Transverse Vibration of a Two-Span Beam Under Action of a Moving Constant Force

By R. S. AYRE,[1] GEORGE FORD,[2] and L. S. JACOBSEN[3]

The problem relates to the transient vibration of a symmetrical, continuous, simply supported two-span beam which is traversed by a constant force moving with constant velocity. The beam is of slender proportions, flexure alone being considered. Damping is zero, and there is no mass associated with the moving force. Exact theoretical solutions for bending stress have been derived in general form. They consist of three infinite series, each related to one of three time eras as follows: (*a*) Where force is crossing first span; (*b*) is crossing second span; (*c*) has left the beam. Each term of a series is related to a natural mode of vibration. Quantitative theoretical studies show the variation in individual terms of the series, and also in summations of the first five terms, as the traversing velocity is varied. A mechanical model with electrical recording of stress was employed to obtain a more complete quantitative solution than was feasible analytically. The agreement between theory and experiment was reasonably good. Large magnifications of stress (of the order of 2.5) were found in the neighborhood of resonance with the fundamental mode.

Nomenclature

The following nomenclature is used in the paper:

- x = horizontal co-ordinate
- y = transverse dynamic deflection of beam; positive downward
- y_i = contribution of ith mode to y
- σ = dynamic flexural stress at lower surface of beam at a given location, x
- σ_i = contribution of the ith mode to σ
- σ_0 = flexural stress at lower surface of beam at mid-point of a span due to force P, when P is fixed at mid-point of same span (static)
- t = time
- l = length of each span
- E = modulus of elasticity for bending
- I = moment of inertia of beam cross section with reference to its neutral axis
- c = half-depth of beam
- Z = section modulus = I/c
- A = cross-sectional area of beam
- γ = weight of material of beam per unit of volume
- g = acceleration due to gravity
- P = magnitude of moving concentrated force
- v = uniform horizontal velocity of force
- i = number of a natural mode
- q_i = generalized co-ordinate for ith mode
- X_i = shape function, that is, normal function
- a_{oi} = etc., boundary-condition constants
- $n_i\pi$ = ith root of frequency equation
- p_i = circular natural frequency of ith mode
- $\tau_1 = \dfrac{2\pi}{p_1}$, natural period of fundamental mode
- $\omega = \dfrac{\pi v}{l}$ = circular forcing frequency
- $N_i = \dfrac{\sin n_i\pi}{\sinh n_i\pi} = \dfrac{\cos n_i\pi}{\cosh n_i\pi}$, constant for ith mode where $i = 2, 4, 6, \ldots$

Introduction

The general problem attracted attention as early as 1847, when a British commission was appointed to study dynamic effects in railway bridges. The commission set up an experimental single-span bridge consisting of a pair of wrought-iron bars 9 ft long and of slender proportions. A carriage was made to pass over the bridge with uniform velocity. The differential equation of deflection was established by neglecting the inertia of the bridge and by considering the moving load as a concentrated mass (1).[4] An exact solution of the equation was obtained by Sir G. G. Stokes (2). A later and more realistic approach was made by A. N. Kryloff (3), by assuming that the mass of the constant load was negligible in comparison with the mass of the beam. The next step was made by S. P. Timoshenko (4), who solved the problem of a pulsating force moving with uniform velocity along a beam. Other work has been done, including that of A. N. Lowan (5), who studied the case in which the velocity of the traversing force is not constant, but the most comprehensive study is that of Sir C. E. Inglis (6, 7). The foregoing investigations were all limited to single-span structures.

In regard to continuous beams, there have been a number of publications (8, 9, 10) on their natural modes and frequencies of vibration and on their steady forced vibration, but to our knowledge the transient problem of a force moving across a continuous beam has not been published previously.

The present study will be extended to include an alternating force moving with constant velocity. Moreover, both of these linear problems will serve as starting points for the contemplated nonlinear problems where appreciable mass is associated with the moving forces.

Theory

Standard classical methods (11) have been used in the analysis which follows. It is assumed: (*a*) the beam is of uniform mass and cross section; (*b*) the material is homogeneous, isotropic, and

[1] Acting Associate Professor of Mechanical Engineering, Stanford University, Stanford University, Calif.

[2] Graduate Student in Mechanical Engineering, Stanford University. Now Assistant Professor of Civil Engineering, University of Alberta, Canada.

[3] Professor of Mechanical Engineering, Stanford University. Mem. ASME.

Contributed by the Applied Mechanics Division and presented at the Semi-Annual Meeting, San Francisco, Calif., June 27–30, 1949, of The American Society of Mechanical Engineers.

Discussion of this paper should be addressed to the Secretary, ASME, 29 West 39th Street, New York, N. Y., and will be accepted until April 10, 1950, for publication at a later date. Discussion received after the closing date will be returned.

Note: Statements and opinions advanced in papers are to be understood as individual expressions of their authors and not those of the Society. Paper No. 49—SA-4.

[4] Numbers in parentheses refer to the Bibliography at the end of the paper.

obeys Hooke's law; (*c*) the beam is free to rotate at all supports, and that no axial stresses are introduced; (*d*) the beam is of such proportions that the effect of shear on the stress distribution and the effect of rotational inertia may be neglected; (*e*) damping is negligible; (*f*) the mass of the moving load is negligible.

Natural Frequencies and Modes of Vibration. Consider a simply supported continuous beam of two equal spans. The instantaneous deflection can be expressed as a product of q, a function of time, and X, a function of location x, referred to as the "shape" function.

$$y = q \cdot X \quad \ldots\ldots [1]$$

FIG. 1

The shape functions of the ith mode for spans a and b are given by

$$X_{ai} = a_{ai} \sin \frac{n_i \pi x}{l} + b_{ai} \cos \frac{n_i \pi x}{l} + c_{ai} \sinh \frac{n_i \pi x}{l} + d_{ai} \cosh \frac{n_i \pi x}{l};\ 0 \leqq x \leqq l \quad \ldots\ldots [1a]$$

and X_{bi} is similar except that a_{ai} becomes a_{bi}, etc.

If the boundary-condition constants a_{ai}, etc., are determined, the following frequency equations result

$$\sin n_i \pi = 0 \quad \ldots\ldots [2]$$

where n_i is an integer

$$\tan n_i \pi - \tanh n_i \pi = 0 \quad \ldots\ldots [3]$$

where n_i is not an integer.

The roots of Equation [2] are exactly π, 2π, 3π, ... , where n_i is 1, 2, 3, ... , and correspond to those for a simply supported beam of one span. The roots of Equation [3] are approximately $(5/4)\pi$, $(9/4)\pi$, $(13/4)\pi$, ... , where n_i is 5/4, 9/4, 13/4, ... , and are equivalent to those for a single-span beam with one end fixed and the other simply supported. The error in the first of the latter set of roots is about 0.01 per cent, and in the higher roots is much smaller.

The natural frequencies are then given by

$$p_i = n_i^2\, p_1 = n_i^2 \frac{\pi^2}{l^2} \sqrt{\frac{EIg}{A\gamma}} \quad \ldots\ldots [4]$$

where p_1 is the circular natural frequency of the fundamental mode.

Values of n_i^2 for the first ten modes are as follows:

Natural mode, i	1	2	3	4	5	6	7	8	9	10
n_i^2	1	1.5625	4.5	9.0625	10	15.5625	16	18.0625	25	27.5625

For any mode, n_i can be determined directly from

$$\left.\begin{aligned} n_i &= \frac{i}{2} + \frac{1}{2}, \text{ for odd-numbered modes} \\ n_i &= \frac{i}{2} + \frac{1}{4}, \text{ for even-numbered modes} \end{aligned}\right\} \quad \ldots\ldots [4a]$$

The shape functions Equation [1*a*] involving boundary conditions and a change in the location variable x, can be reduced to two general forms, Equations [5] and [6]. The new x-co-ordinate systems are shown in Fig. 3

$$X_i = a_{ai}\left[\sin \frac{n_i \pi x}{l}\right];\ 0 \leqq x \leqq 2l \quad \ldots\ldots [5]$$

for odd-numbered modes

$$X_i = a_{ai}\left[\sin \frac{n_i \pi x}{l} - \frac{\sin n_i \pi}{\sinh n_i \pi} \sinh \frac{n_i \pi x}{l}\right];\ 0 \leqq x \leqq l \quad \ldots\ldots [6]$$

for even-numbered modes. The second derivatives of the shape functions, approximately proportional to the stresses, follow at once

$$\frac{d^2 X_i}{dx^2} = a_{ai}\left(\frac{n_i \pi}{l}\right)^2 \left[-\sin \frac{n_i \pi x}{l}\right] \quad \ldots\ldots [5a]$$

for odd modes.

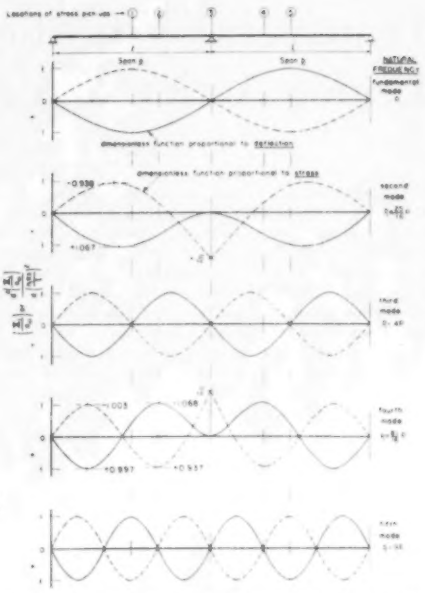

FIG. 2 THEORETICAL DIMENSIONLESS FUNCTIONS PROPORTIONAL TO DEFLECTION AND TO STRESS; FIRST FIVE NATURAL MODES

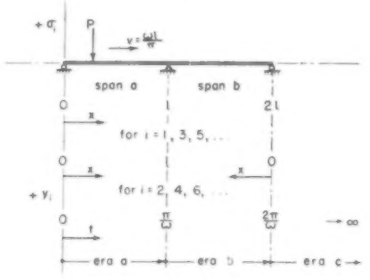

FIG. 3

$$\frac{d^2X_i}{dx^2} = a_{ai}\left(\frac{n_i\pi}{l}\right)^2\left[-\sin\frac{n_i\pi x}{l} - \frac{\sin n_i\pi}{\sinh n_i\pi}\sinh\frac{n_i\pi x}{l}\right] \quad [6a]$$

for even modes.

The dimensionless functions given by the square brackets of Equations [5], [5a], [6], and [6a] have been plotted in Fig. 2 for the first five modes. In regard to stress, the shapes for the odd modes are similar to those for deflection, but for the even modes the stress shapes are characterized by a cusp at the center support. The ordinate at the peak of the cusp is the maximum of the maxima and equals $2\cdot\sin n_i\pi$, or very nearly $= \sqrt{2}$.

Deflections and Stresses: General. Once the roots of the frequency equations have been determined, the total deflection of the beam may be split into its component parts and each part, corresponding to a natural frequency, may be analyzed separately. Each component may be expressed by Equation [1] as follows

$$y_i = q_i \cdot X_i \quad [7]$$

The shape functions X_i have already been derived. The general co-ordinates q_i, are then determined by well-known methods involving the use of Lagrange's equations of motion, and the concept of generalized force. For a beam of more than one span considerable manipulation is involved, but the methods are straightforward. The "symmetrical" two-span case, however, allows of some simplification. Once the deflections y_i have been found the stresses σ_i follow at once.

Moving Constant Force. Let a constant transverse force P move from left to right across the beam with a uniform velocity v. Consider the forcing period as the time necessary for the force to traverse the full length $2l$ of the beam. The forcing frequency is then

$$\omega = \frac{\pi v}{l} \quad [8]$$

Three eras must be considered. In the first, a, the force is crossing span a; in the second, b, it is in span b; in the third, c, it has passed beyond the beam and is no longer acting. The stress contribution of each natural mode is described by three equations, one holding for each era; thus a triple infinity of terms is involved. By examination of the shape functions, Equations [5] and [6], it is evident that the stress equations will fall into two groups, one for the odd-numbered modes, the other for the even. If the derivations are kept in terms of the ith mode, each group reduces to three general equations, one for each era. The phenomenon is then completely described by the six equations for the stress components: σ_{ia}, σ_{ib} and σ_{ic}. When i is odd, use Equations [9a], [10a], and [11a]; when i is even, use Equations [9b], [10b], and [11b].

Odd-numbered natural modes:

$$i = 1, 3, 5, \ldots$$

$$n_i = 1, 2, 3, \ldots, \text{exactly}$$

Force crossing span a (era a)

$$\sigma_{ia} = \frac{Pl}{\pi^2 Z}\cdot\frac{1}{n_i^2}\cdot\frac{\sin n_i\omega t - \dfrac{n_i\omega}{p_i}\sin p_i t}{1-\left(\dfrac{n_i\omega}{p_i}\right)^2}\cdot\sin\frac{n_i\pi x}{l},$$

$$0 \leqq t \leqq \frac{\pi}{\omega} \quad [9a]$$

Force crossing span b (era b):

$$\sigma_{ib} = \frac{Pl}{\pi^2 Z}\cdot\frac{1}{n_i^2}\cdot\frac{\sin n_i\omega t - \dfrac{n_i\omega}{p_i}\sin p_i t}{1-\left(\dfrac{n_i\omega}{p_i}\right)^2}\cdot\sin\frac{n_i\pi x}{l},$$

$$\frac{\pi}{\omega} \leqq t \leqq \frac{2\pi}{\omega} \quad [10a]$$

Note that Equations [9a] and [10a] are identical and therefore hold over the time interval, $0 \leqq t \leqq 2\pi/\omega$.

Force passed beyond the beam (era c)

$$\sigma_{ic} = -\frac{Pl}{\pi^2 Z}\cdot\frac{1}{n_i^2}\cdot 2\cdot\frac{n_i\omega}{p_i}\cdot\sin\frac{p_i\pi}{\omega}\cdot\frac{\cos p_i\left(t-\dfrac{\pi}{\omega}\right)}{1-\left(\dfrac{n_i\omega}{p_i}\right)^2}\cdot\sin\frac{n_i\pi x}{l},$$

$$\frac{2\pi}{\omega} \leqq t \rightarrow \infty \quad [11a]$$

Even-numbered natural modes:

$$i = 2, 4, 6, \ldots$$

$$n_i = 5/4, 9/4, 13/4, \ldots, \text{very nearly}$$

$$N_i = \frac{\sin n_i\pi}{\sinh n_i\pi} = \frac{\cos n_i\pi}{\cosh n_i\pi}$$

Force crossing span a (era a)

$$\sigma_{ia} = \frac{Pl}{\pi^2 Z}\cdot\frac{1}{n_i^2}\cdot\frac{1}{1-N_i^2}\cdot\left\{\frac{\sin n_i\omega t - \dfrac{n_i\omega}{p_i}\sin p_i t}{1-\left(\dfrac{n_i\omega}{p_i}\right)^2} - \frac{N_i\left(\sinh n_i\omega t - \dfrac{n_i\omega}{p_i}\sin p_i t\right)}{1+\left(\dfrac{n_i\omega}{p_i}\right)^2}\right\}$$

$$\times\left(\sin\frac{n_i\pi x}{l} + N_i\sinh\frac{n_i\pi x}{l}\right), \quad 0 \leqq t \leqq \frac{\pi}{\omega} \quad [9b]$$

Force crossing span b (era b)

$$\sigma_{ib} = \frac{Pl}{\pi^2 Z} \cdot \frac{1}{n_i^2} \cdot \frac{1}{1 - N_i^2} \cdot \left\{ \frac{\cos n_i\omega t - \frac{n_i\omega}{p_i}\left\{\sin p_i t - 2 \cdot \cos n_i\pi \cdot \sin p_i\left(t - \frac{\pi}{\omega}\right)\right\}}{1 - \left(\frac{n_i\omega}{p_i}\right)^2} - \frac{N_i\left[\sinh n_i\omega\left(\frac{2\pi}{\omega} - t\right) - \frac{n_i\omega}{p_i}\left\{\sin p_i t - 2 \cdot \cosh n_i\pi \cdot \sin p_i\left(t - \frac{\pi}{\omega}\right)\right\}\right]}{1 + \left(\frac{n_i\omega}{p_i}\right)^2} \right\}$$

$$\times \left(\sin \frac{n_i\pi x}{l} + N_i \sinh \frac{n_i\pi x}{l}\right), \quad \frac{\pi}{\omega} \gtrless t \gtrless \frac{2\pi}{\omega} \quad \ldots\ldots [10b]$$

Force passed beyond beam (era c)

$$\sigma_{ic} = \frac{Pl}{\pi^2 Z} \cdot \frac{1}{n_i^2} \cdot \frac{1}{1 - N_i^2} \cdot 2 \cdot \frac{n_i\omega}{p_i} \cdot \left\{ \frac{\cos n_i\pi - \cos \frac{p_i\pi}{\omega}}{1 - \left(\frac{n_i\omega}{p_i}\right)^2} - \frac{N_i\left(\cosh n_i\pi - \cos \frac{p_i\pi}{\omega}\right)}{1 + \left(\frac{n_i\omega}{p_i}\right)^2} \right\}$$

$$\times \sin p_i\left(t - \frac{\pi}{\omega}\right) \cdot \left(\sin \frac{n_i\pi x}{l} + N_i \sinh \frac{n_i\pi x}{l}\right), \quad \frac{2\pi}{\omega} \gtrless t \to \infty \quad \ldots\ldots [11b]$$

The values of the constants N_i are closely -0.0279, $+0.00121$, -0.0000526, . . . , for modes 2, 4, 6, . . . , respectively. The factor $1/(1 - N_i^2)$ for practical purposes can be considered as unity. It is positive and slightly greater than 1.0; its value for the second mode is 1.00080.

The total stresses are

$$\sigma_a = \sum_{i=1}^{i=\infty} \sigma_{ia}; \quad \sigma_b = \sum_{i=1}^{i=\infty} \sigma_{ib}; \quad \sigma_c = \sum_{i=1}^{i=\infty} \sigma_{ic} \quad \ldots\ldots [12]$$

We now examine some particular values of $n_i\omega/p_i$.

(I) $\qquad v \to \infty; \quad \dfrac{n_i\omega}{p_i} \to \infty$

This case corresponds to that of an infinite velocity of the force P and is trivial; the stresses approach zero. Next, let

(II) $\qquad v \to 0; \quad \dfrac{n_i\omega}{p_i} \to 0$

In this case the problem loses its dynamic aspect, and the summation of the stress components corresponds to what is commonly called the "crawl stress." The summation of the component crawl stresses should then agree with the stresses calculated by methods of statics. Assuming, for example, that the force has reached the mid-point of span a, we determine the stress at the point of loading. The methods of statics give

$$\sigma_c = \frac{Pl}{\pi^2 Z} \cdot \frac{13}{64} \pi^2 = \frac{Pl}{\pi^2 Z} \; 2.0048 \quad \ldots\ldots [13]$$

The summation of the first ten terms results in an appreciable error of -8.2 per cent, of the first fifteen terms in an error of -6.2 per cent. However, if we determine the stress at the mid-support rather than at the point of loading, there is a pronounced difference in the number of terms required to give good agreement with the statical determination, since the first two terms of the series, of which the first is zero, result in an error of about 0.1 per cent.

(III) $\qquad$ Resonance; $\dfrac{n_i\pi}{p_i} = 1$

It can be shown for the odd-numbered modes that σ_i reaches its maximum resonance value at the instant the force leaves the beam, that is, when $t = 2\pi/\omega$. Letting the stress function take its maximum value, unity, we see that the maximum stress at resonance is given by

$$|\sigma_i|_{\substack{\text{res} \\ \max \\ i=1,3,5,\ldots}} = \frac{Pl}{\pi^2 Z} \cdot \frac{\pi}{n_i} \quad \ldots\ldots [14]$$

The relative values are determined by $1/n_i$, and are 1.000, 0.500, 0.333, . . . for modes 1, 3, 5, . . . , respectively.

For the even-numbered modes the maximum resonance stress may be derived from Equation [11b] for σ_{ic}. Setting $\sin p_i[t - (\pi/\omega)]$ equal to unity and letting the stress function take its maximum value, $2 \cdot \sin n_i\pi$, we obtain

$$|\sigma_i|_{\substack{\text{res} \\ \max \\ i=2,4,6,\ldots}} = \frac{Pl}{\pi^2 Z} \cdot \frac{1}{n_i^2} \cdot \frac{1}{1 - N_i^2} \, 2 \sin n_i\pi \, [n_i\pi \sin n_i\pi$$

$$- (1 - N_i) \cos n_i\pi] \approx \frac{Pl}{\pi^2 Z} \cdot \frac{\pi}{n_i}\left[1 - \frac{1 - N_i}{\pi n_i}\right] \quad \ldots\ldots [15]$$

The relative values are given closely by

$$\frac{1}{n_i}\left[1 - \frac{1 - N_i}{\pi n_i}\right]$$

they are 0.590, 0.381, 0.278, . . . for modes 2, 4, 6, . . . , respectively, and for even modes higher than the twelfth they are determined within 5 per cent error by $1/n_i$.

(IV) $\qquad \sigma_{ic} = 0$

For some values of $n_i\omega/p_i$, σ_{ic} becomes zero for all values of t; in other words, the beam is at rest and is dynamically unstrained at the instant the force leaves the beam. This is evident for the two trivial cases (I) and (II). For the odd-numbered modes, the intermediate values of $n_i\omega/p_i$ are readily determined from the fact

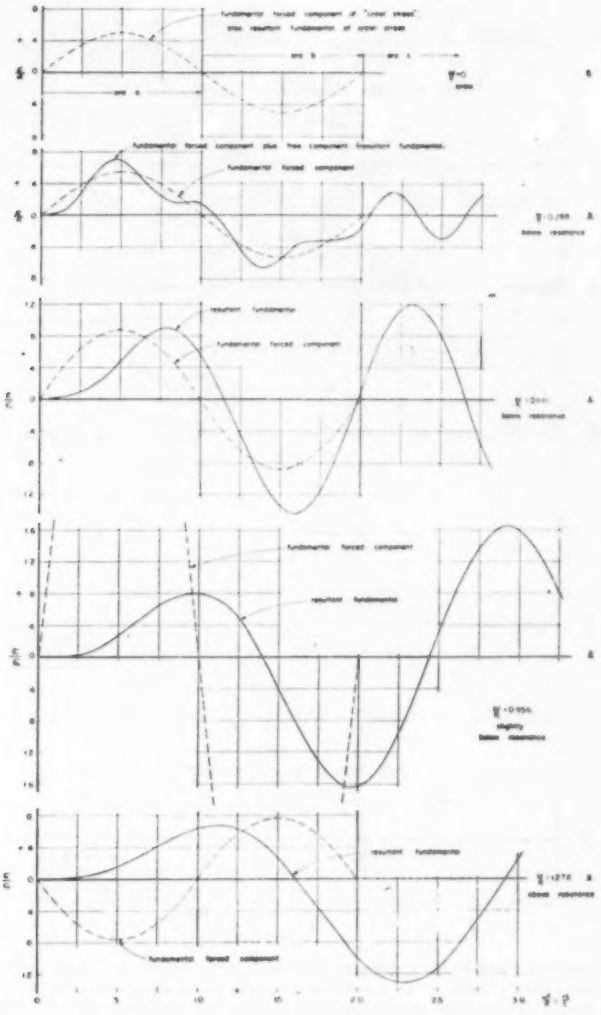

FIG. 4 THEORETICAL STRESS-TIME DIAGRAMS; FUNDAMENTAL-MODE COMPONENT
(For five values of ω/p_1. At mid-span; $x = l/2$.)

that $\sin(p_i\pi/\omega)$ equals zero whenever p_i/ω equals any integer. The condition, $p_i/\omega = n_i$, is an exception, since this results in resonance. Corresponding values of $n_i\omega/p_i$ for the even-numbered modes must be determined by solution of the equation resulting when the bracketed term in Equation [11b] is set equal to zero.

Absolute Maxima. In general, the maximum of the maxima of σ_i for a particular mode can occur during any one of the three time eras depending upon the value of $n_i\omega/p_i$. Since eras *a* and *b* involve two-frequency phenomena the matter of determining the maximum stress while the load is on the beam is a laborious process, especially for the even-numbered components. The determination of the maximum during era *c* is less troublesome, since only single-frequency phenomena are involved, and $n_i\omega/p_i$ alone need be varied. The absolute maximum of σ_{i_c} occurs in the general neighborhood of resonance.

QUANTITATIVE RESULTS

Stress-Time Diagrams Relating to Particular Natural Modes. Figs. 4 to 8, inclusive, show theoretical values of the stress ratios σ_i/σ_0 plotted as functions of the dimensionless time variable $\omega t/\pi$ for the first five natural modes and for five different forcing frequencies. The abscissa or time variable is proportional to the horizontal distance traveled by the force

$$\frac{\omega t}{\pi} = \frac{vt}{l} \qquad [16]$$

The frequency ratio $n_i\omega/p_i$ is used, since it is always unity at

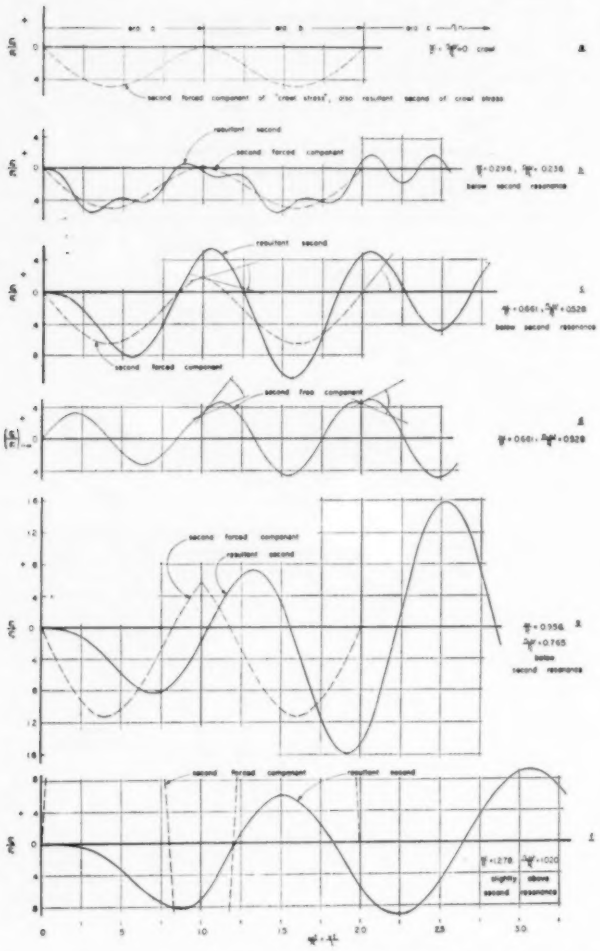

FIG. 5 THEORETICAL STRESS-TIME DIAGRAMS; SECOND-MODE COMPONENT
(For five values of ω/p_1. At mid-support; $x = l$.)

resonance, regardless of i; however, in comparing the effects of a given forcing frequency on several natural-mode stress components, it is often convenient to use the ratio, ω/p_1, which does not change with the mode. The two forms are related as follows

$$\frac{\omega}{p_1} = n_i \cdot \frac{n_i \omega}{p_i} \quad \ldots\ldots\ldots\ldots\ldots\ldots\ldots\ldots [17]$$

Forced-Vibration Terms. When the forcing frequency approaches zero, σ_i becomes one of the components of the crawl stress, the amplitude of the free-vibration term approaches zero, and σ_i is described by the forced-vibration term alone. At forcing frequencies greater than zero, the amplitudes of the forced-vibration terms are modified by the resonance function and by the factor,

$$\frac{1}{1 + \left(\frac{n_i \omega}{p_i}\right)^2}$$

They are illustrated by dashed curves for the fundamental mode in Fig. 4, for the third mode in Fig. 6, and for the fifth mode in Fig. 8. The forced terms for even modes are also shown by dashed curves, for the second mode in Fig. 5, and for the fourth mode in Fig. 7; changes in amplitude as well as in shape occur, due to the presence of the hyperbolic functions.

Free-Vibration Terms. The free-vibration terms describe

$$\frac{p_i}{\omega}, \quad \text{or} \quad \frac{n_i}{\frac{n_i \omega}{p_i}}$$

cycles of motion while the force is crossing the beam. There is no change in either amplitude or phase of the free-vibration stress in passing from era a to era b for the odd-numbered modes. However, in passing into era c, adjustments must be made in amplitude and phase in order to compensate for the abrupt ending of the forced-vibration component at $\omega t/\pi = 2$.

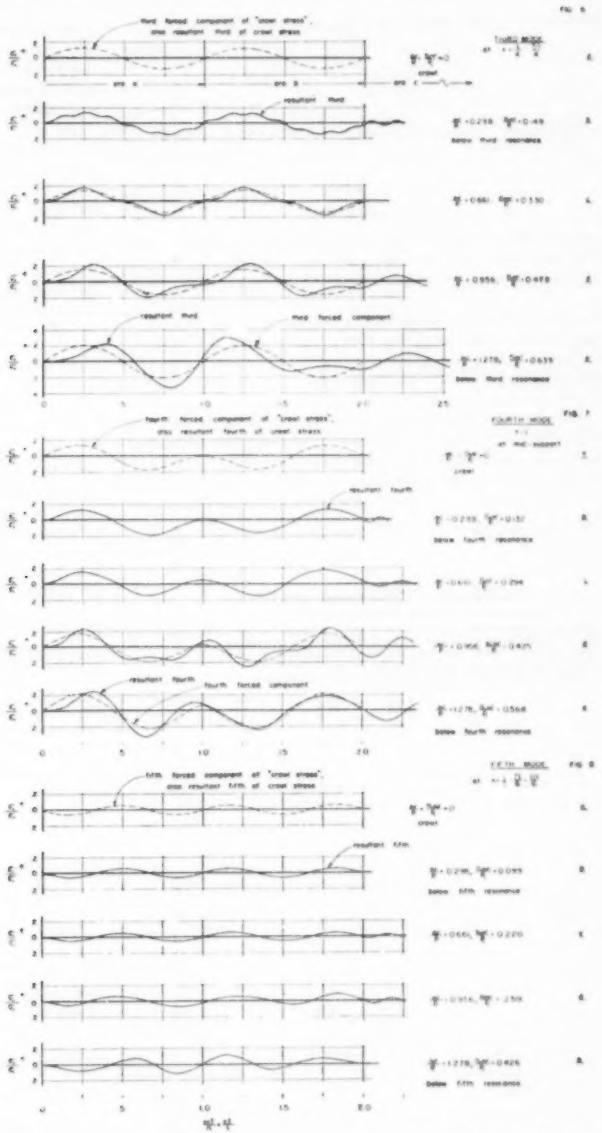

FIGS. 6, 7, 8 THEORETICAL STRESS-TIME DIAGRAMS; THIRD, FOURTH, AND FIFTH-MODE COMPONENTS
(For five values of ω/p_1.)

In regard to the even-numbered modes, the stress Equations [9b] and [10b] indicate that the free-vibration stress component for era b is different from that for era a in amplitude as well as in phase. It is apparent that this is due to the slope discontinuity in the forced-vibration component at the juncture of the two eras. The point is illustrated especially well in Fig. 5(c) for the second mode with $\omega/p_1 = 0.661$, where the free-vibration component is shown separately in Fig. 5(d), and the forced-vibration component and resultant appear in Fig. 5(c). The necessary compensations in slope have been shown by the tangent lines.

Stress-Time Diagrams for the Summation of Several Natural-Mode Components. The number of terms required in a summation to give satisfactory agreement with the total stress (Equations [12]) depends on the position of the force, that is, on time, the location x at which stress is being measured, and on the forcing frequency. Two such examples have already been given. However, these are extreme cases, neither of which should be used as a criterion. In general, the first two terms should always be included in any summation, and higher terms should be added depending upon t, x, and ω. It is probably safe to say that not

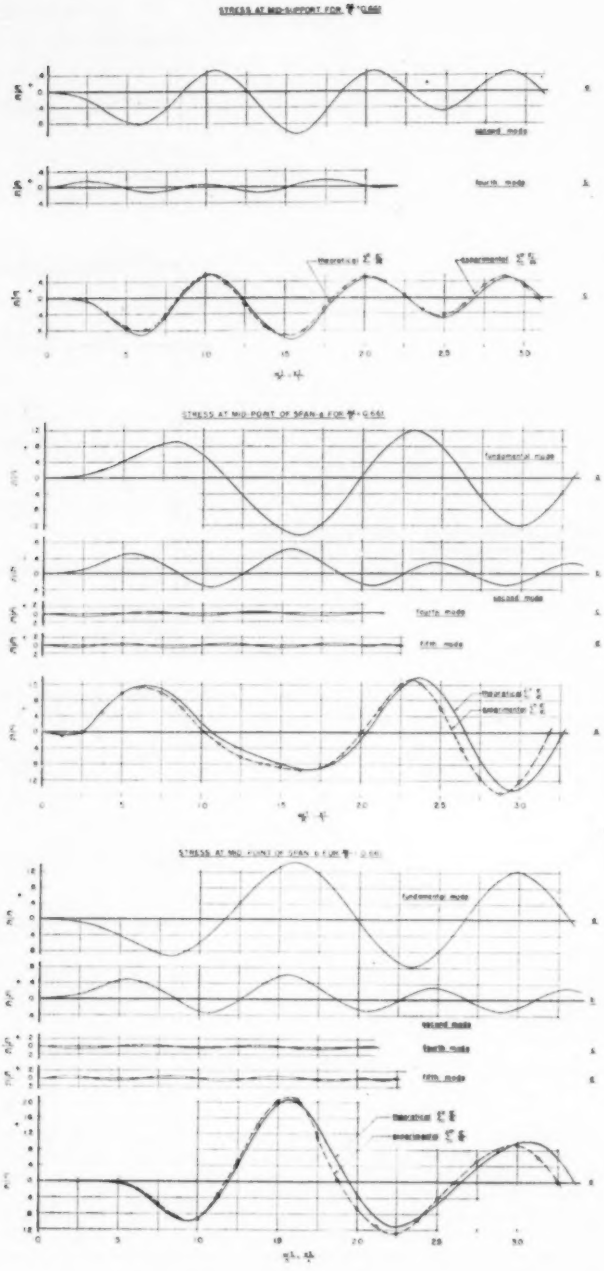

FIG. 9 COMPARISON OF THEORETICAL AND EXPERIMENTAL STRESS-TIME DIAGRAMS

(For three locations; for $\omega/p_1 = 0.661$. The theoretical stress is the summation of the first five natural-mode components. Note that all odd-mode components are zero at mid-support, and that the third-mode component is zero at mid-span. The experimental stress is total stress.)

more than four or five terms are needed for most practical work, except at small values of ω/p_1, and for these the stress magnification is small and not of much practical interest. It is at this point that the need for an experimental apparatus, in effect, a calculating machine for the summation of the series of natural-mode components, becomes most obvious.

Fig. 9 shows the graphical summations of the first five terms of the series for $\omega/p_1 = 0.661$, and for three different locations. The agreement between theory and experiment is reasonably good, particularly in regard to the stress maxima, which are the points of greatest practical concern. The lack of perfect coincidence is ascribable to experimental errors, friction, and to limiting the theoretical summation of the series to a small number of terms. An important source of experimental error is in the traversing velocity, since small errors in ω may sometimes lead to large errors in stress.

Maximum Stress as Function of Frequency Ratio, ω/p_1

Natural-Mode Components. The calculated stress ratios

$$\left|\frac{\sigma_{ia\text{-}b}}{\sigma_0}\right|_{\max} \quad \text{and} \quad \left|\frac{\sigma_{ic}}{\sigma_0}\right|_{\max}$$

for the first five modes have been plotted in Fig. 10 as functions of ω/p_1. During eras *a* and *b* (Fig. 10*a*), the absolute maxima of the fundamental and second mode components occur at values of ω/p_1 less than unity. The stress maxima of the free-vibration era *c* (Fig. 10*b*) are characterized by series of alternating zero values and maxima. The absolute maxima of era *c* occur at approximately the same values of ω/p_1 as do those of eras *a* and *b*. The absolute maxima of era *c* are nearly equal to those of eras *a* and *b*. For low values of ω/p_1, the maximum stress occurs while the force is crossing the beam, but for ω/p_1 greater than unity the maximum stress generally occurs after the force has left the beam. Figs. 10 and 2, when used in conjunction with each other, give the maximum contribution of each component at any location along the beam. (Fig. 2 shows the variation in stress with location.) For example, if the contribution of the two-span second mode is wanted at mid-span, multiply the ordinates of the corresponding curve in Fig. 10 by $0.83/\sqrt{2} = 0.59$.

Total Stresses. Experimentally determined values of the stress ratios

$$\left|\frac{\sigma_{a\text{-}b}}{\sigma_0}\right|_{\max} \quad \text{and} \quad \left|\frac{\sigma_c}{\sigma_0}\right|_{\max}$$

have been plotted in Fig. 11 for three locations. Several theoretical values of

$$\left|\frac{\sigma_{a\text{-}b}}{\sigma_0}\right|_{\max}$$

based upon the first five terms of the series, have also been shown. Theoretical points of total stress for era *c* have not been indicated as the unlimited duration of the era makes their times of occurrence difficult to find.

We can now determine for a given value of ω/p_1 the maximum stress in terms of σ_0, where σ_0 may readily be calculated by Equation [13]. The greatest magnification at mid-span is about 2.4, and occurs when ω/p_1 is approximately 0.85. Since the beam is symmetrical, the curves for era *c* in Figs. 11(*b*) and (*c*), should coincide. They agree at their maxima within about 4 per cent.

Figs. 10 and 2 can also be used to estimate maximum total stress, provided it is assumed that the maxima of the components coincide in sign and in time of occurrence. Examples: Estimate maximum total stress in two-span beam

1 At mid-span when $\omega/p_1 = 0.66$. Use Fig. 10(*a*) and limit to first two modes

$$\left|\frac{\sigma}{\sigma_0}\right|_{\max} \approx 1.43 + 0.59 \times 1.11 = 2.1$$

Compare with bottom diagram in Fig. 9, and with curve for eras *a*, *b*, Fig. 11(*c*), where we obtain 2.1.

2 At mid-span when $\omega/p_1 = 1.2$. Use Fig. 10(*b*) and limit to first two modes

$$\left|\frac{\sigma}{\sigma_0}\right|_{\max} \approx 1.39 + 0.59 \times 1.03 = 2.0$$

Compare with Figs. 11(*b*), (*c*), era *c* curve, where we obtain 1.9.

3 At mid-support when $\omega/p_1 = 1.2$. Use Fig. 10(*b*) and limit to second mode alone

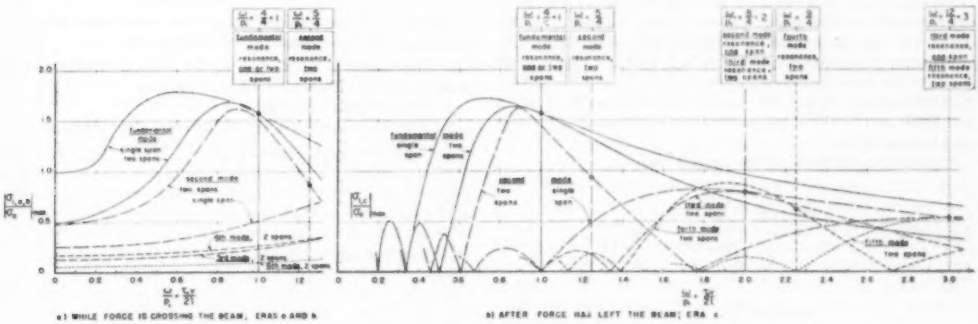
fundamental mode single span two spans
second mode two spans single span
second mode two spans
fundamental mode single span two spans
third mode two spans
fourth mode two spans
fifth mode two spans
a) WHILE FORCE IS CROSSING THE BEAM; ERAS a AND b
b) AFTER FORCE HAS LEFT THE BEAM; ERA c

Fig. 10 Theoretical Absolute Maxima of Stress Components; Comparison of Two-Span Beam With Simply Supported Single-Span Beam

Locations are those giving maximum stress as follows:

Single span: fundamental mode, $x = \frac{l}{2}$; second mode, $x = \frac{l}{4}, \frac{3l}{4}$

Two spans: fundamental mode, $x = \frac{l}{2}, \frac{3l}{2}$; second mode, $x = l$; third mode, $x = \frac{l}{4}, \frac{3l}{4}, \frac{5l}{4}, \frac{7l}{4}$; fourth mode, $x = l$; fifth mode, $x = \frac{l}{6}, \frac{3l}{6}, \frac{5l}{6}, \frac{7l}{6}, \frac{9l}{6}, \frac{11l}{6}$

Note that resonance occurs when $\frac{n_2\omega}{p_2} = \frac{n_1\omega}{n_1^2 p_1} = 1$, i.e., when $\frac{\omega}{p_1} = n_1$

(See Equations [9*a*, *b*], etc.)

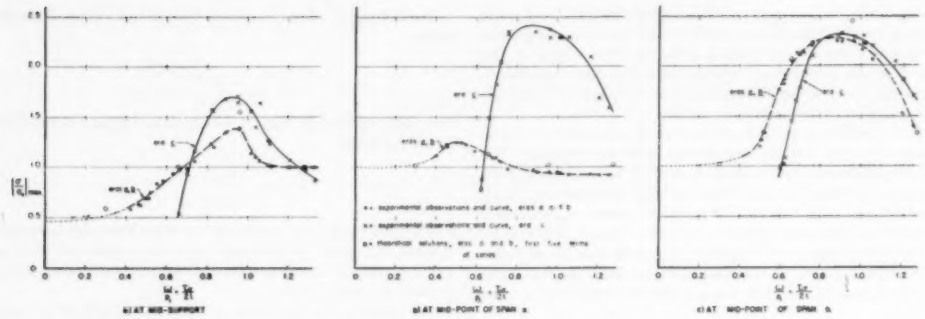

FIG. 11 EXPERIMENTAL ABSOLUTE MAXIMA OF TOTAL STRESSES; THEORETICAL SOLUTIONS FOR ERAS *a* AND *b* SHOWN FOR COMPARISON

$$\left|\frac{\sigma}{\sigma_0}\right|_{\max} \approx 1.0$$

Compare with Fig. 11(*a*), where we obtain 1.1.

Example. If we assume a two-span continuous-girder bridge with span lengths of 100 ft and with a fundamental natural frequency of 2 cycles per sec, the traversing velocity of the force must be 230 mph in order that the maximum stress at mid-span may be reached. The stress is not significantly greater than the static stress σ_0 at speeds up to about 80 mph, while at a speed of 140 mph the stress is nearly 30 per cent greater than σ_0. The foregoing overlooks the fact that actual bridge loads involve mass.

For reasons of uniformity, Fig. 11(*a*) relates stress at mid-support to σ_0; however, it is more indicative of stress magnification at the mid-support to relate this stress to $(^6/_{11})\sigma_0$, which is the static stress at mid-support due to a load at mid-span. The greatest magnification then occurs when ω/p_1 is about 0.9, and is $(^{11}/_6) \times 1.7$ or 3.7. Since beams are often overdesigned with respect to the bending stresses at the supports, the magnification of 3.7 at mid-support is probably of no greater practical importance than that of 2.4 at mid-span.

THE BEAM OF k EQUAL SPANS

The theory can be generalized to cover the case of a beam of any number k of equal spans. However, it is difficult to do this except for the natural modes of purely sinusoidal shape, i.e., modes having the numbers $i = 1, 1 + k, 1 + 2k, 1 + 3k, \ldots$. (all modes of the single-span case, modes 1, 3, 5, 7, ... of the two-span beam, modes 1, 4, 7, 10, ... of the three-span beam, etc.). The equations for the stress components corresponding to these modes are as follows:

Force crossing the beam (forced-vibration era)

$$\sigma_{i(\text{forced})} = \frac{2}{k}\frac{Pl}{\pi^2 Z}\frac{1}{n_i^2}\frac{\sin n_i\omega t - \frac{n_i\omega}{p_i}\sin p_i t}{1-\left(\frac{n_i\omega}{p_i}\right)^2}\sin\frac{n_i\pi x}{l},$$

$$\text{where } 0 \gtrless t \lessgtr \frac{k\pi}{\omega},\ 0 \gtrless x \lessgtr kl \quad \ldots\ldots [18]$$

Force passed beyond the beam (free-vibration era)

$$\sigma_{i(\text{free})} = -\frac{2}{k}\frac{Pl}{\pi^2 Z}\frac{2}{n_i^2}\frac{n_i\omega}{p_i}\frac{\sin\left[\left(\frac{p_i}{\omega}-n_i\right)\frac{k\pi}{2}\right]}{1-\left(\frac{n_i\omega}{p_i}\right)^2}$$

$$\times\cos\left[p_i t-\left(\frac{p_i}{\omega}-n_i\right)\frac{k\pi}{2}\right]\sin\frac{n_i\pi x}{l},\ \text{where } \frac{k\pi}{\omega}$$

$$\gtrless t < \infty,\ 0 \gtrless x \lessgtr kl \quad \ldots\ldots [19]$$

where $i = 1, 1 + k, 1 + 2k, 1 + 3k, \ldots$. and where corresponding values of n_i are $1, 2, 3, 4, \ldots$.

If Equations [18] and [19] for the general case are compared with Equations [9*a*], or [10*a*] and [11*a*], which are the corresponding equations relating specifically to the two-span beam, it can be seen that the general form includes a coefficient $2/k$ and, in Equation [19], some changes made necessary by the fact that the time of starting of the free-vibration era is a function of the number of spans. A very simple relationship exists at resonance. In the sinusoidally shaped modes the resonance stress is independent of the number of spans, i.e., a force crossing a single-span beam at a resonant velocity will induce as large a maximum response in the resonant mode as will the same force in crossing a beam of any number of spans. The resonance stress is given by Equation [14] where i must be taken as just listed. The stress maxima for the fundamental and second modes of a single-span beam have been shown in Fig. 10. They have been related to σ_0 for the two-span case in order to provide a direct comparison.

SUMMARY AND CONCLUSIONS

The principal assumptions which must be kept in mind in application of the foregoing to practice are as follows:

1 The beam is of slender proportions, and consequently bending stresses alone have been considered.

2 Damping has been neglected.

3 Any mass associated with the moving force is negligible.

An exact solution has been obtained. It consists, as one would expect, of an infinite series of stress components, each component corresponding to a natural mode of vibration. There are three such series relating to three time eras, one applying while the force is crossing the first span of the beam, the second while the force is in the second span, and the third after the force has left the beam. Each component of the first two series consists of a forced-vibration term with a frequency proportional to the traversing velocity of the force, and a free-vibration term with a frequency equal to the natural frequency of the mode. Each component of the third series involves only a free-vibration term. The individual terms of the series are not overly complicated, particularly since they reduce to six general types, three holding for the odd-numbered natural modes, one type for each time era, and three for the even Equations [9*a*, *b*], [10*a*,*b*], [11*a*, *b*]; due to the symmetry of the beam those for the odd modes are simple.

The number of terms needed in a summation of the series to re-

sult in satisfactory agreement with the total stress depends upon the requirements of the particular problem, especially on the location x, at which stress is being measured and on the ratio ω/p_1, of forcing frequency to fundamental natural frequency. At least the first two terms must be included, and it is believed that no more than four or five are needed for most practical work. This is in contrast to the single-span case for which the fundamental term alone is often sufficient.

In order to make a quantitative survey of the maxima occurring in the phenomenon one must vary time, location, and forcing frequency. Location may fairly well be restricted to three points, the center of each span and the mid-support. The time of occurrence of the maximum stress associated with a given forcing frequency may lie in any one of the three time eras, depending upon the relationship of the forcing frequency to the natural frequencies; thus all three series must be considered. However, in many cases the maximum occurs either when the force is crossing the second span or after it has left the beam. It has also been found that at forcing frequencies in the neighborhood of the one producing absolute maximum stress a consideration of the third era alone gives good results; this era is more readily handled than the others since it involves only the free-vibration terms. In regard to variation of the maxima with variation in forcing frequency, it has been found that the absolute maximum occurs at a value of ω/p_1 of about 0.85, in other words, a little below resonance with the fundamental mode.

The foregoing indicates that a large number of combinations must be explored; it is obvious that an experimental apparatus is desirable for use in effecting a direct summation of the three series. This is true even for the relatively simple case of a symmetrical two-span beam; beams of unsymmetrical arrangement or of more than two spans would be considerably more difficult to handle theoretically in a quantitative way, but not appreciably more so by experimental means. The experimental apparatus becomes particularly desirable if one is to extend the work to the nonlinear problem involving moving-mass loadings.

The equipment which has been employed is mechanical with electrical stress recording. While electrical analogs are often useful in mechanical-vibration studies, it is believed that the mechanical method is indicated in this case. However, the electrical method of recording strain is certainly desirable. The problem could have been approached by recording deflection, either optically or electrically. However, if one is to explore the higher natural modes, it is desirable to use stress recording since the contributions of the higher modes to stress are of much more significance than their contributions to deflection. Furthermore, stress is often of more practical importance than deflection.

The stress data have been presented as ratios of stress to the static stress σ_0 at mid-span caused by a concentrated load at the same mid-span point. Hence it is possible simply by the calculation of σ_0 and by use of the experimental curves in Fig. 11, to determine the maximum total stress at the center of either span or at the mid-support for any value of ω/p_1 within the limits of the curves.

A hypothetical example applying the magnification factors to a two-span bridge, and overlooking the fact that bridge loads normally involve rather large mass, indicates that large dynamic stresses in bridges, due to velocity loading alone, generally are not to be expected.

Acknowledgment

This investigation is a part of a contract held by Stanford University and sponsored by the Office of Naval Research, titled "The Effects of Transient Disturbances on Structures." The authors are indebted to Mr. Rune L. Evaldson for assistance in carrying out the work.

Bibliography

1 "Appendix to the Report of the Commissioners . . . to Inquire Into the Application of Iron to Railway Structures," by R. Willis, London, England, 1849.

2 "Discussion of a Differential Equation Relating to the Breaking of Railway Bridges," by Sir G. G. Stokes, Mathematics Physics Papers, vol. 2, 1849, p. 179.

3 "Über der erzwungenen Schwingungen von gleichförmigen elastischen Stäben," by A. N. Kryloff, *Mathematische Annalen*, vol. 61, 1905, p. 211.

4 "On the Forced Vibration of Bridges," by S. P. Timoshenko, *Philosophical Magazine*, vol. 43, 1922, p. 1018.

5 "On Transverse Oscillations of Beams Under the Action of Moving Variable Loads," by A. N. Lowan, *Philosophical Magazine*, vol. 19, series 7, 1935, p. 708.

6 "Theory of Transverse Oscillations in Girders and Its Relation to Live Load and Impact Allowances," by Sir C. E. Inglis, Proceedings of the Institution of Civil Engineers, London, England, vol. 218, 1924, p. 225.

7 "A Mathematical Treatise on Vibrations in Railway Bridges," by Sir C. E. Inglis, Cambridge University Press, 1934.

8 "The Transverse Vibrations of Beams and the Whirling of Shafts Supported at Intermediate Points," by E. R. Darnley, *Philosophical Magazine*, vol. 41, 1921, p. 81.

9 "Dynamik der Stabwerke," by K. Hohenemser and W. Prager, Julius Springer, Berlin, Germany, 1933.

10 "Free and Forced Oscillations of Continuous Beams, Treatment by Admittance Method," by W. J. Duncan, *Philosophical Magazine*, vol. 34, 1943, p. 49.

11 "Vibration Problems in Engineering," by S. P. Timoshenko, D. Van Nostrand Company, Inc., New York, N. Y., 1937.

Appendix

Experimental Apparatus

The apparatus is shown in the schematic diagram Fig. 12. It consists essentially of the following:

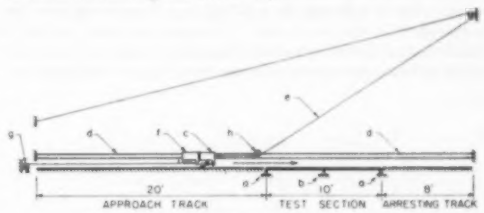

Fig. 12 Schematic Diagram of Apparatus

a, *a*, end supports of beam
b, mid-support of beam
c, force carriage
d, guide rail
e, elastic nylon string
f, release mechanism and dynamometer
g, windlass
h, pulley at which elastic string disengages from carriage

1 The two-span beam (test section) supported at three points (*a*, *b*, *a*) with no constraint against rotation but with complete constraint against vertical translation. The center support (*b*) is the only point at which restraint against horizontal translation is introduced, this is for the purpose of positioning the beam with reference to adjoining parts of the equipment.

2 A moving carriage (*c*) which provides the means for conveying the force along the beam. The force is applied through a roller on the end of a trailing spring-loaded lever attached to the carriage.

3 A guide rail (*d*) for directing the carriage.

4 A horizontal track along which the force approaches and leaves the beam.

5 A device for accelerating the carriage, consisting of an elastic nylon string (*e*) attached to the carriage, a mechanism (*f*) for releasing the carriage, and a windlass (*g*) for stretching the nylon string through a dynamometer built into the releasing mechanism.

6 An arresting device which dissipates most of the kinetic energy of the carriage through friction, and which transforms the remainder into elastic energy.

7 A system for recording dynamic stress as a function of time. This consists of five Wheatstone bridge circuits composed of wire-resistance strain gages, each bridge constituting a stress "pickup;" circuits for selecting and balancing the pickups; amplifiers, and a two-channel Brush oscillograph.

8 A mechanical-electrical timing device for use in computing the average velocity of the force as it moved across each span.

The more important data are as follows:

Beam. Length of each span, 60 in.; width, 4 in.; thickness, $^3/_{16}$ in. Material, cold-rolled steel. Fundamental natural frequency, 4.70 cycles per sec.

Carriage:

Normal weight, about 2 lb; increased to 10 lb at low velocities.

Loading springs, piano wire bent into a U-shape and loaded in bending; spring rate at roller, $^1/_4$ lb per in.; force P, 3 lb.

Effective mass of loading spring, lever, and roller assembly, 0.25 per cent of total mass of beam.

Stress-Recording System. There are five stress pickups located symmetrically on the beam, as shown in Fig. 2. Each consists of eight SR-4 strain gages, two in series in each leg of a Wheatstone bridge. Two legs are attached to the upper surface of the beam and two directly underneath on the lower surface; all gages are active. Flexible wires, offering very little restraint to the beam, connect the bridge circuit with the selecting and balancing circuits.

The locations of the pickups are related to the nodes and points of stress maxima of some of the natural modes of vibration of the beam. Fig. 2 indicates that pickup No. 3, mounted over the mid-support of the beam, records the maxima (with respect to location, x) of all the even-mode components, but records no part of the odd-mode component stresses, they being zero at this point. The locations of pickups Nos. 1 and 5, at the mid-points of spans a and b, respectively, coincide with positions of maximum stress of modes 1, 5, 9, ... and with zero-stress points of modes 3, 7, 11, ... In addition to recording the maxima of every other odd mode, beginning with the fundamental, they record some proportion of the maximum of each even-mode component. Similarly, pickups Nos. 2 and 4, which have been attached at the second third-point of span a, and the first third-point of span b, coincide with zero-stress points of modes 5, 11, 17, ... and record some proportion of all other modes. The latter two pickups are of particular interest in regard to modes 3 and 4, since they record large proportions of their maxima but only a small part of the second-mode component.

By means of the selecting circuits, the pickups can be used individually to record total dynamic stresses, in effect, to make the summation of all terms of the stress series; or a symmetrical pair of pickups can be combined electrically so as to cancel either the odd or the even-mode components. For example, if the output of pickup No. 1 be "subtracted" electrically from that of No. 5, the resultant output will equal twice the sum of the contributions of modes 1, 5, 9, ... This combination gives, at forcing frequencies, in the neighborhood of resonance with the fundamental mode, a very good idea of the fundamental since the contributions of the other recorded modes are relatively small. On the other hand, if the outputs of pickups Nos. 1 and 5 be "added," the odd modes disappear and only the even are shown. The ability to subtract the outputs of Nos. 1 and 5 provided an easy method of checking the behavior of the apparatus.

The amplifier-oscillograph was calibrated for pen response versus input frequency, and for pen response versus peak-input voltage at frequencies up to 80 cycles per sec. To be certain that all factors had been considered, a dynamic calibration of the complete beam and recording system was carried out. This was accomplished by giving the beam a known static deflection of shape equivalent to the fundamental mode, and by then releasing the beam and allowing it to vibrate freely.

Beam-Vibration Analysis With the Electric-Analog Computer

By G. D. McCANN,[1] AND R. H. MacNEAL,[2] PASADENA, CALIF.

The authors have developed a true dynamic analogy which has been used with the Cal Tech electric-analog computer for the rapid and accurate solution of both steady-state and transient beam problems. This analogy has been found well suited to the study of beams having several coupled degrees of freedom, including torsion, simple bending, and bending in a plane. Damping and effects such as rotary inertia may be handled readily. The analogy may also be used in the study of systems involving combined beams and "lumped-constant" elements.

Introduction

SEVERAL electrical analogies have been developed in the past several years for the elastic structures (1, 2).[3] Attempts have been made to use these analogies for the solution of vibrating-beam problems at several computing laboratories. Certain difficulties were encountered which led to the belief that the analog method was not suited to the accurate computation of complex beam problems (3). These difficulties arose from two principal sources. One is the fact that the analogies were not truly dynamic but satisfied only the steady-state form of the beam equations at a single frequency obtained by substituting $j\omega$ for the differential operator $\partial/\partial t$. The other difficulty was that sufficiently accurate electrical components were not employed.

A true dynamic analogy has now been developed which overcomes the first disadvantage and which has been used with the Cal Tech electric-analog computer for the rapid and accurate solution of both steady-state and transient beam problems. The basic analogy presented here actually was developed in 1946,[4] but it has been only recently that its application has been studied in detail and extended to a wider range of elastic media. This analogy has been found to be well suited to the study of beams having several coupled degrees of freedom, including torsion, simple bending, and bending in a plane. Damping and other effects, such as rotary inertia, which are not usually considered in a classical analysis, can be handled readily. Accurate solutions can be obtained for beams having rapid variations in cross section, and the analogy lends itself readily to the study of systems involving combined beams and "lumped constant" elements. Also, as will be discussed in a later paper, the basic analogy can be extended to the static and dynamic analyses of plates with nonuniform thickness and all types of boundary conditions.

Differential Equations for Beams

The following is a tabulation of the beam equations for which analogies are derived in this paper. Although different approaches are possible, the electrical analogy for vibrating beams will be developed in this paper from the fourth-order differential equation for bending deflection, and the second-order differential equation for torsion. The equation for uncoupled torsional vibration is

$$\frac{\partial}{\partial x}\left(K\frac{\partial \alpha}{\partial x}\right) = I_\alpha \frac{\partial^2 \alpha}{\partial t^2} \quad \ldots\ldots [1]$$

where α is the angular displacement, I_α is the moment of inertia per unit length, and K is the torsional rigidity. Both K and I_α may be functions of x.

The equation for uncoupled bending is

$$\frac{\partial^2}{\partial x^2}\left(EI\frac{\partial^2 y}{\partial x^2}\right) + m\frac{\partial^2 y}{\partial t^2} = 0 \quad \ldots\ldots [2]$$

where y is the bending deflection, m is the mass per unit length, E is Young's modulus, and I is the areal moment of inertia with respect to the neutral plane.

If the bending and torsional oscillations are coupled through an unsymmetric load distribution, Equations [1] and [2] become, for the coupled motion

$$\frac{\partial^2}{\partial x^2}\left(EI\frac{\partial^2 y}{\partial x^2}\right) + m\frac{\partial^2 y}{\partial t^2} \pm S_\alpha \frac{\partial^2 \alpha}{\partial t^2} = 0 \quad \ldots\ldots [3]$$

$$-\frac{\partial}{\partial x}\left(K\frac{\partial \alpha}{\partial x}\right) \pm S_\alpha \frac{\partial^2 y}{\partial t^2} + I_\alpha \frac{\partial^2 \alpha}{\partial t^2} = 0 \quad \ldots\ldots [4]$$

where S_α is the first moment per unit length. The choice of sign depends upon the choice of the positive sense of rotation.

If bending deflections in two perpendicular directions are considered, an additional equation is introduced, as well as coupling between the two bending modes through the product of inertia, I_{yz}. The following equations are valid only if α is small

$$\frac{\partial^2}{\partial x^2}\left(EI_z\frac{\partial^2 y}{\partial x^2} + EI_{yz}\frac{\partial^2 z}{\partial x^2}\right) + m\frac{\partial^2 y}{\partial t^2} \pm S_{\alpha y}\frac{\partial^2 \alpha}{\partial t^2} = 0 \quad \ldots [5]$$

$$\frac{\partial^2}{\partial x^2}\left(EI_y\frac{\partial^2 z}{\partial x^2} + EI_{yz}\frac{\partial^2 y}{\partial x^2}\right) + m\frac{\partial^2 z}{\partial t^2} \pm S_{\alpha z}\frac{\partial^2 \alpha}{\partial t^2} = 0 \quad \ldots [6]$$

$$-\frac{\partial}{\partial x}\left(K\frac{\partial \alpha}{\partial x}\right) \pm S_{\alpha y}\frac{\partial^2 y}{\partial t^2} \pm S_{\alpha z}\frac{\partial^2 z}{\partial t^2} + I_\alpha \frac{\partial^2 \alpha}{\partial t^2} = 0 \quad \ldots [7]$$

Besides these principal types of vibration, certain other effects can be included in the electrical analogy. In Equation [2] the effect of rotary inertia has been omitted. Usually this effect is negligible, but it may happen that the beam has a large inertia such as a flywheel attached to it. In this case the differential equation for bending is

---

[1] Professor of Electrical Engineering, California Institute of Technology. Mem. ASME.

[2] Student Graduate, California Institute of Technology.

[3] Numbers in parentheses refer to the Bibliography at the end of the paper.

[4] The basic dynamic analogy for a beam in bending, was developed by H. E. Criner and G. D. McCann in 1946, while both were with Westinghouse Electric Corporation.

Contributed by the Applied Mechanics Division and presented at the Semi-Annual Meeting, San Francisco, Calif., June 27–July 1, 1949, of THE AMERICAN SOCIETY OF MECHANICAL ENGINEERS.

Discussion of this paper should be addressed to the Secretary, ASME, 29 West 39th Street, New York, N. Y., and will be accepted until April 10, 1950, for publication at a later date. Discussion received after the closing date will be returned.

NOTE: Statements and opinions advanced in papers are to be understood as individual expressions of their authors and not those of the Society. Paper No. 49—SA-3.

$$\frac{\partial^2}{\partial x^2}\left(EI\frac{\partial^2 y}{\partial x^2}\right) - \frac{\partial}{\partial x}\left(\rho I'\frac{\partial^2 y}{\partial x \partial t^2}\right) + m\frac{\partial^2 y}{\partial t^2} = 0 \quad [8]$$

where ρ is the volumetric mass density and I' includes besides the areal moment of inertia of the shaft I, the areal moment of inertia of parts that do not contribute to the stiffness. Equation [8] is developed in reference (4).

If the beam is subjected to a tension T, the differential equation of bending becomes

$$\frac{\partial^2}{\partial x^2}\left(EI\frac{\partial^2 y}{\partial x^2}\right) - \frac{T}{\rho}\frac{\partial^2 y}{\partial x^2} + m\frac{\partial^2 y}{\partial t^2} = 0 \quad [9]$$

Equation [9] is also developed in reference (4).

No satisfactory simple theory of the internal damping of elastic bodies is known to the authors. An approximation which gives fair agreement with experimental results and yet is simple to represent is obtained by replacing E by $E + c\partial/\partial t$. In this case Equation [2] becomes

$$\frac{\partial^2}{\partial x^2}\left(EI\frac{\partial^2 y}{\partial x^2} + Ic\frac{\partial^3 y}{\partial t \partial x^2}\right) + m\frac{\partial^2 y}{\partial t^2} = 0 \quad [10]$$

where c is an experimental constant. For an account of this and other theories of damping see reference (5).

Derivation of Electrical Analogies

Electrical Circuit for Torsional Vibration. Although previously derived elsewhere the simple torsion analogies will be considered first to simplify the general analysis. In the electrical network, the derivative with respect to a space co-ordinate is replaced by its finite-difference equivalent. If the value of α is known only at discrete points then

$$\frac{\alpha_{n+1} - \alpha_n}{x_{n+1} - x_n} \doteq \left.\frac{\partial \alpha}{\partial x}\right|_{n+1/2} \quad [11]$$

If α is a smoothly varying function and $\Delta x = x_{n+1} - x_n$ is small, this is a good approximation. It is certainly much better than the approximation

$$\frac{\alpha_{n+1} - \alpha_n}{x_{n+1} - x_n} \doteq \left.\frac{\partial \alpha}{\partial x}\right|_{n} \quad [12]$$

Consequently we replace Equation [1] by the following finite difference equation for the nth node; Δx is assumed to be uniform

$$\frac{1}{\Delta x^2}\left[K_{n+1/2}(\alpha_{n+1} - \alpha_n) - K_{n-1/2}(\alpha_n - \alpha_{n-1})\right] = I_{\alpha n}\left.\frac{\partial^2 \alpha}{\partial t^2}\right|_n \quad [13]$$

$K_{n+1/2}$ is the value of K at

$$x = \frac{x_n + x_{n+1}}{2}$$

and $I_{\alpha n}$ is the value of I_α at $x = x_n$. Rearranging Equation [13]

$$\frac{K_{n+1/2}}{\Delta x}(\alpha_{n+1} - \alpha_n) + \frac{K_{n-1/2}}{\Delta x}(\alpha_{n-1} - \alpha_n) = I_{\alpha n}\Delta x \cdot \frac{\partial^2 \alpha_n}{\partial t^2} \quad [14]$$

Equation [14] can be regarded as a statement of Kirchhoff's law for the sum of the currents at the nth node of an electrical network; α_n is the voltage at the nth node (see Fig. 1), and the coefficients of the α's are the admittances of the branches of the network. If each term in Equation [14] is regarded as the time derivative of current, then

$$\frac{\Delta x}{K_{(n+1/2)}}$$

is an inductance and $I_{\alpha n}\,\Delta x$ is a capacitance. This correlation is the same as that in the mass-capacitance analogy between rigid mechanics and electrical networks. What has been done here essentially, has been to replace a continuous mechanical system by a lumped mechanical system, and then to show the existence of an electrical circuit analogous to this lumped system. If Equation [14] is written for the $n+1$st node, the coefficient of $\alpha_n - \alpha_{n+1}$ is the same as the coefficient of $\alpha_{n+1} - \alpha_n$ in Equation [14] for the nth node. This demonstrates that the electrical analogy is bilateral.

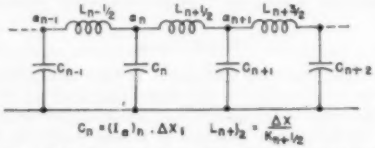

Fig. 1 Equivalent Circuit for Torsional Vibration

Equation [14] can also be regarded as a statement of Kirchhoff's law for the sum of the voltages around the nth loop of an electrical network. In this case α_n is the charge in the nth loop, and the coefficients of the α's are the impedances of the branches of the network. The electrical circuit is identical with that in Fig. 1 where the inductance $L_n = I_{\alpha n}\Delta x$ and the capacitance

$$C_{n+1/2} = \frac{\Delta x}{K_{(n+1/2)}}$$

Electrical analogies for Equation [1] can also be derived in case Δx is not uniform (see Appendix 1). The boundary condition $\alpha = 0$ at $x = x_N$ can be imposed on the circuit in Fig. 1 by shorting the network to ground at $x = x_N$. The boundary condition $(\partial\alpha)/(\partial x) = 0$ at $x = x_{N+1/2}$ is simulated by opening the circuit between the Nth and the $N+1$st nodes. Boundary conditions of the form $(\partial\alpha)/(\partial x) + A\alpha = B$ can be imposed at $x = x_{N+1/2}$.

Electrical Circuit for Uncoupled Bending. Equation [2] applies to the uncoupled bending vibration of a nonuniform beam. If we define the slope

$$\theta = \frac{\partial y}{\partial x} \quad [15]$$

and the shear

$$S = \frac{\partial}{\partial x}\left(EI\frac{\partial \theta}{\partial x}\right) \quad [16]$$

then Equation [2] becomes

$$\frac{\partial}{\partial x}(S) + m\frac{\partial^2 y}{\partial t^2} = 0 \quad [17]$$

It is simpler to write the finite difference equation corresponding to Equations [15], [16], [17] than to write the finite difference equation corresponding to Equation [2]. This method has

the advantage that it immediately reveals the correct form of the electrical network for the solution of transient problems. It also gives simple expressions for the case of unequal lumping. By comparison with Equations [11] and [14], the finite difference equations equivalent to Equations [15], [16], [17] are

$$\theta_{n+1/2} = \frac{y_{n+1} - y_n}{\Delta x} \quad \ldots\ldots\ldots\ldots\ldots\ldots [18]$$

$$\Delta x \cdot S_{n+1/2} =$$

$$(\theta_{n+1/2} - \theta_{n+1/2}) \frac{EI_{n+1}}{\Delta x} + (\theta_{n-1/2} - \theta_{n+1/2}) \frac{EI_n}{\Delta x} \quad \ldots\ldots [19]$$

$$(S_{n+1/2} - S_{n-1/2}) + \Delta x \cdot m_n \frac{\partial^2 y_n}{\partial t^2} = 0 \quad \ldots\ldots [20]$$

If Equations [19] and [20] are to be regarded as statements of Kirchhoff's laws for either current or voltage, S and θ must be quantities of different type (one current, one voltage), and also S and y must be quantities of different type. Consequently, θ and y must be quantities of the same type and Δx in Equation [18] must be a dimensionless ratio in the electrical analogy. The circuit of Fig. 2(*a*), satisfies all three of these equations if θ and y are regarded as voltages. Equation [18] expresses the relationship between the primary and secondary voltages of the transformers where the turns ratio is Δx. Equation [19] is Kirchhoff's law for the sum of the currents entering the node $\theta_{n+1/2}$. The current flowing in the secondary of the transformer is the turns ratio times the current in the primary, i.e., $\Delta x \cdot S_{n+1/2}$. Equation [20] is Kirchhoff's law for the sum of the currents entering the node y_n.

Because of the presence of the second derivative with respect to time in Equation [20], S must be the time derivative of current in the electrical network. By comparison with Equation [14], the network inductance $L_n = (\Delta x)/(EI_n)$, and the network capacitance $C_n = \Delta x \cdot m_n$. The moment

$$M = EI \frac{\partial^2 y}{\partial x^2}$$

is the time derivative of the current flowing in the inductive branches.

The variables θ and y in Equations [18], [19], [20] also can be regarded as circulating electrical charges, and the equations can be regarded as Kirchhoff's laws for the voltages around the loops. The network so obtained is the same and the analogies are shown in Fig. 2(*b*). The shear and moment become the voltages at the nodes. The inductance $L_n = \Delta x \cdot m_n$, while the capacitance $C_n = (\Delta x)/(EI_n)$. In the foregoing analysis we have assumed that Δx is uniform. This assumption is not necessary and the circuit equations for unequal lumping are derived in Appendix 1.

In setting up an actual beam problem, the value of inductance given by $L_n = (\Delta x)/(EI_n)$ may be too large as might also be the case for the capacitors. Also, the turns ratio of the transformers and the unit of time or frequency may be inconvenient. To meet this difficulty arbitrary dimensional scale factors and other constants are introduced into the original equations which are later chosen to give practical values of the electrical components (see Appendix 2). This feature has been eliminated here to simplify the analysis.

Boundary Conditions for Bending Modes. The three principal terminations for a beam are a clamped end, a pinned end, and a free end. The analytical expression of these conditions, together with their electric analog are listed in Fig. 3 for the mass-capacitance analogy alone.

In each case the end of the beam is chosen to coincide with a node of the θ circuit (n = half-integer). The end could as easily have been made to coincide with integral values of n. In the circuit for the clamped end, Fig. 3(*a*), θ should be grounded at $x = 1/2$. And the center tap of the primary of the transformer for cell No. 1/2 should be grounded at $x = 1/2$. Since the secondary is also grounded, y is zero at $x = 1$, and the transformer may be left out. Consequently, in the electrical analogy, the deflection y is always zero at the center of the first section of a cantilever beam. The effect of this approximation will be discussed later.

In the circuit for the free end, Fig. 3(*b*), the current analogous to the shear force S, and the current analogous to the moment M, are both zero at $x = N + 1/2$. By virtue of the first condition, the current in the secondary of the transformer is zero, so that $M_N - M_{N+1} = 0$. Now $M_{N+1/2} = 1/2\,(M_N + M_{N+1}) = 0$ by the second condition. The only way that both of these conditions can be satisfied is to set $M_N = M_{N+1} = 0$.

In the circuit for the pinned end, Fig. 3(*c*), y is zero at $x = 1/2$, and the center tap of the transformer, consequently, is grounded. M is also zero at $x = 1/2$ which means that $M_0 + M_1 = 0$, or that the current in the secondary of the transformer should be twice as great as the current in L_1. But since only one half of the primary winding is used, the same effect can be produced in the primary circuit if the current in the secondary equals M_1, instead of twice M_1. Consequently the θ-circuit to the left of $x = 1/2$ may be omitted. In a similar manner the circuit boundary conditions for the mass-inductance analogy can be determined readily.

Either end of the beam may be part of a lumped mechanical system. This condition also may be imposed easily on the electric network. In fact, the beam (or several beams) may be integrated into a complete mechanical or electromechanical system in any way that is desired.

Equivalent Circuits for Coupled Bending Modes and for Small

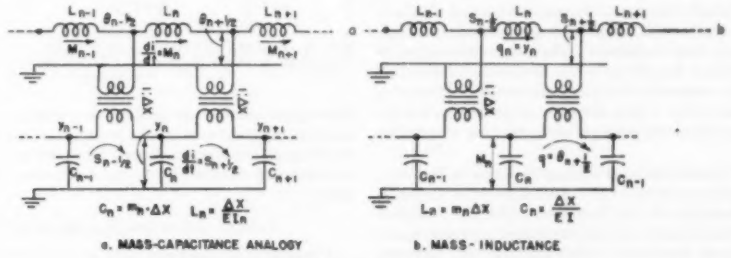

FIG. 2 EQUIVALENT CIRCUITS FOR UNCOUPLED BENDING

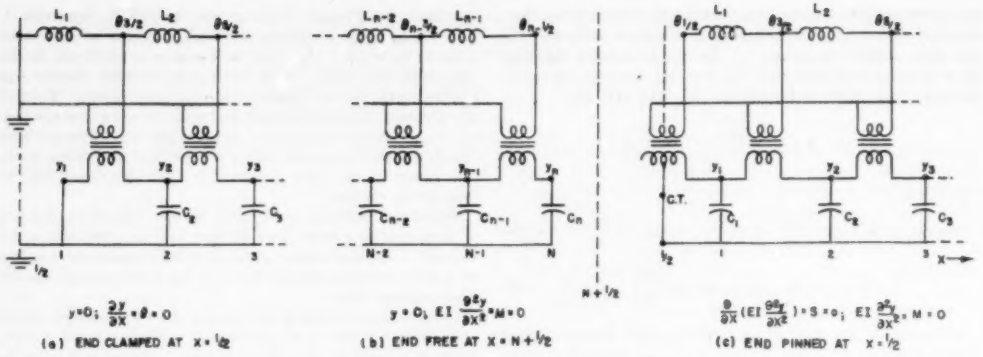

FIG. 3 BOUNDARY CONDITIONS FOR A VIBRATING BEAM

Effects. The equivalent circuit for a beam with coupled bending and torsion is shown in Fig. 13. Coupling between the two modes is by means of capacitors, C_3. The equivalent circuit for this case is derived in Appendix 2. As noted there, S_α in some cases can be negative, requiring a negative capacitor or additional transformer in transient studies. Such electronic elements are available in the CIT computer. However, for steady-state studies, such terms can be represented by inductors.

The equivalent circuit for bending in two dimensions is shown in Fig. 4. The effects of internal damping, rotary inertia, and tension are illustrated also. It will be noted that the circuit is not appreciably complicated by the inclusion of these effects. The circuit derivations are given in Appendix 2.

Static Beam Loading. The foregoing analogies also are applicable to static-beam-loading problems. This will be illustrated with reference to the mass-inductance analogy in Fig. 2(*b*). For this, the shear-loading forces are voltages across the top node points which replace the dynamic forces represented by the inductors *L*. These forces can be simulated by applying alternating-current voltages having a frequency high enough so that the transformers function properly. A single voltage source could be used connected across the points *a b*, Fig. 2(*b*), with a low-impedance divider properly proportioning the voltage along the network. The capacitors also could be replaced by resistors or inductors having the proper impedance at the frequency chosen.

Other Beam Analogies. An analogy involving only capacitors and inductors is shown in Fig. 5(*a*), for the case of uncoupled bending. This network apparently has been used successfully in certain studies of airplane-wing flutter (2). Its chief advantage is that it does not employ transformers, which are rather expensive if sufficiently accurate. Its disadvantage is that it is suitable only for steady-state vibration with the horizontal capacitors depending upon frequency. The authors attempted to determine the natural frequencies of an airplane wing with this network, but were defeated by the continual necessity of varying the horizontal capacitors. This necessity of course makes the capacitor analogy completely unsuited to the solution of transient beam problems.

Kron's double-transmission-line analogy is shown in Fig. 5(*b*). It is discussed fully in reference (1). This network is similar in form to that described in this paper but, like the capacitor analogy, is not a true dynamic one, and the inductances and capacitances depend upon frequency. This network has, however, stimulated the development of digital methods for the solution of

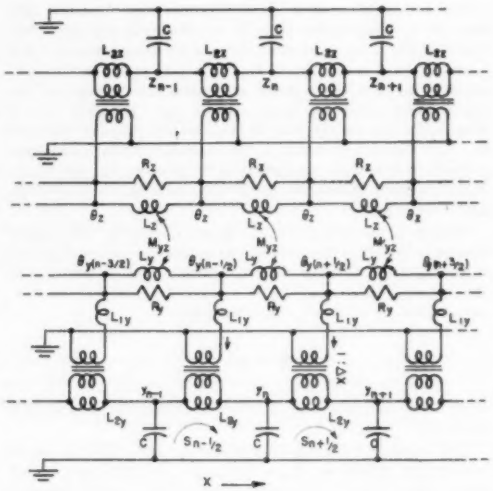

FIG. 4 ELECTRIC NETWORK FOR BENDING IN TWO DIMENSIONS INCLUDING EFFECTS OF INTERNAL DAMPING, ROTARY INERTIA, AND TENSION

beam problems (3). In general, electrical analogies have proved useful in the development of analytical and numerical methods of handling all types of continuous field problems. The relaxation technique of Southwell (6) has its analog in electric-circuit theory (7).

APPLICATION OF THE ELECTRICAL ANALOGIES

A general study has been made of the application of the analogies derived here. The use of such analogies for computer

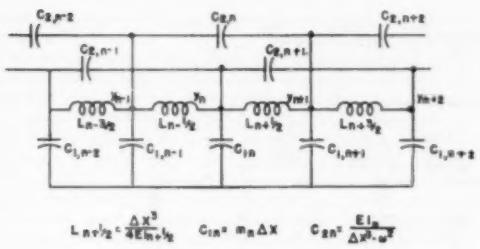

a. CAPACITOR BEAM ANALOGY

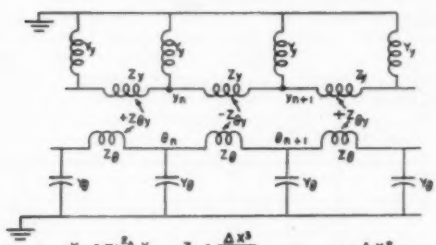

b. KRON'S BEAM ANALOGY

FIG. 5 OTHER ANALOGIES SATISFYING STEADY-STATE EQUATIONS

solutions presents two possible sources of error. One of these is the fact that finite-difference equations are introduced. This is necessary for machine computing methods, and the required number of cells for a specific problem is an important consideration. The second possible source of error lies in the electric-analog components.

In the Cal Tech computer (8), all capacitors and resistors are essentially perfect in the frequency range used. The inductors have "Q's" of 100 or better and thus are representative of low-loss mechanical systems. All elements can be set to better than one per cent of the desired value. Frequency and circuit impedance bases are so chosen that stray capacitance effects are negligible. The only elements with imperfections which need be considered are the transformers. Under certain conditions their leakage impedance may be appreciably high or their magnetizing impedance appreciably low. The transformers are specially designed for a high ratio of magnetizing to leakage impedance as shown by Table 1.

Resonant Modes of a Uniform Cantilever Beam. This type of beam provided a relatively simple and satisfactory method of comparing computer accuracy with theoretical calculations. Consequently a thorough study was made to determine the effect of transformer impedances, number of finite-difference cells, and method of imposing terminal conditions. Also, a comparison was made of the different types of analogies. The uniform cantilever beam is well suited for these tests because it involves two different kinds of boundary conditions, its mode frequencies are well separated, and its analytical solution is readily obtained. This is given by the following equation

$$y = C_3 (\cos k_n x \quad \cosh k_n x) + C_4 (\sin k_n x - \sinh k_n x) \ldots [21]$$

TABLE 1 TRANSFORMER IMPEDANCES AND EFFECT OF TUNING ON ACCURACY OF MODE FREQUENCIES

(a) *Impedances:*
Leakage inductance = 0.025 henries; leakage resistance = 5 ohms
Magnetising inductance range from 55 to 80 henries for range of frequency between 50 and 800 cycles per sec and 1 to 10

(b) *Effect of Tuning Out Transformer Inductances:*

Type of tuning	Mode	Theoretical frequency, cycles per sec	Cross-over freq.[3]	Computer per cent error
None	First	43.75	131	+4.0
Magnetizing[1]	First	43.75	131	+1.2
None	First	21.875	131	+6.0
Magnetizing	First	21.875	131	+2.4
None	Third	767.0	131	−7.7
Leakage[2]	Third	767.0	131	−2.0
None	Second	547.0	262	−2.2
Leakage	Second	547.0	262	+0.4

[1] Tuning capacitors across one winding for 60 henries.
[2] Tuning capacitors in series with one winding for 0.025 henries.
[3] Frequency at which effects of magnetising and leakage cancel each other

where

$$\frac{C_3}{C_4} = -\frac{\sinh k_n l + \sin k_n l}{\cosh k_n l + \cos k_n l} \ldots [22]$$

and k_n is a solution of $(\cos k_n l \cosh k_n l + 1 = 0) \ldots [23]$

The values of $k_n l$ for the first five modes are

n =	1	2	3	4	5
$k_n l$ =	1.875	4.694	7.855	10.996	14.137

The natural frequencies of these modes are proportional to the square of k_n

$$f_n = \frac{k_n^2}{2\pi} \sqrt{\frac{EI}{m}} \ldots [24]$$

In the electrical network, Fig. 2, the resonant frequency is given by

$$f_n = \frac{(k_n l)^2}{2\pi N^2 \sqrt{LC}} \ldots [25]$$

where N is the number of cells.

The capacitor analogy in Fig. 5(a) was first set up and attempts made to determine mode frequencies. It was found that they could not be determined at all accurately. It was necessary to calculate the impedances for a series of assumed values of frequency and attempt to find a resonance condition that indicated a mode. This is a rather tedious process and no sharply defined resonant condition exists which enables determination of the frequencies to within even 10 or 20 per cent. If the frequency is known, however, the circuit gives fairly good mode shapes. It was concluded that this trouble would be encountered with any analogy that is good only for fixed frequencies.

The dynamic analogy derived here was then set up. The complete circuit for eight cells is shown in Fig. 6. The method of imposing the boundary conditions at the clamped and at the free ends has already been discussed. The network was driven by a voltage source connected through a small resistor to the free-end section. The presence of a resonant mode was indicated by a minimum current flowing in the network at the proper frequency. These minima were always very sharp, and resonant frequencies were reproducible to within 0.2 per cent, on consecutive trials.

Results of Steady-State Tests on a Cantilever Beam. The mode-shape data from the steady-state tests are compared with theoretical curves in Fig. 7. The first, second, third, and fifth modes are presented, using analogies with eight, sixteen, and twenty-four cells. Since only relative amplitudes are given by the theoretical curves, one point for each set of data arbitrarily can be

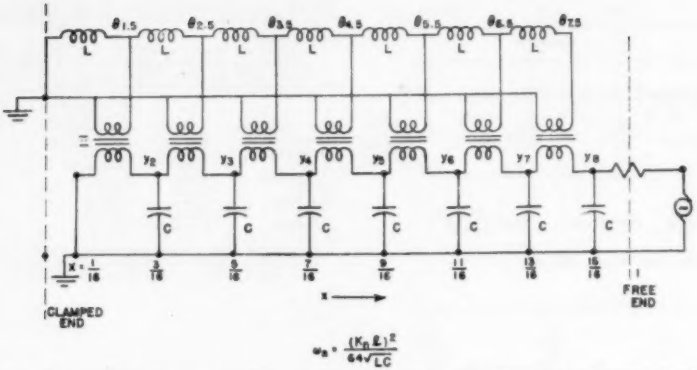

FIG. 6 COMPLETE CIRCUIT FOR STEADY-STATE VIBRATION OF A UNIFORM CANTILEVER BEAM WITH EIGHT CELLS

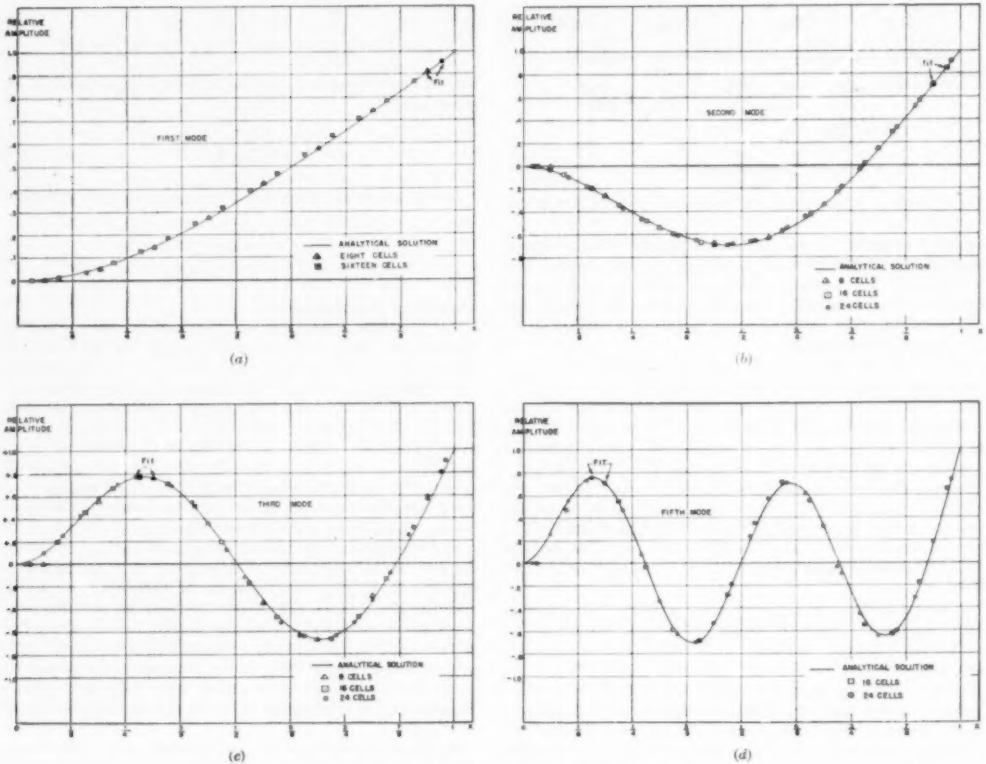

FIG. 7 MODE SHAPES FOR A UNIFORM CANTILEVER BEAM

placed on the curve. The points which are so chosen are indicated in Fig. 7.

In the cantilever-beam analogy, the displacement of the midpoint of the first cell must be zero. It may be seen from the curves that this does not affect seriously the displacement at the second and third cells. An important conclusion which can be drawn from these curves is that, except as just mentioned, cell size has little effect on the accuracy of the mode shapes. Eight cells are sufficient for the first two modes and are nearly sufficient for the third mode. As a consequence, it is possible to represent a uniform beam which, for instance, is part of a larger engineering structure by a small number of cells. This should also be true to a limited extent for nonuniform beams. These conclusions also imply that the boundary conditions have been imposed correctly; for if they were not, marked improvement should have been obtained as the number of cells was increased. The mode-shape data as given by this analogy are much better than those obtained with the capacitor analogy in Fig. 5(*a*).

Effects of Transformer Impedances. In addition to calculating mode shapes, the normal mode frequencies were measured for a large number of combinations of cell size, mode number, and the network components L and C. The difference between the measured frequency and the theoretical frequency given in Equation [25] was calculated. The per cent error is plotted in Fig. 8 as a function of "network" frequency. In this figure it will be noticed that, for a given value of the ratio L/C, the per cent error lies close to a mean curve, so that cell size and mode number have little effect on the error.

The errors are due principally to the leakage and magnetizing inductances of the transformers. The effect of these quantities is studied in Appendix 3. There it is shown that the terms of the differential equation involving magnetizing and leakage impedance have opposite signs. The effects of magnetizing and leakage impedance oppose each other, and the ratio of the two terms is proportional to the square of the frequency. The frequency at which these two effects are equal and opposite is given by

$$f_e = \frac{1}{2\pi}\sqrt{\frac{L}{C}}\sqrt{\frac{I}{L_L L_M}} \qquad [26]$$

where L_L is the leakage inductance and L_M is the magnetizing inductance. As shown in Table 1, the transformers in use with the Cal Tech computer have an $L_L = 0.025$ henry and $L_M \cong 60$ henries.

For $L/C = 10^6$, $f_e = 131$ cycles per sec. The values of f_e for the different ratios L/C are indicated in Fig. 8 along the axis of zero error. The observed errors cross the axis at approximately these points.

The effect of magnetizing and leakage inductances can be eliminated by tuning the transformers. At low frequencies magnetizing impedance is tuned with parallel condensers across the terminals of one winding, and at high frequencies leakage impedance is tuned with condensers in series with one winding. The values of these condensers depend on frequency, but if the resonant frequency is first obtained without them, only a single adjustment has been found to be necessary. In Table 1 the effect of tuning is illustrated for typical cases. The values of tuning capacitors used were the same for all transformers, being calculated from the mean value of leakage and magnetizing impedance. Thus it is seen that the errors in natural frequency plotted in Fig. 8 can be improved considerably, even for extreme values of network frequency, making it possible to guarantee an error in the natural frequency that is in all cases less than $2^1/_2$ per cent. The mode shapes are obtained much more accurately and are not affected appreciably by the error in mode frequency.

For a transient study, where all frequency components are present, it is impossible to tune the transformers; but in this case the accuracy requirements on frequency will usually be less strict.

Response of a Cantilever Beam to an Impulsive Motion of the Base. The transformer beam analogy is suited to the study of transient behavior of beams because the values of the electrical components are not functions of frequency. This is in sharp

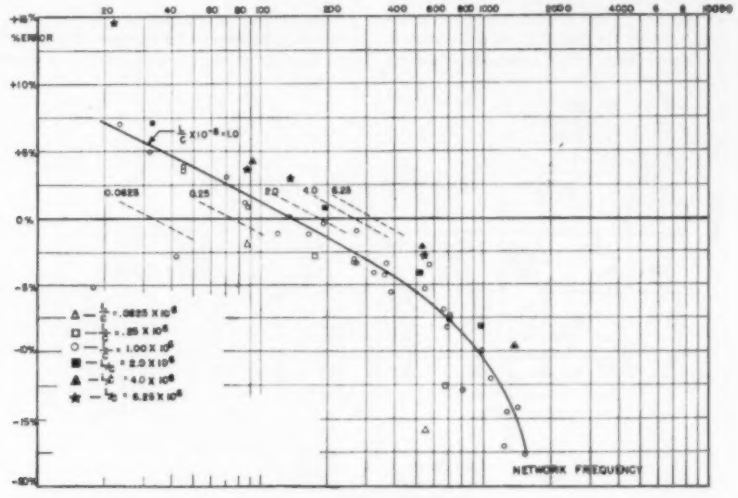

FIG. 8 PER CENT ERROR IN DETERMINATION OF MODE FREQUENCIES OF CANTILEVER BEAM AS A FUNCTION OF NETWORK FREQUENCY AND IMPEDANCE LEVEL

(Points plotted without regard to mode index or number of cells.)

contrast with the other beam analogies mentioned. As an example of transient behavior, the following problem was selected for investigation: A long homogeneous beam has a large mass concentrated at its base. The base may not rotate, but otherwise there are no constraints or supports. The large mass is given an impulse at $t = 0$, so that it moves with nearly constant velocity in direction perpendicular to the axis of the beam. The subsequent motion of points along the beam is required. The mechanical problem and its electrical analogy are illustrated in Fig. 9. This problem was chosen because its analytical solution for the case of of an infinitely large lumped mass is not difficult. In the electrical network, time rate of change of current is the analog of force. Consequently the analog of an impulse is a step current. Closing switch 1 in Fig. 9 allows C_{01} to charge up at a constant rate through R_1. The cyclic repetition process of applying the transient (8) is used so that the solution is displayed as a standing wave on the screen of a cathode-ray oscilloscope. Switches 2, 3, 4, and 5 in Fig. 9 remove the energy from the system while switch 1 is open. For more complex beams a single application would usually be made of the transient forcing function to eliminate a complex switching circuit to remove energy.

Oscillograms showing the response of the system are given in Figs. 10 and 11. In Fig. 10 the solution is given for a beam with a lowest natural frequency of 14.78 cycles per sec. The base has a mass 2.5 times the mass of the beam. From Fig. 10(g) (the solution for $x = {}^{15}/_{16}$), it may be seen that there is no appreciable motion of the end of the beam until the arrival of the initial surge, and that initially the end moves in a direction opposite to the direction of motion of the base.

The electrical solution is compared with an analytical solution for $x = {}^{15}/_{16}$ in Fig. 12. The analytical solution is for a beam whose base has an infinite mass, which accounts for part of the shift between the two curves.

In the oscillograms in Fig. 11 the lowest mode frequency of the cantilever beam has been changed to 43.75 cycles per sec, and the mass of the base is 8.75 times the mass of the beam. Figs. 11(a, b, c) show the deflections $x = {}^{7}/_{16}$, ${}^{11}/_{16}$, and ${}^{15}/_{16}$, respectively. These solutions are similar to those for the corresponding positions of the first beam except that more cycles of oscillation are shown. Figs. 11(d, e, f) show the slope (dy/dx) of the beam at $x = {}^{1}/_{8}$, ${}^{5}/_{8}$, and ${}^{7}/_{8}$, respectively. The importance of higher modes is more evident in these oscillograms than in those of deflection. The second mode, whose frequency is 6.25 times the frequency of the lowest mode, does not appear in Fig. 11(e) for $x = {}^{5}/_{8}$. The reason for this is that at $x = {}^{5}/_{8}$ the slope of the second normal mode is small, see Fig. 7(b).

Moment and shear could have been measured in the network had that been desired. Consequently the stresses in the beam would have been given by the network without the need for computation. This is important because maximum stress is often the desired result in a transient beam study. All of these measurements can be extended without difficulty to the study of nonuniform beams, beams with coupled bending and torsion, and to beams with linear internal damping. In all of these cases numerical calculation is very difficult.

Airplane-Wing Vibration Analysis. An example of one type of practical beam problem which has been solved on the Cal Tech computer is airplane-wing vibration analysis. An illustrative case that was submitted for solution by the El Segundo Engineering Department of the Douglas Aircraft Company is given in Fig. 13. This structure represents a nonuniform beam with coupled bending and torsion, but the nature of the structure was such that the nine cells shown were considered sufficient by the aircraft design engineers for one half of the wing and fuselage.

In Fig. 13 the beam parameters are given in a dimensionless form in terms of the actual electrical parameters set into the computer. The actual dimensional parameters required are given in Appendix 2. It was desired to determine only the first and second torsional and bending-mode frequencies and shapes for both symmetrical and unsymmetrical conditions. The correct boundary conditions are listed in Fig. 13. The unsymmetrical mode case corresponds to pinning the center of the plane in place with no constraint on the slopes at that point. In the symmetric case only the slopes θ and $(\partial\alpha/\partial x)$ are constrained to zero value at the center. As indicated S_{α} is negative for the first two cells, requiring negative capacitors for $C_{2\alpha}$. Since these terms were found to have little effect, it was found simpler to use inductors which were adjusted for the final setting at each mode frequency.

Figs. 14 and 15 present the bending and torsional mode shapes and frequencies for a bending displacement of the wing tip. To show the effect of coupling with the torsional system

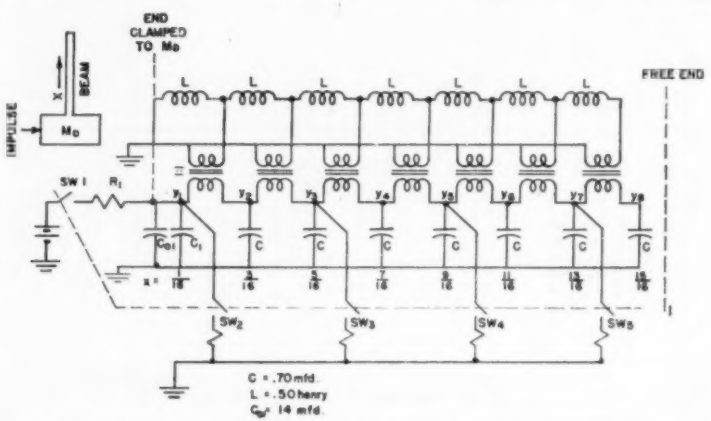

FIG. 9 COMPLETE CIRCUIT FOR TRANSIENT OSCILLATION OF A UNIFORM CANTILEVER BEAM WITH EIGHT CELLS

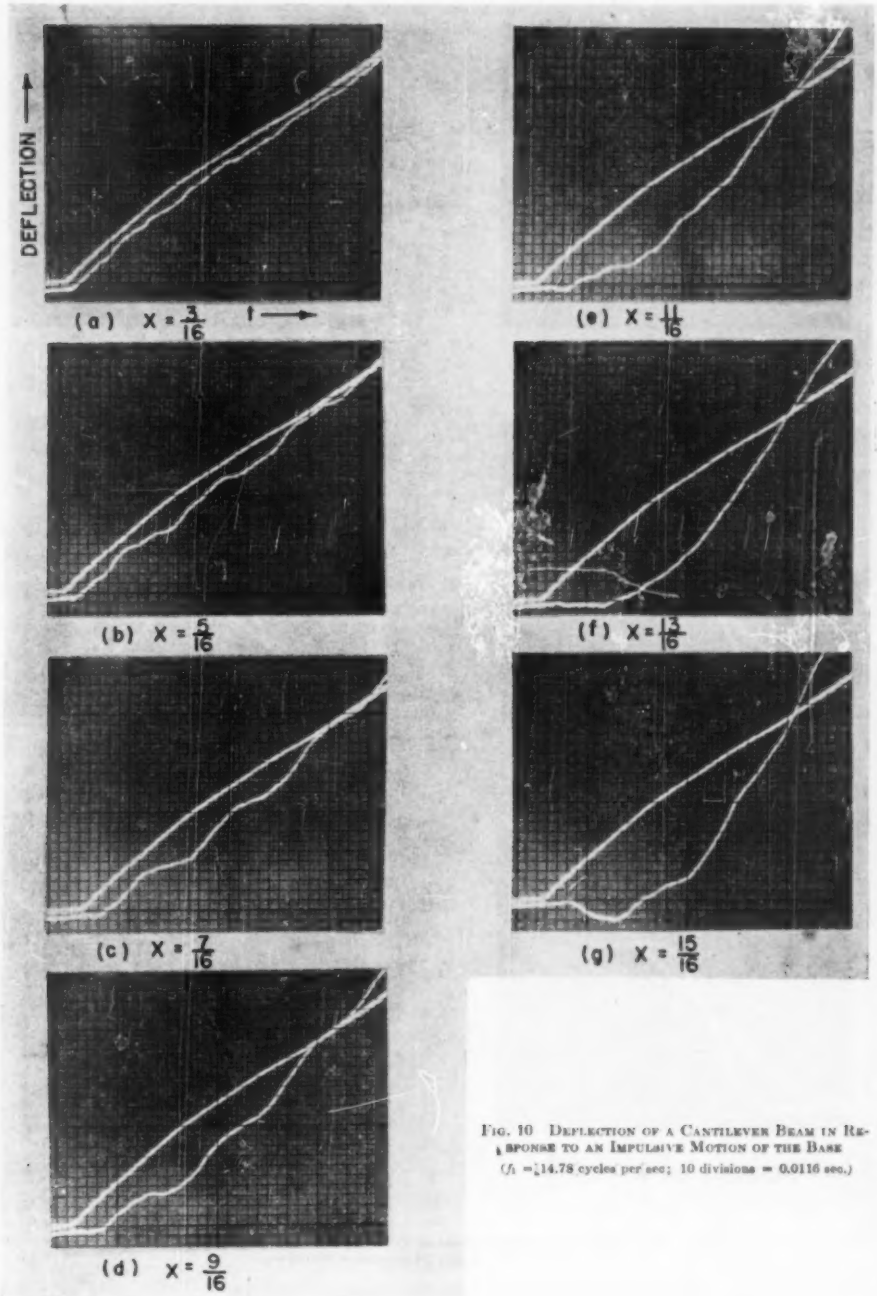

FIG. 10 DEFLECTION OF A CANTILEVER BEAM IN RESPONSE TO AN IMPULSIVE MOTION OF THE BASE
(f_1 = 14.78 cycles per sec; 10 divisions = 0.0116 sec.)

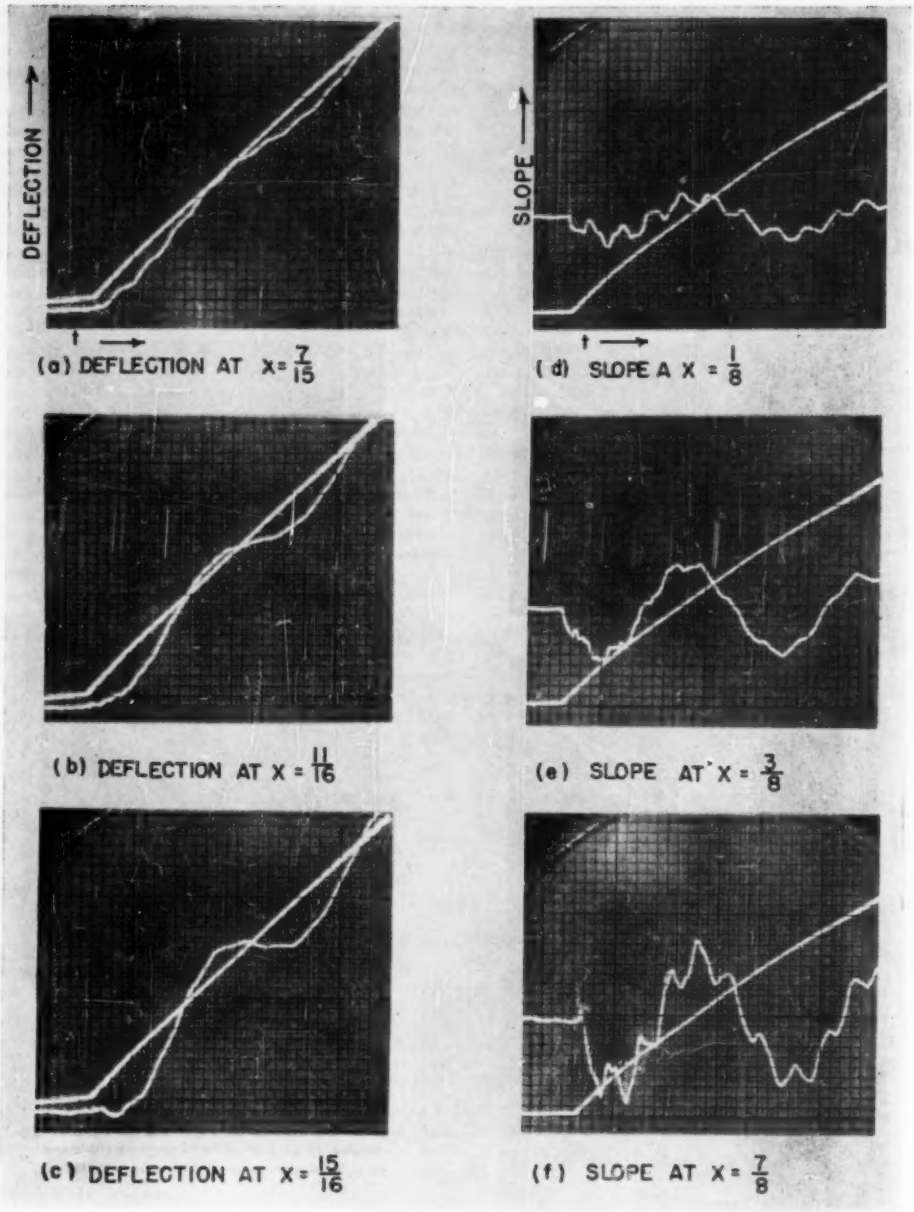
DEFLECTION
(a) DEFLECTION AT X = 7/15
SLOPE
(d) SLOPE A X = 1/8
(b) DEFLECTION AT X = 11/16
(e) SLOPE AT X = 3/8
(c) DEFLECTION AT X = 15/16
(f) SLOPE AT X = 7/8

FIG. 11 RESPONSE OF A CANTILEVER BEAM TO AN IMPULSIVE MOTION OF THE BASE
(f_1 = 43.75 cycles per sec; 10 divisions = 0.0124 sec.)

the bending modes without coupling are plotted also. It is of interest that coupling has little effect except in the case of the second symmetric bending mode, because the frequency for this case is near a resonant frequency of the torsional system.

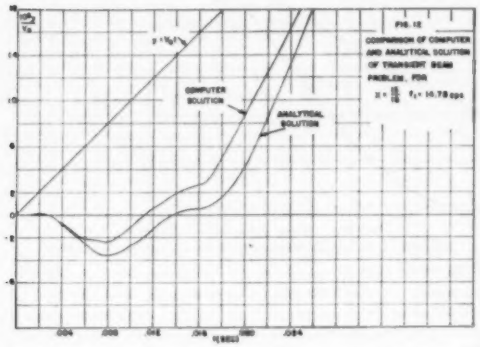

FIG. 12 COMPARISON OF COMPUTER AND ANALYTICAL SOLUTION OF TRANSIENT BEAM PROBLEM FOR $x = \frac{15}{16}$

(f_1 = 14.78 cycles per sec.)

CONCLUSIONS

The general study presented here, together with the problems of this type which have been solved on the Cal Tech computer, has demonstrated that the new beam analogies provide a rapid and accurate method for solving not only static-loading and steady-state dynamic beam-vibration problems, but also transient beam problems. The initial problem and computer set-up time is quite short, and successive solutions can be run off so rapidly that generalized studies also are relatively simple.

BIBLIOGRAPHY

1 "Tensorial Analysis and Equivalent Circuits of Elastic Structures," by G. Kron, *Journal of The Franklin Institute*, vol. 238, December, 1944, p. 400.

2 "The Solution of the Aircraft Wing Flutter Problem by Means of Electric Circuit Analysis," by S. T. Jennings, Ph.D. thesis, The Ohio State University, 1947.

3 "Calculation of the Multiple-Span Critical Speeds of Flexible Shafts by Means of Punched-Card Machines," by A. W. Rankin, JOURNAL OF APPLIED MECHANICS, Trans. ASME, vol. 68, 1946, p. A-117.

4 "Theory of Sound," by Lord Rayleigh, Dover Publications, New York, N. Y., 1945.

5 "Response of Damped Elastic Systems to Transient Disturb-

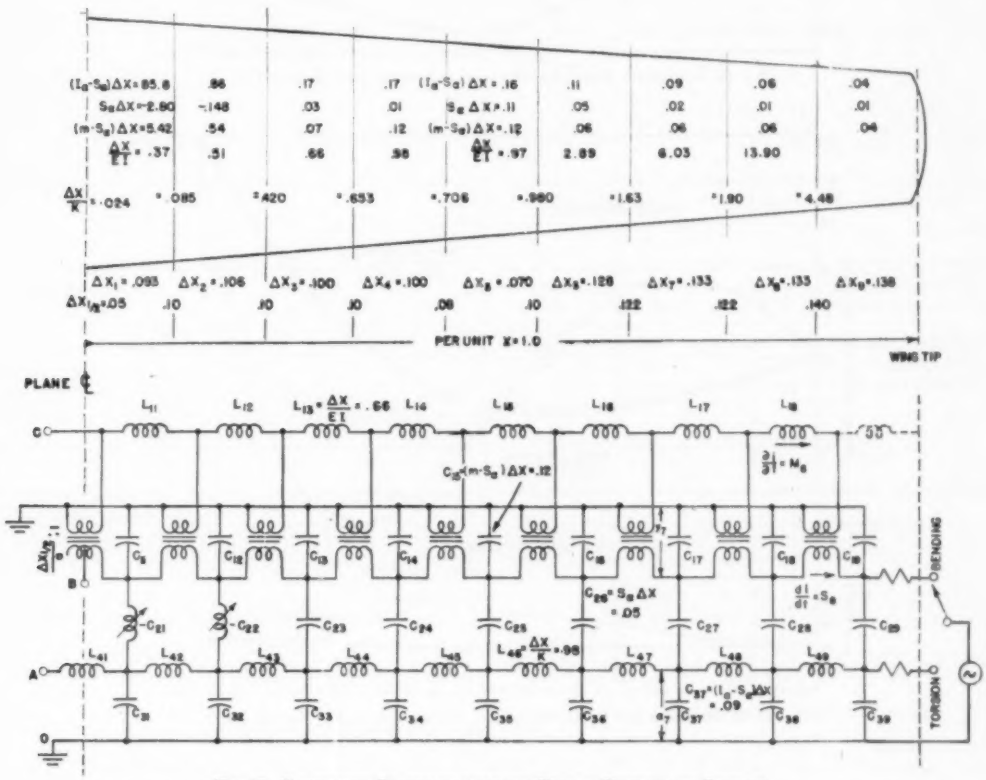

FIG. 13 EQUIVALENT CIRCUIT OF AIRPLANE WING IN TORSION AND BENDING

(Boundary conditions for symmetric modes open A and B, short C to ground. For unsymmetric modes short A and B to ground, open C.)

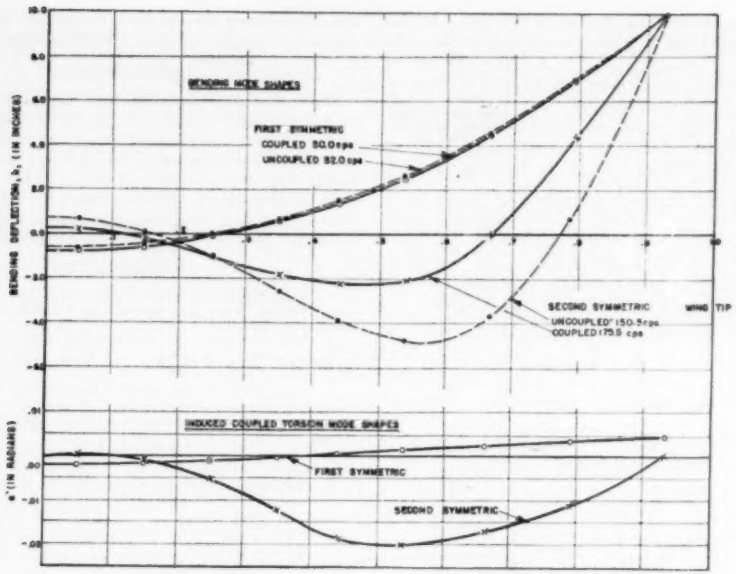

FIG. 14 SYMMETRIC MODE SHAPES AND FREQUENCIES FOR SYSTEM IN FIG. 13

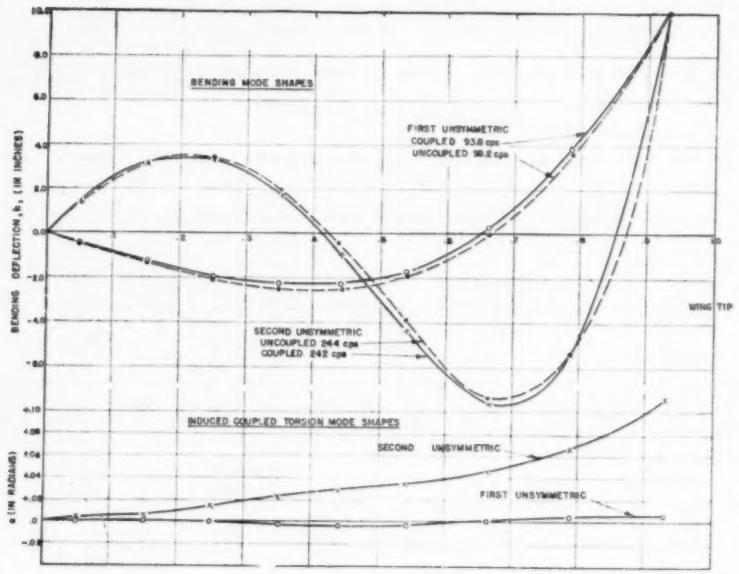

FIG. 15 UNSYMMETRIC MODE SHAPES AND FREQUENCIES FOR SYSTEM IN FIG. 13

ances," by R. D. Mindlin, F. W. Stubner, and H. L. Cooper, Proceedings of the Society for Experimental Stress Analysis, vol. 5, 1948, no. 2.

6 "Relaxation Methods in Theoretical Physics," by R. V. Southwell, Oxford University Press, New York, N. Y., 1946.

7 "Numerical Solution of Ordinary and Partial Differential Equations by Means of Equivalent Circuits," by G. Kron, *Journal of Applied Physics*, vol. 16, 1945, pp. 172–186.

8 "A New Device for the Solution of Transient-Vibration Problems by the Method of Electrical-Mechanical Analogy," by H. E. Criner, G. D. McCann, and C. E. Warren, JOURNAL OF APPLIED MECHANICS, Trans. ASME, vol. 67, 1945, p. A-135.

"Application of Electric-Analog Computers to Heat Transfer and Fluid-Flow Problems," by G. D. McCann and C. H. Wilts. Paper presented at the first Heat Transfer and Fluid Mechanics Institute, Los Angeles, Calif., June 21–23, 1948.

Appendix 1

EQUIVALENT BENDING CIRCUIT FOR UNEQUAL LUMPING

In the text, the equivalent circuit is derived for simple bending with the restriction that Δx remain constant. It is not always convenient to impose this restriction. In the airplane-wing vibration problem, Fig. 13, for instance, the wing was divided into unequal segments, and the constants were calculated for each segment.

Consider the transformation of the space variable

$$\xi = F(x) \quad [27]$$

then

$$\frac{\partial S}{\partial x} = \frac{\partial S}{\partial \xi} \cdot F'(x) \quad [28]$$

and

$$\theta = \frac{\partial y}{\partial x} = \frac{\partial y}{\partial \xi} \cdot F'(x) \quad [29]$$

and also

$$\frac{\partial}{\partial x}\left(EI\frac{\partial \theta}{\partial x}\right) = \frac{\partial}{\partial \xi}\left(EIF'(x)\frac{\partial \theta}{\partial \xi}\right) \cdot F'(x) \quad [30]$$

Substituting these expressions into Equations [15], [16], and [17] gives the following

$$\theta = \frac{\partial y}{\partial \xi} \cdot F'(x) \quad [31]$$

$$\frac{S}{F'(x)} = \frac{\partial}{\partial \xi}\left(EI\,F'(x)\frac{\partial \theta}{\partial \xi}\right) \quad [32]$$

$$\frac{\partial S}{\partial \xi} + \frac{1}{F'(x)} \cdot m\frac{\partial^2 y}{\partial t^2} = 0 \quad [33]$$

The finite-difference expressions equivalent to these equations with $\Delta\xi$ held constant are

$$\theta_{n+1/2} = \frac{y_{n+1} - y_n}{\Delta\xi} \cdot F'(x)_{n+1/2} \quad [34]$$

$$\frac{\Delta\xi \cdot S_{n+1/2}}{F'(x)_{n+1/2}} = (\theta_{n+1/2} - \theta_{n+1/2})\frac{[EIF'(x)]_{n+1}}{\Delta\xi} + (\theta_{n-1/2} - \theta_{n+1/2})\frac{[EIF'(x)]_n}{\Delta\xi} \quad [35]$$

$$S_{n+1/2} - S_{n-1/2} + \frac{\Delta\xi}{F'(x)_n} \cdot m_n\frac{\partial^2 y_n}{\partial t^2} = 0 \quad [36]$$

Define

$$\Delta x_{n+1/2} = \frac{\Delta\xi}{F'(x)_{n+1/2}} \quad \text{and} \quad \Delta x_n = \frac{\Delta\xi}{F'(x)_n} \quad [37]$$

Then, in the foregoing equations, x may be regarded as the independent variable. The physical elements of the network are given by

$$C_n = m \cdot \Delta x_n, \quad L_n = \frac{\Delta x_n}{EI_n}$$

and the transformer turns ratio $T = \Delta x_{n+1/2}$.

A further investigation reveals that the only restrictions on Δx_n and $\Delta x_{n+1/2}$ are that their sums should each separately equal the length of the bar. Hence it is convenient to take Δx_n as the width of the nth cell and $\Delta x_{n+1/2}$ as the distance between the centers of the nth and $n+1$ cells.

Appendix 2

DERIVATION OF ELECTRICAL ANALOGY FOR COUPLED MODES AND FOR SPECIAL EFFECTS

Coupled Bending and Torsion. In Equations [3] and [4] the terms containing S_α represent mutual coupling. Choosing the negative sign and replacing $\partial/(\partial t)$ by $j\omega$ for convenience

$$m\frac{\partial^2 y_n}{\partial t^2} - S_\alpha\frac{\partial^2 \alpha_n}{\partial t^2} = -m\omega^2 y_n + S_\alpha\omega^2\alpha_n = -y_n[\omega^2(m - S_\alpha)] - \omega^2 S_\alpha(y_n - \alpha_n) \quad [38]$$

and similarly

$$-S_\alpha\frac{\partial^2 y_n}{\partial t^2} + I_\alpha\frac{\partial^2 \alpha}{\partial t^2} = -\alpha_n[\omega^2(I_\alpha - S_\alpha)] - \omega^2 S_\alpha(\alpha_n - y_n) \quad [39]$$

Since the admittance of a capacitor is $-\omega^2 C$ (with respect to rate of change of current), we have in Fig. 13

$$C_{1n} = \Delta x\,(m - S_\alpha)_n \quad C_{2n} = \Delta x \cdot S_{\alpha n} \quad C_{3n} = \Delta x(I_\alpha - S_\alpha)_n \quad [40]$$

If both positive and negative values of S_α are present, some C_2 terms must be replaced with inductors for the steady-state case or with the electronic equivalent of a negative capacitor for transient studies.

The use of dimensionless parameters mentioned in the text will be discussed in connection with the equations for coupled bending and torsion. Introduce the following changes into Equations [3] and [4]:

Replace t by $N\bar{t}$ (N = time-base change)
Replace x by $p\bar{x}$ (p = metric-scale change)
Replace α by $\frac{\alpha'}{b}$ (b = dependent variable scale change)
Divide through by a (a = impedance base change)

Then Equations [3] and [4] become

$$\frac{\partial^2}{\partial \bar{x}^2}\left(\frac{EI}{ap^4}\frac{\partial^2 y}{\partial \bar{x}^2}\right) + \frac{m}{aN^2}\frac{\partial^2 y}{\partial \bar{t}^2} - \frac{S_\alpha}{abN^2}\frac{\partial^2 \alpha'}{\partial \bar{t}^2} = 0 \quad [41]$$

$$-\frac{\partial}{\partial \bar{x}}\left(\frac{K}{ab^2p^2}\frac{\partial \alpha'}{\partial \bar{x}}\right) - \frac{S_\alpha}{abN^2}\frac{\partial^2 y}{\partial \bar{t}^2} + \frac{I_\alpha}{ab^2N^2}\frac{\partial^2 \alpha}{\partial \bar{t}^2} = 0 \quad [42]$$

The values of the physical elements in Fig. 13 become

$$C_{1n} = \frac{\Delta\bar{x}}{aN^2}\left(M - \frac{S_\alpha}{b}\right) \quad C_{2n} = \frac{\Delta\bar{x}}{aN^2}\frac{S_\alpha}{b} \quad C_{3n} = \frac{\Delta\bar{x}}{aN^2}\left(\frac{I_\alpha}{b^2} - \frac{S_\alpha}{b}\right)$$

$$L_{1x} = ap^4 \frac{\Delta x}{EI} \qquad L_{2x} = \frac{ab^2p^2\,\Delta x}{K} \qquad T = \Delta x$$

The four factors a, b, p, and N permit these electrical parameters to be chosen in such a way that they fit the range of available physical elements.

Bending in Two Perpendicular Directions. For simple bending, $(EI)/(\Delta x)$ is the admittance between nodes in the slope circuit. For two bending modes we see from Equations [5] and [6] that $(EI_{yz})/(\Delta x)$ represents a mutual admittance between the slope circuits. In terms of mutual impedance as obtained from the determinantal equations

$$Z_y = \frac{\Delta x}{E}\left[I_z - \frac{I_{yz}^2}{I_z}\right]^{-1} \quad \ldots\ldots\ldots\ldots [43]$$

$$Z_z = \frac{\Delta x}{E}\left[I_z - \frac{I_{yz}^2}{I_y}\right]^{-1} \quad \ldots\ldots\ldots\ldots [44]$$

$$Z_{yz} = \frac{\Delta x}{E}\left[I_{yz} - \frac{I_y I_z}{I_{yz}}\right]^{-1} \quad \ldots\ldots\ldots\ldots [45]$$

Effects of Rotary Inertia and Tension. The method we will use here will be to write the circuit equations for the network in Fig. 4, then to replace them by the equivalent expressions for a continuous system (differential equations); then to identify the circuit elements by reference to the equations of a beam.

In Fig. 4 the arrows indicate the direction of assumed current flow. Summing the currents at node y_n, we obtain

$$S_{n+1/2} - S_{n-1/2} = C\omega^2 y \quad \ldots\ldots\ldots\ldots [46]$$

The voltage in the slope circuit is given by

$$\theta_{n+1/2} = \frac{y_{n+1} - y_n}{\Delta x} + L_{1y} \cdot \Delta x \left[S_{n+1/2} - (y_n - y_{n+1}) \cdot \frac{1}{L_{2y}}\right] \quad \ldots\ldots\ldots\ldots [47]$$

or, ignoring $(y_n - y_{n+1})/L_{2y}$ compared with $S_{n+1/2}$

$$\theta_{n+1/2} = \frac{y_{n+1} - y_n}{\Delta x} + L_{1y} \cdot \Delta x \cdot S_{n+1/2} \quad \ldots\ldots [48]$$

Sum the currents at the node $\theta_{n+1/2}$

$$\frac{1}{L_y}(\theta_{n+1/2} - 2\theta_{n+1/2} + \theta_{n-1/2}) = \Delta x\left[S_{n+1/2} - (y_n - y_{n+1})\frac{1}{L_{2y}}\right] \quad \ldots\ldots [49]$$

In these equations, replacing the difference expressions by the corresponding differential expressions, we have

$$\frac{\partial S}{\partial x} = \frac{C\omega^2 y}{\Delta x} = -\frac{C}{\Delta x}\frac{\partial^2 y}{\partial t^2} \quad \ldots\ldots\ldots\ldots [50]$$

$$\theta = \frac{\partial y}{\partial x} + L_{1y} \cdot \Delta x \cdot S \quad \ldots\ldots\ldots\ldots [51]$$

$$\frac{1}{L_y}\frac{\partial^2 \theta}{\partial x^2} = \frac{1}{\Delta x} S + \frac{\partial y}{\partial x} \cdot \frac{1}{L_{2y}} \quad \ldots\ldots\ldots\ldots [52]$$

Differentiate Equation [52]

$$\frac{1}{L_y}\frac{\partial^3 \theta}{\partial x^3} = \frac{1}{\Delta x}\frac{\partial S}{\partial x} + \frac{\partial^2 y}{\partial x^2} \cdot \frac{1}{L_{2y}} \quad \ldots\ldots\ldots\ldots [53]$$

Substitute for θ from Equation [51]

$$\frac{1}{L_y}\frac{\partial^4 y}{\partial x^4} + \frac{L_{1y}}{L_y}\Delta x \cdot \frac{\partial^2 S}{\partial x^2} = \frac{1}{\Delta x}\frac{\partial S}{\partial x} + \frac{\partial^2 y}{\partial x^2} \cdot \frac{1}{L_{2y}} \quad \ldots\ldots [54]$$

Substitute for $(\partial S)/(\partial x)$ from Equation [50]

$$\frac{1}{L_y}\frac{\partial^4 y}{\partial x^4} - \frac{L_{1y}C}{L_y}\frac{\partial^4 y}{\partial x^2 \partial t^2} + \frac{C}{\Delta x^2}\frac{\partial^2 y}{\partial t^2} - \frac{\partial^2 y}{\partial x^2}\frac{1}{L_{2y}} = 0 \quad \ldots [55]$$

If we let

$$C = m\,\Delta x \qquad L_{2y} = \Delta x \cdot \frac{\rho}{T}$$

$$L_y = \frac{\Delta x}{EI} \qquad L_{1y} = \frac{\rho I'}{EIm\,\Delta x}$$

we see that Equation [55] is equivalent to Equations [8] and [9]. Thus the effects of rotary inertia and tension can be included in the network analogy of a vibrating beam.

Internal Damping. For simple bending $(EI)/(\Delta x)$ is the admittance between nodes in the slope circuit. For internal damping, we see from Equation [10] that

$$\frac{Ic}{\Delta x} \cdot \frac{\partial}{\partial t}$$

represents an additional admittance (to rate of change of current) caused by the internal damping. Consequently in Fig. 4

$$R_y = \frac{\Delta x}{I_y \cdot c} \quad \text{and} \quad R_z = \frac{\Delta x}{I_z \cdot c}$$

Appendix 3

Effect of Leakage and Magnetizing Impedances. In a physical transformer there is leakage reactance which may be represented as a small inductance in series with one of the terminals. The magnetizing impedance may be represented by a large coil in shunt with either the primary or secondary terminals. In Fig. 4, L_{2y} may be regarded as the magnetizing impedance referred to the primary terminals, and L_{1y} as the leakage impedance referred to the secondary terminals. If $(\partial^2)/(\partial t^2)$ is replaced by $-\omega^2$ in Equation [55] of Appendix 2, there results

$$\frac{1}{L_y}\frac{\partial^4 y}{\partial x^4} + \frac{C}{\Delta x^2}\frac{\partial^2 y}{\partial t^2} + \frac{\partial^2 y}{\partial x^2}\left[\frac{\omega^2 L_{1y} C}{L_y} - \frac{1}{L_{2y}}\right] = 0 \quad \ldots [56]$$

The term involving leakage and magnetizing inductance will vanish if

$$\omega = \sqrt{\frac{L_y}{C}}\sqrt{\frac{1}{L_{1y}L_{2y}}} \quad \ldots\ldots\ldots\ldots [57]$$

The Behavior of Long Beams Under Impact Loading

By P. E. DUWEZ,[1] D. S. CLARK,[2] AND H. F. BOHNENBLUST,[3] PASADENA, CALIF.

This paper presents the results of a theoretical and experimental investigation of the plastic deformation of long beams which are subjected to a concentrated transverse impact of constant velocity. In the theoretical analysis, the beam is supposed to be of infinite length, and plane cross sections are assumed to remain plane. The bending moment is assumed to depend on the curvature according to a function that is obtained from the stress-strain curve of the material. The theory neglects both the lateral displacement of the cross sections against each other due to the shearing force and the rotary kinetic energy of the motion of the beam. The theory shows that a strain is not propagated along a beam at constant velocity, as in the case of longitudinal impact. The strain depends on the ratio between the square of the distance from the point of impact and the time. This is correct regardless of the shape of the moment - curvature curve. If certain approximations are applied to the bending moment - curvature curve, the theory provides a method of computing the deflection curve of a beam at any instant during impact. An experimental study has been made in which the deflection curves of long simply supported beams have been obtained during impact. The deflection characteristics of a cold-rolled steel and an annealed-copper beam have been computed by approximating the bending moment - curvature curves. It is shown that for materials such as cold-rolled low-carbon steel, for which plastic deflection is localized at the point of impact, the observed deflection curve is closely approximated by computing a curve based on the assumption that the beam remains elastic. For a soft material like annealed copper, plastic deformation extends over a relatively large distance from the point of impact and, taking plastic deformation into account, a satisfactory agreement is obtained between theory and experimental results.

Introduction

THE theory of the elastic deformation of a beam subjected to a transverse impact was developed by Boussinesq[4] and others several decades ago. This theory will now be extended to the case of plastic deformation. The success of this extension depends on the fact that Boussinesq's solution gives a clue to the form of the solution for the plastic case. Boussinesq's theory is not an exact study of the three-dimensional stress-strain distribution in the beam, but it is based on the simplified equations commonly used in this type of problem. The present theory uses the same simplifications, but the linear equation between bending moment and curvature is replaced by a more general relation.

Experiments have been conducted for the purpose of verifying the theoretical developments. The dimensions of the beams and the experimental conditions were chosen in order to be as close as possible to the hypotheses used in the theory. Since the theory was developed for infinitely long beams, it was necessary to test beams for which the ratio of length to depth was very large. The tests were made in such a way that the impact velocity remained essentially constant for a predetermined period of deflection referred to as the duration of impact. This period was made sufficiently small for only the central portion of the beam to be influenced by the impact. In this way the effect of the supports was reduced as much as possible.

In the theoretical analysis, approximations to the true bending moment - curvature curve were studied. Tests have been made with two metals in order to illustrate both approximations. The bending moment - curvature curve of cold-rolled low-carbon steel may be approximated by an extended elastic line terminating in a horizontal line in the plastic region. This is one of the approximations made in the theory. The other approximation to the moment - curvature curve, which consists of an elastic line terminating in a straight line with an upward slope, may be used for copper.

In order to study separately the influence of the impact velocity and the duration of impact on the deflection characteristics, two series of experiments were made on beams for each of the two materials. One series of tests were made with an impact velocity of 100 fps with the duration of impact ranging from 0.5 to 5 millisec. In another series of tests, the duration of impact was held constant at 1.25 or 3.34 millisec, and the impact velocity was varied from 25 to 150 fps.

The investigations presented in this paper were conducted in 1943, at the California Institute of Technology, under a contract with the National Defense Research Committee of the Office of Scientific Research and Development. The portion of this paper concerned with theoretical developments is the work of H. F. Bohnenblust.

Theoretical Considerations

The Equation of Motion. The differential equation for the elastic motion of a beam is obtained from the equilibrium conditions

$$Q = \frac{\partial M}{\partial x} \quad [1]$$

$$\frac{\partial Q}{\partial x} + \rho A \frac{\partial^2 y}{\partial t^2} = 0 \quad [2]$$

In these equations x is the distance along the beam, y the deflec-

[1] Associate Professor of Mechanical Engineering, California Institute of Technology.

[2] Associate Professor of Mechanical Engineering, California Institute of Technology. Mem. ASME.

[3] Professor of Mathematics, California Institute of Technology.

[4] "Application des Potentiels," by J. Boussinesq, Paris, 1855.

Contributed by the Applied Mechanics Division and presented at the Semi-Annual Meeting, San Francisco, Calif., June 27–30, 1949, of THE AMERICAN SOCIETY OF MECHANICAL ENGINEERS; this paper was presented also at the Seventh International Congress of Applied Mechanics, London, England, September 5–10, 1948.

Discussion of this paper should be addressed to the Secretary, ASME, 29 West 39th Street, New York, N. Y., and will be accepted until April 10, 1950, for publication at a later date. Discussion received after the closing date will be returned.

NOTE: Statements and opinions advanced in papers are to be understood as individual expressions of their authors and not those of the Society. Paper No. 49—SA-1.

tion, ρ the mass per unit volume, A the cross-sectional area, M the bending moment, and Q the shearing force. The bending moment M is assumed to be a function of the curvature k only

$$k = \frac{\partial^2 y}{\partial x^2}$$

As Nadai[5] has shown, the bending moment can be computed from the stress-strain relations in tension and in compression, provided suitable assumptions are made. The first part of the bending moment - curvature curve corresponds to the elastic bending and is a straight line given by

$$M = E I k \quad [3]$$

in which E is Young's modulus and I is the moment of inertia of the cross section of the beam.

Boussinesq gave the solution of the problem for small values of the velocity of impact V_1, for which the deformation of the beam is elastic. His results show that the ratio y/t is a function of x^2/t alone. This fact remains true even when the deformation of the beam is plastic. To verify this statement, which is assumed to be true, the equations are integrated and the solution is shown to satisfy the boundary and initial conditions of the problem.

It is convenient to replace x by the new variable

$$\eta = \frac{1}{4a^2} \frac{x^2}{t} \quad [4]$$

where

$$a^2 = \sqrt{\frac{EI}{\rho A}}$$

Taking $y = tf(\eta)$ then

$$k = \frac{1}{2a^2} [f' + 2\eta f'']$$

$$\frac{\partial^2 y}{\partial t^2} = \frac{\eta^2}{t} f'' \quad [5]$$

The curvature is a function of η alone, and the same is true for the bending moment M, since M is a function of k. The shearing force is given by

$$Q = \frac{1}{a\sqrt{t}} \sqrt{\eta} \frac{dM}{d\eta} \quad [6]$$

and, in order to deal with functions of η alone, the quantity

$$S = \frac{2a^2}{EI} \sqrt{t}\, Q = \frac{2a^2}{EI} \sqrt{\eta} \frac{dM}{d\eta} \quad [7]$$

is introduced. Equation [2] becomes

$$S' + \eta^{1/2}(2a^2 k - f') = 0 \quad [8]$$

By differentiation and Equations [5] and [7], it follows that

$$S'' + EIS \frac{dk}{dM} = 0 \quad [9]$$

Any solution S of Equation [9] for which $S'(0) = 0$ is a solution of Equation [8] and gives the shear distribution for an impact of a certain velocity. Every other quantity can be expressed in terms of S by integrations. The upper limit of the integrals is infinite, since for $x = \infty$, the bending moment, the curvature, the slope, and the deflection are equal to zero. Therefore

$$M = -\frac{EI}{2a^2} \int_\eta^\infty \frac{S(\eta)}{\sqrt{\eta}}\, d\eta \quad [10]$$

$$Q = \frac{EI}{2a^2} \frac{1}{\sqrt{t}} S(\eta) \quad [11]$$

$$k = \frac{1}{2a^2} \int_\eta^\infty \frac{S''(\eta)}{\sqrt{\eta}}\, d\eta \quad [12]$$

$$y = -\frac{t}{2} \int_\eta^\infty \frac{S'(\eta)}{\sqrt{\eta}}\, d\eta + \frac{t}{2} \eta \int_\eta^\infty \frac{S'(\eta)}{\eta^{3/2}}\, d\eta \quad [13]$$

Equation [13], evaluated at $\eta = 0$, shows that the velocity at $x = 0$ for all t is a constant, say, V_1, and

$$V_1 = -\frac{1}{2} \int_0^\infty \frac{S'(\eta)}{\sqrt{\eta}}\, d\eta \quad [14]$$

Finally, $(\partial y)/(\partial x)$ at $x = 0$ is equal to zero for all t and $y = y' = 0$ for $t = 0$ and any $x > 0$. All initial conditions are satisfied and the assumption that y is of the form

$$y = tf(\eta) = tf\left(\frac{x^2}{t}\right)$$

is justified. As a consequence, two deflection curves for the same impact velocity but at different times, become identical when y is divided by t, and x is divided by $\sqrt{t}$. In particular, the point x_0 at which $y = 0$ is proportional to $\sqrt{t}$.

The force $P = P(t)$ necessary to produce the impact is twice the shear Q evaluated at $\eta = 0$

$$P = \frac{EI}{a^2} S(0) \frac{1}{\sqrt{t}} \quad [15]$$

The force P is seen to be inversely proportional to the square root of t. The energy W is therefore proportional to this square root, or

$$W = 2 \frac{EI}{a^2} V_1 S(0) \sqrt{t} \quad [16]$$

The Case of an Elastic Beam. The general theory given in the preceding section includes the case of an elastic beam under impact. Equation [9] takes the simple form

$$S'' = S = 0$$

and Equation [14] gives the solution

$$S = 2 \sqrt{\frac{2}{\pi}}\, V_1 \cos \eta \quad [17]$$

Equation [12] shows that the maximum curvature is attained at $x = 0$; it is given by

$$k(0) = V_1 \sqrt{\frac{A}{EI}} \quad [18]$$

The limiting velocity of impact which does not produce a plastic deformation is obtained by equating $k(0)$ to the elastic curvature k_e. This gives

$$V_e = k_e \sqrt{\frac{EI}{A}} \quad [19]$$

Under a concentrated impact the beam is deformed in the shape of a wavy curve, the waves traveling away from the point of impact. At each of its points the beam is successively concave and convex. By evaluating the integrals in Equation [13], it is

[5] "Plasticity," by A. Nadai, McGraw-Hill Book Company, Inc., New York, N. Y., 1931, p. 165.

seen that x_0, i.e., the first value of x for which $y = 0$, is obtained by the formula

$$x_0 = 2.13 \sqrt[4]{\frac{EI}{A\rho}} \sqrt{t} \quad \ldots\ldots\ldots\ldots\ldots\ldots [20]$$

or

$$x_0 = 2.13 \sqrt[4]{\frac{I}{A}} \sqrt{c_0 t}$$

where $c_0 = \sqrt{E/\rho}$ is the speed of sound in the material.

The Case of the Plastic Beam. The fundamental equation, Equation [9], can be solved only by graphical methods when the bending moment - curvature curve obtained experimentally is not expressed analytically. It is necessary, however, to know the relation between the bending moment and the curvature in the hysteresis region, because reversal of curvature will occur in the plastic part of the bending moment - curvature curve. It may be assumed that, if the curvature decreases after reaching a maximum value k_1, the corresponding value of the moment follows the hysteresis curve indicated in Fig. 1. The hysteresis curve is similar to the moment - curvature curve in the ratio 2:1.

A computation can be carried through in a simple case in which it is assumed that the bending moment - curvature curve consists of two straight lines. The first straight line corresponding to the elastic bending passes through the origin and has a slope equal to EI. The second straight line starts at the elastic limit k_e, M_e, and has a smaller slope. A still simpler case is to suppose that the bending moment is independent of the curvature in the plastic range.

For a bending moment - curvature relation, consisting of two straight lines, the derivative $(dM)/(dk)$ is equal to either EI or IEa^2. Equation [9] shows, then, that S is composed of sections of curves of the form $A\cos(\eta - \eta_1)$ or $A\cos(1/\alpha)(\eta - \eta_1)$. At the points of junction, both S and its derivative S' are continuous. A typical case is illustrated in Fig. 2. In the regions I to IV, S is given by

$$\text{I} \quad S = A\cos\left(\frac{1}{\alpha}\right)\eta \qquad 0 \le \eta \le \eta_0$$

$$\text{II} \quad S = -B\sin(\eta - \eta_1) \qquad \eta_0 \le \eta \le \eta_1$$

$$\text{III} \quad S = -C\sin\left(\frac{1}{\alpha}\right)(\eta - \eta_1) \qquad \eta_1 \le \eta \le \eta_2$$

$$\text{IV} \quad S = D\sin(\eta - \eta_1) \qquad \eta_2 \le \eta$$

The eight unknowns η_0, η_1, η_2, η_3; A, B, C, and D are determined by the five conditions of continuity of S and S' and the following three integral conditions

$$-2\int_{\eta_2}^{\infty} \frac{S}{\sqrt{\eta}}\,d\eta = \int_{\eta_0}^{\eta_1} \frac{S}{\sqrt{\eta}}\,d\eta = 4V_e$$

$$\int_0^{\infty} \frac{S'}{\sqrt{\eta}}\,d\eta = -2V_1$$

The last equation is Equation [14], and the first two are obtained from the following facts:

1 At η_2 the bending moment M equals M_e.

2 The change in M between η_0 and η_1 is equal to $2M_e$. This is true, first, because the curvature decreases as η varies from η_1 to η_0 and thus the bending moment decreases along the hysteresis curve; also because the slope of this hysteresis curve is EI until M has decreased by the amount $2M_e$.

Fig. 3 illustrates these facts by exhibiting the values of k and M for the different values of η. The actual computations proceed as follows:

A pair of values η_2 and η_3 is chosen. From the continuity relations of S and S' the ratios $A:B:C:D$ and the values of η_1 and η_0 are determined. Then, by trial and error, a pair of values, η_2 and η_3 is found for which the first two integral conditions are satisfied. The impact velocity is then computed. This calculation is repeated until the given impact velocity is obtained. It will be noticed that the integrals involved are easily reduced to the Fresnel integrals and their values may be taken from the table of C. M. Sparrow.[6]

As the impact velocity decreases, region III becomes smaller and disappears. Then only two regions need be considered, since II and IV combine into a single region. Finally, region I disappears when the impact velocity is the elastic velocity.

For higher velocities of impact the integral

$$\int_{\eta_2}^{\infty} \frac{S}{\sqrt{\eta}}\,d\eta$$

increases. When its value equals $2V_e$, a new region appears at η_2 similar to the region III between η_1 and η_2. This complication occurs in the computation for the copper beam.

[6] "Table of Integrals," by C. M. Sparrow, Edward Brothers, Ann Arbor, Mich., 1934.

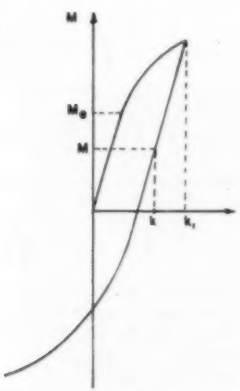

FIG. 1 HYSTERESIS IN BENDING MOMENT - CURVATURE CURVE

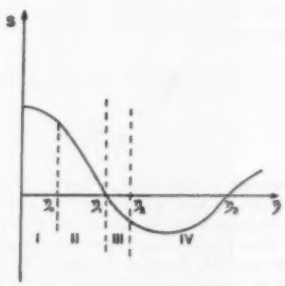

FIG. 2 REPRESENTATION OF FUNCTION $S(\eta)$

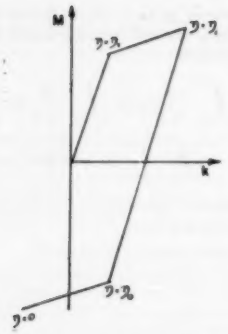

FIG. 3 BENDING MOMENT AND CURVATURE FOR DIFFERENT VALUES OF η_0

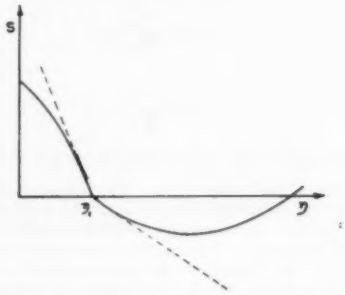

FIG. 4 FUNCTION $S(\eta)$ FOR $V_1 > 2.087\ V_e$

If the second straight line of the bending moment - curvature curve is taken to be horizontal, the value of α is zero and the foregoing computations are greatly simplified. It will be necessary to consider two cases depending upon the magnitude of the impact velocity.

Case 1: $V_e < V_1 < 2.087\ V_e$. This case corresponds to an impact velocity greater than the elastic velocity but small enough to avoid the region III of the preceding section. The fact that $V_1 = 2.087\ V_e$ is the limiting value for this case will be shown presently. Starting from the results of the preceding section, let α tend toward zero. Since $\eta_0 < \alpha(\pi/2)$, the region I will shrink to the point $\eta = 0$. But the derivative S' at $\eta = 0$ tends to a finite limit, different from zero. The function S is then of the form

$$S = -B \sin (\eta - \eta_1)$$

The unknowns η_1 and B are determined from the integral conditions

$$-B \int_0^\infty \frac{\sin (\eta - \eta_0)}{\sqrt{\eta}}\, d\eta = 2V_e \quad \ldots\ldots\ldots [21]$$

$$B \int_0^\infty \frac{\cos (\eta - \eta_0)}{\sqrt{\eta}}\, d\eta = 2V_1 \quad \ldots\ldots\ldots [22]$$

or

$$B = 2\sqrt{\frac{V_1^2 + V_e^2}{\eta}}, \quad \eta_1 = \frac{\pi}{4} + \tan^{-1}\frac{V_e}{V_1} \quad \ldots\ldots [23]$$

The slope $(\partial y)/(\partial x)$ can be computed at $x = 0$ from Equation [13]. As $S'(0)$ no longer vanishes, this slope is different from zero. It is given by

$$\tan\theta = -\left(\frac{\partial y}{\partial x}\right)_{x=0} = \sqrt{\frac{2}{\pi}}\,\frac{1}{a}\,(V_1 - V_e)\sqrt{t}$$

$$= \sqrt{\frac{2k_e}{\pi V_e}}\,(V_1 - V_e)\sqrt{t} \quad \ldots\ldots [24]$$

The appearance of this angle is due to the special bending moment - curvature curve considered; as soon as the moment reaches M_e the material flows and the curvature can increase indefinitely. Case 1 is valid as long as the moment M for $\eta \neq 0$ remains less than M_e in absolute value. The integral representation of M, (Equation [10]) shows that M is an oscillating function of decreasing amplitude. The bending moment M reaches its first and largest extremum at $\eta = \eta_1$. The limiting velocity V_1 for Case 1 is determined from the equation

$$\frac{BEI}{2a^2}\int_{\eta_1}^\infty \frac{\sin(\eta - \eta_1)}{\sqrt{\eta}}\, d\eta = M_e = \frac{EIV_e}{a^2}$$

The coefficient B can be expressed in terms of η_1 and V_e. Substitution of this expression in the last equation gives

$$\sin\eta_1 \frac{1}{\sqrt{2\pi}}\int_0^{\eta_1}\frac{\cos\eta}{\sqrt{\eta}}\, d\eta - \cos\eta_1 \frac{1}{\sqrt{2\pi}}\int_0^{\eta_1}\frac{\sin\eta}{\sqrt{\eta}}\, d\eta$$

$$= \sin\eta_1 - \cos\eta_1$$

for the limiting value of η_1. Its solution is $\eta_1 = 70.6$ deg; and from Equation [23] the corresponding value of the velocity is $V_1 = 2.087\ V_e$.

Case 2: $V_1 > 2.087\ V_e$. For such velocities, region III should appear, but since $\eta - \eta_1 < \epsilon(\pi/2)$ it must shrink to a point when $\alpha = 0$. The influence of this point region is to allow a break in the continuity of S'. The graph of the function S is given in Fig. 4.

$$S = -B \sin (\eta - \eta_1), \quad 0 \leq \eta \leq \eta_1$$

$$S = -D \sin (\eta - \eta_1), \quad \eta_1 \leq \eta$$

The unknowns B, D, and η_1 are given again by the integral conditions

$$2D\int_{\eta_1}^\infty \frac{\sin(\eta - \eta_1)}{\sqrt{\eta}}\, d\eta = -B\int_0^{\eta_1}\frac{\sin(\eta - \eta_1)}{\sqrt{\eta}}\, d\eta = 4V_e \quad \ldots\ldots [25]$$

$$B\int_0^{\eta_1}\frac{\cos(\eta - \eta_1)}{\sqrt{\eta}}\, d\eta + D\int_{\eta_1}^\infty \frac{\cos(\eta - \eta_1)}{\sqrt{\eta}}\, d\eta = 2V_1 \quad \ldots [26]$$

Here also the deflection curve has an angle θ at $x = 0$. Its value is given by

$$\tan\theta = -\left(\frac{\partial y}{\partial x}\right)_{x=0} = \frac{\sqrt{t}}{a}\, B\cos\eta_1 = \sqrt{t}\sqrt{\frac{k_e}{V_e}}\, B\cos\eta_1 \quad \ldots [27]$$

At the point $x_1 = 2a\sqrt{t}\sqrt{\eta_1}$, which corresponds to the value η_1, for η, the slope of the beam is continuous, but the curvature changes suddenly due to the discontinuity of S' at η_1. The change of the curvature is

$$\Delta k = \frac{k_e}{2V_e}\,\frac{1}{\sqrt{\eta}}\,(B - D)$$

The values of η_1 and $\tan\theta/\sqrt{tV_s k_s}$ can be plotted from Equations [25], [26], [27] as functions of V_1/V_s. For large values of impact velocity the approximate expressions obtained are as follows

$$\eta_1 = \frac{3V_s}{V_1} \quad \text{and} \quad \tan\theta = \sqrt{t}\,\sqrt{\frac{k_s}{3}}\,\frac{V_1^{3/2}}{V_s}$$

Experimental Investigation

Testing Procedure. The beam specimens were of rectangular cross section $^3/_8$ in. × $^3/_4$ in., or $^3/_8$ in. × 1 in. and were 10 ft long; they were tested in a position such that the long side of the rectangular cross section was in the plane of the motion of the beam. The ends of the beam were restricted from moving vertically by pins passing horizontally through the beam and resting in slots parallel to the beam, thus permitting horizontal motion and rotation about the pin. In this way the bending moment at the ends of the beam was zero. The impact of desired velocity and duration was applied by means of a $5^3/_4$-lb hammer striking the beam in the center. The length of the contact of the hammer along the beam was $^3/_4$ in. The hammer was accelerated to the desired velocity by means of rubber bands, and the velocity was measured electrically.[7] The duration of the impact was controlled by adjusting the distance D between the top of the test beam and the stopping anvils. The stopping anvils were so arranged that they stopped the motion of the hammer, but permitted the test beam to continue its motion downward due to its inertia after the impact load was released.

The deflection curve at the end of the impact, i.e., at the instant the hammer hit the stopping anvils, was obtained by means of a spark photograph. For this purpose, a "Strobolux" (gas-filled electric discharge tube) was used; it gave a single flash of light of about 30 microsec duration. The tube was fired by the hammer crushing and grounding an insulated wire placed on the stopping anvils. The shutter of a camera equipped with a f:11 lens was opened manually just prior to the test and closed just after the test. The side of the beam toward the camera was painted optical black and a thin white line was painted on the side and adjacent to the top of the beam. A piece of black cardboard with white horizontal and vertical inch scales was placed directly behind the beam. A typical photograph is shown in Fig. 5. In taking the photographic record an exposure was made with the beam in the static position, and then a second exposure was made when the hammer came in contact with the anvils. The photographic negatives were projected at an enlarged scale, and the curves traced for purposes of analysis.

Experiments were made with two different metals, namely, cold-rolled low-carbon steel, and annealed copper. These two metals served for tests of the two types of approximation of the bending moment-curvature curves discussed in the theory. The results of tests on each metal will be considered separately.

Tests on Cold-Rolled Low-Carbon-Steel Beams:

1 *Bending Moment - Curvature Curve.* Tension and compression stress-strain curves were first obtained experimentally for the material studied. The bending moment - curvature curve was then computed by the method of Nadai[8] for a beam $^3/_8$ inch wide and 1 inch deep. The approximate bending moment-curvature curve taken for the computation of the deflection curves under impact consists of two straight lines as indicated in curve 2, Fig. 6. The plastic part of the curve is approximated by a horizontal straight line. The approximate curve is determined

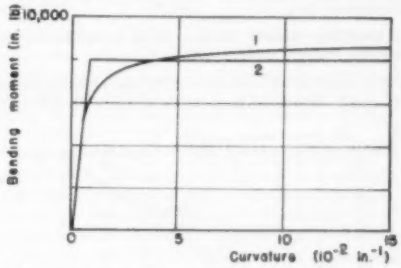

Fig. 6 Bending Moment - Curvature Curve for Cold-Rolled-Steel Beam
(1, Actual curve. 2, Approximate curve.)

by the values of the bending moment and the curvature at the elastic limit, which are 8000 in-lb and 0.853×10^{-2}/in., respectively.

2 *Comparison Between Theoretical and Experimental Deflection Curves.* The theoretical deflection curve based on the approximate bending moment - curvature curve has been computed for an impact velocity of 100 fps and a deflection of 1.04 in. at the point $x = 0$. The duration of impact in this case is 0.87 millisec. The value of the elastic velocity V_s, computed by Equation [19] and using the approximate bending moment-curvature curve, is 40.9 fps. Therefore, in this case, in which the impact velocity is 100 fps, the beam must be deformed plastically. The theoretical deflection curve is plotted, together

[7] "An Experimental Study of the Propagation of Plastic Deformation Under Conditions of Longitudinal Impact," by P. E. Duwez and D. S. Clark, Trans. ASTM, vol. 47, 1947, pp. 502–532.

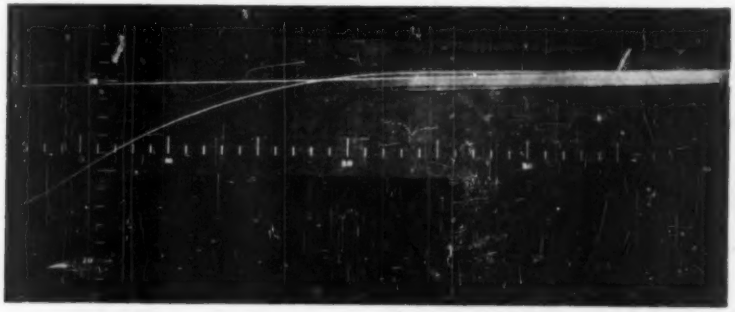

Fig. 5 Typical Photographic Record of Beam-Deflection Curves

FIG. 7 DEFLECTION CURVES FOR COLD-ROLLED-STEEL BEAM
(Impact velocity 100 fps; duration of impact 0.87 millisec. Experimental curve ——, theoretical – – – –, and theoretical assuming elastic beam —·—·)

with one experimental curve in Fig. 7. The angle θ and the distance x_0 from this theoretical curve are compared with the experimental values taken from two different tests made under the same impact conditions in the following table:

	Theoretical	Experimental
Angle θ (per cent)[a]	8.0	7.0 – 7.7
Distance x_0 (in.)	12.6	17.0 –15.8

[a] For simplicity, angle θ which is small, is expressed as a percentage slope, or θ (per cent) = 100 tan θ.

The agreement between the theoretical and experimental angles is fairly good. However, there is an appreciable difference between the theoretical and the experimental values of x_0. Two conditions may account for this: (1) The bending moment-curvature curve taken for the computation is an approximation; (2) the beam is not infinite, as required by the theory; hence the support may have had some influence. In Fig. 7 is plotted a second theoretical deflection curve which was obtained by considering the beam to act elastically. In such a case, the theoretical angle θ at the point of impact is obviously zero, which is not of course in agreement with the experiment. Regardless of this difference, it is interesting to note that the elastic deflection curve is not so far from the experimental deflection curve. The theoretical value of x_0 on the elastic basis (15.2 in.) is even closer to the experimental value than the x_0 computed by considering the beam to behave plastically.

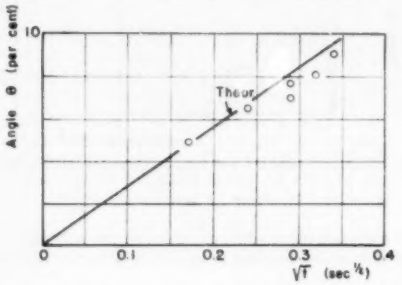

FIG. 8 ANGLE θ VERSUS $\sqrt{t}$ FOR COLD-ROLLED-STEEL BEAMS

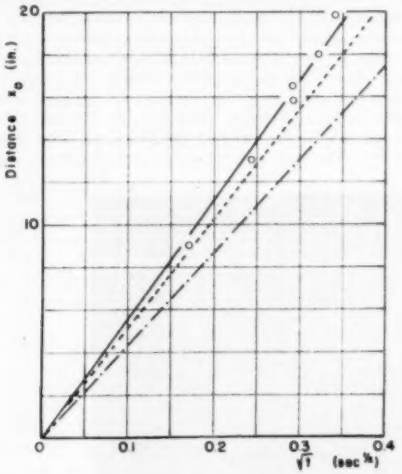

FIG. 9 DISTANCE x_0 VERSUS $\sqrt{t}$ FOR COLD-ROLLED-STEEL BEAMS
(Computed lines assuming the beam elastic – – – –, and plastic —·—·)

3. *Variation of Angle θ and Distance x_0 With Time.* According to the theory, the angle θ at the point of impact and the distance x_0 should be proportional to $\sqrt{t}$. A series of experiments have been made on 10-ft cold-rolled-steel beams with an impact velocity of 100 fps. The values of θ and x_0 are plotted against $\sqrt{t}$ in Figs. 8 and 9. The agreement between experiments and theory is satisfactory. The two dashed lines in the x_0, $\sqrt{t}$ diagram are theoretical. One is computed on the hypothesis that the beam behaves plastically, while the other is computed on the hypothesis that the beam remains elastic indefinitely. Here, as previously shown in comparing the deflection curves, the experimental value of x_0 seems to be in better agreement with the value computed on the basis of elastic behavior of the beam.

It is significant that the experimental points in Figs. 8 and 9 lie on a straight line, which means that the experimental results follow the $\sqrt{t}$ law obtained in the theory. The difference between the slopes of the experimental and the theoretical straight line can be attributed to the approximation made for the bending moment-curvature curve.

4 *Variation of Angle θ With Impact Velocity.* From the theory it is possible to compute θ as a function of V_1, employing the approximate bending moment-curvature curve (given in Fig. 6). The angle θ is zero for impact velocities up to V_e, which in this case is 47.9 fps. From V_e to 2.087 V_e, i.e., between 40.9 and 85.5

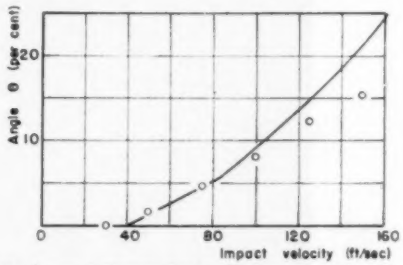

FIG. 10 ANGLE θ VERSUS IMPACT VELOCITY FOR COLD-ROLLED-STEEL BEAM
(Duration of impact 1.22 millisec.)

fps, θ varies linearly with the impact velocity V_1 (Equation [24]). For impact velocities above 2.087 V_y, the function θ is determined by means of graphs, as explained in the theory. The theoretical value of θ as a function of V_1 is given in Fig. 10.

To check these theoretical considerations, a series of experiments has been made with the impact velocity ranging from 25 to 150 fps and the duration of impact about 1.22 millisec. The experimental values of the angle θ are plotted, together with the theoretical curve in Fig. 10. The measurement of the angle θ from the experimental deflection curve is not accurate for impact velocities under 75 fps, because the angle is too small. For 25 fps, the tangent to the deflection curve at the point of impact appeared to be horizontal and the value of θ was taken as zero. For 50 fps, however, there was a measurable angle. The agreement obtained here between the experimental and theoretical relations between θ and V_1 is not as satisfactory as the agreement between experimental and the theoretical relations between θ and t. For impact velocities up to 100 fps, the discrepancy might be due to experimental errors. However, for greater impact velocities it is too large to be ascribed to such an error. On the other hand, for the relatively long durations of impact chosen for these experiments, the discrepancy might well be related to the influence of the supports.

5 *Variation of Distance x_0 With Impact Velocity.* Equation [20] gives the distance x_0 as a function of the dimensions of the beams and the time of impact t, and shows that x_0 is independent of the impact velocity. This formula, however, is valid only for impact velocities smaller than V_y. For higher velocities, the distance x_0 cannot be expressed by a simple analytical formula, but a few computations have shown that the variation of x_0 is negligible within the range of impact velocities used in the experiments.

As shown in the following table, the distance x_0 found experimentally does not seem to have any systematic variation with the impact velocity and can be considered as essentially constant:

Impact velocity V_1, fps	Distance x_0, in.
25	18.5
50	19.0
75	18.0
100	19.0
125	17.5
150	18.0

Tests on Annealed-Copper Beams:

1 *Bending Moment - Curvature Curve.* Tension and compression stress-strain curves were first obtained and the bending moment - curvature curve shown in Fig. 11 was computed.

The bending moment - curvature curve was approximated by two straight lines, as shown in curve 2, Fig. 11. This approximation differs from the one taken for cold-rolled steel in that the straight line in the plastic range of the curve makes an angle with the horizontal axis instead of being horizontal.

2 *Comparison Between Theoretical and Experimental Deflection Curves.* The theoretical deflection curve has been computed for an impact velocity of 97.1 fps, and a deflection of 4 in. at the point $x = 0$. The duration of impact in this case is 3.44 millisec. The curve computed from the theory and the curve obtained from the experiment are plotted in Fig. 12, in which it will be noted that the shapes of the two curves are similar. An upward curvature is observed in the vicinity of the impact, which occurs over an appreciable distance, and the angle θ at $x = 0$ is negligible in contrast with the angle found in the case of cold-rolled steel. In the latter case the angle may be attributed to a very localized curvature. The curvature in the experimental curve is greater than in the theoretical curve, probably as a result of the approximation taken for the bending moment - curvature curve. The value of x_0 computed from the theory is smaller than the observed value (9 in. instead of 14 in.). This difference also may be attributed to the choice of the approximate bending moment - curvature curve and the influence of the supports.

A deflection curve was also computed on the assumption that the beam remains perfectly elastic; this is also given in Fig. 12. In the case of the cold-rolled beams, the elastic deflection curve agrees rather well with the experimental curve, Fig. 7, except for the angle θ at the point of impact. In the case of annealed copper, the elastic deflection curve is not in good agreement with the measured deflection curve. This fact shows that for copper beams the influence of the plasticity cannot be overlooked. Plastic strains are found at some distance from the point of impact, whereas in cold-rolled steel, the plastic deformation was localized in a very small region near the point of impact.

3 *Variation of Distance x_0 With Time.* It has been shown in the theory that, for a given impact velocity, the distance x_0 between the point of impact and the point at which the deflection

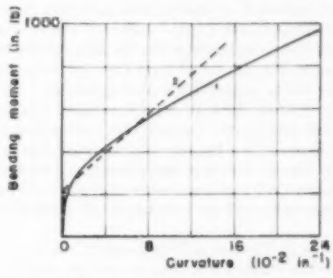

FIG. 11 BENDING MOMENT - CURVATURE CURVE FOR ANNEALED-COPPER BEAM
(Actual curve ——; approximate curve — — — —.)

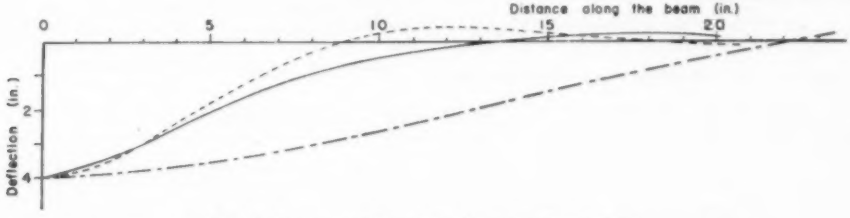

FIG. 12 DEFLECTION CURVES FOR ANNEALED-COPPER BEAM
(Impact velocity 97 fps; duration of impact 3.44 millisec. Experimental curve ——, theoretical — — — —, and theoretical assuming elastic beam — · — ·)

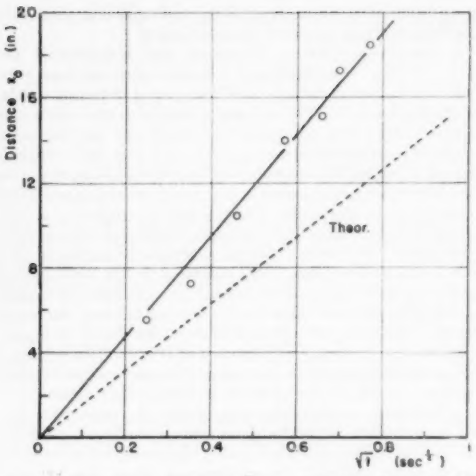

FIG. 13 DISTANCE x_0 VERSUS $\sqrt{t}$ FOR ANNEALED-COPPER BEAM

curve cuts the horizontal axis varies directly with $\sqrt{t}$. This relation is general and independent of the shape of the bending moment - curvature curve. This fact has been verified by a series of experiments made with an impact velocity of 100 fps and different durations of impact.

In Fig. 13 it is shown that x_0 varies linearly with $\sqrt{t}$. The theoretical straight line drawn on the same diagram is far from the experimental points. Another approximation of the bending moment - curvature curve could have given closer agreement. This could be accomplished by taking a straight line in the plastic range of the curve making a larger angle with the horizontal axis. However, for such an approximation, the shape of the theoretical deflection curve, Fig. 12, would have been far from the experimental curve in the region of the point of impact. In fact, the approximate bending moment - curvature curve cannot lead to a theoretical deflection curve that will be in perfect agreement with the experimental curve. In order to accomplish this, it would be necessary to choose different approximations for each of the different portions of the beam, since the different portions of the beam are subjected to curvatures of markedly different values.

4 *Variation of Distance x_0 With Impact Velocity.* Deflection curves have been measured for beams tested at velocities ranging from 25 to 150 fps for which the duration of impact was approximately constant (about 3.34 millisec). The principal result of these tests (see table) is the evidence they provide that the distance x_0 does not present any systematic variation with the impact velocity, and that it can be considered as independent of the velocity of impact.

Impact velocity V_1, fps	Distance x_0, in.
25	12.2
50	12.0
75	13.0
100	13.0
125	13.3
150	13.8

SUMMARY AND CONCLUSIONS

The deflection of a beam subjected to an impact is influenced by the bending due to the bending moment, the displacement due to the shear force, and the tension in the beam produced by the localized deflection. The results of this investigation verify the relations established in a theory based on the bending alone. Therefore it can be concluded that shear and tension are of secondary importance.

The comparison of experimental and theoretical results is based on the deflection curves at the end of the impact. In these curves, the distance along the beam (x_0) at which the deflection curve crosses the horizontal axis was measured, and for cold-rolled low-carbon steel, the angle θ formed at the point of impact was also measured.

The fundamental result of the theory is the fact that the strain is not propagated along the beam at constant velocity, as is the case in a longitudinal impact on a rod. The strain depends here on the ratio x^2/t and therefore the distance x_0 and the angle θ must vary as $\sqrt{t}$ for a given impact velocity. This holds true independently of the shape of the bending moment - curvature curve and was found strictly verified within experimental errors. The computation of the factor of proportionality had to be based on simple approximations to the bending moment - curvature curve, and no perfect agreement can be expected. However, for cold-rolled low-carbon steel and copper beams, the agreement is satisfactory, particularly in the measurement of θ. The discrepancy, especially in x_0, may also be attributed to the influence of the supports. The dependence of x_0 and θ on the impact velocity is also in satisfactory agreement with the theory. The higher the velocity of impact, the more localized is the plastic deformation in the region of the blow. Hence the higher the velocity the less important are the supports.

It should be noted that for cold-rolled low-carbon steel, the deflection curve may be predicted on the basis of elastic behavior outside a neighborhood of the point of impact. This is not the case for copper beams.

ACKNOWLEDGMENTS

The authors wish to acknowledge the assistance of D. S. Wood, who performed a large portion of the laboratory tests, and of J. V. Charyk, who helped in carrying through some of the computations.

The Effect of an Axial Force on the Vibration of Hinged Bars

By S. WOINOWSKY-KRIEGER[1]

It can be shown that the vibration of an extensible bar, carrying no transverse load and having the ends fixed at the supports, causes an axial tensile force with a period equal to the half-period of the vibration of the bar. This force modifies the process of the vibration to a nonlinear one and produces an increase of the frequency of vibration according to the increase of the amplitude.

Nomenclature

The following nomenclature is used in the paper:

l = length of bar
y = instantaneous deflection of any point x, of bar
E = Young's modulus of material
A = cross-sectional area of bar
B = EI = flexural rigidity of bar
r = $\sqrt{I/A}$ = radius of gyration
β = spring constant of supports of bar relative to axial displacement
S_0 = initial axial tensile force of bar
S_1 = axial tensile force due to deflection
q = transverse load per unit length
t = time
ψ = a function of t alone
μ = vibration mass per unit length of bar
a = half amplitude of vibration
α = a/r
ω = frequency in radians per sec
n = positive integers
$P_n = \dfrac{n^2\pi^2 B}{l^2}$ = Euler's load of bar for buckling form with n half waves
$P_0 = -S_0$ = initial compressive load of bar

Vibration of Bars

The usual theory of vibration of the bars is based on the assumption that one end of the bar, being free to move in an axial direction, an extensionless deflection of the bar is obtained. In technical practice we often have to deal with immovable end hinges, or with hinges connected with supports in such a manner that, as the ends approach each other, a tensile force is produced in the bar which is proportional to the amount of that motion. In these cases the effect of the axial force on the process of vibration must be investigated. Further, we assume an initial tensile force and an extensibility of the bar. The deflection of the bar does not need to be small in comparison with its transverse dimensions; however, it must be small enough to represent the curvature of the deflected bar by the approximate expression $\partial^2 y/\partial x^2$.

In the absence of transverse load, the deflection of the vibrating bar, Fig. 1, is defined by the differential equation

$$B\frac{\partial^4 y}{\partial x^4} = -\mu\frac{\partial y^2}{\partial t^2} + (S_0 + S_1)\frac{\partial^2 y}{\partial x^2} \quad \ldots\ldots [1]$$

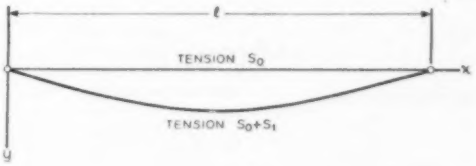

FIG. 1

The value S_0 being given, we will first express the unknown force S_1 through the deflection y. The amount of approach of both hinged ends of the bar due to the deflection is

$$\Delta l = \frac{1}{2}\int_0^l \left(\frac{\partial y}{\partial x}\right)^2 dx \quad \ldots\ldots [2]$$

Now, the axial force S_1 produces an elongation of the bar

$$\Delta l = S_1\left(\frac{l}{EA} - \frac{1}{\beta}\right) = \frac{S_1 l}{EA}\left(1 - \frac{EA}{l\beta}\right) \quad \ldots\ldots [3]$$

It may be seen from the last expression that the constant $1/\beta$ can be omitted in our further investigation without any loss of generality. If, in fact, the actual constant $1/\beta \neq 0$, we should only replace the actual area A in our final results by the reduced value

$$A' = \frac{A}{1 - \dfrac{EA}{l\beta}} \quad \ldots\ldots [4]$$

Equating now the Expressions [2] and [3], we get

$$S_1 = EA\,\frac{\Delta l}{l} = \frac{B}{2lr^2}\int_0^l \left(\frac{\partial y}{\partial x}\right)^2 dx \quad \ldots\ldots [5]$$

Substituting the last expression in Equation [1], we obtain

$$\frac{\partial^2 y}{\partial t^2} = -\frac{B}{\mu}\frac{\partial^4 y}{\partial x^4} + \frac{1}{\mu}\left[S_0 + \frac{B}{2lr^2}\int_0^l \left(\frac{\partial y}{\partial x}\right)^2 dx\right]\frac{\partial^2 y}{\partial x^2} \quad \ldots [6]$$

Putting

$$y = a\psi \sin\frac{n\pi x}{l} \quad \ldots\ldots [7]$$

the geometrical conditions at the hinged ends of the bar are

---

[1] Frankfort-on-Main, Germany.

Presented at the National Meeting of the Applied Mechanics Division, Ann Arbor, Mich., June 13-15, 1949, of The American Society of Mechanical Engineers.

Discussion of this paper should be addressed to the Secretary, ASME, 29 West 39th Street, New York, N. Y., and will be accepted until April 10, 1950, for publication at a later date. Discussion received after the closing date will be returned.

Note: Statements and opinions advanced in papers are to be understood as individual expressions of their authors and not those of the Society. Paper No. 49—APM-2.

satisfied. Using Equation [6], we get the following equation for ψ

$$\frac{d^2\psi}{dt^2} = -\frac{n^4\pi^4\alpha^2 B}{4\mu l^4}\psi^3 - \left(\frac{n^4\pi^4 B}{\mu l^4} + \frac{n^2\pi^2 S_0}{\mu l^2}\right)\psi = 0 \quad [8]$$

Multiplying this by $(d\psi)/(dt)$ and integrating the result between the maximum deflection ($\psi = 1$, $[d\psi]/[dt] = 0$) and any deflection ψ, we obtain

$$\left(\frac{d\psi}{dt}\right)^2 = \frac{n^4\pi^4\alpha^2 B}{8\mu l^4}(1 - \psi^4) + \left(\frac{n^4\pi^4 B}{\mu l^4} + \frac{n^2\pi^2 S_0}{\mu l^2}\right)(1 - \psi^2) \quad [9]$$

Using the abbreviations

$$p^2 = \frac{n^4\pi^4 B}{\mu l^4}\left(1 + \frac{\alpha^2}{4}\right) + \frac{n^2\pi^2 S_0}{\mu l^2} \quad [10]$$

and

$$k^2 = \frac{1}{2 + \frac{8}{\alpha^2}\left(1 + \frac{S_0 l^2}{n^2\pi^2 B}\right)} \quad [11]$$

Equation [9] becomes

$$\left[\frac{d\psi}{d(pt)}\right]^2 = (1 - \psi^2)(k^2\psi^2 + 1 - k^2) \quad [12]$$

The solution of this equation is

$$\psi = cn[p(t + t_0), k] \quad [13]$$

where k is the modulus of the elliptic function and t_0 a constant of integration, which we can make zero. Now, by Equation [7], each expression of the form

$$y = a \sin\frac{n\pi x}{l}\, cn\,(pt, k) \quad [14]$$

with $n = 1, 2, 3, \ldots$ is a possible solution of Equation [1]. But this equation is nonlinear in y, and for this formal reason a superposition of any solutions of the form, Equation [14], is not practicable. The obvious mechanical reason for difficulty in obtaining a general solution of the problem is the coupling effect of axial forces resulting from each particular solution of the form of Equation [14].

The period of the function $cn(pt, k)$ is

$$4K = 4\int_0^{\pi/2} \frac{d\varphi}{\sqrt{1 - k^2\sin^2\varphi}} \quad [15]$$

and the corresponding frequency

$$\omega = \frac{\pi p}{2K} \quad [16]$$

In the absence of axial forces (we can get this case assuming $S_0 = 0$, $r \to \infty$ and thus obtaining $\alpha = 0$, $k = 0$, $K = \pi/2$) the frequency becomes

$$\omega_0 = p_0 \quad [17]$$

where $p_0^2 = n^4\pi^4 B/\mu l^4$. Comparing this well-known result with the case in which the ends of the bar are fixed ($S_0 \neq 0$), but the initial axial force is zero ($S_0 = 0$), we have by Equation [10]

$$\frac{\omega}{\omega_0} = \frac{\pi}{2K}\sqrt{1 + \frac{\alpha^2}{4}} \quad [18]$$

The effect of the amplitude on the increase of the frequency is seen from Table 1.

TABLE 1 EFFECT OF AMPLITUDE ON INCREASE OF FREQUENCY

α	ω/ω_0	α	ω/ω_0
0	1	1.0	1.089
0.1	1.0008	1.5	1.190
0.2	1.0038	2	1.316
0.4	1.015	3	1.626
0.6	1.038	4	1.976
0.8	1.058	5	2.35

By Equation [5] the tensile force due to the deflection alone is

$$S_1 = \frac{B\psi^2}{2lr^2}\int_0^l \left(\frac{an\pi}{l}\right)^2 \cos^2\frac{n\pi x}{l}\, dx = \frac{P_n\alpha^2}{4}\, cn^2(pt,\ k) \quad [19]$$

Hence the frequency of this force is equal to 2ω and its maximum value is

$$\max S_1 = \frac{P_n\alpha^2}{4} \quad [20]$$

P_n being that Euler load which corresponds to the orthogonal function $y = \sin(n\pi x)/l$.

We have now to consider the effect of the initial axial force S_0. At first let S_0 be positive, by Equations [10] and [16] the frequency ω then increases if the value S_0 is increasing. Now let S_0 become negative. While $|S_0| = P_0$ increases, the frequency ω decreases, and it vanishes if

$$P_0 = P_n\left(1 + \frac{\alpha^2}{4}\right) \quad [21]$$

Consequently the critical value of the compressive force in a vibrating bar is larger than the Euler load P_n when the deflection is zero, and it decreases to the value

$$P = P_0 - \max S_1 = P_n \quad [22]$$

at the instant of the maximum deflection ($\psi = 1$). Until now, no transverse load on the bar has been assumed. Treating the problem more rigorously, we should introduce at least a load commensurate to the mass of the bar. This load can be replaced with sufficient accuracy by a transvere load following the law

$$q = q_0 \sin\frac{\pi x}{l} \quad [23]$$

Introducing the load q in Equation [1], we can reduce our problem to the evaluation of an elliptic integral of the first kind

$$t = \int_0^t \frac{d\psi}{\sqrt{\Psi}} \quad [24]$$

where Ψ denotes a quadric in ψ. The inverse of this integral is again an elliptic function. Contrary to the result given in Equation [13], it would represent a nonsymmetrical vibration about the axis $y = 0$ of the undeflected bar.

Solution by Bessel Functions

A solution analogous to Equation [14] can be obtained, by means of Bessel functions, for the case of a vibrating circular plate with fixed edge, if the deflected surface of the plate is assumed a surface of revolution. However, such a solution would be of little practical interest. In fact, if the amplitude of the vibration of the plate remains small, as compared with its thickness, the influence of the external forces acting in the middle plane can be practically neglected. However, if the deflections of the plate are comparable with its thickness, the well-known theory of bending of plates with large deflections must be taken as the basis for further investigation, and the whole problem of vibrations then becomes much more complicated.

Graphical, Mechanical, and Electrical Aids for Compressible Fluid Flow

By H. PORITSKY,[1] B. E. SELLS,[2] and C. E. DANFORTH[3]

Graphical, mechanical, and electrical methods of studying two-dimensional and axially symmetrical irrotational flow of nonviscous compressible fluids are described and examples are given of problems solved by these methods. Rules for the construction of compressible flux plots using wires, beads, and a suitable device for obtaining the desired length-width ratios of the rectangles are derived, and the apparatus used is described. An analogy is described by means of which these problems can be solved by the use of a d-c resistance board, employing variable resistances which are adjusted to conform to the derived relations. Designers and aerodynamicists in need of solution for problems for which no analytical solutions are available can use the methods described in this paper to obtain the required solutions.

Nomenclature

The following nomenclature is used in the paper:

a = local velocity of sound
a_0 = velocity of sound at stagnation pressure and density
B = magnetic flux density
C, C' = constants
C_p = specific heat at constant pressure
C_v = specific heat at constant volume
c = radius of circle
E = electric-field intensity
E_x = component of electric-field intensity acting in x-direction
E_y = component of electric-field intensity acting in y-direction
H = magnetic-field intensity
h = tank depth
I_x = component of electric current acting in x-direction
I_y = component of electric current acting in y-direction
I_∞ = element current at large distance from disturbances
$\mathbf{M}$ = Mach number
Δn = distance along streamline
p = local pressure
p_0 = stagnation pressure
q = local velocity
R = element resistance
R_∞ = element resistance at large distance from disturbances
r = distance from axis of symmetry
r_0 = distance from axis of symmetry at which rectangles become squares under stagnation conditions
Δs = distance along equipotential line
u = local velocity in x-direction
V = electric-field potential
v = local velocity in y-direction
x = either dimensionless variable or horizontal co-ordinate
y = either dimensionless variable or vertical co-ordinate
z = distance parallel to axis of symmetry
γ = ratio of specific heats of fluid
δ = mesh spread
η = vertical distance along network
λ = conductance
μ = magnetic permeability
ξ = horizontal distance along network
ρ = local mass density
ρ_0 = stagnation mass density
ρ_∞ = density of fluid at large distance from disturbances
φ = velocity-potential function
$\tilde{\varphi}$ = electric potential (voltage)
$\Delta\varphi$ = incremental velocity-potential function
ψ = streamline function
$\tilde{\psi}$ = current function
$\Delta\psi$ = incremental streamline function

1 Introduction

In the following are described several graphical, mechanical, and electrical aids for the study of irrotational flow of a compressible nonviscous fluid.

The graphical method, also known as "flux plotting," consists in drawing equipotentials and flow lines, and utilizing certain relations between the sides Δn, Δs of the rectangles formed by them. (For incompressible fluids these rectangles form curvilinear squares.) Sections 2–4 contain these rules for two-dimensional flows; Section 5 for flows with axial symmetry. Illustrative examples for the two-dimensional case are given in Figs. 8 and 9.

The two-dimensional flux plotting method is not new, and references to the literature are given in Section 6. However, the method does not seem to be well known, and this is one of the reasons for including it in the present paper.

An electrical analogy is described in Section 7. This utilizes a d-c board and requires adjustment of resistances as a proper function of the local voltage gradient.

Mechanical aids based on utilizing wires and pins, the wires sliding through holes in the pins, are described in Section 8. For incompressible flow, following a suggestion by Lord Rayleigh, four sets of wires are used, two orthogonal sets making 45 deg angles with each other. A flow of an incompressible fluid through a grid of turbine blades determined by this model is shown in Fig. 15.

For handling compressible flow, only one orthogonal set of wires is used, and the wire and pin mechanical model is used with either proper double calipers, Fig. 18, or pairs of mutually perpendicular cams, Fig. 20. The calipers are so designed that

[1] Apparatus Engineering Division, General Electric Company, Schenectady, N. Y. Mem. ASME.
[2] Aircraft Gas Turbine Engineering Division, General Electric Company, Lynn River Works, Lynn, Mass.
[3] Technical Education Division, General Electric Company, Schenectady, N. Y.

Presented at the Annual Conference of the Applied Mechanics Division, Ann Arbor, Mich., June 13–15, 1949, of The American Society of Mechanical Engineers.
Discussion of this paper should be addressed to the Secretary, ASME, 29 West 39th Street, New York, N. Y., and will be accepted until April 10, 1950, for publication at a later date. Discussion received after the closing date will be returned.
Note: Statements and opinions advanced in papers are to be understood as individual expressions of their authors and not those of the Society. Paper No. 49—APM-24.

when one pair of opposite caliper legs is adjusted to a proper value of Δn, the other automatically opens to the distance Δs. The cams perform the same function by being shaped so that, when dropped into a rectangle, the four edges of the cams should come into contact with the mid-points of the sides of the rectangle. A problem solved by the use of the calipers is given in Fig. 19, and one solved by the use of the cams is given in Fig. 22.

2 Flux Plotting Rules for Two-Dimensional Flow of Compressible Fluids

As stated in the preceding section, the assumptions made regarding the flow are that it possesses no vorticity and no viscosity. As a consequence of the former, the flow may be described by means of a velocity-potential function φ, such that the velocity is equal to the gradient of φ. From the condition of continuity (conservation of fluid mass) there exists a flux function or streamline function ψ, whose gradient is the mass transport per unit length at right angles to the flow. The curves of constant potential

$$\varphi = \text{const} \quad [1]$$

and the streamlines

$$\psi = \text{const} \quad [2]$$

intersect each other at right angles (with exception of the isolated points at which the velocity q vanishes). Denote by Δn, Δs the sides of the rectangles obtained by drawing the flow lines Equation [2] for values of ψ differing by the same amount $\Delta\psi$, and curves of constant velocity potential Equation [1] at right angles to the former, and for constant values of φ differing by the same amount $\Delta\varphi$, with Δn the distance along the streamlines, and Δs the distance along the equipotentials, see Fig. 1. The following

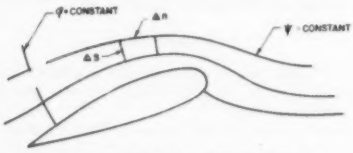

Fig. 1 Flow-Field Nomenclature

relations will be proved for a proper ratio of $\Delta\varphi$: $\Delta\psi$ and for small increments $\Delta\varphi$, $\Delta\psi$

$$y = \frac{x}{\left[1 - \dfrac{\gamma - 1}{2x^2}\right]^{1/(\gamma-1)}} \quad [3]$$

where

$$x = \frac{(\Delta n)a_0}{\Delta\varphi} = \frac{a_0}{q} \quad [4]$$

$$y = \frac{(\Delta s)a_0}{\Delta\varphi} = \frac{(\Delta s)a_0\rho_0}{\Delta\psi} \quad [5]$$

Here a_0 is the velocity of sound at the stagnation pressure and density (p_0, ρ_0), q is the local velocity, and x, y are two dimensionless variables proportional to the sides Δn, Δs, respectively

$$\Delta n = Cx, \quad \Delta s = Cy \quad [6]$$

where C is a constant. The graph of Equation [3] is plotted in Fig. 2 for the case $\gamma = 1.4$ and in Fig. 3 for $\gamma = 1.33$. In deriving Equation [3] it is assumed that at low velocities, that is, for large rectangles, the rectangles become squares. This shows up in Fig. 2 as a 45-deg-line asymptote.

In passing from x to Δn, and y to Δs it is not necessary to compute the $\Delta\varphi$, $\Delta\psi$-values in Equations [4], [5]. Generally, for some part of the flow q, p, ρ are known, and either Δn or Δs is given. Thus either x or y may be found there and the constant of proportionality C in Equation [6] may be determined. Both x and y are dimensionless, while C has the units of length.

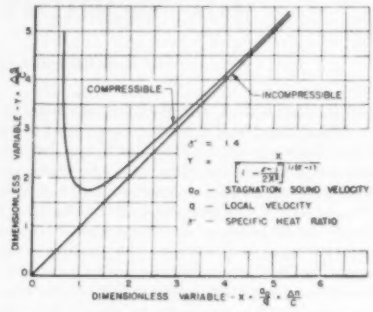

Fig. 2 Compressible Flux Plotting Function

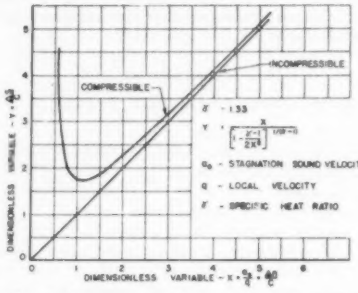

Fig. 3 Compressible Flux Plotting Function

For any one value of γ, Equation [3] represents a universal curve applicable to all flows satisfying the conditions noted. However, for particular plots, a curve of Δn plotted directly versus Δs may be preferred, and this may be plotted readily by carrying out a change of scale along the axes after C in Equation [6] has been evaluated. This is illustrated in detail in the examples described in Section 4. Again, different constants may be preferred in Equation [6], replacing it by

$$\Delta n = Cx, \quad \Delta s = C'y \quad [7]$$

This is the case when one adjusts the plot to obtain squares at infinity, when the fluid velocity there does not vanish. In such cases the curve of Δn versus Δs is obtained from the universal curve Equation [3] by means of a different change of scale along each axis.

After the plot has been completed, the pressure on solid boundaries may be determined from it by means of the equation

$$\frac{p}{p_0} = \left[1 - \frac{\gamma - 1}{2x^2}\right]^{\gamma/(1-\gamma)} = \left(\frac{y}{x}\right)^{\gamma} \quad [8]$$

Here p is the pressure at any point, p_0 the stagnation pressure, x

the local value of x, which may be found from Equation [6] and measured values of Δn or Δs.

A plot of p/p_0 versus x for $\gamma = 1.4$ is given in Fig. 4.

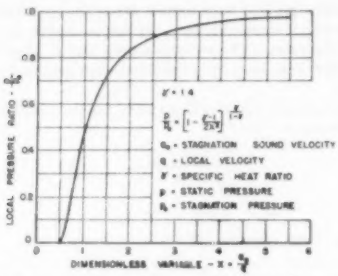
LOCAL PRESSURE RATIO - p/p0
DIMENSIONLESS VARIABLE - x = q/a0
γ = 1.4
p/p0 = [1 - ((γ-1)/2)(q²/a0²)]^(γ/(γ-1))
a0 = STAGNATION SOUND VELOCITY
q = LOCAL VELOCITY
γ = SPECIFIC HEAT RATIO
p = STATIC PRESSURE
p0 = STAGNATION PRESSURE

FIG. 4 COMPRESSIBLE FLUX PLOTTING PRESSURE VARIATION WITH VELOCITY

3 DERIVATION OF EQUATION [3]

From the definition of φ, ψ, one obtains for sufficiently small rectangle sides Δn, Δs and correspondingly small $\Delta\varphi$, $\Delta\psi$

$$\Delta\varphi = (\Delta n)q \quad [9]$$

$$\Delta\psi = (\Delta s)\rho q \quad [10]$$

where q is the velocity, ρ the density. We proceed to eliminate ρ by means of the Bernoulli equation.

The general form of the Bernoulli equation is given by

$$\frac{q^2}{2} + \int_{p_0}^{p} \frac{dp}{\rho} = 0 \quad [11]$$

where p_0 is the stagnation pressure, that is, the pressure from which a stationary gas can be made to reach the state in question by isentropic expansion. Under the assumption of perfect gas laws and constant specific heats the isentropic relation is given by

$$p = \frac{p_0}{\rho_0^{\gamma}} \rho^{\gamma} \quad [12]$$

where $\gamma = C_p/C_v$ is the ratio of specific heats.

Substituting in Equation [11] and carrying out the integration one obtains

$$0 = \frac{q^2}{2} + \frac{\gamma - 1}{\gamma} \frac{p_0}{\rho_0^{\gamma}} \left[\rho^{\gamma-1} - \rho_0^{\gamma-1}\right] \quad [13]$$

which may be written in either of the forms

$$\frac{q^2}{2} + \frac{\gamma}{\gamma - 1} \frac{p_0}{\rho_0} \left[\left(\frac{\rho}{\rho_0}\right)^{\gamma-1} - 1\right] = 0 \quad [14]$$

$$\left(\frac{\rho}{\rho_0}\right)^{\gamma-1} = 1 - \frac{\gamma-1}{2} q^2 \Big/ \frac{\gamma p_0}{\rho_0} = 1 - \left[\frac{\gamma-1}{2} q^2\right] \left[\frac{\gamma p_0}{\rho_0}\right]^{-1} \quad [15]$$

Recalling the following expression for the velocity of sound

$$a^2 = \frac{dp}{d\rho} \quad [16]$$

one obtains from Equation [12]

$$a^2 = \frac{\gamma p_0}{\rho_0^{\gamma}} \rho^{\gamma-1} = \frac{\gamma p_0}{\rho_0} \left[\frac{\rho}{\rho_0}\right]^{\gamma-1} \quad [17]$$

so that the sound velocity a_0 at the stagnation pressure p_0 is given by

$$a_0^2 = \frac{\gamma p_0}{\rho_0} \quad [18]$$

This enables one to change the Bernoulli Equation [14] into the form

$$\left(\frac{\rho}{\rho_0}\right) = \left[1 - \frac{\gamma-1}{2} \frac{q^2}{a_0^2}\right]^{1/(\gamma-1)} \quad [19]$$

From Equations [9], [10], [19] one obtains

$$\Delta n = \frac{\Delta\varphi}{q} \quad [20]$$

$$\Delta s = \frac{\Delta\psi}{\rho q} = \frac{\Delta\psi}{\rho_0 q \left[1 - \frac{\gamma-1}{2} \frac{q^2}{a_0^2}\right]^{1/(\gamma-1)}} \quad [21]$$

Assume now that near the stagnation pressure, where the velocity q is low and the rectangles are large, the rectangle sides Δn, Δs become equal, and the rectangles become squares. Then, for $q = 0$ and $\Delta n = \Delta s$ Equations [20], [21]

$$\Delta n = \frac{\Delta\varphi}{q} = \Delta s = \frac{\Delta\psi}{\rho q} \quad [22]$$

so that

$$\Delta\psi = \rho_0 \Delta\varphi \quad [23]$$

Since $\Delta\varphi$ and $\Delta\psi$ are constants for the whole plot, the last relation holds for the whole plot.

Multiplying Equation [20] by a_0, dividing by $\Delta\varphi$ and introducing x as a_0/q, one is led to Equation [4]. Similarly, multiplying Equation [21] by a_0, replacing $\Delta\psi$ from Equation [23], dividing by $\Delta\varphi$, and introducing y for $\Delta s\, a_0/\Delta\varphi$, one is led from Equation [21] to Equation [5], and to Equation [3].

Examination of Equation [4] shows that x, being a ratio of velocities, is dimensionless; similarly y is dimensionless. This is a further advantage in using these variables and Equation [3].

A well-known dimensionless variable is the Mach number

$$\mathbf{M} = q/a \quad [24]$$

that is, the ratio of the fluid velocity to the local velocity of sound. The relation between x and $\mathbf{M}$ is obtained from the alternative form of Bernoulli equation

$$a_0^2 = a^2 + \frac{\gamma-1}{2} q^2 \quad [25]$$

which is readily obtained from Equations [14], [17], [18]. Dividing Equation [25] by a^2 yields

$$\frac{a_0^2}{a^2} = \left(\frac{a_0}{q}\right)^2 \left(\frac{q}{a}\right)^2 = 1 + \frac{\gamma-1}{2} \left(\frac{q}{a}\right)^2 \quad [26]$$

and introducing x and $\mathbf{M}$

$$\mathbf{M}^2 x^2 = 1 + \frac{\gamma-1}{2} \mathbf{M}^2 \quad [27]$$

so that

$$x^2 = \frac{1}{M^2} + \frac{\gamma - 1}{2} \quad [28]$$

In practice, one may prefer a curve of Δn, Δs in inches to the dimensionless universal curve Equation [3]. To obtain it one calculates C by applying Equation [6] at some place in the flow where the dimensions and flow conditions are given. With C evaluated, the x-, y-values on the plot of Equation [3] are read off, converted by means of Equation [6] into Δn, Δs values and plotted. A similar procedure is followed in applying Equation [7].

Equation [8] for the pressure is obtained by writing Equation [12] in the form

$$\frac{p}{p_0} = \left(\frac{\rho}{\rho_0}\right)^{\gamma} \quad [29]$$

and substituting for (ρ/ρ_0) from Equation [19], at the same time introducing x for a_0/q.

4 Examples

To illustrate the application of the foregoing, consider the flow through a grid of vanes shown in Fig. 5 for a flow for air with

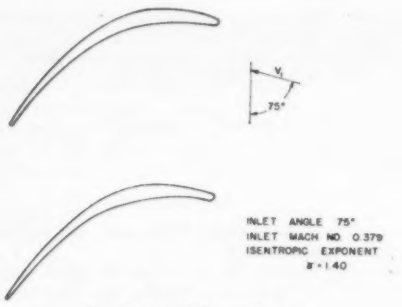

Fig. 5 Basic Grid of Blades

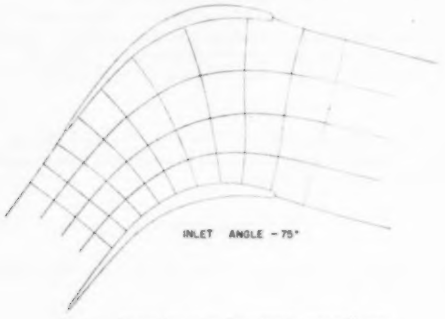

Fig. 6 Flux Plot of Incompressible Flow

$\gamma = 1.4$ corresponding to a Mach number $M = 0.375$ at an angle of 75 deg to the base line. As usual it will be assumed that the Kutta-Joukovski condition is satisfied at the trailing end of the blades; since this end is not absolutely sharp, the application of this condition is somewhat vague and a slight discrepancy between different plots may be expected on that account.

In applying the rules previously stated to the present example, it is convenient though not necessary to start first with an incompressible plot through the grids in question. It will be recalled that this divides the plane into small squares. After this plot is made, the flow lines from it are taken as a first approximation to the compressible flow, subject to change as a result of applying the rules. The incompressible plot is given in Fig. 6. Since its flow lines have to be modified, high accuracy in it is not necessary.

From Equation [28] it follows that for the incoming flow at infinity (with $\gamma = 1.4$)

$$x^2 = \frac{1}{(0.375)^2} + 0.2 = 7.315$$

$$x = 2.704$$

From Fig. 2 this corresponds to

$$y = 2.899$$

Direct measurement of the period space of the grid in Fig. 5 yields 4.45 in., so that with a 75-deg angle for the inlet flow, one obtains for the inlet flow, assuming four flow spaces per space between adjacent vanes

$$\Delta s = \frac{4.45}{4} \sin 75 \text{ deg} = 1.1125 \times 0.9659 = 1.073$$

Hence the value of C in Equation [6] is now equal to

$$C = \frac{\Delta s}{y} = \frac{1.073}{2.899} = 0.3705$$

A direct plot of Δs versus Δn is obtained by applying Equation [6] to Fig. 2, and leads to Fig. 7.

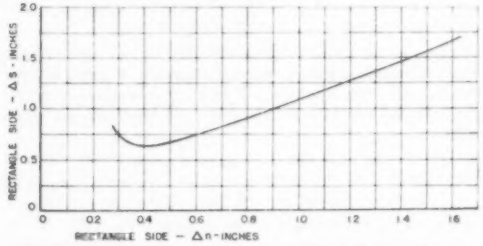

Fig. 7 Variation of Δs With Δn for Flux Plot in Fig. 8

A plot of the compressible flow, utilizing Fig. 7, is given in Fig. 8. Fig. 9 is another, independent, plot for the same inlet conditions and for the same shape vanes. In Fig. 9 the squares were chosen not at stagnation pressure but at infinity at the inlet side. This corresponds to utilizing Equation [7] with the same value of C' as before, namely, $C' = 0.3853$, but with $C = 1.023$. To obtain the latter it will be recalled that at infinity the values of x and y are, respectively, equal to 2.865 and 2.886. The calculation of C can now be obtained by making Δn equal to Δs at infinity. It will be noted that there is a fair amount of discrepancy between Figs. 8 and 9.

A plot of the pressure ratio p/p_0 along the blade boundaries derived from Fig. 8 is shown in Fig. 10. This is obtained from Equation [7] by measuring the distances Δn along both sides of the blade boundaries.

5 Axially Symmetric Flows

For flows with axial symmetry, where the flow lines always he

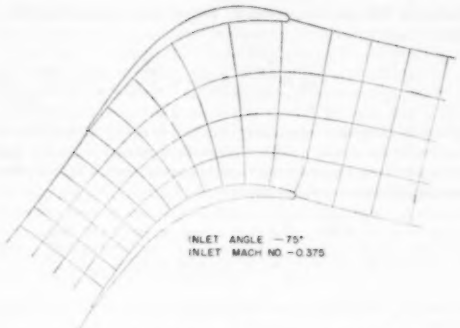

FIG. 8 FLUX PLOT OF COMPRESSIBLE FLOW

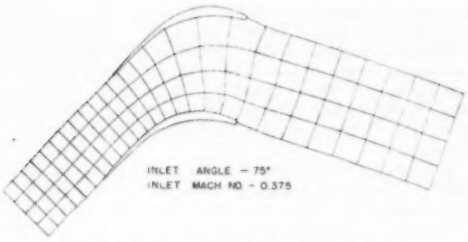

FIG. 9 FLUX PLOT OF COMPRESSIBLE FLOW

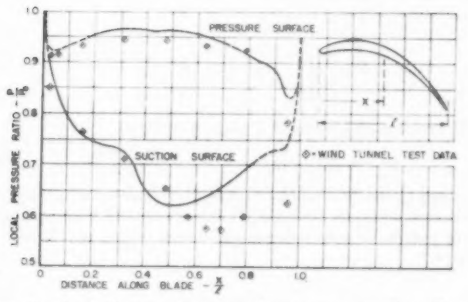

FIG. 10 BLADE SURFACE PRESSURE DISTRIBUTION FOR FLUX PLOT IN FIG. 8

in axial planes, a set of rules similar to those of Section 2 can be derived. By definition the streamline function $\psi(r, z)$, where r is the distance from the symmetry axis, z the distance parallel to it, is defined as the total flow through a circle through the point (r, z) with axis along the z-axis, see Fig. 11.

FIG. 11 CO-ORDINATES FOR AXIALLY SYMMETRIC FLOW

If in an axial plane the curves Equations [1], [2] be drawn for fixed values of φ, ψ differing by amounts $\Delta\varphi$, $\Delta\psi$, respectively, then Equation [9] holds; however, Equation [10] is replaced by

$$\Delta\psi = 2\pi r\rho q\, \Delta s \qquad [30]$$

Hence one now obtains

$$\Delta n = \frac{\Delta\varphi}{q}, \quad \Delta s = \frac{\Delta\psi}{2\pi r q \rho} \qquad [31]$$

Suppose now that $\Delta\varphi$, $\Delta\psi$ be so picked that the rectangles of the plot become squares, $\Delta n = \Delta s$ at $p = p_0$, $\rho = \rho_0$, $r = r_0$ under stagnation conditions

$$\Delta\varphi = \frac{\Delta\psi}{2\pi r_0 \rho_0} \qquad [32]$$

Then one obtains from Equation [31] at any point of the plot

$$\Delta s = \Delta n \frac{r_0}{r} \frac{\rho_0}{\rho} \qquad [33]$$

Introducing x, y as in Equations [4], [5] one rewrites Equation [33] in the form

$$y = x \frac{r_0}{r} \frac{\rho_0}{\rho} \qquad [34]$$

and utilizing Equations [19] and [4], one obtains

$$y = \frac{x}{\left[\frac{r}{r_0}\right]\left[1 - \frac{\gamma - 1}{2x^2}\right]^{1/(\gamma-1)}} \qquad [35]$$

Unlike the two-dimensional case where a universal curve Equation [3] was obtained, now a relation holds involving x, y as well as the ratio r/r_0. The relation Equation [35] may be plotted as a series of curves, one for each value of r/r_0. These are obtained from the curve of Figs. 2 and 3 by dividing the ordinates y by r/r_0. The rectangle side Δn now depends not only upon Δs but also upon the distance from the axis. However, a universal curve can be obtained by writing Equation [35] in the form

$$\frac{yr}{r_0} = \frac{x}{\left[1 - \frac{\gamma - 1}{2x^2}\right]^{1/(\gamma-1)}} \qquad [36]$$

and represented by Figs. 2 and 3 by renaming y as yr/r_0.

6 REFERENCE TO LITERATURE. ANALOGIES

The earliest account of the rules for plotting compressible fluid flow that have come to the authors' attention is in Prandtl and Busemann, reference (1),[4] where a curve of the potential and streamline distances is given, and the flow around a cylinder at a Mach number $M = 0.4$ is shown. Reference is made there to two papers by G. H. Bryan (2) although examination of these reports failed to disclose the plotting rule.

A graphical method applicable to two-dimensional compressible flow and flow with axial symmetry is described briefly by Stodola (3). This consists in sketching the flow lines, and using the relation which in the present notation can be written as

$$\log q = \int \frac{ds}{R} \qquad [37]$$

where R is the radius of curvature of the streamlines and the integration is carried out along the equipotential lines. This relation is used to correct a preliminary sketch of the streamlines. The method is due to Fliegel (4).

An unpublished Westinghouse report on the subject of compressible fluid flow entitled "Air Flow Determination by Graphi-

[4] Numbers in parentheses refer to the Bibliography at the end of the paper.

cal Methods" was prepared by W. C. Brenner and Lee A. Kilgore (5) as a preprint of the Institute of Aeronautical Sciences for its national meeting in 1944. The meeting was canceled due to war travel restrictions and the paper was not presented. It is not available as a published paper.

The basic relation between the rectangle width and its length is given in (5) in the form of a family of curves rather than a single curve due to the fact that unit squares are employed in the undisturbed stream, rather than at the stagnation pressure.

The paper includes several plots about a single airfoil (graphical methods are relatively inaccurate in such a problem). It also contains several flows through a grid for $\mathbf{M} = 0, \mathbf{M} = 0.6$.

A useful method suggested in the Brenner-Kilgore paper employs beads with strings running through them in mutually perpendicular directions. This method enables one to modify a construction after the dimensions of the rectangles have been checked without considerable erasing.

An analogy can be built up between compressible two-dimensional flow and the flow of an incompressible fluid in a tank with variable depth, the depth being adjusted to depend on the velocity. This analogy has been used by G. I. Taylor and C. F. Sharman (6) as a basis for solving compressible flow by starting with a flow in a tank of uniform depth, modifying its depth in accordance with the resultant velocity, and repeating this process.

This analogy follows from the compressible fluid-flow equations

$$u = \frac{\partial \varphi}{\partial x}, \quad v = \frac{\partial \varphi}{\partial y} \qquad [38]$$

$$\rho u = \frac{\partial \psi}{\partial y}, \quad \rho v = -\frac{\partial \psi}{\partial x} \qquad [39]$$

by applying them to the flow of an incompressible fluid in a tank in which ρ is made proportional to the tank depth h, and identifying u, v as the "average" velocity over the depth h. To avoid surface waves, a flat plate may be placed over the water surface. Equation [19] shows that ρ is a function of the velocity $q = \sqrt{u^2 + v^2}$ only. Hence the tank depth must be adjusted in accordance with Equation [19], so that its depth is a proper function of the local velocity q.

7 Electrical and Magnetic Analogies

The tank analogy requires Pitot-tube measurement and suffers from boundary-layer effects, from velocity disturbances in the z-direction (normal to the top boundary), and from other difficulties. A more convenient analogy is offered by the conduction of electric currents in a plate for which the conductance is a function of the voltage gradient or of the current density. This analogy follows from the plate-conduction equations

$$E = -\frac{\partial \bar{\varphi}}{\partial x}, \quad E_y = -\frac{\partial \bar{\varphi}}{\partial y} \qquad [40]$$

$$I_x = \lambda E_x, \quad I_y = \lambda E_y \qquad [41]$$

$$\frac{\partial I_x}{\partial x} + \frac{\partial I_y}{\partial y} = 0 \qquad [42]$$

where $\bar{\varphi}$ is the electric potential (voltage), E_x, E_y the electric-field components, λ the plate conductance, and I_x, I_y the current components across the plate thickness per unit normal length.

Equation [42] may be solved by means of a current function $\bar{\psi}$ thus

$$I_x = \frac{\partial \bar{\psi}}{\partial y}, \quad I_y = -\frac{\partial \bar{\psi}}{\partial x} \qquad [43]$$

It is now clear that an analogy can be set up by identifying the fluid-velocity vector q with electric-field intensity E, the mass transport vector ρq with the electric-current vector I, and ρ with the plate conductance λ as follows

φ	$u,\ v,\ q = \sqrt{u^2 + v^2}$	ψ	$\rho u,\ \rho v,\ \rho q$	ρ
$\bar{\varphi}$	$E_x,\ E_y,\ E = \sqrt{E_x^2 + E_y^2}$	$\bar{\psi}$	$I_x,\ I_y,\ I = \sqrt{I_x^2 + I_y^2}$	λ

[44]

where corresponding elements are made proportional to each other.

Equation [19] requires that the conductance be made a function of the voltage gradient (or of the current density I—the gradient of $\bar{\psi}$). This presumably could be accomplished by varying the plate thickness, but this method would suffer from many of the inconveniences of Taylor's tank model. It is further conceivable that materials could be developed whose resistivity will vary in the proper manner either with the voltage gradient or with the current density (possibly by utilizing the temperature effect due to the heat developed by the current). Until that is done, however, the most convenient procedure is to resort to the d-c board.

By replacing the derivatives in Equations [38], [39], [40] to [43] by difference quotients of values of φ, ψ at corners of a square lattice net of mesh spread $\delta = \Delta x = \Delta y$ over the region in question, one converts these differential equations into difference equations which may be interpreted as the circuit equations of a network of resistances connected in the same manner as the lattice, the resistance R of each element (both vertical and horizontal) being given by

$$\frac{R}{R_\infty} = \frac{1}{\left[1 - \frac{\gamma - 1}{2}\left(\frac{E}{E_\infty}\right)^2\right]^{1/(\gamma-1)}} \qquad [45]$$

The resultant field strength E can be found from

$$E = \sqrt{E_x^2 + E_y^2} = \sqrt{[(\Delta_x \bar{\varphi})^2 + (\Delta_y \bar{\varphi})^2]}/\delta \qquad [46]$$

It may further be found by reading the voltage values $\bar{\varphi}$, plotting the equipotentials Equation [1] for constant $\Delta\bar{\varphi}$, measuring Δn, the normal distance between the equipotentials, and finding E from

$$E = \frac{\Delta \bar{\varphi}}{\Delta n} \qquad [47]$$

If the orthogonal trajectories of Equation [1] (namely, the curves of Equation [2]) also be drawn as in the flux plotting procedure, the local conductance $\lambda = \rho$ is further given by

$$\lambda \sim \rho = \frac{\Delta \bar{\psi}}{\Delta \bar{\varphi}} \frac{\Delta n}{\Delta s} = \rho_0 \frac{\Delta n}{\Delta s} \qquad [48]$$

(see Equations [9], [10]). Thus it varies as the "ratio" of the rectangle sides. From Equations [3] to [6] now follows

$$\lambda \sim \rho = \frac{\Delta \bar{\psi}}{\Delta \bar{\varphi}} \frac{x}{y} = \frac{\Delta \bar{\psi}}{\Delta \bar{\varphi}} \left(1 - \frac{\gamma - 1}{2x^2}\right)^{1/(\gamma-1)}$$

$$x = \frac{a_0}{\gamma} \qquad [49]$$

In setting up compressible flow problems on the d-c board, one may start with constant resistances, read the voltages of the lattice points, calculate E from Equation [46], or from a plot based on these voltages and Equation [47]; changing the resistances in accordance with Equation [45] one now reads the new voltage values, recomputes the electric gradient and adjusts the resistances once more. This process is repeated till no further change in resistances is required.

The d-c board procedure may be combined profitably with the flux plotting method where the resistance values are evident from the ratio of rectangle sides and the voltage gradient varies inversely as the distance between equipotentials.

The electric analogy may be carried out in an alternative way by utilizing the replacements

ψ	ρv, $-\rho u$, ρq	φ	u, v, q	ρ
$\bar{\varphi}$	E_x, E_y, E	$\bar{\psi}$	$-I_y$, $+I_x$, I	$\frac{1}{\lambda}$

. . . [50]

rather than Equation [44], so that the fluid streamlines correspond to the lines of constant electric potential, and the density ρ corresponds to the plate resistance.

As an example, the foregoing electrical analogy was used to set up on the d-c board the flow of a compressible fluid, at a Mach number $\mathbf{M} = 0.5$, around a circular cylinder placed normally to the stream. In view of the symmetry of the assumed flow (disregarding the possibility of shocks) only one quadrant was set up on the d-c board. The network utilized is shown in Fig. 12, where in terms of the length units used, the circle was taken of

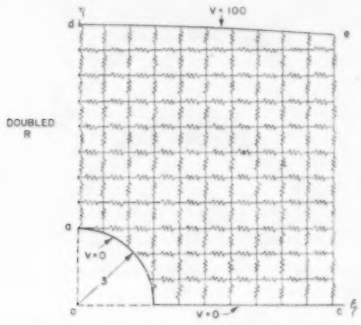

FIG. 12 NETWORK FOR D-C BOARD TEST

radius $c = 3$, and the region covered extended to $\xi = 10$, $\eta = 10+$. The analogy indicated in Equation [50] rather than in Equation [44] was utilized, due to the greater convenience of applying the boundary condition of a constant electrical potential V (which is equal to $\bar{\varphi}$ and ψ in Equation [50]) along the lower boundary *abc* and the upper boundary *de*, corresponding to constant values of the flow function ψ, rather than applying the condition of vanishing normal derivative of the electric potential V (zero normal current) corresponding to $\partial\varphi/\partial n = 0$, which would be required if Equation [44] had been used.

The choice of the "grain size," it must be admitted, is a rather coarse one, especially near the circular boundary, but was dictated by the total number of 288 available resistances, and the possible need of using two resistances in series to represent some of the elements.

The conditions along the boundary were computed from the Rayleigh-Janzen theory (8), including $\mathbf{M}^4$ corrections obtained by Imai (9) and Kawamura (10), and these were used to calculate the boundary potentials along $\xi = 10$ and to find the shape of *de*. The vertical resistances joining the points along $\eta = 10$ to the upper boundary *de* were chosen proportional to the corresponding length of the vertical line segments representing them, and similarly for the irregular segment abutting the circle. The values of the vertical resistances along $\xi = 10$ were adjusted to obtain the prescribed border voltages. Finally, along *ad* ($\xi = 0$) the resistances were doubled, corresponding to one of two resistances in parallel which would be obtained if a similar network were set up for negative ξ; the measured currents I_y in the elements along $\xi = 0$, after being read, were doubled in value.

The method of solution was as follows: All the internal resistances were chosen equal to a constant ($R = 10{,}000$ ohms) corresponding to the flow of an incompressible fluid, and with the modification of the resistances near the boundaries which were adjusted (relative to R_∞) as previously described. For a uniform flow the voltage $V = 100$ applied at $\eta = 9$ corresponds to current $I_\infty = 1/900$ amp. The boundary potentials were next applied, and the voltages at the various points of the network were read, as well as the currents I_x, I_y in the individual resistances. From the analogy Equation [50], it is evident that the current $I = (I_x^2 + I_y^2)^{1/2}$ corresponds to the velocity q of the fluid, while the voltage gradient E corresponds to the fluid mass flow ρq, and the resistances of the elements correspond to the density ρ. The currents I were calculated; since I_x, I_y were measured at different points, interpolation equivalent to taking the mean of the four surrounding I_y was used to obtain the value of I_y at the mid-point of a horizontal resistance, and similarly for I_x at the mid-points of vertical resistances. The resistances were then determined as a function of the current I by means of

$$R/R_\infty = [1.05 - 0.05(I/I_\infty)^2]^{5/2} \quad \ldots\ldots\ldots [51]$$

This equation is obtained from Equations [48], [49], and the equations of Sections 2 and 3, by noting from Equation [49] that

$$\frac{R}{R_\infty} = \frac{\rho}{\rho_\infty} = \frac{y}{x}\Big/\frac{y_\infty}{x_\infty} = \left(1 - \frac{\gamma - 1}{2x^2}\right)^{1/(\gamma-1)} \Big/ \left(1 - \frac{\gamma - 1}{2x_\infty^2}\right)^{1/(\gamma-1)} \quad \ldots\ldots [52]$$

$$x/x_\infty = q_\infty/q = I/I_\infty \quad \ldots\ldots\ldots [53]$$

by obtaining from Equation [28] $x^2 = 4.2$ for $\mathbf{M} = 0.5$, putting $\gamma = 1.4$, and simplifying. The resistances were then adjusted to correspond to the computed values of R, the readings taken again, and the process repeated.

As a further check, the resistances were also computed as a function of the voltage gradient, $E = \Delta V/\Delta s$, or of Δs. Noting that ρ is proportional to y/x of Equations [3] to [5] while Δs is proportional to y, a curve of R/R_∞ versus $\Delta s = y/y_\infty$ was computed. The equipotentials corresponding to the measured V-values were plotted, Δs measured, and the resistances adjusted to correspond to the R versus Δs-curve. This curve, similarly to Figs. 2 and 3, showed a minimum value for Δs at sonic velocity.

Four tests of this kind were carried out. The results of the last tests showed fair agreement between the values of resistances set up and those determined from the current readings and from the voltage readings. The final plot of V is shown in Fig. 13. For comparison, three broken lines of incompressible flow are also shown in Fig. 13.

While the foregoing renders highly probable the existence of a solution of a potential flow without shock around a circular cylinder with $\mathbf{M} = 0.5$, it does not assure it, in view of the low

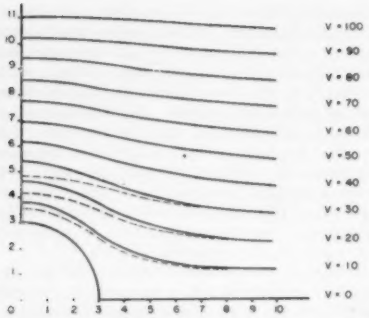

FIG. 13 FLOW LINES FOR COMPRESSIBLE FLOW AROUND CIRCULAR CYLINDER FOR $M = 0.5$

accuracy of present-day d-c boards, the rather large "grain size" used, the assumed nearness of constant boundary conditions, as well as the relatively small number of iterations; yet the tests show that the use of the board for the purpose of eliminating tedious relaxation calculations is quite attractive. Since present d-c boards were not built for the purpose of solving field problems but rather for the analysis of short circuits of power systems, it is planned to build a new d-c board with more units and of higher accuracy which will be more suitable for field problems.

It is also of interest to point out the existence of a "magnetic analogy" to the fluid-flow or electrical-conductance problem in a material with a nonlinear (H, B)-relation. In the analogy Equation [44] ϕ becomes the magnetic potential, E, I are replaced by H, B, and the conductance λ by the permeability μ defined by

$$\mu = \frac{B}{H} \qquad [54]$$

In identifying Equation [3] or [49] with (B, H)-curves or μ versus H-curves it must be kept in mind that H, B, μ vary as $1/x$, $1/y$, x/y.

While the analogy is complete, it offers no obvious possibility of utilization for fluid flow since the (B, H)-curves for ferromagnetic materials do not resemble the curve Equation [3].

8 MECHANICAL MODELS UTILIZING WIRES AND PINS

The network of beads and strings previously described has an inherent difficulty in that drilling the holes at right angles in the beads does not satisfy the condition that the strings intersect in right angles. In fact, due to the curvature of the flux and equipotential lines, the string angles must depart from right angles, but there is no way of determining these departures from right angles. To satisfy more nearly the condition of orthogonality, small spring-steel wires can be used in conjunction with pins having holes in them drilled at right angles. Except for the effect of clearance between the wires and the holes, the wires then intersect in the prescribed right angle despite their curvature in the flow field. Such an arrangement is shown in Fig. 14.

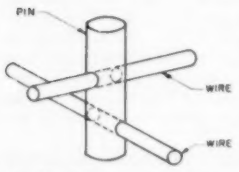

FIG. 14 INTERSECTION OF FLUX PLOTTING WIRES

To satisfy Laplace's equation for two-dimensional, incompressible flow, the units of the network must have a constant length-width ratio which leads to curvilinear squares. Lord Rayleigh (7) proposed that superimposing a second orthogonal network on the original, forming ± 45 deg with the original network, and using common intersections for the double mesh would produce such a network of curvilinear squares. It may be shown that such a superimposed mesh forms a more perfect realization of the small square plotting rule that can be accomplished by the usual method of equating the length between mid-points of the curvilinear square. This is true because the small square rule is exact only in the limit when the size of the squares approaches zero, while the 45-deg rule regarding the curvilinear diagonals is exact even for finite-size squares. The angle requirements are then exact and produce a more accurate plot.

A working model utilizing this principle was constructed by using music wire, 0.020 in. diam, with brass pins $^3/_{32}$ in. diam. Some difficulty was encountered with the permanent set of coiled wire but this was alleviated by obtaining straight wire from the mill. After some experimentation, it was possible to mass-produce the small pins so that the angular variation due to clearance and machining tolerances did not exceed $^1/_2$ deg from the prescribed angle.

This device has been used satisfactorily, and Figs. 15 and 16 show an example of its use in obtaining a conception of the flow

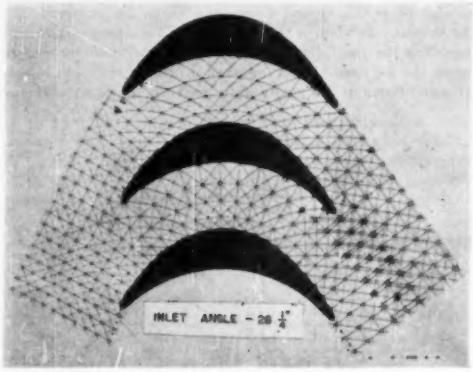

FIG. 15 FLUX PLOT OF INCOMPRESSIBLE FLOW

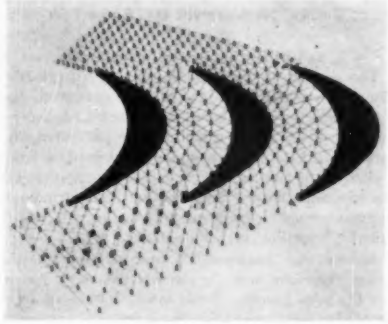

FIG. 16 OBLIQUE VIEW SHOWING CONSTRUCTION OF INCOMPRESSIBLE FLUX PLOT

around a grid of turbine blades. Experience has shown that it is better to use a minimum of two passages between three successive blades in plotting the cascade field. Because the circulation around the blade is seldom an integral number, an overlapping of the equipotential lines is to be expected between the two flow paths. This has been found to have no serious difficulty since the per cent overlap is constant throughout the field. A similar duplication also occurs for the 45-deg network.

It may be pointed out, however, that a single passage between adjacent blades will give exact results if the condition of periodicity of the flow lines be imposed by means of additional pins which are maintained apart at a constant pitch by means of additional rigid bars running above the regular pins and wires.

Several sets of pins were used to perform the plotting: special pointed pins were used to form the flux lines to the blade boundary and a special pin was used for the stagnation point on the central blade of the cascade.

A flux plot of the flow of an incompressible fluid through a hyperbolic channel made to check the results obtained from the wire mesh against an analytical solution is shown in Fig. 17.

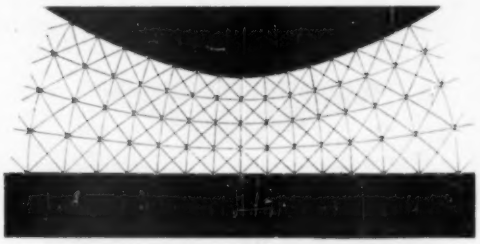

FIG. 17 FLOW OF INCOMPRESSIBLE FLUID IN A HYPERBOLIC CHANNEL

Comparison of velocities obtained from the flux plot with velocities obtained from the analytical solution showed a maximum discrepancy of approximately 10 per cent. This discrepancy was considered justified since only approximate boundary conditions were used in setting up the problem.

The value of this apparatus lies in indicating the nature of the flow for problems where no analytical solutions are known. It is best adapted to problems such as cascades of blades where the boundary conditions are fairly well defined. For such problems an accuracy of approximately 3 per cent may be expected.

In considering the flux plotting of a compressible flow field, one no longer has the condition of small squares, although the specification of an orthogonal network still obtains. The relationship of rectangles of constant length-width ratio is now replaced by the relationship given in Sections 2 through 5, where it is shown that one side of the rectangle, Δn, is a definite function of the second side Δs. While it is possible to incorporate the principle in some mechanism which will prescribe automatically proper relationship of Δs to Δn for the entire wire mesh, such schemes thus far investigated appear unduly complicated and expensive, since any such method postulates the existence of such a device for each small mesh of the network.

A rather simple caliper device for the solution of compressible flow fields has been constructed and is shown in Fig. 18. Essentially, it is a pair of four-legged calipers with the width between one pair of opposite legs being set as a function of the width between the other pair of legs. This latter set of legs, for the view shown, has a width of $^3/_4$ in. for Δs at a true Mach number of unity.

This setting is accomplished by pivoting the caliper legs at a definite point and regulating the opening of each caliper pair by means of a screw carrying a disk working against cam surfaces on the legs. The one pair of cam surfaces is straight and yields a linear change of Δs with the rotation of the screw, while the other side is curved and has the shape of Fig. 2 incorporated in it.

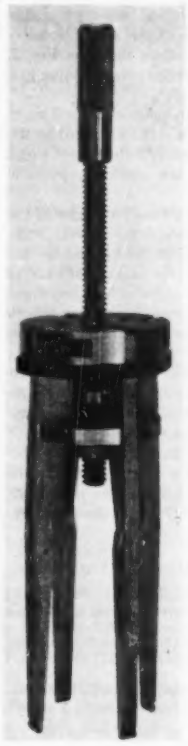

FIG. 18 COMPRESSIBILITY CALIPERS

To construct a compressible plot, the basic 90-deg network is used without the 45-deg diagonal wires. Again, experience has shown some advantage in using two adjacent passages for cascade flow plots. Such a plot is shown in Fig. 19. The cascade is identical with the one for incompressible flow shown in Fig. 15, with the same inlet flow angle and the Mach number equal to 0.5. This plot was made by starting in the center of the upper passage and testing each rectangle while working against the direction of flow, and then completing the lower passage in the direction of flow. The complete mesh was tested several times to obtain a good degree of accuracy. Approximately 40 hr were required to perform such a plot satisfactorily.

FIG. 20 FLUX PLOTTING WEDGE

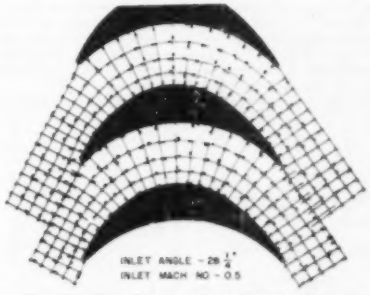

FIG. 19 FLUX PLOT OF COMPRESSIBLE FLOW

Another device which may be used for the solution of compressible flow fields is shown in Fig. 20. This device consists of two thin, flat leaves—one trapezoidal, the other having curved sides. These leaves are rigidly joined together along their verti-

cal center lines at right angles to each other, forming a wedge whose vertical height is 2 in. The shape of this wedge is determined by the relationship given by the curve shown in Fig. 2, each point along the vertical axis of the wedge corresponding to a point on the curve.

In performing a plot, the same basic wire network is used but is constructed 2 in. above the working surface as shown in Fig. 21, to permit the wedges to be inserted vertically into the rectangles formed by the wires. Special long pins are used to support the network away from its boundaries.

The length-width ratios of the sides of all the rectangles of the network are then adjusted until the device may be inserted, without forcing, into any rectangle to a depth determined by the size of the rectangle. When so inserted, the edges of the leaves must just touch the mid-points of the sides of the rectangle. As soon as all of the rectangles have been so adjusted the network is complete. In performing this operation several of the wedges may be used simultaneously.

It is felt that these wedges are superior to the calipers just described, in that their first cost is lower and that the time required to perform a plot with their use is less, through the elimination of the time required to adjust the calipers.

A flux plot made using the wedges of the flow of compressible fluid through a hyperbolic channel with a Mach number at the center of the channel of approximately 0.8 is shown in Fig. 22. This figure may be compared with Fig. 17 which shows incompressible flow through the same channel.

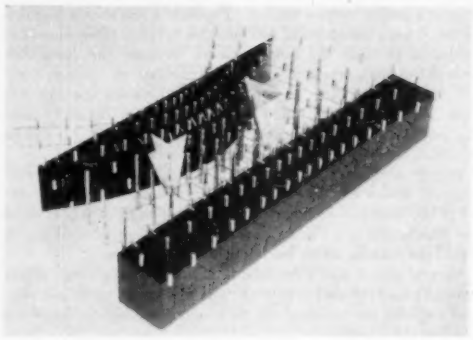

FIG. 21 OBLIQUE VIEW SHOWING CONSTRUCTION OF COMPRESSIBLE FLUX PLOT

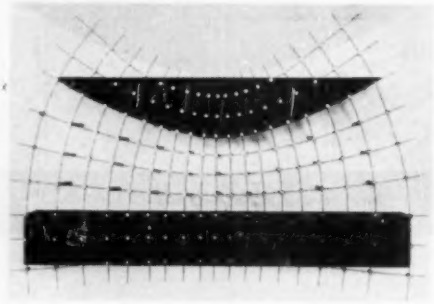

FIG. 22 FLOW OF COMPRESSIBLE FLUID IN A HYPERBOLIC CHANNEL

BIBLIOGRAPHY

1 "Handbuch der Experimentalen Physik," by L. Prandtl and A. Busemann, Julius Springer, Leipzig, Germany, vol. 4, 1931, pp. 407–444.

2 "Technical Report of the Advisory Committee for Aeronautics," by G. H. Bryan, London, England, Report no. 55, 1918; Report no. 640.

3 "Steam and Gas Turbines," by A. Stodola and L. C. Lowenstein, McGraw-Hill Book Company, Inc., New York, N. Y., 1927, sect. 170, p. 992.

4 "Mehrdimensionale Strömmung von Gasen," by Gustav Flügel, *Zeitschrift für das gesamte Turbinenwesen*, vol. 16, 1919, pp. 161–165 and 178–180.

5 "Air Flow Determination by Graphical Methods," by W. C. Brenner and L. A. Kilgore, unpublished Westinghouse report.

6 "A Mechanical Method for Solving Problems of Flow in Compressible Fluids," by G. I. Taylor and C. F. Sharman, Proceedings of the Royal Society of London, series A, vol. 121, 1928, pp. 194–217.

7 "Collected Works," by Lord Rayleigh, The Macmillan Company, New York, N. Y., vol. 6, 1911–1919, p. 153; or *Philosophical Magazine*, vol. 25, 1913, pp. 698–702.

8 "On the Flow of Compressible Fluid Past an Obstacle," by Lord Rayleigh, *Philosophical Magazine*, vol. 32, 1916, pp. 1–6; also "Collected Works," by Lord Rayleigh, vol. 6, 1911–1919, pp. 402–406.

9 "On the Flow of a Compressible Fluid Past a Circular Cylinder, II," by I. Imai, Proceedings of the Physical Mathematical Society of Japan, vol. 23, 1941, p. 181.

10 "A Study of the Subsonic Flow of a Compressible Fluid Past a Circular Cylinder," by T. Kawamura, Proceedings of the Physical Mathematical Society of Japan, vol. 24, 1942, p. 110.

Introduction to the Comprex

By F. W. BARRY,[1] CAMBRIDGE, MASS.

This paper describes the construction and operation of a comprex, or pressure exchanger, together with its application to a gas-turbine cycle. A simple analysis is also developed, which is intended to indicate the performance characteristics of a comprex. This analysis shows that the pressure ratio, relative gas flow, and the ratio of the temperature of the leaving gas to that of the entering air are all functions of scavenging velocity and of the nature of the compression and expansion processes (as is shown graphically). Some irreversibility is found to be essential to the useful operation of a comprex. Finally, formulas for the major dimensions of a comprex are presented.

Nomenclature

The following nomenclature is used in the paper, with subscripts corresponding to the numbers in Fig. 1:

A = area of port normal to rotor axis
c = absolute velocity (see Fig. 1), fps
c_p, c_v = specific heats, Btu/lb deg R
d = mean diameter of cells
g = acceleration of gravity
h = specific enthalpy
J = mechanical equivalent of heat
k = ratio of specific heats, assumed = 1.4
L = length of rotor (see Fig. 1)
m = circumferential distance (see Fig. 1), ft
n = polytropic exponent
p = pressure
q = velocity of wave relative to rotor
R = gas constant, 53.35 ft per deg R
r = radial height of cells, ft
T = absolute temperature, deg R
U = internal energy
u = rotor peripheral velocity at mean diameter
v = specific volume
W = weight rate of flow, lb per sec
w = velocity of flow relative to rotor (see Fig. 5), fps
α = helix angle of cells (see Fig. 1)
β = angle (see Fig. 5)
ρ = density, $1/v$

Introduction

For years engineers have attempted to devise a purely rotary machine which, like an internal-combustion engine, may utilize a fluid at temperatures greatly in excess of those reached by the materials employed. Such a device would enjoy the mechanical simplicity of a turbine, yet, by virtue of a higher permissible maximum temperature, could attain a higher thermal efficiency. Claude Seippel of Brown Boveri achieved this goal in 1940, by inventing the comprex, or pressure exchanger, which compresses one stream and expands another in its rotor. As in an internal-combustion engine, the working space of a comprex contains alternately hot and cold gas, in order that the wall temperature will remain below that which ordinary metals will withstand. For example, if the expansion process operates between temperatures of 1540 and 1200 F, and the compression process between 360 and 660 F, the wall temperature would be the average of these, or only 940 F. Due to the high speed of operation, the temperature at the wall surface will deviate but little from this mean.

Fig. 1 shows two sections of a comprex on the right. It is seen to consist of but two components; the casing and the rotor. The casing has two inlet ports at one end and two exit ports at the other. The rotor has around its periphery a number of shrouded helical cells in which the compression and expansion processes take place. Since, in the Brown-Boveri design, there are 30 cells, and the rotor revolves at 6000 rpm, it is plain that the flow in the ports is essentially continuous. A motor or turbine is connected to the rotor to serve as a governor.

Cycle of Operation

A developed view of the cells and ports, showing the waves accomplishing the compression and expansion processes, is on the left in Fig. 1. The inlet ports are on the right, and the exit ports, on the left, that is, the flow is from right to left. The two long vertical lines are the ends of the rotor, which is moving upward.

In order to explain the cell mechanics, it is most convenient to consider an observer on the rotor. To him, any one cell appears stationary, and the ports appear to pass by the ends of this cell in the correct sequence.

To start, let us say that he sees the cell full of gas flowing to

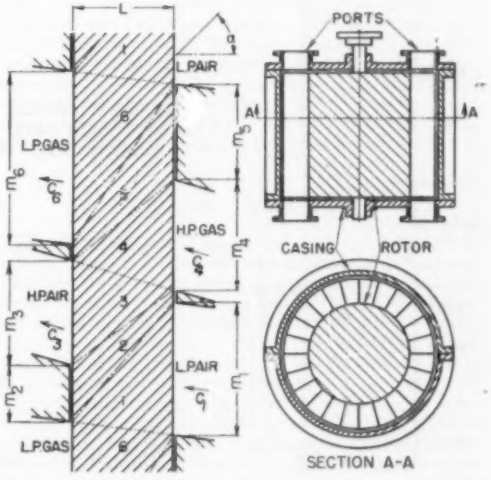

Fig. 1 Developed View of Rotor and Sections of Comprex

[1] Research Assistant, Gas Turbine Laboratory, Massachusetts Institute of Technology. Jun. ASME.

Presented at the National Meeting, Applied Mechanics Division, Ann Arbor, Mich., June 13–15, 1949, of The American Society of Mechanical Engineers.

Discussion of this paper should be addressed to the Secretary, ASME, 29 West 39th Street, New York, N. Y., and will be accepted until April 10, 1950, for publication at a later date. Discussion received after the closing date will be returned.

Note: Statements and opinions advanced in papers are to be understood as individual expressions of their authors and not those of the Society. Paper No. 49—APM-18.

the left and that a port on the right has just opened to admit low-pressure air in state 1. (The terms "gas" and "air" are used to distinguish between the two streams; they do not imply differences in composition.) This air also flows to the left behind a surface of separation between air and gas with the same velocity, relative to the observer on the rotor, as does the gas. As the last gas leaves the cell the port on the left closes and, as a result, produces a pneumatic ram effect on the moving air. The associated pressure increase occurs in a wave which travels back along the cell at about the speed of sound. The inlet port closes as this wave reaches the end, so as to trap a charge of stagnant medium-pressure air, in state 2, in the cell.

The port on the right next opens to admit high-pressure gas, in state 4, which compresses the air still further. As before, the pressure increase occurs in a wave moving, in this case, to the left. The high-pressure air port opens when this wave reaches the left end to permit the air, in state 3, to be scavenged out of the cell by the following gas. While the cell is filled with a stream of air and gas flowing to the left, the observer sees the gas port close. By virtue of its momentum the gas expands to a lower pressure behind the closed port. The closing of the gas port is timed so that the expansion wave, in which this pressure drop occurs, reaches the left end at the same instant as the last air leaves the cell. Since the high-pressure air port closes at the same time, a charge of stagnant medium-pressure gas, in state 5, is thus trapped in the cell.

Now the low-pressure gas port opens at the left. As a result, a second expansion wave shoots to the right and leaves behind it low-pressure gas, in state 6, flowing to the left out of the port. Finally, as this wave reaches the right end, the low-pressure air port opens. Thus one complete cycle of operation has occurred in one revolution of the rotor.

In order to get away from certain restrictions inherent in the design just described, it is necessary to make some alterations in the cycle of operation. For example, there is the arrangement shown in Fig. 2 which employs two-stage (a stage consists of two waves) compression and expansion. Such a unit would operate at a higher pressure ratio without any increase in pressure ratio across each wave. An important feature is that air must be supplied at two pressures and that gas is exhausted also at two pressures. Another excellent variation uses single-stage compression with two-stage expansion. Such a unit does not have the disadvantage of requiring that air be supplied at two pressures, although it still produces gas at two pressure levels, and it has the advantage that the ratio of the temperature of low-pressure gas to that of low-pressure air may be greater than for the other two designs mentioned previously.

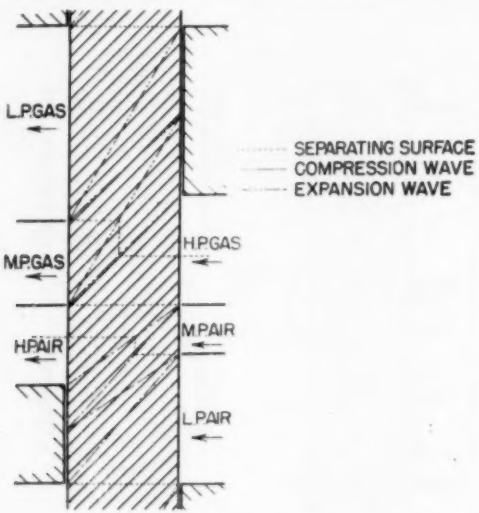

FIG. 2 LAYOUT OF TWO-STAGE COMPREX

GAS-TURBINE APPLICATION

Having discussed the operation of a comprex, let us now investigate one of its most promising applications, namely, its use as a high-pressure stage in a gas turbine. Fig. 3 shows schematically a possible arrangement, and Fig. 4 shows the temperature-entropy diagram for the corresponding cycle. Air is first compressed by compressor A and flows through duct G to the comprex C. It is there compressed further, as just described, and then passes through fan F. The fan may be necessary to overcome pressure drops in the high-pressure ducts and combustor B. Fuel is then burned in the air entering the combustor. Some of the resulting gas expands in the comprex and flows through duct P to the turbines. Since all of the gas cannot expand in the comprex, the remainder, tempered by cool air from duct D, flows through E to the high-pressure turbine H. The gas leaving this turbine mixes with that from the comprex and expands in the low-pressure turbine T. The comprex rotor is connected to a motor or turbine, M.

At this point one would naturally ask how this cycle, using a comprex, compares with the familiar simple cycle. One might expect that the performance would be similar to that of a simple cycle having the same over-all pressure ratio and having a turbine-inlet temperature equal to that of the gas entering the comprex. Alternatively, one might consider that the additional power, over that of a simple cycle using the same compressor and low-pressure turbine, is about that developed by the high-pressure turbine, H. Dr. Meyer (1)[1] expects that for a particular unit the power would be increased by 80 per cent and the efficiency by 25 per cent.

FLOW ANALYSIS

In the remaining part of this paper an analysis of the operation of the comprex is presented. Its purposes are to relate the various flow parameters to each other, thereby determining which may be independent, and to provide a means for making a preliminary design. For this analysis the following assumptions are made:

1 The problem is considered as one-dimensional within each cell.

2 There is no heat or work transfer to the cell walls. The former assumption is justified by statements made by Dr. Meyer (1); the latter is true for constant cell diameter and helix angle.

3 The pressure and velocity on each side of a surface of separation between gas and air are equal, that is,

$$p_1 = p_6, \text{ and } w_1 = w_6$$

also

$$p_2 = p_4, \quad \text{and} \quad w_2 = w_4$$

In drawing the curves presented herein it is further assumed that $w_1 = w_3$, which is equivalent to requiring that $\beta_1 = \beta_3$ or $c_1 = c_3$. This assumption is not essential to the analysis, provided that angles β_1 and β_3 and velocities c_1 and c_3 are so chosen

[1] Numbers in parentheses refer to the Bibliography at the end of the paper.

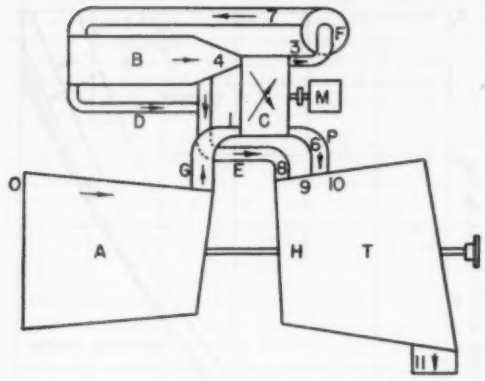

FIG. 3 GAS TURBINE WITH COMPREX AS HIGH-PRESSURE STAGE

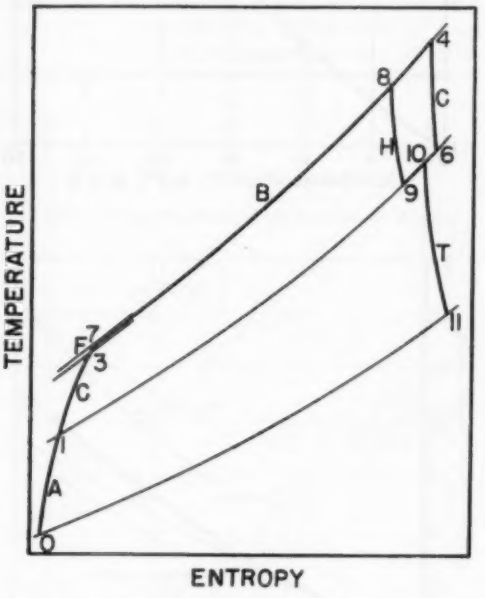

FIG. 4 TEMPERATURE-ENTROPY DIAGRAM FOR GAS-TURBINE CYCLE WITH COMPREX

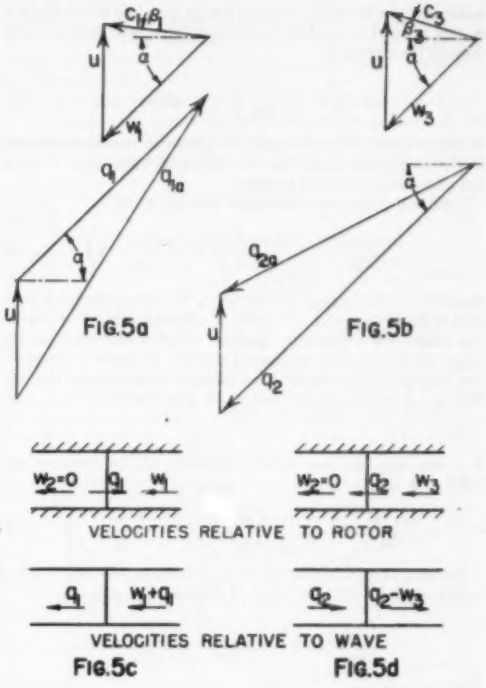

FIG. 5 VELOCITY DIAGRAMS

that the helix angle α and the rotor velocity u are the same in both the low and high-pressure-velocity triangles, Fig. 5(*a*) and (*b*).

4 Losses due to mixing and leakage are neglected. The former may be minimized by keeping the angle β small and thereby reducing radial pressure gradients at the surfaces of separation.

5 Pressure and velocity changes occur only in moving waves of negligible thickness which do not reflect from the cell ends. A method of reducing the resulting errors for the expansion waves is briefly discussed.

6 The air and gas obey the perfect gas law, $pv = RT$.

The first task is to relate the over-all pressure ratio, p_2/p_1, to the scavenging velocity w_1. As a first approach, let us assume that the waves causing the pressure increments in the air are normal shocks. Consider the first compression wave, moving to the right with speed q_1, which separates the inlet air moving to the left at w_1 from the air in state 2, which is at rest relative to the rotor. These velocities are shown in the top part of Fig. 5(*c*); below, the flow velocities are shown relative to the moving shock which then appears to be stationary. The well-known normal-shock relations now enable one to calculate the properties of the air in state 2, if the Mach number before the shock is set equal to

$$\frac{w_1 + q_1}{\sqrt{kgRT_1}} = \frac{w_1 + q_1}{49.04\sqrt{T_1}}$$

Consider now the second shock, which separates region 2 from region 3. Fig. 5(*d*) illustrates the corresponding transformation of velocities. Upon relating w_1 and w_2, one may calculate similarly the air properties in state 3 which are those of the leaving high-pressure air. By carrying through a number of such calculations, with $w_1 = w_3$, one may draw a curve, such as the line marked "normal shock" in Fig. 6, relating the over-all pressure ratio to the scavenging velocity, as was required.

Unfortunately, the preceding analysis cannot be applied to the expansion process, since the resulting decrease in entropy cannot occur without heat transfer, which has been barred out. Also, losses other than those inherent in a shock are not allowed for. Focusing attention on the first compression wave separating states 1 and 2, one may write the first law of thermodynamics which

states that the change in internal energy plus kinetic energy of a system is equal to the heat transferred (zero here) less the work done by the system, as

$$U_2 - \left(U_1 + \frac{w_1^2}{2gJ}\right) = -p_1(v_2 - v_1) \quad [1]$$

It will be noted that this equation applies to a system comprising a unit weight of air and that the flow-work term, $p_1(v_2 - v_1)$, is not a function of variable pressure.

Equation [1] may be rearranged into the form

$$\frac{(w_1/\sqrt{T_1})^2}{2gJ} = \frac{h_2 - h_1}{T_1} + R\frac{T_2}{T_1}\left(\frac{p_1}{p_2} - 1\right) \quad [2]$$

in which the scavenging velocity $w_1/\sqrt{T_1}$, is expressed as a function of T_2/T_1 and p_2/p_1. In order to relate these latter two ratios one might use a dynamic equation, which would result in the same solution as that for normal shocks. In order to allow for the presence of friction or other losses one may assume that the flow is polytropic, as expressed by the following equation

$$pv^n = \text{const} \quad [3]$$

For this case one may rewrite Equation [2], for constant specific heats, as

$$\frac{(w_1/\sqrt{T_1})^2}{2gJc_p} + 1 = \left(\frac{p_2}{p_1}\right)^{\frac{n}{n-1}}\left(\frac{k-1}{k}\frac{p_1}{p_2} + \frac{1}{k}\right) \quad [4]$$

Turning attention now to the second wave, between states 2 and 3, one may write the first law of thermodynamics as

$$\left(\frac{w_3^2}{2gJ} + U_3\right) - U_2 = -p_2(v_3 - v_2) \quad [5]$$

This rearranges to

$$\frac{(w_3/\sqrt{T_3})^2}{2gJ} = \frac{h_2 - h_3}{T_3} + R\left(\frac{p_2}{p_3} - 1\right) \quad [6]$$

or, for polytropic flow, to

$$\frac{(w_3/\sqrt{T_3})^2}{2gJc_p} + \left(\frac{p_3}{p_2}\right)^{\frac{n}{n-1}} = \frac{k-1}{k}\frac{p_2}{p_3} + \frac{1}{k} \quad [7]$$

Curves of p_2/p_1 against $w_1/\sqrt{T_1}$ and p_3/p_2 against $w_3/\sqrt{T_3}$ may now be plotted from Equations [4] and [7]. By assuming a value for $w_1/\sqrt{T_1}$, one may calculate the corresponding value of $w_3/\sqrt{T_3}$ and, as a result, the over-all pressure ratio p_3/p_1, can be found. Fig. 6 shows the resulting curves for a number of values of n, with $w_1 = w_3$ and $k = 1.4$.

Either by writing the corresponding equations, or by comparing the flow patterns, it may be seen that Equations [2] and [6] apply to the expansion waves if the subscripts are altered suitably. Therefore, Figs. 6 and 7 also apply to the expansion process, provided that in order not to violate the second law of thermodynamics, one uses values for n of 1.4 and 1.45 for the compression and of 1.3, 1.35, and 1.4 for the expansion process. (The curve for $n = 1.45$, in Fig. 6, lies between those marked "$n = 1.4$" and "normal shock" for values of $w_1/\sqrt{T_1} > 18$; it is omitted for clarity.)

For gas-turbine applications the expanding gas will be hot. Consequently, the assumptions that the gas has constant specific heats and that their ratio equals 1.4, used in the curves cited, are hardly satisfactory. Therefore a curve is presented, marked "$T_6 = 1660$," for which Equations [2] and [6] were used and for which it was assumed arbitrarily that $T_6 = 1660$ deg R, and that the flow is isentropic. This curve may be compared with that marked $n = 1.4$ which it closely approximates.

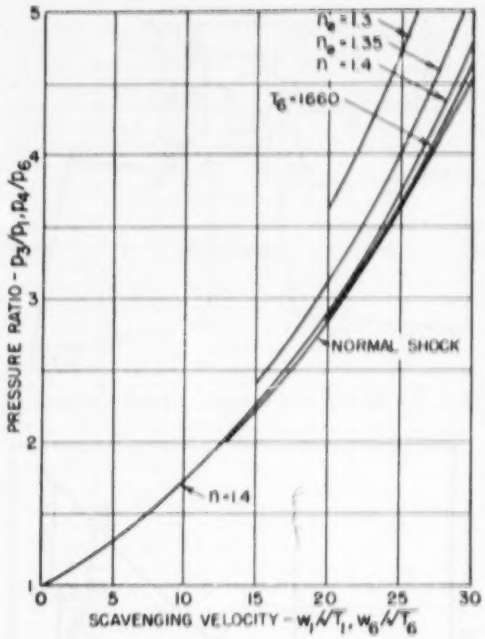

FIG. 6 PRESSURE RATIO VERSUS SCAVENGING VELOCITY

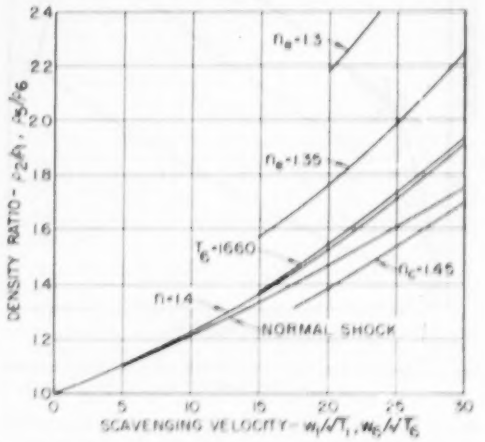

FIG. 7 DENSITY RATIO VERSUS SCAVENGING VELOCITY

It must be emphasized that the author does not intend that any of the curves of this paper will represent actual operating characteristics. In Fig. 6, for example, it is expected that an actual curve for the compression process would be nearly the same as that marked normal shock for low scavenging veloci-

ties and would be below it for higher velocities. It would intersect the curve marked "n = 1.45" at one point. Similarly, a curve for the expansion process would be asymptotic to that marked n = 1.4 for low scavenging velocity and would be above it for higher velocities, intersecting that marked "n = 1.35" at one point. In Figs. 9 and 10 the operating curve would be in a single line.

The main weakness of the foregoing analysis, and of the design procedure based upon it, is that the expansion waves are not very thin, as was assumed, but increase in thickness with time. Among the methods for obtaining a more accurate idea of the flow is the method of characteristics. This was used to obtain Fig. 8 which shows the isentropic expansion of the gas for a scavenging velocity $w_6/\sqrt{T_6}$ of 13.6. The expansion wave has been divided into three equal parts, each being indicated by a dashed line. It may be noted that the disturbances in the expanding gas flow produce corresponding disturbances in the entering air flow. Therefore, for an accurate design, it would be necessary to apply the method of characteristics, or an equivalent method, to the whole flow in the rotor. The hydraulic analogy (2) might be used to study the wave patterns qualitatively.

If, now, one chooses an over-all pressure ratio and makes suitable assumptions regarding the compression and expansion processes, one may find from Fig. 6, values for $w_1/\sqrt{T_1}$ and $w_6/\sqrt{T_6}$. Since $w_1 = w_6$, one may calculate the required ratio T_6/T_1. Fig. 9 shows the results of a number of such calculations, with each line labeled to indicate the assumptions regarding the compression and expansion processes used. This figure shows that for gas-turbine applications, where T_6/T_1 must be greater than 1, some irreversibility in the expansion process is essential—a surprising result.

To show this, consider, for example, the limiting case of isentropic compression and expansion, and let low-pressure air be introduced at any arbitrary velocity. Then the air will be compressed to the required pressure, as given by the curve marked

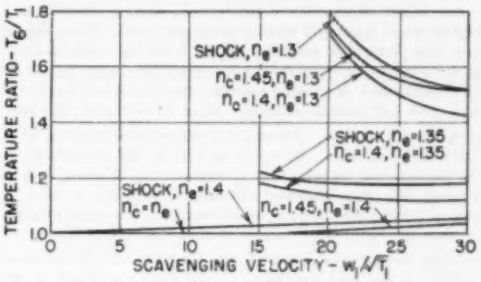

FIG. 9 TEMPERATURE RATIO VERSUS SCAVENGING VELOCITY

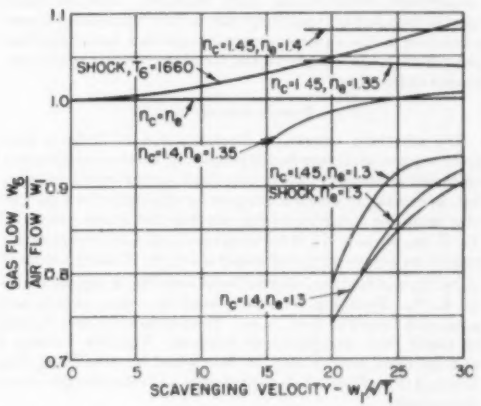

FIG. 10 FLOW RATE RATIO VERSUS SCAVENGING VELOCITY

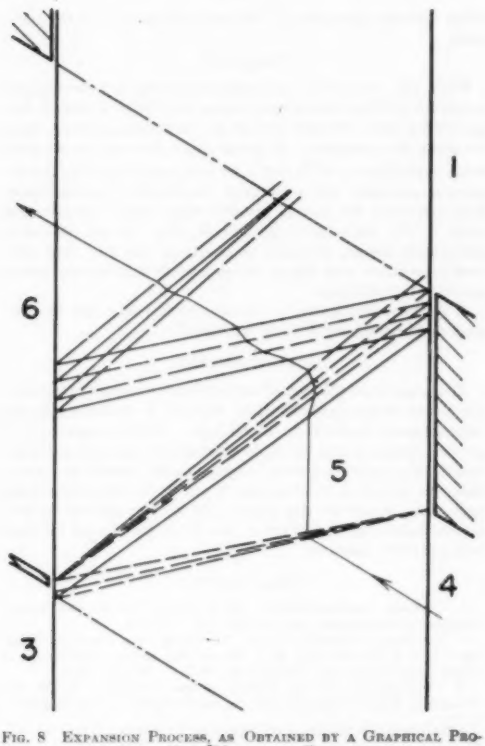

FIG. 8 EXPANSION PROCESS, AS OBTAINED BY A GRAPHICAL PROCEDURE BASED UPON METHOD OF CHARACTERISTICS

n = 1.4 in Fig. 6. Since the over-all pressure ratio is the same function of scavenging velocity for the isentropic expansion as for the isentropic compression, because one process is the reverse of the other, the values of $w_1/\sqrt{T_1}$ and $w_6/\sqrt{T_6}$ must be the same. Because $w_1 = w_6$, the gas temperature T_6 must equal the air temperature T_1 (as is shown by the line marked "$n_c = n_e$" in Fig. 9, and, consequently, $T_3 = T_6$. It is therefore apparent that no fuel may be burned in the high-pressure air. Equation [8], presented later, shows that all of the air which is compressed must be expanded again in the comprex; the line marked $n_c = n_e$ in Fig. 10 shows the same result. In this limiting case, the comprex thus serves to compress and expand an air stream reversibly and exhausts it in the same state as that in which it entered. Therefore it may be omitted from a cycle in which it occurs without any effect on that cycle. Consequently, a gas-turbine unit in which combustion may occur only on the high-pressure side of the comprex would not operate.

A turbosupercharger is a machine which may perform the same functions as a comprex, namely, to compress air and expand gas without requiring any net shaft power. However, one may not mentally replace a comprex by a turbosupercharger, because the latter has one more degree of freedom than the comprex. Unlike the comprex, fixing the compressor and turbine efficiencies and the compressor entering and turbine leaving temperatures does not fix the pressure ratio. A turbosupercharger therefore operates usefully, indeed, most usefully, when the flow in the compressor and turbine is isentropic.

One might inquire how a gas turbine, using a comprex as a high-pressure stage, will operate under part load. Some insight into this problem is provided by the following considerations: If, for example, under part-load operation the volume flow of air after compressor A remains constant, the flow velocity c_1 in the inlet port will remain constant. Since T_1 will drop, the ratio $c_1/\sqrt{T_1}$ will increase. Because c_1 is proportional to w_1, $w_1/\sqrt{T_1}$ will likewise increase. As shown in Fig. 9, the temperature of the gas entering the low-pressure turbine must decrease, and, as a result, the cycle efficiency will drop. Therefore, in order to help maintain high efficiency under part load, one would attempt to have the compressor operate so that the volume flow of air entering the comprex decreases, and the ratio $c_1/\sqrt{T_1}$ decreases slightly as the load decreases. Under such conditions, if the flow efficiencies in the comprex did not alter, the turbine-inlet temperature could remain fairly constant. This conclusion must be modified for a particular case to take into account altered efficiencies in the comprex, due to its operation under part load away from design conditions, and the characteristics of the compressor and turbines.

Design Procedure

The next task, namely, to determine how to design a comprex, requires an answer to the problem of which quantities may be chosen arbitrarily. There is no single answer to this question, but, in general, to design a comprex for application to a gas turbine using the foregoing results, one will first choose values for T_6, T_1, p_1, air flow W_1, n for compression and for expansion (or equivalent parameters), and angles α and β. Then the value of $w_1/\sqrt{T_1}$, and hence w_1, may be found from Fig. 9, against the ratio T_6/T_1. From Fig. 7 one may read the values of ρ_2/ρ_1 and ρ_5/ρ_6, and from Fig. 6 of p_2/p_1. Temperatures T_3 and T_4 may be found from the polytropic relations. The flow velocity c and the rotor speed u may be determined by considering Fig. 5(*a*) and (*b*). Thus all state properties and velocities have been determined.

The gas flow W_4, which is different from the air flow, is found by recollecting the assumption that no energy is transferred to the rotor. Consequently, for steady flow

$$\frac{W_5}{W_1} = \frac{h_2 - h_1}{h_4 - h_6} \cong \frac{T_2 - T_1}{T_4 - T_6} \quad \ldots\ldots [8]$$

The gas flow may also be found by noting that the volume flow of gas in state 5 must equal that of air in state 2, or

$$\frac{W_5}{\rho_5} = \frac{W_6}{\rho_5} = \frac{W_2}{\rho_2} = \frac{W_1}{\rho_2}$$

Therefore

$$\frac{W_6}{W_1} = \frac{\rho_5}{\rho_2} = \frac{\rho_5/\rho_6}{(\rho_2/\rho_1)(T_6/T_1)} \quad \ldots\ldots [9]$$

Equations [8] and [9] have been found to check satisfactorily, which is rather encouraging in the light of their totally different derivations. Fig. 10, based upon Equation [9], shows that the scavenging velocity, and therefore the over-all pressure ratio, is limited if the gas flow is to be less than the air flow.

Since all fluid properties, velocities, and flow rates have been determined, the dimensions of the comprex may now be found. The port areas, normal to the axis of rotation, are calculated from

$$A_1 = rm_1 = \frac{W_1 T_1 R}{p_1 c_1 \cos \beta_1} \quad \ldots\ldots [10]$$

$$A_2 = rm_2 = \frac{W_1 T_2 R}{p_2 c_2 \cos \beta_2} \quad \ldots\ldots [11]$$

$$A_4 = rm_4 = \frac{W_6 T_4 R}{p_6 c_4 \cos \beta_4} = \frac{W_6 T_4}{W_1 T_2} A_2 \quad \ldots\ldots [12]$$

$$A_6 = rm_6 = \frac{W_6 T_6 R}{p_6 c_6 \cos \beta_6} = \frac{W_6 T_6}{W_1 T_1} A_1 \quad \ldots\ldots [13]$$

if the flow in the ports is assumed to be uniform.

By noting that $m_1 + m_6$ nearly equals the total circumference, and by assuming a value for r/d, one may compute the mean cell diameter d, and the radial cell height r. The continuity relation

$$W_1 = \rho_2 u r L = \rho_1 w_1 r m_1 \cos \alpha \quad \ldots\ldots [14]$$

may be solved for the rotor length L

$$L = \frac{m_1 w_1 \cos \alpha}{u(\rho_2/\rho_1)} \quad \ldots\ldots [15]$$

These formulas determine all the major dimensions of the comprex.

Conclusion

While the analysis of the comprex developed here neglects a detailed study of the various losses, it is believed that it has provided a fairly accurate idea of the restrictions existing upon the design of a comprex. In particular, it has been shown that fixing values for $w_1/\sqrt{T_1}$ and n for compression and for the expansion processes (or equivalent parameters) automatically fixes values for the over-all pressure ratio, p_2/p_1; temperature ratio, T_6/T_1; and relative gas flow, W_4/W_1. On the basis of a preliminary design, obtained as described, one may next proceed to evaluate each loss so far as possible and thereby arrive at a more refined design.

A further investigation of the application to a gas turbine, such as described, seems to be warranted.

Acknowledgments

This paper is an abstract of two seminars presented in a graduate course on gas turbines under Prof. C. R. Soderberg at the Massachusetts Institute of Technology. Written reports (3, 4) on the seminars are on file in the mechanical-engineering department. The author is greatly indebted to Mr. Harold M. Coverdale[3] the author of the first report, and to the Department for permission to publish this paper. He is most grateful to Professors Soderberg, E. S. Taylor, and W. R. Hawthorne for their help and encouragement.

Bibliography

1 "Recent Developments in Gas Turbines," by Adolph Meyer, *Mechanical Engineering*, vol. 69, 1947, pp. 274–275.

2 "A Study of Gas Flow in the 'Comprex' by a Hydraulic Analogy," by J. J. Hinchey and R. F. Sweek, MS thesis, Department of Naval Construction and Engineering, M.I.T., Jan. 16, 1948.

3 "Introduction to the Theory of the Comprex," by H. M. Coverdale, Term Project No. 10, Course 2.214, M.I.T., April, 1947.

[3] Consolidated Mining and Smelting Company, Trail, B. C., Canada.

4 "Theory of the Comprex," by F. W. Barry, Term Project No. 11, Course 2.214, M.I.T., May, 1947.

5 "Swiss Develop New Gas Turbine Units," by Adolph Meyer, *Electrical World*, vol. 127, Jan. 4, 1947, pp. 38–40.

6 "Recent Gas Turbine Developments at Brown Boveri," by P. R. Sidler, Proceedings of the Midwest Power Conference, sponsored by the Illinois Institute of Technology, vol. 9, 1947, 345 pp.

7 "Pressure Exchanger," U. S. Patent no. 2,399,394, April 30, 1946.

8 "Where Gas Turbine Will Fit in Future Power Fields," by Hans Pfenninger, *Power*, vol. 69, January, 1947, pp. 87(25)–88(26).

Appendix

The second analysis did not yield the wave velocities q_1 and q_2 explicitly. In case these should be desired, they may be found easily from the requirement that the directions of wave motions shown in Fig. 1 must be the same as those of the absolute wave velocities q_{1a} and q_{2a}, shown in Fig. 5(*a*) and (*b*). Thus for the first compression wave

$$\frac{L}{m_1 - L \tan \beta_1} = \frac{q_1 \cos \alpha}{q_1 \sin \alpha + u} \quad \ldots\ldots\ldots [16]$$

By introducing the continuity relation, Equation [14], one may solve for q_1

$$q_1 = \frac{w_1 u}{(\rho_2/\rho_1)u - w_1(\sin \alpha + \cos \alpha \tan \beta_1)} = \frac{w_1}{(\rho_2/\rho_1) - 1} \quad \ldots [17]$$

Similarly

$$q_2 = \frac{w_2 u}{w_2(\sin \alpha + \cos \alpha \tan \beta_2) - u(\rho_2/\rho_2)} = \frac{w_2}{1 - (\rho_2/\rho_2)} \quad \ldots [18]$$

Use of an Optical Property of Glycerine-Water Solutions to Study Viscous Fluid-Flow Problems

By W. W. HAGERTY,[1] ANN ARBOR, MICH.

It is a property of certain concentrations of glycerine-water solutions, when in a state of steady flow, that the planes of equal shear in the liquid become visible in ordinary light, if viewed along a path tangent to the shear plane. This phenomenon has been used successfully to study a fluid-flow problem at the University of Michigan. The nature and scope of application of this optical property is currently being studied further. This report gives details of what may prove to be a useful tool in certain phases of experimental fluid-flow problems.

IN order to facilitate the description of the property of certain concentrations of glycerine-water solutions, for the planes of equal shear in the liquid to become visible in ordinary light when in a state of steady flow, its application to a particular problem will be described. It was desired to study further the secondary motion of a fluid in an annulus in the case where the inner cylinder or annulus wall is rotating about its axis, the outer wall is stationary, and the annulus is bounded on the ends by fixed planes. Figs. 1 and 2 show the apparatus used in this study. The inner cylinder is a metal tube of $4^1/_4$ in. OD. The outer tube is made of lucite and has an inner diameter of $5^1/_2$ in., so the thickness of the annulus is $^5/_8$ in. A plexiglas box is provided around the annulus; and when filled with liquid of suitable index of refraction, eliminates the optical distortion caused by the curved surface of the cylinders.

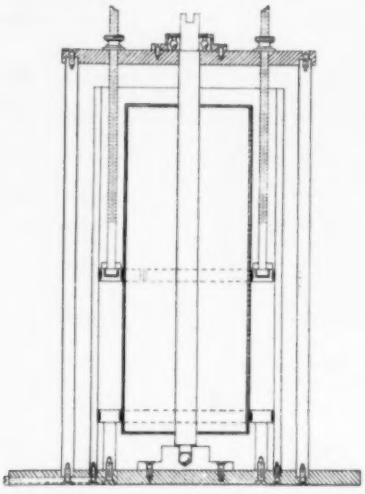

FIG. 1 SKETCH OF EXPERIMENTAL APPARATUS

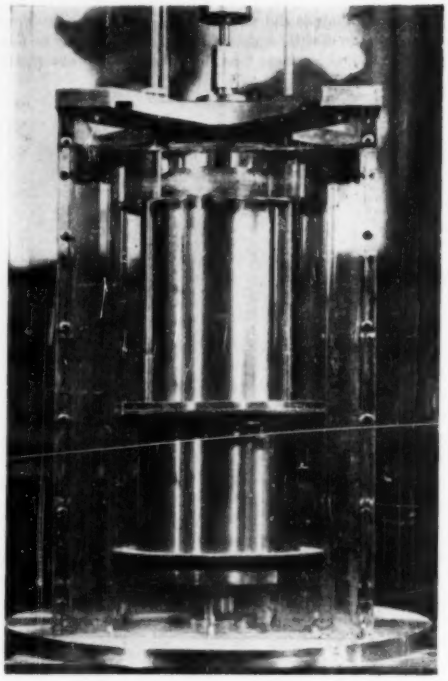

FIG. 2 EXPERIMENTAL APPARATUS

There are three modes of flow when the annulus is very long:

1 When the inner cylinder rotates slowly, all particles move in circular paths concentric with the axis of the cylinders. This is a form of Couette motion.

2 As the speed of rotation of the inner cylinder is increased, a stable secondary motion develops. Pairs of ring vortices appear as shown in Fig. 3. In this motion each particle of fluid rotates

[1] Assistant Professor of Engineering Mechanics, University of Michigan. Jun. ASME.

Presented at the National Meeting of the Applied Mechanics Division, Ann Arbor, Mich., June 13–15, 1949, of THE AMERICAN SOCIETY OF MECHANICAL ENGINEERS.

Discussion of this paper should be addressed to the Secretary, ASME, 29 West 39th Street, New York, N. Y., and will be accepted until April 10, 1950, for publication at a later date. Discussion received after the closing date will be returned.

NOTE: Statements and opinions advanced in papers are to be understood as individual expressions of their authors and not those of the Society. Paper No. 49—APM-21.

simultaneously about the axis of the rotating cylinder and about the core of the ring vortex of which it is a part.

3 At relatively high speeds of rotation, the vortex motion becomes unstable, and the motion becomes generally irregular or turbulent.

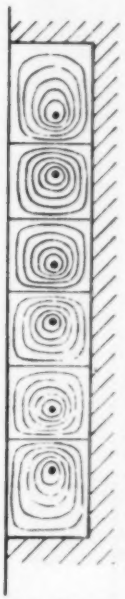

FIG. 3 PATTERN OF SECONDARY FLOW, SHOWING A 3-PAIR SYSTEM OF VORTICES (Moving wall is on left side.)

EXPERIMENTAL WORK

G. I. Taylor solved the problem, theoretically and experimentally, of determining the critical speed at which the vortex motion first appeared.[2] He also established its initial form and reported his observations on the changes in the form of the motion as the speed of rotation of the inner cylinder was increased. The specific object of the recent study was to learn more about the stability of the vortex motion and to determine the effect of the fixed end planes with an annulus of short axial length.[3]

A typical observation is made by causing the inner cylinder to rotate at a speed below that speed at which the secondary motion will develop. The fluid then moves with Couette motion. The speed is then slowly increased until the first evidences of secondary motion appear as shown in Fig. 4. The speed is then held constant while the development continues as in Figs. 5, 6, and 7. The particular vortices shown in these illustrations are the second and third from the top in Fig. 3. In this case the second vortex will develop more rapidly than the third due to its proximity to the end plane. Farther from the end plane, all vortices develop at more or less the same rate. Fig. 4 shows the initial phase of the development of the secondary flow. It should be borne in mind that the thickness of the annulus is $^5/_8$ in. and that eventually the vortices will be approximately square. Initially the disturbance is of a random nature. The developed vortex shown at the top in Fig. 4 was due to the presence of the end plates. This vortex was caused by the boundary conditions of the problem, and is a disturbance of a different nature from the one under discussion. After a time one of the disturbances will develop as shown in Fig. 5. This view was taken at the same position but does not represent a development of any of the particular disturbances in Fig. 4. However, it represents the next stage in the development of a vortex.

Fig. 6 shows a later stage in the development. The top vortex has developed from the disturbance, and by its motion has caused the adjacent fluid to start the vortex motion, rotating in the opposite direction. Fig. 7 shows a late stage with both vortices about fully developed. Fig. 8 shows an intermediate stage of development of vortices some distance from the end plane. It can be seen that they are about equally developed and that adjacent vortices are rotating in the opposite sense.

The lines which appear look something like the lines which result from an imperfect mixture of two liquids having different indexes of refraction, such as glycerine and water, or alcohol and water. In order for the lines to be readily visible, the solution should contain at least 70 per cent glycerine. The clarity of the lines increases with the glycerine concentration, at least up to 95 per cent glycerine. To obtain higher percentages of glycerine, the experimental apparatus must be protected against exposure to the atmosphere. Due to its strong hygroscopic action, the glycerine will absorb about 4 or 5 per cent water from the air. The kinematic viscosity of a 95 per cent concentration is about 20 times that of a 70 per cent concentration, so this is a useful range of values.

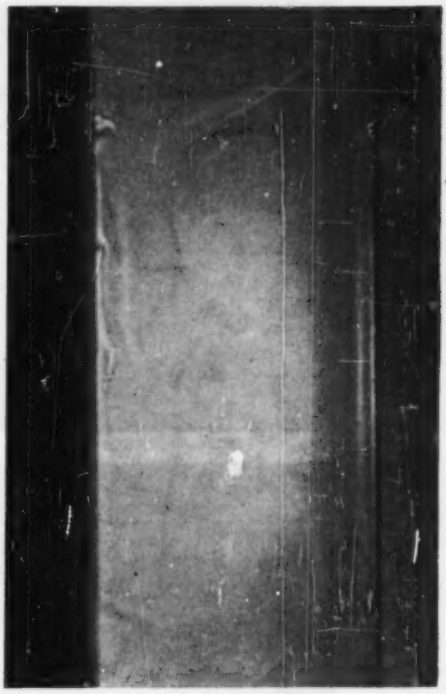

FIG. 4 INITIAL DEVELOPMENT OF SECONDARY MOTION (Moving wall is on left side.)

The number of lines observed seems to be proportional to the speed of rotation of the ring vortices. With increasing speeds the lines become increasingly finer and more numerous, and finally they become so close together that they no longer can be distinguished separately by eye. Actually, hundreds or thousands of lines are seen, but the clearest are those normal to the line of vision. As one moves about the annulus at the same elevation, the picture does not change, since the disturbance is independent of angular position. Additives in the liquid obscure the lines, so the solution should be as clean as possible.

VISIBILITY OF LINES OR EDGES OF PLANES

It is not known at this time just why the lines or edges of planes are visible. Several different concepts have been considered. Some of these have been rejected and some are still being considered and studied. The principal ideas that have been entertained to date follow:

[2] "Stability of a Viscous Fluid Contained Between Two Rotating Cylinders," by G. I. Taylor, Philosophical Transactions of the Royal Society of London, series A, vol. 223, 1923, pp. 289–343.

[3] "A New Factor in the Design of Hydraulic Seals," by W. W. Hagerty, Proceedings of the National Conference on Industrial Hydraulics, 1947, pp. 122–129.

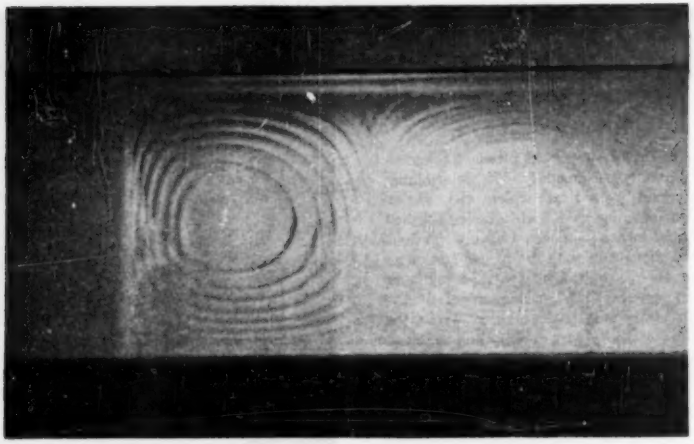

FIG. 7 WELL-DEVELOPED SECONDARY MOTION

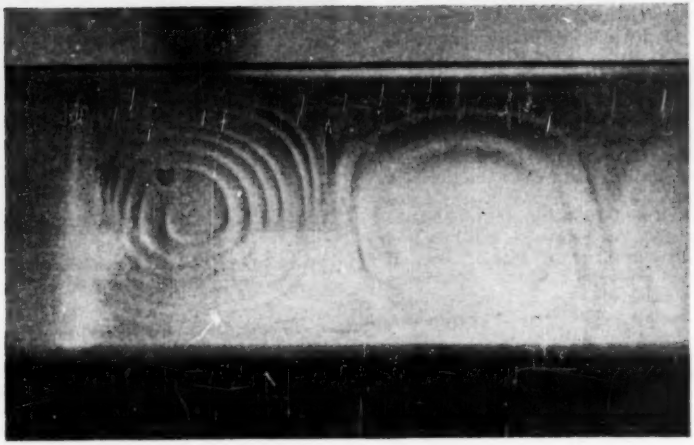

FIG. 6 CONTINUED DEVELOPMENT OF SECONDARY MOTION
(Top vortex is more developed than bottom one because it is near fixed end plane of annulus.

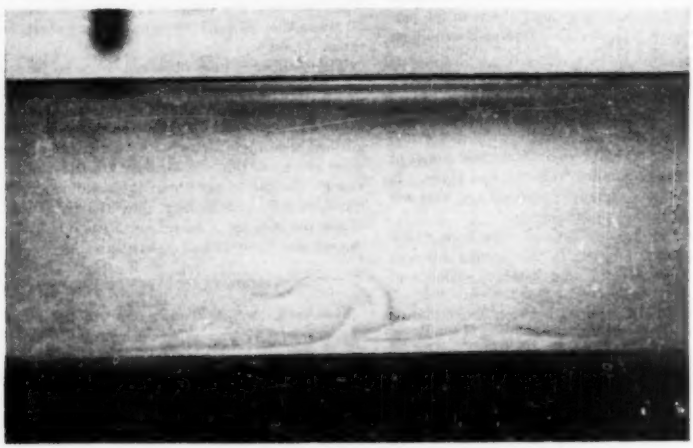

FIG. 5 EARLY STAGE IN DEVELOPMENT OF SECONDARY MOTION

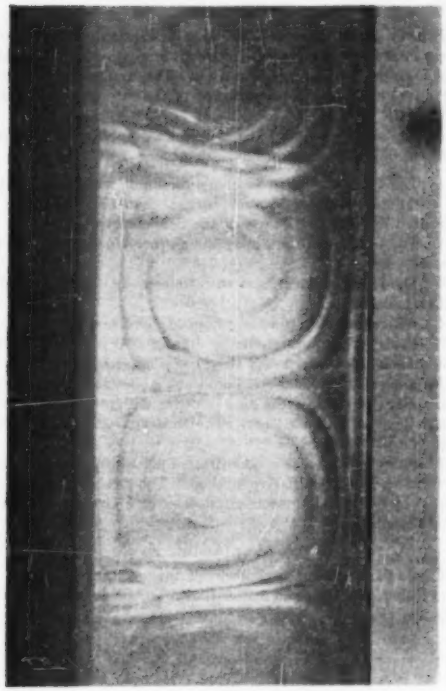

FIG. 8 INTERMEDIATE STAGE OF DEVELOPMENT OF SECONDARY MOTION AT A POSITION IN ANNULUS SOME DISTANCE FROM END PLANES
(Note adjacent vortices are rotating in opposite sense.)

1 The first thought was that the axes of the glycerine molecules became oriented in some regular manner due to the steady nature of the flow. The appearance of the lines could then be explained by double-refractive properties of the glycerine. When this was investigated, it was found that the length of glycerine molecules is too short to affect the visible light waves. Water and glycerine molecules apparently do combine in certain proportions to form molecular chains, which are no doubt longer than single glycerine molecules. The manner of formation of these chains seems to be somewhat obscure, but the best information that has been received is that these chains are not long enough for their orientation to produce a visible effect.

2 It was found rather early that the lines appeared to be clearer if the background was a bright surface which reflected sunlight. This led to the idea that the light was partially polarized. Apparatus similar to the optical benches used in photoelasticity was set up to test this idea. No improvement of any kind was noticed with any arrangement of polarizing screens and lights that could be tried. Apparently this phenomenon is not the same as the double refraction of Canadian balsam, for example.

3 The lines were viewed using Schlieren apparatus, but no improvement was noticed.

4 It was observed that the lines became fainter with time when the motion is continued in steady state for periods of 5 to 30 min, depending upon the speed of rotation. At very low speeds, when the secondary flow just appears, the lines are clearly visible for longer periods than at high speeds. This gave rise to the idea that the lines were due to thermal gradients which decrease with time due to thixotropic behavior of the glycerine-water solution. When the solutions used were tested in a viscosimeter, they did exhibit a mild thixotropy in that the viscosity decreased about 5 per cent under continuous testing. This did not account for the eventual complete vanishing of the lines. In addition, several oils of equal or greater viscosity and with about the same specific heat were tested in the annulus, but nothing could be seen in any of those tested. Therefore the phenomenon did not seem to be due to thermal gradients alone.

5 Another observed fact is that when the rotation is suddenly stopped and the whole system is at rest, the lines are still visible. After a time they become irregular and sink very slowly as though by gravity. To explain this, it was thought that the fluid motion produces an actual separation of the water from the glycerine, and that the lines are due to the difference, in the index of refraction, of the pure glycerine from that of the glycerine-water solution. It has not been possible to make a critical test of this motion by using absolutely pure glycerine. Due to its hygroscopic property and to the open construction of the test apparatus, the glycerine used thus far has always had some water in solution. In addition, the entire notion of separation seems to be weakened somewhat, since the visibility of the lines improves with increasing concentrations of glycerine. This means that the contrast between the refractive index of pure glycerine and that of the glycerine-water solution would be rather slight. Another critical test yet to be made is to conduct the test with the machine on its side to see whether the lines still sink in the direction of gravity. Brief tests with other containers indicate that such is the case.

TECHNIQUE FOR STUDYING FLUID FLOW

At the present time, the polarized light and Schlieren techniques have been abandoned, at least temporarily, but the other ideas listed are being studied. The technique now being used to study fluid flow is to provide a diffused indirect light so that the lines may be viewed against a white background which is bright but not shiny, Fig. 9. The light is directed against a screen of ordinary white vellum, and the observer or camera is then normal to the screen. Satisfactory results are also obtained by backlighting the vellum.

From the illustrations shown it is evident that this technique has been very useful in the study of this particular problem. It is believed that this method may help to obtain the shear pattern,

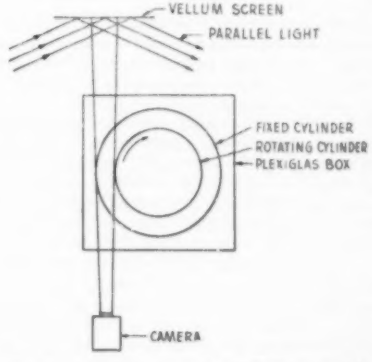

FIG. 9 ARRANGEMENT FOR TAKING PHOTOGRAPHS

in many cases, of steady flow. For example, in the case of rotating cylinders, the effect of the corners on the Couette motion is clearly visible. It is also possible to see the effect of the velocity discontinuity where the inner rotating cylinder and the fixed end plane are very close together.

Furthermore, it may be possible to do some useful work in boundary-layer studies. It may show the exact state of flow or the laminar boundary layers, and the development of instabilities in the boundary layer. Where the flow near the boundaries is observed, however, the number of lines increases as the velocity gradient increases. They are then more difficult to distinguish separately. It may be necessary, therefore, to devise fairly elaborate equipment such as is used to determine the so-called surface stresses in three-dimensional photoelasticity.

It is believed that the relation between the velocity gradient and the spacing of the lines can be calibrated from known laminar-flow configurations. This would then be a quantitative method as well as a qualitative one. Such known flows include the Couette motion in the case of long cylinders, Poiseuille flow in pipes, and flow around a flat disk due to its rotation about its axis.

The residual pattern may also be useful. When small balls and sticks are dropped or moved through a body of the glycerine-water solution, the disturbance is visible and lines remain after the motion has ceased.

Apparatus to study flow around objects of various shapes and to study boundary-layer separation is now being constructed. Only preliminary tests have been made, but these indicate that the flow pattern does become visible when the motion is steady or when the changes take place slowly. The latter is the case when critical speeds are approached with care.

Conclusion

When a glycerine-water solution is in a state of steady rate of shear or slowly changing rate of shear, lines appear in the liquid which show the flow configuration. The number of lines observed on each area is proportional to the rate of shear in that area.

An explanation of why the visible lines appear should agree with the following observations:

1 The lines appear in ordinary daylight, without additives in the fluid. The appearance is not changed by the use of polarized light or by the use of the Schlieren technique.

2 The number of lines increases as the velocity gradient increases.

3 The lines become fainter with time as the status quo of the fluid is maintained.

4 Where motion is suddenly stopped, the lines are still visible.

5 The residual lines gradually diffuse, as if by molecular action and sink downward very slowly as if by gravity.

An adequate explanation should aid in devising a technique and apparatus to bring the lines out to maximum clarity. They could then be magnified and thereby separated for cases with high velocity gradient.

This may prove to be a quantitative method of flow measurement as well as a qualitative method. The method may be calibrated by studying flow configurations which already have been solved theoretically.

Acknowledgment

The author wishes to acknowledge the assistance rendered by Mr. Robert W. Peach and Mr. Larry Talbot in studying this problem.

Holzer Method for Forced-Damped Torsional Vibrations[1]

By T. W. SPAETGENS,[2] VANCOUVER, B. C.

The forced and resonant-vibration characteristics of a torsional system are easily enough determined by the well-known Holzer methods, in the case where the only major damping influences available in the system are those of the prime-mover itself, or of the propeller, in the case of a propeller-propulsion system. Where a damper exists within the system, the classic solution confines itself to the determination of the *resonant*-vibration characteristics under optimum damping conditions, and utilizes the principle of energy balance in conjunction with an equivalent system. The problem of *forced* vibration in a system having a damper is not susceptible, however, to such simple treatment regardless of whether or not the damping is optimum. This paper outlines an exact method, whereby both the forced- and the resonant-vibration characteristics of a viscously damped system may be calculated for any existing damping condition, optimum or otherwise, and which utilizes the ever-popular Holzer form.

Introduction

THE conventional Holzer methods for treating free and forced vibration problems are well known. These conventional methods are applicable only to those systems wherein the damping effects are small enough so as to have no appreciable effect upon the natural frequencies and the vibrating shapes of the systems. As Den Hartog and Li point out,[3] in most practical systems having only inherent damping, the vibratory shapes, and the natural frequencies (as determined by free vibration) are not affected appreciably by this inherent damping and thus the widespread use of the conventional Holzer methods for the treatment of these practical systems is justified.

Nomenclature

The following nomenclature is used in the paper:

I = moment of inertia
ω = frequency
θ = torsional amplitude
m = harmonic forcing torque
$m' = m/10^6$
K = torsional spring constant
J = imaginary unit
ϕ = phase angle
C = torsional damping coefficient (general)
C_i = "inner" (mass to mass) torsional damping coefficient
C_o = "outer" (mass to ground) torsional damping coefficient
n = subscript, mass number

For torsional systems wherein the damping is derived chiefly from extrinsic sources of appreciable magnitude, the well-known Holzer methods no longer apply. Examples of such systems are those employing dampers and those in which the power transmission is affected by hydraulic or by electrical couplings. Den Hartog and Li[3] have discussed this and have shown the development of an extension to Holzer's conventional method whereby it is possible to treat systems which have large extrinsic (viscous) damping forces. In the case of a system with unequal discrete masses (most of the practical systems fall into this category) this method will permit the determination of the damped natural frequency and the amplitudes of the various masses (vibratory shape), where there is a forcing torque applied to one end of the system.

By utilizing this extended type of damped Holzer table and by introducing into it, in complex fashion, the harmonic forcing torques at the various masses (corresponding to the various cylinders of the prime mover under consideration) the author has found that the forced-vibration characteristics of a viscously damped system of any configuration can be determined completely. Since such a Holzer table contains the damping effects as well as the forcing effects, it can be used for the determination of the absolute amplitudes at all forcing frequencies, including the damped natural frequency, and the peak amplitude thus found indicates the value of the damped natural frequency.

Theory

In the paper[3] by Den Hartog and Li it is shown that when damping of a viscous nature is present in a system, the equations of torsional motion for the damped system differ from the equations of motion for the undamped system in that $I_n\omega^2 - j\omega C_{o_n}$ replaces $I_n\omega^2$, and $K_n + j\omega C_{n_i}$ replaces K_n, where C_{o_n} is the (outer) damping coefficient between the nth mass and the "ground" and C_{n_i} is the (inner) damping coefficient between the n and $n + 1$ masses. Hence these substitutions can be carried into the undamped Holzer table, some of the computations thereby becoming complex. As already inferred, it is only in those cases where the viscous damping torques are of such magnitude as to affect the natural frequency and vibratory shape of the system that these substitutions must be made.

In the more usual case, where the damping is not of sufficient magnitude to affect substantially either the natural frequency or vibratory shape, the free steady-state vibratory motions of the various masses are harmonic and in time phase with one another. Therefore the inertia torques of the various masses are in phase and when adding harmonic forcing torques (which are in phase

[1] After the author had investigated the problem of forced-damped torsional vibration, a rough draft was submitted to Prof. J. P. Den Hartog who commented kindly and pointed out that a similar development was shown in the book "Die Berechnung der Drehschwingungen," by H. Holzer, J. Springer, Berlin, 1922. However, not knowing of an account of this important problem in English literature the author feels that presentation of his investigation may be of interest, especially so since the Holzer book appears to be virtually impossible to procure.

[2] Stress and Vibration Analyst, Vivian Diesels and Munitions, Ltd.

[3] "Forced Torsional Vibrations With Damping: An Extension of Holzer's Method," by J. P. Den Hartog and J. P. Li, JOURNAL OF APPLIED MECHANICS, Trans. ASME, vol. 68, 1946, p. A-276.

Presented at the National Meeting of the Applied Mechanics Division, Ann Arbor, Mich., June 13–15, 1949, of THE AMERICAN SOCIETY OF MECHANICAL ENGINEERS.

Discussion of this paper should be addressed to the Secretary, ASME, 29 West 39th Street, New York, N. Y., and will be accepted until April 10, 1950, for publication at a later date. Discussion received after the closing date will be returned.

NOTE: Statements and opinions advanced in papers are to be understood as individual expressions of their authors and not those of the Society. Paper No. 49—APM-12.

or antiphased with each other) to the system, we compound them algebraically with the inertia torques because, for a system with zero damping, force and motion are either in phase or are antiphased.[4] When the forcing torques are not in phase at the various masses, a time dimension enters into the Holzer computations. Here, the forcing torque system is broken down into sine and cosine (quadrature, in time) components. The effect of these component force systems upon the corresponding sine and cosine motions is computed; remembering that there is either 0-deg or 180-deg phase angle between component torque and component motion so that here again the various Holzer table entries are compounded algebraically. Such a computation has been shown by Porter.[5]

When there is appreciable damping in the system, however, the motions of the masses are not in time phase even for "major" orders of excitation. Also, the component forcing torques at each mass are no longer in phase or antiphased with their respective components of motion at each mass, due to the damping. Thus it is that the conventional Holzer methods described thus far will not treat the forced-damped torsional-vibration problem. Since the phase angle between torque and motion, for damping, is neither 0 deg nor 180 deg but rather is an unknown, the harmonic forcing torques must be expressed as complex numbers in terms of this unknown and must be entered into the Holzer table as such. The Holzer table, it is noted, is already complex in nature due to the quadrature stiffness term of the damper.

Fig. 1(*a*) shows a simple single-mass system acted upon by an external damping torque $C(d\theta/dt)$

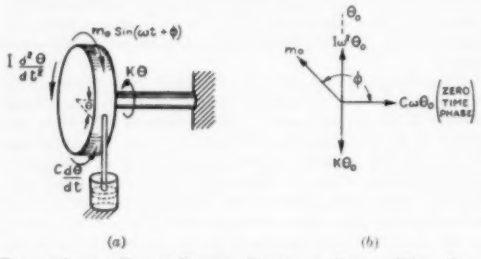

FIG. 1 SIMPLE FORCED-DAMPED TORSIONAL SYSTEM WITH CORRESPONDING VECTOR DIAGRAM

and by a harmonic forcing torque $m_0 \sin(\omega t + \phi)$. The differential equation of motion for this system is

$$I\frac{d^2\theta}{dt^2} + C\frac{d\theta}{dt} + K\theta = m_0 \sin(\omega t + \phi)$$

Fig. 1(*b*) is the vectorial representation of this equation. The solution is a sine wave $[\theta = \theta_0 \sin(\omega t + 90)]$, and the four torques of the foregoing equation are sine waves. The three torques on the left side of the equation are separated from each other by a phase angle of 90 deg since one differentiation of a sine wave results in another sine wave ahead of the first by 90 deg.

In a multimass system, a vector diagram, somewhat similar to that of Fig. 1(*b*), applies to each mass of the system. The diagram is of course different for each mass in that the vectors change in magnitude and phase; also the expressions for restoring torques of the shafts become $K(\theta_n - \theta_{n+1})$. If the damping exists "between" the various masses, then $C\omega\theta_n$ becomes $C\omega(\theta_n - \theta_{n+1})$. The harmonic forcing torques remain constant at each mass at which they act, that is, if we are considering an engine with identical cylinders, but the phase angle ϕ will remain the same only for a major order of excitation. The manner in which the vector diagram changes from mass to mass is, in reality, the physical concept of the two-dimensional Holzer table.

APPLICATION

The author first had occasion to investigate the problem of forced-damped torsional vibration while analyzing the vibration characteristics of a certain 10-cylinder Vivian marine Diesel-engine design. It was apparent, despite numerous attempts to retune the system and alter its vibratory shape, that a very serious 5th order critical existed only some 10 per cent above the maximum operating speed. The forced vibratory shear stress (nominal) set up in the crankshaft by this critical (calculated by the conventional Holzer method for forced vibration with zero damping) at the maximum operating speed was 9000 psi, while the resonant stress was 24,000. A Houdaille-Hershey viscous damper was then "applied" to the system, and the calculated resonant stress was lowered to 7000 with the peak of the damped critical now at some 8 per cent above the top operating speed. Since we consider that 4500 is about the maximum allowable vibratory stress (for continuous running) for the 10-cylinder crankshaft of this particular design, it was very important in this particular case to know in advance the behavior of the viscous damper away from resonance. Accordingly, the type of investigation shown here was made.

In order to illustrate the application of the theory in a brief manner, we will consider a fictitious 3-cylinder Diesel generator unit for which it is required to find the third-order vibratory amplitude at the front flywheel for a speed range of 675 to 725 rpm for the case where the unit is undamped (that is, where inherent damping only is present), and also for the case where a viscous damper is installed.

For simplicity, the harmonic torque, m, is considered to remain constant over the entire speed range under consideration. Torque-curve analysis has not been made for the model of engine used in this illustration, and the torque harmonic coefficients of Andriola,[6] which are well-suited to this engine, are used instead, although any other source of coefficients might have been used

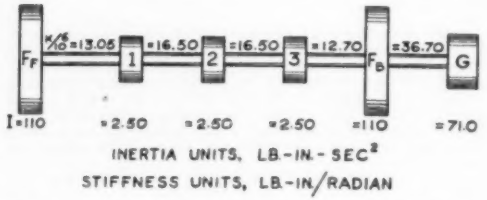

FIG. 2 EQUIVALENT ELASTIC SYSTEM OF 3-CYLINDER DIESEL-GENERATOR UNIT

since the problem is fictitious. Inherent damping in the undamped system is calculated by the formula of Lewis and Porter.[7] The equivalent elastic system is shown in Fig. 2.

[4] "Mechanical Vibrations," by J. P. Den Hartog, McGraw-Hill Book Company, Inc., New York, N. Y. third edition, 1947, p. 66.

[5] "Evaluation of Effects of Torsional Vibration," by the War Engineering Board of the SAE, New York, N. Y., 1945, pp. 226–229.

[6] "The Problem of Flywheel Effect and Speed Regulation for Diesel-Engine-Driven Machinery," by A. D. Andriola, Trans. ASME, vol. 60, 1938, pp. 119–125.

[7] Reference 5, p. 155.

TABLE 1 FREE VIBRATION HOLZER—FIRST MODE; $\omega^2 = 51{,}700$

MASS NO.	I	$I\omega^2/10^6$	θ	$I\omega^2\theta/10^6$	$\Sigma I\omega^2\theta/10^6$	$K/10^6$	TWIST
F_F	110	5.690	1.000	5.690	5.690	13.05	.436
1	2.50	.129	.564	.073	5.763	16.50	.350
2	2.50	.129	.214	.028	5.791	16.50	.351
3	2.50	.129	−.137	−.018	5.773	12.70	.455
F_B	110	5.690	−.592	−3.370	2.403	36.70	.065
G	71.0	3.670	−.657	−2.410	−.007		

(*a*) *Undamped Case.* The natural frequency of the first-mode vibration is 2170 cycles per min and third-order resonance is at 723 rpm

$$m = m_1 A.R. = 1220 \text{ lb-in. allowing for inertia}$$
$$\text{Damping} = 2{,}386{,}000\ \theta_1^{2.5}$$

from which

$$\theta_1 = \left[\frac{1220 \times \pi \times 0.641}{2{,}386{,}000}\right]^{0.77}$$
$$= 0.0050 \text{ radians at } F_f$$

TABLE 2 FORCED-UNDAMPED VIBRATION OF THIRD ORDER AT 690 RPM; $\omega^2 = 47{,}000$

I	$I\omega^2/10^6$	θ	$I\omega^2\theta/10^6$	$m/_{10}$	Σ TORQUE	$K/10^6$	TWIST
110	5.170	1.000	5.170	—	5.170	13.05	.396
2.50	.117	.604	.071	m'	$5.241 + m'$	16.50	$.317 - .061m'$
2.50	.117	$.287 - .061m'$	$.034 - .007m'$	m'	$5.275 + 1.993m'$	16.50	$.320 + .121m'$
2.50	.117	$-.033 - .182m'$	$-.004 - .021m'$	m'	$5.271 + 2.972m'$	12.70	$.415 + .234m'$
110	5.170	$-.448 - .416m'$	$-2.320 - 2.150m'$	—	$2.951 + .822m'$	36.70	$.081 + .022m'$
71.0	3.340	$-.529 - .438m'$	$-1.765 - 1.462m'$	—	$1.1860 - .642m'$		

$m' = m/10^6$

From Table 2 θ_1 at 690 rpm $= \dfrac{0.642 \times 1220}{10^6 \times 1.186}$

$= 0.00066$ radians at F_f

Several tables similar to Table 2 were computed to give the undamped amplitude-speed curve shown in Fig. 4.

(*b*) *Damped Case.* Fig. 3 shows the application of a viscous damper to the front flywheel. The damper mass, D_1 becomes part of the dynamic system, and thus the damping of the interconnecting fluid is C_i (inner). While it is possible and sometimes preferable to calculate the simultaneous effects of both inherent and external damping by use of the forced-damped Holzer table, nevertheless the effect of the inherent system damping is neglected for now (Table 5 displays the computation for inherent damping), since we are interested primarily in speeds other than damped resonance. However, even at damped resonance, the effect of inherent damping is small compared to that of the damper. The "spring" stiffness of the damper-flywheel connection is zero so that when K is replaced by $K + j\omega C_i$, we have $0 + j\omega C_i$. The complex expression for the harmonic forcing torque m of Fig. 1(*b*) is

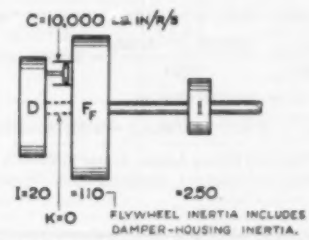

FIG. 3 APPLICATION OF VISCOUS DAMPER TO SYSTEM OF FIG. 2

$$-m \cos (180 - \phi) + jm \sin (180 - \phi)$$

where ϕ is the phase angle between m at No. 1 cylinder and the damper torque. The foregoing expression simplifies to

$$m \cos \phi + jm \sin \phi$$

for any quadrant.

Table 3 has two unknowns, the amplitude θ and the phase angle ϕ. The two equations necessary for a solution are made available by setting both the real and imaginary components of the end torque equal to zero, from which we obtain

$$\cos \phi = -\frac{0.235\,\theta}{0.689\,m'} = -0.341\,\theta/m'$$

$$\sin \phi = \frac{0.459\,\theta}{0.689\,m'} = 0.666\,\theta/m'$$

TABLE 3 FORCED-DAMPED* (EXTERNALLY) HOLZER TABLE; THIRD ORDER AT 695 RPM; $\omega^2 = 47{,}600$

I	$I\omega^2/10^6$	θ	$I\omega^2\theta/10^6$	$m/10^6$	Σ TORQUE	$K/10^6$	TWIST
20.0	.953	1.000θ (ZERO TIME PHASE)	$.953\theta$	—	$.953\theta$	$0 + j2.18$	$-.437j\theta$
110	5.24	$1.000\theta + .437j\theta$	$5.240\theta + 2.290j\theta$	—	$6.193\theta + 2.290j\theta$	13.05	$.474\theta + .175j\theta$
2.50	.119	$.526\theta + .262j\theta$	$.063\theta + .031j\theta$	$m'\cos\phi + jm'\sin\phi$	$6.256\theta + m'\cos\phi + j(2.321\theta + m'\sin\phi)$	16.50	$.380\theta + .061m'\cos\phi + j(.141\theta + .061m'\sin\phi)$
2.50	.119	$.146\theta - .061m'\cos\phi + j(.121\theta - .061m'\sin\phi)$	$.017\theta - .007m'\cos\phi + j(.014\theta - .007m'\sin\phi)$	$m'\cos\phi + jm'\sin\phi$	$6.273\theta + 1.993m'\cos\phi) + j(2.335\theta + 1.993m'\sin\phi)$	16.50	$.380\theta + .121m'\cos\phi + j(.141\theta + .121m'\sin\phi)$
2.50	.119	$-.234\theta - .182m'\cos\phi + j(-.020\theta - .182m'\sin\phi)$	$-.028\theta - .022m'\cos\phi - j(.002\theta + .022m'\sin\phi)$	$m'\cos\phi + jm'\sin\phi$	$6.245\theta + 2.971m'\cos\phi + j(2.333\theta + 2.971m'\sin\phi)$	12.70	$.492\theta + .234m'\cos\phi + j(.184\theta + .234m'\sin\phi)$
110	5.24	$-.726\theta - .416m'\cos\phi + j(-.204\theta - .416m'\sin\phi)$	$-3.805\theta - 2.180m'\cos\phi - j(1.070\theta + 2.180m'\sin\phi)$	—	$2.440\theta + .791m'\cos\phi + j(1.263\theta + .791m'\sin\phi)$	36.70	$.066\theta + .022m'\cos\phi + j(.034\theta + .022m'\sin\phi)$
71.0	3.38	$-.792\theta - .438m'\cos\phi + j(-.238\theta - .438m'\sin\phi)$	$-2.675\theta - 1.480m'\cos\phi + j(-.804\theta - 1.480m'\sin\phi)$		$-.236\theta - .689m'\cos\phi + j(.459\theta - .689m'\sin\phi)$		

$j\omega C_i/10^6 = j \times 2.18 \times .010 = 2.18j$

* EXTERNAL DAMPING ONLY

$$\tan \phi = 0.666/-0.341 = -1.955 \qquad \phi = 117° 05'$$

$$\theta = \frac{m' \cos \phi}{-0.341} = \frac{0.00122 \times -0.455}{-0.341} = 0.00163 \text{ radians}$$

Amplitude at the front flywheel is

$$\sqrt{1 + (0.437)^2} \times 0.00163 = 0.00178 \text{ radians}$$

Eight forced-damped Holzer tables, similar to Table 3, were computed to obtain the damped amplitude-speed curve shown in Fig. 4.

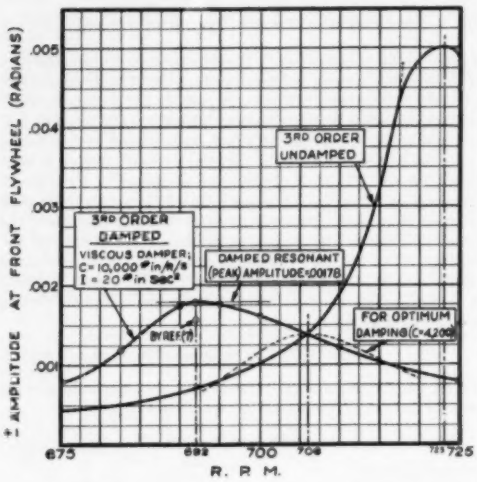

FIG. 4 DAMPED AND UNDAMPED AMPLITUDE-SPEED CURVES

O'Connor[3] has developed a method of determining the resonant amplitude at the damped natural frequency for a damped system such as we are dealing with. It is of interest to know how well the amplitude thus obtained agrees with that (0.00178) obtained by the damped-Holzer calculation. Equation [33] of O'Connor's paper is given as follows

$$I_a = \frac{2 I_e W_i}{\pi \omega_m^2 I_e \theta^2 - W_i}$$

where

I_a = damper-mass inertia (= 20)
ω_m^2 = (frequency)² of undamped engine (=51,700)
I_e = $\Sigma I \theta^2$ from free Holzer table (1) (= 180.3)
W_i = (work input)—(inherent damping work)
θ = damper-housing amplitude at damped resonance

Since we have neglected inherent damping in our work so far, W_i = work input = 2460 θ. Solving for θ, we obtain 0.00160 radians. The agreement of this value with the exact value of 0.00178 radians is fair enough since the O'Connor equation is meant for the optimum damping condition which, in accordance with O'Connor's work (Equation [27]), is calculated to be 4200 lb-in./radians sec, while the actual damping coefficient used (10,000) is considerably greater. An additional reason for the value of 0.00160 being lower is that it is based on a free Holzer table of the first-mode vibration and, therefore, includes only first-mode effects, while the value 0.00178 obtained by Holzer computation necessarily includes the effects of all possible modes of torsional vibration, as influenced by the third order.

In passing, it is noted that while the mathematical properties of the common-point frequency are such that a system having the optimum damping can be solved for the amplitude and vibratory shape at damped resonance with fair accuracy by manipulation of the system's free-vibration characteristics, a system with either considerably more or considerably less damping can be solved accurately only by the forced-damped Holzer method, which provides us with not only the flank but also the peak of the damped amplitude-speed curve.

If we define the common-point frequency as the natural frequency of a system having a front-end inertia of $I_{F_f} + I_D/2$ (= 120), we obtain for the common-point frequency a value of 706 rpm for the third order, which value is identical with that found from the intersection of the curves in Fig. 4.

OTHER CONSIDERATIONS

Computing the forced-damped amplitudes for a "minor" order of vibration involves some complexity. For purposes of illustration the first-order damped amplitude will be calculated at 695 rpm. With cranks at 120 deg, the expressions for the gas torque harmonics of the first order are

$m \cos \phi + jm \sin \phi$ for No. 1 cylinder
$-m \cos (\phi - 60) - jm \sin (\phi - 60)$ for No. 2 cylinder
$-m \cos (\phi + 60) - jm \sin (\phi + 60)$ for No. 3 cylinder

For greater ease in execution of the Holzer computations, the following substitutions are made

$m' \cos \phi \equiv A_c$, $m' \sin \phi \equiv A_s$, $m' \cos (\phi - 60) \equiv B_c$, $m' \sin (\phi - 60) \equiv B_s$, etc.

Table 4 shows the first-order forced-damped calculation.

Equating the end-torque components to zero and simplifying, we get

$$1.483 \theta - 0.088 m' \cos \phi + 0.048 m' \sin \phi = 0$$
$$0.207 \theta - 0.088 m' \sin \phi - 0.048 m' \cos \phi = 0$$

from which

$$\theta = 0.059 m' \cos \phi - 0.032 m' \sin \phi = 0.125 m' \sin \phi + 0.232 m' \cos \phi$$

where m = 2500 lb-in., $\tan \phi = -0.379$, $\phi = 159° 14'$

$$\theta = (0.059 \times 0.0025 \times -0.935) - (0.032 \times 0.0025 \times 0.354)$$
$$\theta = 0.000166 \text{ radians}$$

At the beginning of this paper it is stated that in most practical systems having inherent damping only, the vibratory shape as determined by free vibrations is not affected appreciably by this inherent damping. It will be of interest to show the truth of this statement by applying the forced-damped Holzer method to the equivalent system of Fig. 2, and comparing the vibratory shape thus determined with the free vibratory shape as determined by Table 1 in conjunction with energy balance. In order to treat the system by the damped-forced Holzer method, it is necessary to consider that there are several viscous-damping torques acting on the system at the location of the inertia masses. These damping torques will be considered as acting at each of the three cylinder center lines (Shannon treated the inherent-damping phenomenon on such a basis), and to be of such magnitude as to result in the front-end amplitude of 0.0050 radian as calculated by energy balance. While the inherent damping is not totally linear or viscous in character, the vibratory shape obtained by considering it as such will be very near to the true vibratory shape.

Inherent damping per cycle = 2460 × 0.0050 = 12.3 lb-in. per cycle

[3] "The Viscous Torsional Vibration Damper," by B. E. O'Connor, Quarterly Transactions, SAE, vol. 1, January, 1947, pp. 87–97.

TABLE 4 FORCED-DAMPED* (EXTERNALLY) HOLZER TABLE; FIRST ORDER AT 695 RPM; $\omega^2 = 5290$

I	$I\omega^2/10^6$	Θ	$I\omega^2\Theta/10^6$	$m/10^6$	Σ TORQUE	$K/10^6$	TWIST
20.0	.106	1.000Θ (ZERO TIME-PHASE)	$.106\Theta$	—	$.106\Theta$	$0+j.727$	$-.146j\Theta$
110	.582	$1.000\Theta + .146j\Theta$	$.582\Theta + .085j\Theta$	—	$.686\Theta + .085j\Theta$	13.05	$.053\Theta + .006j\Theta$
2.50	.013	$.947\Theta + .140j\Theta$	$.012\Theta + .002j\Theta$	[1] $A_c + jA_s$	$.700\Theta + A_c + j(.087\Theta + A_s)$	16.50	$.042\Theta + .061A_c + j(.005\Theta + .061A_s)$
2.50	.013	$.905\Theta - .061A_c + j(.135\Theta - .061A_s)$	$.012\Theta - .001A_c + j(.002\Theta - .001A_s)$	[2] $-B_c - jB_s$	$.712\Theta + .999A_c - B_c + j(.089\Theta + .999A_s - B_s)$	16.50	$.043\Theta + .061A_c - .061B_c + j(.005\Theta + .061A_s - .061B_s)$
2.50	.013	$.862\Theta - .122A_c + .061B_c + j(.130\Theta - .122A_s + .061B_s)$	$.011\Theta - .002A_c + .001B_c + j(.002\Theta - .002A_s + .001B_s)$	[3] $-C_c - jC_s$	$.723\Theta + .997A_c - .999B_c - C_c + j(.091\Theta + .997A_s - .999B_s - C_s)$	12.70	$.057\Theta + .078A_c - .078B_c - .079C_c + j(.007\Theta + .078A_s - .078B_s - .079C_s)$
110	.582	$.805\Theta - .200A_c + .140B_c + .079C_c + j(.123\Theta - .200A_s + .140B_s + .079C_s)$	$.469\Theta - .116A_c + .081B_c + .046C_c + j(.071\Theta - .116A_s + .081B_s + .046C_s)$	—	$1.132\Theta + .881A_c - .918B_c - .954C_c + j(.162\Theta + .881A_s - .918B_s - .954C_s)$	36.70	$.032\Theta + .024A_c - .025B_c - .026C_c + j(.004\Theta + .024A_s - .025B_s - .026C_s)$
71.0	.376	$.773\Theta - .224A_c + .165B_c + .105C_c + j(.119\Theta - .224A_s + .165B_s + .105C_s)$	$.291\Theta - .084A_c + .062B_c + .040C_c + j(.045\Theta - .084A_s + .062B_s + .040C_s)$	—	$1.483\Theta + .797A_c - .856B_c - .914C_c + j(.207\Theta + .797A_s - .856B_s - .914C_s)$		

$j\omega C_c/10^6 = j \times 72.75 \times .010$

$m = 2500$ LB. IN.

* EXTERNAL DAMPING ONLY

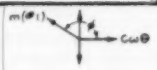

TABLE 5 FORCED-DAMPED* (INHERENTLY) HOLZER TABLE; THIRD ORDER AT 723 RPM; $\omega^2 = 51{,}530$

I	$I\omega^2/10^6$	Θ	$I\omega^2\Theta/10^6$	$m/10^6$	Σ TORQUE$/10^6$	$K/10^6$	TWIST
110	5.67	1.000Θ (ZERO TIME-PHASE)	5.670Θ	—	5.670Θ	13.05	$.435\Theta$
2.50	.129-.411j	$.565\Theta$	$.073\Theta - .232j\Theta$	$m'\cos\phi + jm'\sin\phi$	$5.743\Theta + m'\cos\phi + j(-.232\Theta + m'\sin\phi)$	16.50	$.348\Theta + .061m'\cos\phi + j(-.014\Theta + .061m'\sin\phi)$
2.50	.129-.411j	$.217\Theta - .061m'\cos\phi + j(.014\Theta - .061m'\sin\phi)$	$.034\Theta - .008m'\cos\phi - .025m'\sin\phi + j(.087\Theta - .008m'\sin\phi + .025m'\cos\phi)$	$m'\cos\phi + jm'\sin\phi$	$5.777\Theta + 1.982m'\cos\phi - .025m'\sin\phi + j(-.319\Theta + 1.982m'\sin\phi + .025m'\cos\phi)$	16.50	$.350\Theta + .121m'\cos\phi - .001m'\sin\phi + j(-.019\Theta + .121m'\sin\phi + .001m'\cos\phi)$
2.50	.129-.411j	$-.133\Theta - .182m'\cos\phi + .001m'\sin\phi + j(.033\Theta - .182m'\sin\phi - .001m'\cos\phi)$	$-.004\Theta - .024m'\cos\phi - .075m'\sin\phi + j(.059\Theta - .024m'\sin\phi + .075m'\cos\phi)$	$m'\cos\phi + jm'\sin\phi$	$5.773\Theta + 2.968m'\cos\phi - .100m'\sin\phi + j(-.260\Theta + 2.968m'\sin\phi + .100m'\cos\phi)$	12.70	$.455\Theta + .234m'\cos\phi - .008m'\sin\phi + j(-.020\Theta + .234m'\sin\phi + .008m'\cos\phi)$
110	5.67	$-.588\Theta - .416m'\cos\phi + .009m'\sin\phi + j(.053\Theta - .416m'\sin\phi - .009m'\cos\phi)$	$-3.33\Theta - 2.360m'\cos\phi + .051m'\sin\phi + j(.300\Theta - 2.360m'\sin\phi - .051m'\cos\phi)$	——	$2.443\Theta + .608m'\cos\phi - .049m'\sin\phi + j(.040\Theta + .608m'\sin\phi + .049m'\cos\phi)$	36.70	$.067\Theta + .017m'\cos\phi - .001m'\sin\phi + j(.001\Theta + .017m'\sin\phi + .001m'\cos\phi)$
71.0	3.66	$-.655\Theta - .433m'\cos\phi + .010m'\sin\phi + j(.052\Theta - .433m'\sin\phi - .010m'\cos\phi)$	$-2.400\Theta - 1.59m'\cos\phi + .036m'\sin\phi + j(.190\Theta - 1.590m'\sin\phi - .036m'\cos\phi)$	——	$+.043\Theta - .982m'\cos\phi - .013m'\sin\phi + j(.230\Theta - .982m'\sin\phi + .013m'\cos\phi)$		

$j\omega C_0/10^6 = 227.0 \times 1810/10^6 = .411j$

* INHERENT DAMPING ONLY

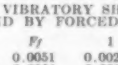

therefore

$$C\omega\pi \sum_{n=1}^{n=3} \theta_n^2 = 12.5$$

$\sum_{n=1}^{n=3} \theta_n^2$ from free Holzer Table 1 = 0.0000960

whence $C = 1810$ in-lb per radian per sec

The damping coefficients are effective between the three cylinder masses and the "ground," which in this case is the engine frame. Consequently, the proper substitution in the damped-Holzer table is $I\omega^2 - j\omega C_e$ for $I\omega^2$. The computations are shown in Table 5.

By equating the component end torques to zero and simplifying as before, we obtain

$$\phi = 80° 11'$$
$$\theta = 0.0051 \text{ radians}$$

The absolute amplitude curve (vibratory shape) is obtained from Column 3 of Table 5. Using 0.0051 as the value of θ for both methods, the vibratory shapes may be compared as in Table 6.

TABLE 6 RESONANT VIBRATORY SHAPES AS DETERMINED BY ENERGY BALANCE AND BY FORCED-DAMPED HOLZER METHOD

θ	F_f	1	2	3	F_b	G
By energy balance	0.0051	0.00288	0.00109	—0.00070	—0.00302	—0.00335
By forced-damped Holzer	0.0051	0.00288	0.00110	—0.00072	—0.00308	—0.00343
Difference, per cent	0	0	1.0	2.9	2.0	2.3

The percentage differences, for equal amplitudes at the front flywheel, are shown to be of negligible extent for the practical solution of vibration problems. For purposes of research work on the inherent damping problem, where it is in order to assess the damping effects at resonance very accurately, the use of the more exact vibratory shape may be warranted.

ACKNOWLEDGMENT

The author acknowledges, with thanks, the kind encouragement and advice rendered by Prof. J. P. Den Hartog; also the kind encouragement of W. P. Haggerty, Chief Engineer, Vivian Diesels and Munitions Limited.

A Comparative Study of Some Variational Principles in the Theory of Plasticity

By RODNEY HILL,[1] SHEFFIELD, ENGLAND

The variational principle of Markov for velocity distributions in a plastic state is extended to a work-hardening material and to more general boundary conditions. A relationship is shown to exist between Markov's principle and the maximum work principle of Hill.

Nomenclature

The following nomenclature is used in the paper:

σ_{ij} = stress tensor; σ_{11}, σ_{22}, σ_{33} are the normal stresses in the direction of the co-ordinate axes x_1, x_2, x_3, corresponding to σ_x, σ_y, σ_z, in the usual notation; σ_{12}, σ_{23}, σ_{31} are the shearing stresses, corresponding to τ_{xy}, τ_{yz}, τ_{zx}

σ_{ij}' = deviatoric part of the stress tensor

$\bar{\sigma}$ = stress intensity

$\dot{\epsilon}_{ij}$ = strain-rate tensor; $\dot{\epsilon}_{11}$, $\dot{\epsilon}_{22}$, $\dot{\epsilon}_{33}$ are the normal strain rates, but $\dot{\epsilon}_{12}$, $\dot{\epsilon}_{23}$, $\dot{\epsilon}_{31}$ are half the engineering shear-strain rates, corresponding to $\frac{1}{2}\dot{\gamma}_{xy}$, etc.

$\frac{\cdot}{\epsilon}$ = strain-rate intensity

u_i = components of velocity

l_j = direction cosines of outward normal to a surface

F_i = external stress components acting on a surface

λ = factor of proportionality in stress-strain relations

k = yield stress in shear

dS, dV = elements of surface and volume, respectively

Introduction

Recently several variational principles, and corresponding uniqueness theorems, have been established for certain boundary-value problems in the theory of plasticity. These may be classified broadly in two groups: namely, (*a*) those which apply to a plastic-elastic material (1, 2);[2] and (*b*) those which apply to a plastic-rigid material (3, 4), where the elastic component of strain is disregarded. This classification should not be taken to imply that the respective boundary-value problems are unrelated, since the plastic-rigid body must, in general, be regarded as a plastic-elastic body in which Young's modulus is allowed to assume an infinitely great value. The interesting question of the precise nature of the relationship will, however, not be discussed here, the present paper being concerned solely with boundary-value problems appropriate for a plastic-rigid material.

Two variational principles, apparently very different in character, have been proved by Hill and Markov for a nonhardening plastic-rigid material obeying the laws of classical plasticity and undergoing loading everywhere. For convenience, the proofs are repeated here, Markov's original proof being appreciably shortened and, at the same time, extended to more general boundary conditions and to a work-hardening material. The theorems are then expressed in a form such that the connection between them becomes apparent. It is finally shown how both can be applied to the proof of the uniqueness of solutions under certain boundary conditions.

Principle of Maximum Plastic Work

Consider a plastic mass in quasi-static equilibrium, no element of which is being unloaded. Each element is supposed to be stressed to the yield point, according to the law of von Mises

$$\sigma_{ij}'\sigma_{ij}' = 2k^2 \qquad [1]$$[3]

where k is the yield stress in shear, and σ_{ij}' is the deviatoric part of the stress tensor σ_{ij}. Stress k may vary throughout the mass (because of different previous strain histories), but is regarded as specified at each point at the moment under consideration. The plastic stress-strain relations are taken to be those of Lévy and von Mises

$$\dot{\epsilon}_{ij} = \frac{1}{2}\left(\frac{\partial u_i}{\partial x_j} + \frac{\partial u_j}{\partial x_i}\right) = \lambda\sigma_{ij}' \qquad [2]$$

where $\dot{\epsilon}_{ij}$ is the tensor representing the rate of strain, u_i is the flow velocity, and λ is a factor of proportionality which varies in space and time. A necessary consequence of Equation [2] is that $\dot{\epsilon}_{ii} = 0$, or that the volume of each element does not change. During continued plastic deformation the rate $\dot{W}$ of plastic work done must be positive. Since

$$\dot{W} = \sigma_{ij}\dot{\epsilon}_{ij} = \lambda\sigma_{ij}'\sigma_{ij}' = 2k^2\lambda,$$

this is ensured if λ is positive. The equations of equilibrium are

$$\frac{\partial \sigma_{ij}}{\partial x_j} = 0 \qquad [3]$$

Let σ_{ij}^* represent any stress distribution satisfying the yield condition, Equation [1], and the equilibrium Equation [3]. Now, by the inequality of Schwartz

$$(\sigma_{ij}'\sigma_{ij}')(\sigma_{ij}^{*\prime}\sigma_{ij}^{*\prime}) \geqslant (\sigma_{ij}'\sigma_{ij}^{*\prime})^2,$$

and so $\sigma_{ij}'\sigma_{ij}' \geqslant \sigma_{ij}'\sigma_{ij}^{*\prime}$, since $\sigma_{ij}'\sigma_{ij}' = \sigma_{ij}^{*\prime}\sigma_{ij}^{*\prime}$. Multiplying through by the positive factor λ and integrating through the volume of the plastic mass

$$0 \leqslant \int \lambda\sigma_{ij}'(\sigma_{ij}' - \sigma_{ij}^{*\prime})dV$$

$$= \int (\sigma_{ij}' - \sigma_{ij}^{*\prime})\frac{\partial u_i}{\partial x_j}\,dV$$

---

[1] British Iron and Steel Research Association, Metal Flow Research Laboratory.

[2] Numbers in parentheses refer to the Bibliography at the end of the paper.

Presented at the National Meeting of the Applied Mechanics Division, Ann Arbor, Mich., June 13–15, 1949, of The American Society of Mechanical Engineers.

Discussion of this paper should be addressed to the Secretary, ASME, 29 West 39th Street, New York, N. Y., and will be accepted until April 10, 1950, for publication at a later date. Discussion received after the closing date will be returned.

Note: Statements and opinions advanced in papers are to be understood as individual expressions of their authors and not those of the Society. Paper No. 49—APM-16.

[3] In this and subsequent equations, the summation convention is to be understood. If a subscript i or j appears twice in the same term, the term is to be summed for all values i, j = 1, 2, 3. Thus $\sigma_{ii} = \sigma_{11} + \sigma_{22} + \sigma_{33}$, and $\sigma_{ij}'\sigma_{ij}' = \sigma_{11}'^2 + \sigma_{22}'^2 + \sigma_{33}'^2 + 2\sigma_{23}^2 + 2\sigma_{31}^2 + 2\sigma_{12}^2$.

using Equation [2] and the fact that the stress tensor is symmetric

$$= \int \frac{\partial}{\partial x_j} \{(\sigma_{ij} - \sigma_{ij}^*)u_i\}\, dV$$

since the material is incompressible and σ_{ij} and σ_{ij}^* satisfy the equilibrium equations. Using Green's theorem to transform the volume integral into an integral over the surface

$$0 \leqslant \int (\sigma_{ij} - \sigma_{ij}^*)u_i l_j\, dS$$

where l_i are the direction cosines of the outward normal. This equation states that the work $\int \sigma_{ij} u_i l_j dS$ done by the actual surface forces is greater than the work $\int \sigma_{ij}^* u_i l_j dS$ done by any other stress system for the same surface velocities, provided σ_{ij}^* satisfies the equilibrium equations and the yield criterion.[4] More generally, if the surface velocities are prescribed only over a part S_U of the surface, and the external stresses $F_i = \sigma_{ij} l_j$ over the rest S_F, then

$$\int_{SU} F_i u_i\, dS \geqslant \int_{SU} F_i^* u_i\, dS \ldots\ldots\ldots\ldots [4]$$

where the stress system σ_{ij}^* is such that $F_i^* = \sigma_{ij}^* l_j = F_i$ on S_F.[5] The equal sign corresponds to systems differing only by a uniform hydrostatic pressure or tension. This theorem states an absolute maximum of the plastic work for varying stresses (3). The theorem of Markov, now to be proved, states an absolute minimum for a related function when the velocities are varied.

Markov's Theorem

The original proof by Markov of his variational principle was restricted to a nonhardening material (k = const) obeying Equations [1] and [2]. His statement of the principle is equivalent to the following: If a plastic mass is subjected to continued deformation at all points, under surface velocities u_i, the expression

$$\int \sqrt{\dot{\epsilon}_{ij}^* \dot{\epsilon}_{ij}^*}\, dV, \quad \dot{\epsilon}_{ij}^* = \frac{1}{2}\left(\frac{\partial u_i^*}{\partial x_j} + \frac{\partial u_j^*}{\partial x_i}\right)$$

takes an absolute minimum value in the actual state, the u_i^* being any velocity distribution satisfying the boundary conditions and the equation of incompressibility $(\partial u_i^*)/(\partial x_i) = 0$. When expressed in this form, Markov's theorem appears to have no obvious connection with the maximum work principle. In the more general statement which will now be proved for a work-hardening material, the connection will become apparent.

It is supposed, as before, that the value of $\sqrt{\sigma_{ij}'\sigma_{ij}'}$, or $\sqrt{2}k$, is given at each point of the body. From Equation [2]

$$\dot{\epsilon}_{ij}\dot{\epsilon}_{ij} = \lambda^2 \sigma_{ij}'\sigma_{ij}'$$

and hence by eliminating λ

$$\frac{\dot{\epsilon}_{ij}}{\sqrt{\dot{\epsilon}_{ij}\dot{\epsilon}_{ij}}} = \frac{\sigma_{ij}'}{\sqrt{\sigma_{ij}'\sigma_{ij}'}} \ldots\ldots\ldots\ldots [5]$$

where the square roots are to be taken positive. Now, by Schwartz's inequality

$$\sqrt{\dot{\epsilon}_{ij}\dot{\epsilon}_{ij}}\sqrt{\dot{\epsilon}_{ij}^*\dot{\epsilon}_{ij}^*} \geqslant \dot{\epsilon}_{ij}\dot{\epsilon}_{ij}^*$$

The equality holds if, and only if, the components of the tensors $\dot{\epsilon}_{ij}$ and $\dot{\epsilon}_{ij}^*$ are proportional. Introducing the factor $\sqrt{\sigma_{ij}'\sigma_{ij}'}$, and integrating through the volume

$$\int \sqrt{\sigma_{ij}'\sigma_{ij}'}\sqrt{\dot{\epsilon}_{ij}^*\dot{\epsilon}_{ij}^*}\, dV \geqslant \int \sqrt{\sigma_{ij}'\sigma_{ij}'}\,\frac{(\dot{\epsilon}_{ij}\dot{\epsilon}_{ij}^*)}{\sqrt{\dot{\epsilon}_{ij}\dot{\epsilon}_{ij}}}\, dV \ldots [6]$$

But, from Equation [5]

$$\sqrt{\sigma_{ij}'\sigma_{ij}'}\,\frac{\dot{\epsilon}_{ij}(\dot{\epsilon}_{ij}^* - \dot{\epsilon}_{ij})}{\sqrt{\dot{\epsilon}_{ij}\dot{\epsilon}_{ij}}} = \sigma_{ij}'(\dot{\epsilon}_{ij}^* - \dot{\epsilon}_{ij}) = \sigma_{ij}(\dot{\epsilon}_{ij}^* - \dot{\epsilon}_{ij})$$

since both $\dot{\epsilon}_{ij}^*$ and $\dot{\epsilon}_{ij}$ satisfy the equation of incompressibility. Now σ_{ij} is the actual stress and therefore must satisfy the equilibrium equations. Hence with the use of Green's theorem

$$\int \sqrt{\sigma_{ij}'\sigma_{ij}'}\,\frac{\dot{\epsilon}_{ij}(\dot{\epsilon}_{ij}^* - \dot{\epsilon}_{ij})}{\sqrt{\dot{\epsilon}_{ij}\dot{\epsilon}_{ij}}}\, dV = \int \sigma_{ij}\left(\frac{\partial u_i^*}{\partial x_j} - \frac{\partial u_i}{\partial x_j}\right) dV$$
$$= \int \frac{\partial}{\partial x_j}\{\sigma_{ij}(u_i^* - u_i)\}\, dV$$
$$= \int \sigma_{ij}(u_i^* - u_i) l_j\, dS \ldots [7]$$

Combining Equations [6] and [7]

$$\int \sqrt{\sigma_{ij}'\sigma_{ij}'}\sqrt{\dot{\epsilon}_{ij}^*\dot{\epsilon}_{ij}^*}\, dV \geqslant \int \sqrt{\sigma_{ij}'\sigma_{ij}'}\sqrt{\dot{\epsilon}_{ij}\dot{\epsilon}_{ij}}\, dV + \int \sigma_{ij}(u_i^* - u_i) l_j\, dS \ldots\ldots\ldots [8]$$

If the velocity is given over a part S_U of the surface, and the external stress $F_i = \sigma_{ij} l_j$ over the remainder S_F, then

$$\int \sqrt{\sigma_{ij}'\sigma_{ij}'}\sqrt{\dot{\epsilon}_{ij}\dot{\epsilon}_{ij}}\, dV - \int_{S_F} F_i u_i\, dS \leqslant \int \sqrt{\sigma_{ij}'\sigma_{ij}'}\sqrt{\dot{\epsilon}_{ij}^*\dot{\epsilon}_{ij}^*} - \int_{S_F} F_i u_i^*\, dS \ldots\ldots [9]$$

If the material does not work-harden, $\sigma_{ij}'\sigma_{ij}'$ is the same at all points of the body, and

$$\int \sqrt{\dot{\epsilon}_{ij}\dot{\epsilon}_{ij}}\, dV - \frac{1}{\sqrt{2}\,k}\int_{S_F} F_i u_i\, dS \leqslant \int \sqrt{\dot{\epsilon}_{ij}^*\dot{\epsilon}_{ij}^*}\, dV - \frac{1}{\sqrt{2}\,k}\int_{S_F} F_i u_i^*\, dS$$

Markov's original theorem is obtained by setting $S_F = 0$.

Relation Between the Two Variational Principles

Equation [8] may be interpreted in terms of stress, and strain rate, intensity (alternatively called generalized, equivalent, or effective stress and strain rate). By definition, the stress intensity is

$$\bar{\sigma} = \sqrt{\frac{3}{2}}\sqrt{\sigma_{ij}'\sigma_{ij}'}$$

and the strain-rate intensity is

$$\dot{\bar{\epsilon}} = \sqrt{\frac{2}{3}}\sqrt{\dot{\epsilon}_{ij}\dot{\epsilon}_{ij}}$$

Hence Equation [8] can be written as

$$\int \bar{\sigma}\dot{\bar{\epsilon}}\, dV - \int_{SF} F_i u_i\, dS \leqslant \int \bar{\sigma}\dot{\bar{\epsilon}}^*\, dV - \int_{SF} F_i u_i^*\, dS \ldots [10]$$

Now it is well known that, when the Lévy-Mises law applies, the rate $\dot{W}$ of plastic work is equal to $\bar{\sigma}\dot{\bar{\epsilon}}$. This may be immediately proved from Equation [5] as follows

$$\dot{W} = \sigma_{ij}\dot{\epsilon}_{ij} = (\sigma_{ij}'\sigma_{ij}')\frac{\sqrt{\dot{\epsilon}_{ij}\dot{\epsilon}_{ij}}}{\sqrt{\sigma_{ij}'\sigma_{ij}'}} = \sqrt{\sigma_{ij}'\sigma_{ij}'}\sqrt{\dot{\epsilon}_{ij}\dot{\epsilon}_{ij}} = \bar{\sigma}\dot{\bar{\epsilon}}$$

[4] For the relation between this principle and Sadowsky's principle of maximum plastic resistance (5) see reference (3).

[5] More generally still, certain components of the surface stress and velocity may be given on the same part of the surface. The modified interpretation of Equation [4] is obvious.

The left-hand side of Equation [10] therefore is equal to

$$\int \sigma_{ij}\dot{\epsilon}_{ij}\,dV - \int_{S_F} F_i u_i\,dS = \int_{S_U} F_i u_i\,dS$$

by the use of Green's theorem. Substituting this in Equation [10], and combining with Equation [4], there results

$$\int_{S_U} F_i^* u_i\,dS \leqslant \int_{S_U} F_i u_i\,dS \leqslant \int \vartheta\dot{\epsilon}^*\,dV - \int_{S_F} F_i u_i^*\,dS. \quad [11]$$

The relation between Markov's variational principle and the author's is now apparent. The work done by the actual surface forces over S_U is the absolute maximum of the expression in the author's theorem for varying stress, and the absolute minimum of the expression in Markov's theorem for varying velocity. This result provides a means of obtaining upper and lower bounds in the approximate solution of special problems.

Extension to More General Stress-Strain Laws

It is easy to extend the maximum work principle to a stress-strain law of the form

$$\dot{\epsilon}_{ij} = \lambda \frac{\partial f}{\partial \sigma_{ij}} \quad [12]$$

where f, the plastic potential, is a general function of the invariants J_2 and J_3 of the deviatoric stress tensor. Since f is then independent of the hydrostatic component of the stress, $(\partial f)/(\partial \sigma_{ii}) = 0$, and Equation [12] implies that there is no change in volume. The condition for yielding is

$$f(\sigma_{ij}) = \text{const.} \quad [13]$$

where the value of the constant depends on the strain history. For any stress σ_{ij}^* satisfying Equation [13]

$$\sigma_{ij}' \frac{\partial f}{\partial \sigma_{ij}} \geqslant \sigma_{ij}^{*\prime} \frac{\partial f}{\partial \sigma_{ij}} \quad [14]$$

provided f is a positive convex function of the stress components. Suppose that the function f is represented by a closed curve (the yield locus) in the plane $\sigma_1 + \sigma_2 + \sigma_3 = 0$, where the principal stresses σ_1, σ_2, σ_3 are taken as Cartesian co-ordinates. Equation [14] may be interpreted as stating that the scalar product of the vector $\sigma_{ij}^{*\prime}$ and the outward normal to the yield locus at the point σ_{ij}' can never be greater than the scalar product of the vector σ_{ij}' and the same normal. Multplying Equation [14] by the positive factor λ, and integrating

$$\begin{aligned} 0 &\leqslant \int \lambda(\sigma_{ij}' - \sigma_{ij}^{*\prime}) \frac{\partial f}{\partial \sigma_{ij}}\,dV \\ &= \int (\sigma_{ij}' - \sigma_{ij}^{*\prime})\,\dot{\epsilon}_{ij}\,dV \qquad \text{from Equation [12]} \\ &= \int (\sigma_{ij} - \sigma_{ij}^*)\,u_i l_j\,dS \end{aligned}$$

provided σ_{ij} and σ_{ij}^* both satisfy the equilibrium equations. This proves the principle of maximum plastic work.

Markov's theorem, on the other hand, does not seem capable of generalization in this way.

Uniqueness Theorem

Both variational principles can be applied readily to prove the uniqueness of a stress solution under given boundary conditions. Suppose, if possible, that σ_{ij}, u_i, and σ_{ij}^*, u_i^*, could be two distinct solutions (i.e., not differing merely by a uniform hydrostatic stress), satisfying Equations [1], [2], and [3], and the boundary conditions. Now, by the maximum work principle

$$\int F_i u_i\,dS > \int F_i^* u_i\,dS, \quad \int F_i^* u_i^*\,dS > \int F_i u_i^*\,dS$$

if, and only if, the stress systems are not identical. Hence

$$\begin{aligned} &\int (F_i - F_i^*)(u_i - u_i^*)\,dS \\ &= \int (F_i u_i - F_i^* u_i)\,dS + \int (F_i^* u_i^* - F_i u_i^*)\,dS \\ &> 0 \end{aligned}$$

But if the boundary conditions are such that

$$(F_i - F_i^*)(u_i - u_i^*) = 0 \quad [15]$$

everywhere on the surface, we arrive at a contradiction. Hence it is impossible that there can be two distinct stress solutions. In general, of course, there will be no solution at all, since the boundary conditions must be such as to produce continued plastic deformation at all points in the body.

The boundary condition of Equation [15] includes the following special cases: (*a*) The velocity is given on S_U and the external stress on S_F. Then $F_i^* = F_i$ on S_F and $u_i^* = u_i$ on S_U, and so Equation [15] is satisfied everywhere. (*b*) The normal component of velocity and the resultant tangential stress are given at all points on the surface. The vector $F_i - F_i^*$ lies in the tangent plane, and the vector $u_i - u_i^*$ is directed along the normal, so that their scalar product is zero.

Alternatively, uniqueness may be proved by Markov's principle. From Equation [8]

$$\begin{aligned} &\int \sqrt{\sigma_{ij}'\sigma_{ij}'}\,\sqrt{\dot{\epsilon}_{ij}^*\dot{\epsilon}_{ij}^*}\,dV - \int \sqrt{\sigma_{ij}'\sigma_{ij}'}\,\sqrt{\dot{\epsilon}_{ij}\dot{\epsilon}_{ij}}\,dV \\ &\qquad > \int F_i(u_i^* - u_i)\,dS \\ &\int \sqrt{\sigma_{ij}^{*\prime}\sigma_{ij}^{*\prime}}\,\sqrt{\dot{\epsilon}_{ij}\dot{\epsilon}_{ij}}\,dV - \int \sqrt{\sigma_{ij}^{*\prime}\sigma_{ij}^{*\prime}}\,\sqrt{\dot{\epsilon}_{ij}^*\dot{\epsilon}_{ij}^*}\,dV \\ &\qquad > \int F_i^*(u_i - u_i^*)\,dS \end{aligned}$$

if and only if $\dot{\epsilon}_{ij}$ and $\dot{\epsilon}_{ij}^*$ do not differ merely by a scalar factor at every point. Adding these equations, and recalling that $\sigma_{ij}'\sigma_{ij}' = \sigma_{ij}^{*\prime}\sigma_{ij}^{*\prime}$, we obtain

$$0 < \int (F_i - F_i^*)(u_i - u_i^*)dS$$

The proof continues as before. Hence $\dot{\epsilon}_{ij}$ and $\dot{\epsilon}_{ij}^*$ are either equal or differ only by a scalar factor of proportionality at each point. In both cases σ_{ij}' and $\sigma_{ij}^{*\prime}$ are identical.

BIBLIOGRAPHY

1 "A Variational Principle for Plastic Materials With Strain-Hardening," by P. Hodge and W. Prager, *Journal of Mathematics and Physics*, vol. 27 (i), 1948, p. 1.

2 "Complementary Minimum Principles for an Elastic-Plastic Material," by H. J. Greenberg; to be published.

3 "A Variational Principle of Maximum Plastic Work in Classical Plasticity," by R. Hill, *The Quarterly Journal of Mechanics and Applied Mathematics*, vol. 1 (i), 1948, p. 18.

4 "On Variational Principles in the Theory of Plasticity," by A. A. Markov, *Prikladnaia Matematika i Mekhanika*, vol. 11, 1947, p. 339.

5 "A Principle of Maximum Plastic Resistance," by M. A. Sadowsky, JOURNAL OF APPLIED MECHANICS, Trans. ASME, vol. 65, 1943, p. A-65.

Deflections and Moments Due to a Concentrated Load on a Cantilever Plate of Infinite Length

By T. J. JARAMILLO,[1] CHICAGO, ILL.

This paper contains an exact solution in terms of improper integrals for the deflections and moments due to a transverse concentrated load acting at an arbitrary point of an infinitely long cantilever plate of constant width and thickness. The solution is transformed into series form by means of contour integration, and is illustrated by numerical examples. In particular, comparisons are made with the known solution (1)[2] for the special case where the load is applied at the free edge of the plate. The results obtained are of practical significance in connection with the design of certain types of monorail cranes.

Nomenclature

The following nomenclature is used in this paper:

(X, Y, Z) = Cartesian co-ordinates
a = width of plate
h = thickness of plate
c = distance of load from clamped edge

$\left(\xi = \frac{x}{a},\ \eta = \frac{y}{a},\ \zeta = \frac{c}{a}\right)$ = dimensionless co-ordinates

ν = Poisson's ratio
E = Young's modulus

$\gamma = \frac{1+\nu}{1-\nu}$

$N = \frac{Eh^3}{12(1-\nu^2)}$ = flexural rigidity of plate

w = deflection
Q_x, Q_y; M_x, M_y; M_{xy} = shear forces, bending moments, and twisting moments, respectively
P = magnitude of concentrated load

$\nabla^4 = \frac{\partial^4}{\partial x^4} + 2\frac{\partial^4}{\partial x^2 \partial y^2} + \frac{\partial^4}{\partial y^4}$ = biharmonic operator

Statement of Problem, Boundary, and Transition Conditions

Consider a plate in the shape of an infinitely long strip of width a and thickness h, which is clamped along one of its parallel edges, the other edge being free, Fig. 1. Let the plate be acted on by a transverse concentrated load P, whose point of application is arbitrary. We introduce a Cartesian co-ordinate system $Oxyz$ such that the xy-plane coincides with the median plane of the plate, the y-axis is taken coincident with the clamped edge, and the xz-plane is assumed to contain the load P, which intersects the median plane at the point A $(c, 0)$.

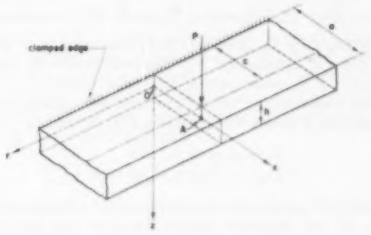

Fig. 1 Cantilever Plate, Loading, and Co-Ordinate System

It is expedient for what follows to divide the plate into the two strip-shaped regions separated by the line $x = c$, and to designate functions defined in the regions $0 \leq x \leq c$ and $c \leq x \leq a$ by the subscripts 1 and 2, respectively. If the weight of the plate is neglected, the transverse deflections $w_j(x, y)$ $(j = 1, 2)$, within the assumptions of the classical small deflections theory, are characterized by the homogeneous biharmonic equation

$$\nabla^4 w_j(x, y) = 0 \ (j = 1, 2) \quad \ldots\ldots\ldots\ldots [1]$$

which is valid throughout the regions under consideration except for the singular load point A.

The equations relating the deflections to the shearing forces, bending moments, and twisting moments are

$$\left.\begin{aligned} Q_{jx} &= -N(w_{j,xxx} + w_{j,xyy}) \\ M_{jx} &= -N(w_{j,xx} + \nu w_{j,yy}) \\ M_{jxy} &= -M_{jyx} = N(1-\nu)w_{j,xy} \end{aligned}\right\} \quad \ldots\ldots\ldots [2][3]$$

where ν is Poisson's ratio and N denotes the flexural rigidity of the plate. In view of Equations [2], the boundary conditions written in terms of the deflections w, appear as follows

Along the clamped edge $x = 0$

$$w_1(0, y) = w_{1,x}(0, y) = 0 \quad \ldots\ldots\ldots\ldots [3]$$

and along the free edge $x = a$, $M_{2x} = Q_{2x} = M_{2xy} = 0$ so that

$$[w_{2,xx} + \nu w_{2,yy}]_{(a,y)} = 0 \quad \ldots\ldots\ldots\ldots [4]$$

$$[w_{2,xxx} + (2-\nu)w_{2,xyy}]_{(a,y)} = 0 \quad \ldots\ldots\ldots\ldots [5]$$

---

[1] Research Mathematician, Armour Research Foundation.

[2] Numbers in parentheses refer to the Bibliography at the end of the paper.

Presented at the National Meeting of the Applied Mechanics Division, Ann Arbor, Mich., June 13–15, 1949, of The American Society of Mechanical Engineers.

Discussion of this paper should be addressed to the Secretary, ASME, 29 West 39th Street, New York, N. Y., and will be accepted until April 10, 1950, for publication at a later date. Discussion received after the closing date will be returned.

Note: Statements and opinions advanced in papers are to be understood as individual expressions of their authors and not those of the Society. Paper No. 49—APM-15.

[3] See reference (3). The subscripts x and y attached to functions which originally bear no such subscripts, indicate partial derivatives. Thus, $w_{j,xyy} = \partial^3 w_j / \partial x \partial y^2$.

where Equation [5] is Kirchhoff's condition, which is equivalent to the requirements

$$Q_{1x}(a, y) = M_{1xy}(a, y) = 0$$

In addition to the boundary conditions, the solution must conform to the transition conditions at $x = c$. From the continuity requirements for the deflections, slopes, and bending moments, we have

$$w_1(c, y) = w_2(c, y) \quad \ldots\ldots [6]$$

$$w_{1,x}(c, y) = w_{2,x}(c, y) \quad \ldots\ldots [7]$$

$$[w_{1,xx} + \nu w_{1,yy}]_{(c,y)} = [w_{2,xx} + \nu w_{2,yy}]_{(c,y)} \quad \ldots\ldots [8]$$

The shearing force Q_x must be continuous along $x = c$, except for the point of application A of the load, where Q_x has a discontinuity. The corresponding transition condition is formulated most conveniently for our purposes by replacing the concentrated load P with a force function $F(y)$ defined by

$$\left.\begin{aligned} F(y) &= p \text{ for } |y| \leq \delta \\ F(y) &= 0 \text{ for } \delta < |y| < \infty \end{aligned}\right\} \quad \ldots\ldots [9]$$

where $2p\delta = P$, and by subsequently passing to the limit as $\delta \to 0$. By use of the familiar Fourier integral representation for $F(y)$, the required condition on Q_x now becomes

$$-N\,[w_{1,xxx} + w_{1,yyx}]_{(c,y)} + N\,[w_{2,xxx} + w_{2,yyx}]_{(c,y)} = \int_0^\infty \frac{2p \sin \alpha\delta}{\pi\alpha} \cos \alpha y \, d\alpha. \quad [10]$$

Solution for Deflections in Integral Form

The problem formulated in the preceding section consists of determining the biharmonic functions $w_j(x, y)$ $(j = 1, 2)$ which satisfy the foregoing boundary and transition conditions. To this end we recall that

$$w_j(x, y) = \int_0^\infty f_j(x, \alpha)\cos \alpha y \, d\alpha; \quad (j = 1, 2) \quad \ldots\ldots [11]$$

with

$$f_j(x, \alpha) = (A_j + B_j\alpha x)\cosh \alpha x + (C_j + D_j \alpha x)\sinh \alpha x \quad \ldots [12]$$

is a solution of Equation [1] for arbitrary choice of the functions $A_j(\alpha)$, $B_j(\alpha)$, $C_j(\alpha)$, $D_j(\alpha)$, $(j = 1, 2)$ provided the improper Integral [11] and its required partial derivatives exist. This solution, moreover, conforms to the symmetry of the problem under consideration. Since Equations [3], [4], [5], [6], [7], [8], [10] are to hold identically in y, we have from these and Equations [11], [12]

$$\left.\begin{aligned} &f_{1,x}(o, \alpha) = f_{1,xx}(o, \alpha) = 0 \\ &f_{2,xx}(a, \alpha) - \alpha^2 f_2(a, \alpha) = 0 \\ &f_{2,xxx}(a, \alpha) - \alpha^2(2 - \nu)f_{2,x}(a, \alpha) = 0 \\ &f_1(c, \alpha) - f_2(c, \alpha) = 0 \\ &f_{1,x}(c, \alpha) - f_{2,x}(c, \alpha) = 0 \\ &f_{1,xx}(c, \alpha) - f_{2,xx}(c, \alpha) = 0 \\ &f_{2,xxx}(c, \alpha) - f_{1,xxx}(c, \alpha) = \frac{P}{\pi N} \end{aligned}\right\} \quad \ldots\ldots [13]$$

Substitution of Equations [12] into Equations [13] leads to eight simultaneous equations in the eight unknown coefficients A_j, B_j, C_j, D_j $(j = 1, 2)$, and after introducing the solution of these equations into Equations [12], we arrive at the complete integral representation of the deflections $w_j(x, y)$. Before citing the results so obtained, we define the dimensionless co-ordinates ξ, η, ζ by means of

$$\xi = \frac{x}{a}, \quad \eta = \frac{y}{a}, \quad \zeta = \frac{c}{a} \quad \ldots\ldots [14]$$

and let

$$\mu = \alpha a \quad \ldots\ldots [15]$$

Clearly

$$0 \leq \xi \leq 1, \quad -\infty < \eta < \infty, \quad 0 \leq \zeta \leq 1 \quad \ldots\ldots [16]$$

With the notations adopted in Equations [14] and [15], we finally arrive at

$$w_j(\xi, \eta, \zeta) = \frac{Pa^2}{8\pi N} \int_0^\infty \frac{\varphi_j(\xi, \zeta, \mu)}{\mu^3 \, \Delta(\mu)} \cos \mu\eta d\mu \quad \ldots\ldots [17]$$

$$(j = 1, 2)$$

where

$$\left.\begin{aligned} \Delta(\mu) &= \mu^2 + \gamma^2 + (2\gamma + 1)\cosh^2\mu \\ \gamma &= \frac{1 + \nu}{1 - \nu} \end{aligned}\right\} \quad \ldots\ldots [18]$$

and for

$$j = 1 \; (0 \leq \xi \leq \zeta)$$

$$\left.\begin{aligned} \varphi_1(\xi, \zeta, \mu) &= (1 + 2\gamma)[S_1 + \mu(\zeta - \xi)C_1 - (1 + 2\mu^2\xi)S_2 \\ &\quad -\mu(\xi + \zeta)C_2] + [1 + 2\gamma + 2\gamma^2 + 2\mu^2(1 - \xi)(1 - \zeta)]S_4 \\ &\quad +\mu(2 - \xi - \zeta)C_4 - [1 + 2\gamma + 2\gamma^2 + 2\mu^2(1 - \zeta + \xi)]S_5 \\ &\quad -[2 - \zeta + (1 + 2\gamma)^2\,\xi + 4\mu^2\xi(1 - \zeta)]\mu C_5 \end{aligned}\right\} \quad \ldots [19]$$

Here, the auxiliary symbols S_i and $C_i (i = 1, 2, 3, 4, 5)$ are accounted for by

$$\left.\begin{aligned} \left.\begin{matrix} S_1 \\ C_1 \end{matrix}\right\} &= \left.\begin{matrix} \sinh \\ \cosh \end{matrix}\right\} (2 - \zeta + \xi)\mu \\ \left.\begin{matrix} S_2 \\ C_2 \end{matrix}\right\} &= \left.\begin{matrix} \sinh \\ \cosh \end{matrix}\right\} (2 - \zeta - \xi)\mu \\ \left.\begin{matrix} S_3 \\ C_3 \end{matrix}\right\} &= \left.\begin{matrix} \sinh \\ \cosh \end{matrix}\right\} (2 + \zeta - \xi)\mu \\ \left.\begin{matrix} S_4 \\ C_4 \end{matrix}\right\} &= \left.\begin{matrix} \sinh \\ \cosh \end{matrix}\right\} (\zeta + \xi)\mu \\ \left.\begin{matrix} S_5 \\ C_5 \end{matrix}\right\} &= \left.\begin{matrix} \sinh \\ \cosh \end{matrix}\right\} (\zeta - \xi)\mu \end{aligned}\right\} \quad \ldots\ldots [20]$$

For $j = 2$ $(\zeta \leq \xi \leq 1)$

$$\varphi_2(\xi, \zeta, \mu) = \varphi_1(\zeta, \xi, \mu) \quad \ldots\ldots [21]$$

Thus φ_2 is obtained from Equations [19] by interchanging ξ and ζ, which follows also from Maxwell's reciprocal theorem applied to the deflections $w_j(x, y)$.

Bending and Twisting Moments in Integral Form

The integral representations for the bending moments M_x, M_y, and the twisting moment M_{xy} are now readily deduced from Equations [17], [18], [19], [20], [21] by means of Equations [2]. This computation yields

$$\left.\begin{aligned} M_{jx}(\xi, \zeta, \eta) &= \frac{-P(1 - \nu)}{8\pi} \int_0^\infty \frac{\psi_j(\xi, \zeta, \mu)\cos \mu\eta}{\mu\,\Delta(\mu)} \, d\mu \\ M_{jy}(\xi, \eta, \zeta) &= \frac{-P(1 - \nu)}{8\pi} \int_0^\infty \frac{\chi_j(\xi, \zeta, \mu)\cos \mu\eta}{\mu\,\Delta(\mu)} \, d\mu \\ M_{jxy}(\xi, \eta, \zeta) &= \frac{P(1 - \nu)}{8\pi} \int_0^\infty \frac{\phi_j(\xi, \zeta, \mu)\sin \mu\eta}{\mu\,\Delta(\mu)} \, d\mu \end{aligned}\right\} \quad \ldots [22]$$

$(j = 1, 2)$

where $\Delta(\mu)$ is as in Equations [18], and the definitions of the integrands are completed by

$$\left.\begin{aligned}\psi_1(\xi,\zeta,\mu) &= (1+2\gamma)\{-\gamma S_1+(\zeta-\xi)\mu C_1\\ &+(\gamma-2\mu^2\xi\zeta)S_2+[(1+2\gamma)\zeta-\xi]\mu C_2\}+[\gamma(1+2\gamma)\\ &+2\mu^2(1-\xi)(1-\zeta)]S_4+[(1+2\gamma)\zeta-\xi-2\gamma]\mu C_4\\ &+[\gamma(3+6\gamma+4\gamma^2)+2\mu^2(1+2\gamma)(1-\zeta)-2\mu^2\xi]S_5\\ &+[2\gamma+\zeta-(1+2\gamma)^2\xi-4\mu^2\xi(1-\zeta)]\mu C_5\end{aligned}\right\}\ldots[23]$$

$$\left.\begin{aligned}\chi_1(\xi,\zeta,\mu) &= (1+2\gamma)\{-\gamma S_1-(\zeta-\xi)\mu C_1\\ &+(\gamma+2\mu^2\xi\zeta)S_2+[(2\gamma-1)\zeta-\xi]\mu C_2\}-[\gamma(3+2\gamma)\\ &+2\mu^2(1-\xi)(1-\zeta)]S_4-[2\gamma-\xi-(2\gamma-1)\zeta]\mu C_4\\ &+[\gamma(4\gamma^2+2\gamma-1)+2\mu^2(2\gamma-1)(1-\zeta)+2\mu^2\xi]S_5\\ &+[2\gamma-\zeta+(1+2\gamma)^2\xi+4\mu^2\xi(1-\zeta)]\mu C_5\end{aligned}\right\}\ldots[24]$$

$$\left.\begin{aligned}\phi_1(\xi,\zeta,\mu) &= (1+2\gamma)[\mu(\zeta-\xi)S_1-\mu(\zeta-\xi)S_2\\ &+2\mu^2\xi\zeta C_2]+\mu(\zeta-\xi)S_4+[2\gamma(\gamma+1)\\ &+2\mu^2(1-\xi)(1-\zeta)]C_4+[(1+2\gamma)^2\xi-\zeta\\ &+4\mu^2\xi(1-\zeta)]\mu S_4-2[\gamma(\gamma+1)+\mu^2(1-\xi-\zeta)]C_5\end{aligned}\right\}\ldots[25]$$

$$\left.\begin{aligned}\psi_2''(\xi,\zeta,\mu) &= (1+2\gamma)\{-\gamma S_2+\mu(\xi-\zeta)C_2\\ &+(\gamma-2\mu^2\xi\zeta)S_2+[(1+2\gamma)\zeta-\xi]\mu C_2\}\\ &+[\gamma(1+2\gamma)+2\mu^2(1-\xi)(1-\zeta)]S_4+[(1+2\gamma)\zeta\\ &-\xi-2\gamma]\mu C_4+\{\gamma(1+2\gamma)+2\mu^2[1-\xi-(1\\ &+2\gamma)\zeta]\}S_4-[(1+2\gamma)^2\zeta-2\gamma-\xi\\ &+4\mu^2\zeta(1-\zeta)]\mu C_4\end{aligned}\right\}\ldots[26]$$

$$\left.\begin{aligned}\chi_2(\xi,\zeta,\mu) &= (1+2\gamma)\{-\gamma S_2-\mu(\xi-\zeta)C_2\\ &+(\gamma+2\mu^2\xi\zeta)S_2+[(2\gamma-1)\zeta+\xi]\mu C_2\}-[\gamma(3+2\gamma)\\ &+2\mu^2(1-\xi)(1-\zeta)]S_4+[(2\gamma-1)\zeta+\xi-2\gamma]\mu C_4\\ &-\{\gamma(3+2\gamma)+2\mu^2[1-\xi+(2\gamma-1)\zeta]\}S_4\\ &+[(1+2\gamma)^2\zeta+2\gamma-\xi+4\mu^2\zeta(1-\zeta)]\mu C_5\end{aligned}\right\}\ldots[27]$$

$$\left.\begin{aligned}\phi_2(\xi,\zeta,\mu) &= (1+2\gamma)[-\mu(\xi-\zeta)S_2+\mu(\xi-\zeta)S_2\\ &+2\mu^2\xi\zeta C_2]+[2\gamma(\gamma+1)+2\mu^2(1-\xi)(1-\zeta)]C_4\\ &-\mu(\xi-\zeta)S_4+[(1+2\gamma)^2\zeta-\xi+4\mu^2\zeta(1-\zeta)]\mu S_4\\ &-2[\gamma(\gamma+1)+\mu^2(1-\xi-\zeta)]C_5\end{aligned}\right\}\ldots[28]$$

Series Representation of Deflections and Moments

The numerical determination of the deflections and moments as functions of the position parameters ξ and η, the load parameter ζ, and Poisson's ratio ν, necessitates the evaluation of the improper integrals appearing in Equations [17], [22]. In view of the fact that the foregoing integrals are not expressible in terms of elementary functions, numerical integration provides one possible method for their evaluation.[4] However, this approach is exceedingly cumbersome if a complete and sufficiently accurate coverage of the solution is to be achieved. For this reason it is advantageous to resort instead to contour integration[5] in order to obtain series expansions of the integrals under consideration in terms of the residues at the singularities of the corresponding integrands. To this end we observe that the singularities of the integrands in Equations [17], [22] are simple poles and coincide with the zeros of $\Delta(\mu)$ which, by Equation [18], are the solutions of

$$\Delta(\mu)\equiv\mu^3+\gamma^2+\gamma+1/4+(\gamma+1/2)\cosh 2\mu=0\ldots[29]$$

Since $\gamma>0$, $\Delta(\mu)$ has no real roots. Moreover, it is readily shown that, considering only the upper half plane, the roots of Equation [29] are of the form

$$\left.\begin{aligned}&\mu_n=\pm\alpha_n+i\beta_n\ (n=0,1,2,\ldots\infty)\\ &\alpha_0=0,\ \alpha_n>0\ (n\geq 1)\\ &\beta_n>0\ (n\geq 0)\end{aligned}\right\}\ldots\ldots[30]$$

Thus in the region under consideration there is a single purely imaginary root, the remaining roots occurring in complex pairs which are located symmetrically with respect to the axis of imaginaries. We find that both α_n and β_n, regardless of the value of ν, are monotonically increasing functions of n for $n\geq 1$ and tend to infinity together with n. It is interesting to note that for large values of n, β_n asymptotically approaches $n\pi$. The distribution of the roots of Equation [29] in the first quadrant of the complex plane is indicated in Fig. 2, which is based on the values of α_n and β_n for $n=0,1,2,\ldots.7$ given in Table 1. These values were established by application of Newton's method[6] to the solution of the two real, transcendental equations corresponding to the complex Equation [29].

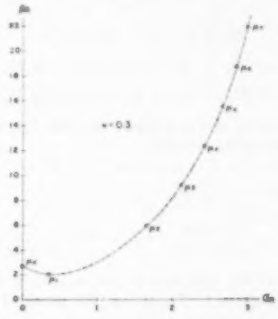

Fig. 2 Location of the Roots of $\Delta(\mu)=0$

TABLE 1 VALUES OF $\mu_n=\alpha_n+i\beta_n$, $\nu=0.3$

n	0	1	2	3	4	5	6	7
α_n	0	0.35654	1.6742	2.1312	2.4346	2.6642	2.8498	3.0058
β_n	2.7068	2.0272	5.9639	9.1813	12.3648	15.534	18.696	21.853

By virtue of a theorem on residues,[7] we now have

$$\left.\begin{aligned}&\int_0^\infty\theta(\mu)\cos\mu\eta d\mu=\pi i\sum_{n=0}^{\infty}R_n\\ &\text{for}\\ &\theta(\mu)=\frac{\varphi_i}{\mu^2\Delta(\mu)},\ \frac{\psi_i}{\mu\Delta(\mu)},\ \frac{\chi_i}{\mu\Delta(\mu)}\end{aligned}\right\}\ldots\ldots[31]$$

and

$$\left.\begin{aligned}&\int_0^\infty\theta(\mu)\sin\mu\eta d\mu=\pi\sum_{n=0}^{\infty}R_n\\ &\text{for}\\ &\theta(\mu)=\frac{\varphi_i}{\mu\Delta(\mu)}\end{aligned}\right\}\ldots\ldots[32]$$

where R_n is the residue at the simple pole μ_n of $\theta(\mu)e^{i\mu\eta}$. On evalu-

[4] This procedure is followed by MacGregor, reference (1), in the special case referred to previously.

[5] See reference (4), p. 45 et seq. and reference (5), chapt. VI.

[6] Reference (6), p. 90, et seq.

[7] Reference (5), p. 114, et seq. The extension of the theorem to our case, where the number of poles is infinite, is established by means of the Mittag-Leffler theorem.

ating the foregoing residues on the basis of Equations [19], [23], [24], [25], [26], [27], [28], we reach by aid of Equations [31], [32] the desired expansions for the deflections and moments whose integral forms are Equations [17], [22]. We first record the results of this lengthy computation for the deflections $w_j(\xi, \eta, \zeta)$

$$\left.\begin{aligned} w_j(\xi, \eta, \zeta) &= -\frac{Pa^2}{\pi N} K_j(\xi, \eta, \zeta) \ (j = 1, 2) \\ K_1 &= \frac{\pi}{8}\left\{\frac{\varphi_0(\xi, \zeta)e^{-\beta_0\eta}}{2\beta_0{}^4 + (2\gamma + 1)\beta_0 \sin 2\beta_0}\right. \\ &\quad \left. + 2\sum_{n=1}^{\infty}[p_n(\xi, \zeta)\sin \alpha_n\eta + q_n(\xi, \zeta)\cos \alpha_n\eta]e^{-\beta_n\eta}\right\} \\ K_2(\xi, \eta, \zeta) &= K_1(\xi, \eta, \xi) \end{aligned}\right\} \quad \ldots [33]$$

where

$$\left.\begin{aligned} p_n(\xi, \zeta) &= f_n r_n(\xi, \zeta) + g_n t_n(\xi, \zeta) \\ q_n(\xi, \zeta) &= f_n t_n(\xi, \zeta) - g_n r_n(\xi, \zeta) \end{aligned}\right\} \quad \ldots [34]$$

$$\left.\begin{aligned} f_n &= \frac{E_n}{E_n{}^2 + F_n{}^2}, \ g_n = \frac{F_n}{E_n{}^2 + F_n{}^2} \\ E_n &= 2\alpha_n + (2\gamma + 1)\sinh 2\alpha_n \cos 2\beta_n \\ F_n &= 2\beta_n + (2\gamma + 1)\cosh 2\alpha_n \sin 2\beta_n \end{aligned}\right\} \quad \ldots [35]$$

The functions φ_0, r_n, and t_n in Equations [33], [34] will be defined by aid of the auxiliary functions

$$\left.\begin{aligned} \delta_n &= \frac{\alpha_n}{\alpha_n{}^2 + \beta_n{}^2}, \quad \epsilon_n = \frac{\beta_n}{\alpha_n{}^2 + \beta_n{}^2} \\ \lambda_n &= \frac{\alpha_n{}^2 - 3\beta_n{}^2}{(\alpha_n{}^2 + \beta_n{}^2)^2}, \quad \rho_n = \frac{3\alpha_n{}^2 - \beta_n{}^2}{(\alpha_n{}^2 + \beta_n{}^2)^2} \end{aligned}\right\} \quad \ldots [36]$$

and in terms of the functions Si, Ci, si, ci $(i = 1, 2, 3, 4, 5)$. Here S_i, C_i are given by Equations [20] provided that μ is replaced by α_n; the analogous definitions of s_i, c_i are obtainable from Equations [20] by replacing the hyperbolic functions with the corresponding trigonometric functions and μ with β_n. Following these agreements, we may write

$$\left.\begin{aligned} r_n(\xi, \zeta) &= (1 + 2\gamma)\,[\lambda_n\delta_n S_1c_1 + \epsilon_n\rho_n C_1s_1 \\ &\quad + (\zeta - \xi)\left(\frac{\lambda_n + \rho_n}{4}\right)C_1c_1 + 2(\zeta - \xi)\delta_n\epsilon_n S_1s_1 \\ &\quad - (\lambda_n\delta_n + 2\xi\zeta\delta_n)S_2c_2 - (\rho_n\epsilon_n + 2\xi\zeta\epsilon_n)C_2s_2 \\ &\quad - (\xi + \zeta)\left(\frac{\lambda_n + \rho_n}{4}\right)C_2c_2 - 2(\xi + \zeta)\delta_n\epsilon_n S_2s_2] \\ &\quad + [(1 + 2\gamma + 2\gamma^2)\lambda_n\delta_n + 2(1 - \xi)(1 - \zeta)\delta_n]S_4c_4 \\ &\quad + [(1 + 2\gamma + 2\gamma^2)\rho_n\epsilon_n + 2(1 - \xi)(1 - \zeta)\epsilon_n]C_4s_4 \\ &\quad + (2 - \xi - \zeta)\left(\frac{\lambda_n + \rho_n}{4}\right)C_4c_4 + 2(2 - \xi - \zeta)\delta_n\epsilon_n S_4s_4 \\ &\quad - [(1 + 2\gamma + 2\gamma^2)\delta_n\lambda_n + 2(1 - \zeta + \xi)\delta_n]S_5c_5 \\ &\quad - [(1 + 2\gamma + 2\gamma^2)\rho_n\epsilon_n + 2(1 - \zeta + \xi)\epsilon_n]C_5s_5 \\ &\quad - [2 - \zeta + (1 + 2\gamma)^2\xi + 4\xi(1 - \zeta)(\alpha_n{}^2 - \beta_n{}^2)]\left(\frac{\lambda_n + \rho_n}{4}\right)C_5c_5 \\ &\quad - [2 - \zeta + (1 + 2\gamma)^2\xi + 4\xi(1 - \zeta)(\alpha_n{}^2 - \beta_n{}^2)]\,2\delta_n\epsilon_n S_5s_5 \\ &\quad + 8\alpha_n\beta_n{}^2\xi(1 - \zeta)\left(\frac{\lambda_n + \rho_n}{4}\right)S_5s_5 \\ &\quad - 16\,\alpha_n\beta_n\xi(1 - \zeta)\delta_n\epsilon_n C_5c_5 \end{aligned}\right\} \quad \ldots [37]$$

$$\left.\begin{aligned} t_n(\xi, \zeta) &= (1 + 2\gamma)\,[\delta_n\lambda_n C_1s_1 - \epsilon_n\rho_n S_1c_1 \\ &\quad + (\zeta - \xi)\left(\frac{\lambda_n + \rho_n}{4}\right)S_1s_1 - 2(\zeta - \xi)\delta_n\epsilon_n C_1c_1 \\ &\quad - (\lambda_n\delta_n + 2\xi\zeta\delta_n)C_2s_2 + (\epsilon_n\rho_n + 2\xi\zeta\epsilon_n)S_2c_2 \\ &\quad - (\xi + \zeta)\left(\frac{\lambda_n + \rho_n}{4}\right)S_2s_2 + 2(\xi + \zeta)\delta_n\epsilon_n C_2c_2] \\ &\quad + [(1 + 2\gamma + 2\gamma^2)\delta_n\lambda_n + 2(1 - \xi)(1 - \zeta)\delta_n]C_4s_4 \\ &\quad - [(1 + 2\gamma + 2\gamma^2)\epsilon_n\rho_n + 2(1 - \xi)(1 - \zeta)\epsilon_n]S_4c_4 \\ &\quad + (2 - \xi - \zeta)\left(\frac{\lambda_n + \rho_n}{4}\right)S_4s_4 - 2(2 - \xi - \zeta)\delta_n\epsilon_n C_4c_4 \\ &\quad - [(1 + 2\gamma + 2\gamma^2)\delta_n\lambda_n + 2(1 - \zeta + \xi)\delta_n]C_5s_5 \\ &\quad + [(1 + 2\gamma + 2\gamma^2)\epsilon_n\rho_n + 2(1 - \zeta + \xi)\epsilon_n]S_5c_5 - [2 - \zeta \\ &\quad + (1 + 2\gamma)^2\xi + 4\xi(1 - \zeta)(\alpha_n{}^2 - \beta_n{}^2)]\left(\frac{\lambda_n + \rho_n}{4}\right)S_5s_5 \\ &\quad + [2 - \zeta + (1 + 2\gamma)^2\xi + 4\xi(1 - \zeta)(\alpha_n{}^2 - \beta_n{}^2)]\,2\delta_n\epsilon_n C_5c_5 \\ &\quad - 8\,\alpha_n\beta_n\xi(1 - \zeta)\left(\frac{\lambda_n + \rho_n}{4}\right)C_5c_5 \\ &\quad - 16\,\alpha_n\beta_n\xi(1 - \zeta)\delta_n\epsilon_n S_5s_5 \end{aligned}\right\} \quad \ldots [38]$$

$$\left.\begin{aligned} \varphi_0(\xi, \zeta) &= (1 + 2\gamma)\,[\beta_1 + \beta_0(\zeta - \xi)c_1 - (1 - 2\beta_0{}^2\xi\zeta)s_2 \\ &\quad - \beta_0(\xi + \zeta)c_2] + [(1 + 2\gamma + 2\gamma^2) - 2\beta_0{}^2(1 - \xi)(1 - \zeta)]s_1 \\ &\quad + (2 - \xi - \zeta)\beta_0 c_4 - [1 + 2\gamma + 2\gamma^2 \\ &\quad - 2\beta_0{}^2(1 - \zeta + \xi)]s_3 - [2 - \zeta + (1 + 2\gamma)^2\xi \\ &\quad - 4\beta_0{}^2\xi(1 - \zeta)]\beta_0 c_5 \end{aligned}\right\} \quad \ldots [39]^*$$

Equations [33] to [39] together with the roots μ_n of Equation [29] constitute the complete series representation of the deflections $w(\xi, \eta, \zeta)$. The series in Equation [33] was found to be rapidly convergent, and only the leading four terms had to be taken into account in subsequent numerical computations. The values of

$$K_j = -w_j \Big/ \frac{Pa^2}{\pi N}$$

for $\nu = 0.3$ and various values of ξ, η, ζ are listed in Tables 2, 3, and 4.

TABLE 2 VALUES OF K_j FOR $\eta = 0$ AND VARIOUS VALUES OF ξ AND ζ, $\nu = 0.3$

$\xi \backslash \zeta$	0.25	0.50	0.75	1.00
0.25	0.0168	0.0272	0.0388	0.0499
0.50	0.0272	0.0794	0.118	0.160
0.75	0.0388	0.118	0.220	0.318
1.00	0.0499	0.160	0.318	0.525

TABLE 3 VALUES OF K_j FOR $\zeta = 0.75$ AND VARIOUS VALUES OF ξ AND η, $\nu = 0.3$

$\xi \backslash \eta$	0	0.25	0.50	1.00	1.50	2.00	∞
0	0	0	0	0	0	0	0
0.25	0.0388	0.0233	0.0207	0.0116	0.00543	0.00142	0
0.50	0.1183	0.1080	0.0867	0.0463	0.0217	0.00939	0
0.75	0.2201	0.1129	0.0586	0.0162	0.00462	0.00133	0
1.00	0.3178	0.2942	0.2435	0.1379	0.0687	0.0312	0

TABLE 4 VALUES OF K_j FOR $\zeta = 1$ AND VARIOUS VALUES OF ξ AND η, $\nu = 0.3$

$\xi \backslash \eta$	0	0.25	0.50	1.00	1.50	2.00	∞
0	0	0	0	0	0	0	0
0.25	0.0499	0.0409	0.0341	0.0189	0.00886	0.03379	0
0.50	0.1595	0.1455	0.1218	0.0691	0.0335	0.0147	0
0.75	0.3178	0.2942	0.2435	0.1379	0.0687	0.0312	0
1.00	0.5245	0.4703	0.3804	0.2154	0.1076	0.0495	0
	(0.527)[a]	(0.470)	(0.380)	(0.213)	(.....)	0.0496)	

[a] Numbers in parentheses in this table are values obtained by MacGregor, reference (1).

* The argument of s_i, c_i $(i = 1, 2, 3, 4, 5)$ in Equations [39] is understood to be β_0.

General series representations, analogous to Equation [33], were also obtained for the bending moments $M_{1y}(\xi, \eta, \zeta)$, $M_{1\eta}(\xi, \eta, \zeta)$, and the twisting moment $M_{1xy}(\xi, \eta, \zeta)$ for $j = 1, 2$. However, in view of space limitations, we cite here merely the results for the clamped edge $\xi = 0$

$$\left.\begin{aligned} M_x(0, \eta, \zeta) &= PK_x(\eta, \zeta) \\ M_y(0, \eta, \zeta) &= \nu M_x(0, \eta, \zeta) \\ M_{xy}(0, \eta, \zeta) &= 0 \\ K_x(\eta, \zeta) &= -\frac{1}{2}\left\{\frac{\psi_0 e^{-\beta_0\eta}}{2\beta_0^2 + (2\gamma + 1)\beta_0 \sin 2\beta_0}\right. \\ &\quad \left. -2\sum_{n=1}^{\infty} e^{-\beta_n\eta}\left[p_{\zeta n}(\zeta)\sin \alpha_n\eta + q_{\zeta n}(\zeta)\cos \alpha_n\eta\right]\right\} \end{aligned}\right\} \quad \ldots [40]$$

where

$$\left.\begin{aligned} p_{\zeta n}(\zeta) &= f_n r_{\zeta n}(\zeta) + g_n t_{\zeta n}(\zeta) \\ q_{\zeta n}(\zeta) &= f_n t_{\zeta n}(\zeta) - g_n r_{\zeta n}(\zeta) \end{aligned}\right\} \quad \ldots [41]$$

with f_n and g_n given by Equations [35], [36], whereas

$$\left.\begin{aligned} r_{\zeta n}(\xi) &= (1 + 2\gamma)\xi \cosh (2 - \zeta)\alpha_n \cos(2 - \zeta)\beta_n \\ &\quad + \xi \cosh \xi\alpha_n \cos \xi\beta_n \\ &\quad + 2\left[\gamma(\gamma + 1)\delta_n + (1 - \zeta)\alpha_n\right] \sinh \xi\alpha_n \cos \zeta\beta_n \\ &\quad + 2\left[\gamma(\gamma + 1)\epsilon_n - (1 - \zeta)\beta_n\right] \cosh \xi\alpha_n \sin \xi\beta_n \\ t_{\zeta n}(\xi) &= (1 + 2\gamma)\xi \sinh (2 - \zeta)\alpha_n \sin (2 - \zeta)\beta_n \\ &\quad + \xi \sinh \xi\alpha_n \sin \xi\beta_n \\ &\quad + 2\left[\gamma(\gamma + 1)\delta_n + (1 - \zeta)\alpha_n\right] \cosh \xi\alpha_n \sin \xi\beta_n \\ &\quad - 2\left[\gamma(\gamma + 1)\epsilon_n - (1 - \zeta)\beta_n\right] \sinh \xi\alpha_n \cos \xi\beta_n \end{aligned}\right\} \quad \ldots [42]$$

and δ_n, ϵ_n are as in Equations [36]. Finally

$$\psi_0(\xi) = (2\gamma + 1)\beta_0\xi \cos(2 - \zeta)\beta_0 + \beta_0\xi \cos \xi\beta_0 + 2[\gamma(\gamma + 1) - \beta_n^2(1 - \xi)] \sin \xi\beta_0 \quad \ldots [43]$$

The series in Equations [40] again was found to converge rapidly with the exception of the neighborhood of $\eta = 0$, where the convergence is slow. The values of $K_x = M_x/P$ at $\xi = 0$ and for various choices of ζ, η are given in Table 5. Most of these K_x-values were checked independently by numerical integration based upon Equations [22], and in all instances the agreement is seen to be satisfactory.

Discussion of Results

According to the solution obtained for the problem under consideration, the deflections w depend on the dimensionless coordinates $\xi = x/a$, $\eta = y/a$, as well as on the relative load position, i.e., on $\zeta = c/a$, and on Poisson's ratio ν. Moreover, for fixed values of ξ, η, ζ, and ν, the deflection w is directly proportional to Pa^2/N where P is the load, a the plate width, and N the flexural rigidity of the plate. The maximum deflections occur along the ξ-axis (Fig. 3), and there at the free edge $\xi = 1$. Figs. 4 and 5 show illustrative profiles of the deflection surface for $\zeta = 3/4$ and $\zeta = 1$, respectively. We observe that w is practically negligible beyond $\eta = 2$. The curve for $\xi = 1$ in Fig. 4 is identical with that for $\xi = 3/4$ in Fig. 5 by virtue of the reciprocal relation $w(\xi, \eta, \zeta) = w(\zeta, \eta, \xi)$. From Fig. 4 we note that if $\zeta < 1$ and $\eta \neq 0$, w is not necessarily a steadily increasing function of ξ. The values of $w(\eta)$ for $\zeta = 1$, $\xi = 1$ are found to be in very close agreement with those obtained by MacGregor (1).

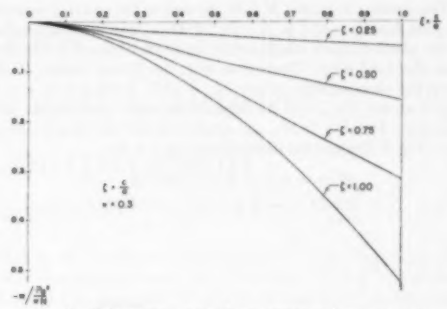

Fig. 3 ξ-Dependence of Deflection w Along η = 0

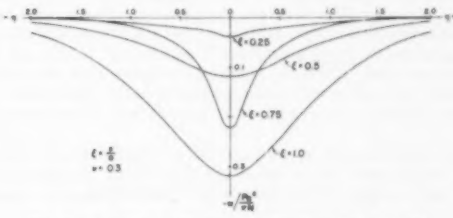

Fig. 4 Profiles of Deflection Surface for ζ = 3/4

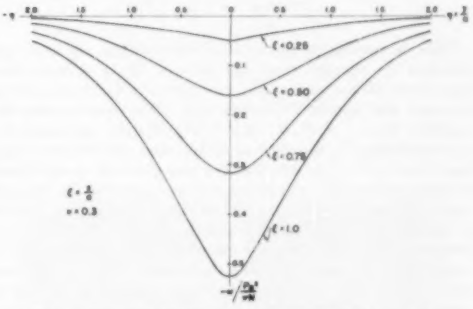

Fig. 5 Profiles of Deflection Surface for ζ = 1.0

TABLE 5 VALUES OF M_x/P FOR $\xi = 0$ AND VARIOUS VALUES OF ζ AND η, $\nu = 0.3$

	$\zeta = 0.25$		$\zeta = 0.50$		$\zeta = 0.75$		$\zeta = 1.00$	
η	(1)	(2)	(1)	(2)	(1)	(2)	(1)	(2)
0	[c]	−0.332	[c]	−0.370	[c]	−0.428	−0.509	−0.509[b]
0.25	−0.174	−0.172	−0.302	−0.302	−0.385	−0.387	−0.474	[c]
0.50	−0.074	−0.073	−0.196	−0.196	−0.298	−0.294	−0.390	[c]
1.00	−0.022	−0.022	−0.076	−0.076	−0.140	−0.141	−0.205	[c]
1.50	−0.0075	−0.009	−0.029	−0.029	−0.059	−0.051	−0.091	[c]
2.00	−0.0026	−0.0026	−0.0108	−0.010	−0.023	−0.023	−0.037	[c]

1 By numerical integration, Equation [22].
2 By series expansion, Equation [40].
[c] Not computed.
[b] MacGregor's result, reference (1).

The bending moments M_x, M_y as well as the twisting moment M_{xy} are functions of ξ, η, ζ, ν, and P alone, and are independent of the absolute plate width or the absolute distance of the load from the fixed edge. Regardless of ζ, the largest values of M_x along the clamped edge, where $M_y = \nu M_x$, occur at $\xi = \eta = 0$. Fig. 6 shows $M_{x,\max}$ in its dependence upon the relative load position. For $\zeta = 1$, $M_{x,\max}$ coincides with MacGregor's result (1). Fig. 6 displays the discontinuity at $\zeta = 0$

$$M_x(\xi = 0, \eta = 0, \zeta = 0) = 0$$

$$\lim_{\zeta \to 0} M_x(\xi = 0, \eta = 0, \zeta) = -0.32\,P \quad \ldots\ldots\ldots [44]$$

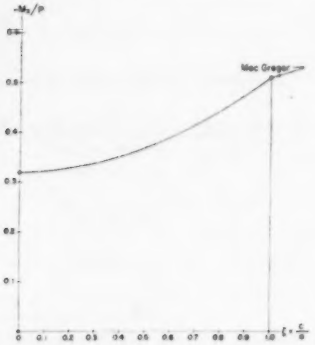

FIG. 6 ζ-DEPENDENCE OF BENDING MOMENT M_x AT $\xi = 0$, $\eta = 0$, FOR $\nu = 0.3$

Thus, according to the solution obtained, as the load approaches the clamped edge, the moment $M_{x,\max}$ is never less than about 60 per cent of the corresponding value induced by the same load applied at the free edge. The discontinuous dependence upon ζ of $M_{x,\max}$ at $\zeta = 0$ is formally accounted for by considering the distribution of M_x along the clamped edge, shown in Fig. 7. It is seen that the load gives rise to significant bending moments M_x only over a certain segment of the clamped edge, and that the relative width of this "influence zone" tends to zero with ζ. It should of course be emphasized that if the distance of the load from the clamped edge is of the order of magnitude of the plate thickness, the solution ceases to be physically valid, since in this instance the shearing deformations, neglected in the elementary plate theory, are no longer unimportant.

The foregoing discontinuity is also confirmed by observing that the limit as $\zeta = c/a \to 0$ alternatively admits the interpretation $a \to \infty$ with c fixed, which corresponds to the cantilever plate of infinite width. An exact solution in closed form for this case was given by Michell (7). According to Michell's solution the bending moment M_x at $\xi = \eta = 0$ is $-P/\pi$, and is here independent of ζ. Our present limit, Equation [44] is seen to be in very good agreement with this result.

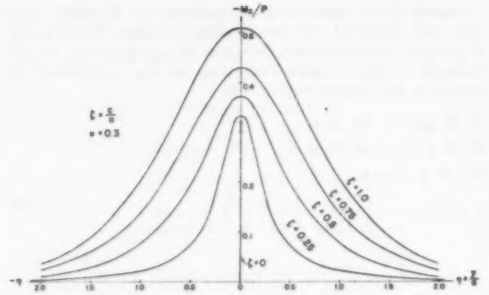

FIG. 7 η,ζ-DEPENDENCE OF BENDING MOMENT M_x ALONG CLAMPED EDGE

ACKNOWLEDGMENT

The author is greatly indebted to Dr. Eli Sternberg, Associate Professor of Mechanics at Illinois Institute of Technology, for his invaluable advice and assistance in the preparation of this paper. Particular thanks are also due to Dr. LeVan Griffis, Chairman of Mechanics at Illinois Institute of Technology and Armour Research Foundation, who secured Foundation sponsorship for this investigation. Finally, acknowledgment is made to Mr. R. L. Calvin and Mr. C. E. Spurrier who assisted in the numerical calculations.

BIBLIOGRAPHY

1 "Deflection of a Long Helical Gear Tooth," by C. W. MacGregor, *Mechanical Engineering*, vol. 57, 1935, p. 225.

2 "Cantilever Plate With Concentrated Edge Load," by D. L. Holl, Trans. ASME, vol. 59, 1937, p. 8.

3 "Theory of Plates and Shells," by S. Timoshenko, McGraw-Hill Book Company, Inc., New York, N. Y., 1940.

4 "Complex Variables and Operational Calculus With Technical Applications," by N. W. MacLachlan, The Macmillan Company, New York, N. Y., 1946.

5 "A Course in Modern Analysis," by E. T. Whittaker and G. N. Watson, The Macmillan Company, New York, N. Y., 1944.

6 "Calculus of Observations," by E. T. Whittaker and G. Robinson, Blackie & Sons, Ltd., London and Glasgow, 1937.

7 "The Flexure of a Circular Plate," by J. H. Michell, Proceedings of the London Mathematical Society, vol. 34, 1902, p. 223.

Effect of Imperfections on Buckling of Thin Cylinders and Columns Under Axial Compression[1]

By L. H. DONNELL[2] and C. C. WAN[3]

Von Kármán and Tsien have shown that under elastic conditions the resistance of perfect thin cylinders subjected to axial compression drops precipitously after buckling. It is considered that this indicates that this type of buckling is very sensitive to imperfections or disturbances. In this paper the effects of certain imperfections of shape (assumed to be equivalent to all the actual defects or disturbances combined) are studied by the large-deflection shell theory developed in a previous paper (2).[4]

It is found that two types of buckling failure may occur. One is of a purely elastic type which occurs when the peak of the average stress versus average strain curve is reached, while the other type is precipitated by yielding, which for thicker cylinders or lower-yield material may occur before such a peak is reached. Curves are derived giving the dependence of each type of failure upon the dimensions and elastic and yield properties of the specimen and also upon an "unevenness factor" U which determines the magnitude of the initial imperfections and is assumed to depend on the method of fabrication. The relations derived are in line with test results, and similar studies of the buckling of struts indicate that the magnitude of the initial imperfections which have to be assumed to explain test strengths are reasonable.

Introduction

THE problem of buckling of a thin-walled circular cylinder under simple axial compression has received a great deal of study, and, although this is a very fundamental case, it is still a subject for controversy. The present discussion will be limited to cylinders long enough (say, more than $^3/_4$ of a diameter) so that end conditions are unimportant, as has been shown by Nojima and Kanemitsu (1), and short enough (say, less than 10 or 20 diameters) so that there is no danger of buckling of the cylinder as a tubular column. Most practical applications fall in such a range.

Let us first review briefly the known facts concerning this case. If a thin cylinder, Fig. 1, of mean radius r and wall thickness t is subjected to sufficient axial compressive stress σ, it actually buckles into many comparatively small waves, as indicated by the photographs (2) of Fig. 2. Buckling comes suddenly, almost explosively, and usually occurs over only a part of the wall, as at (*a*) or (*b*), rather than in the complete manner of (*c*) or (*d*). The number of waves around the circumference n is of the order of ten or so, and the wave shape ratio m (ratio of wave length in the circumferential to that in the axial direction) is always close to unity, with an average value of about 0.75.

The classical theory for this case, developed by Lorenz (3), Southwell (4), Timoshenko (5), Robertson (6), and others, is based on small-deflection shell theory and the assumptions of

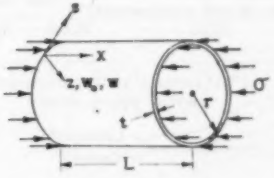

Fig. 1

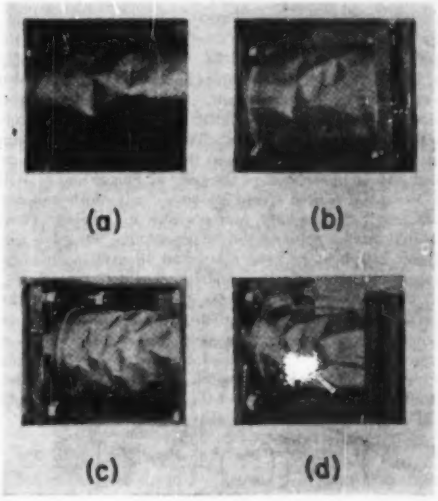

Fig. 2

[1] This work was done partly at Illinois Institute of Technology and partly at Chance Vought Aircraft. The authors wish to thank these institutions for the opportunities afforded them, and in particular Dr. LeVan Griffis, Chairman of Mechanics at I.I.T. Presented at the Seventh International Congress of Applied Mechanics, London, England, 1948.

[2] Research Professor, Illinois Institute of Technology, Chicago, Ill. Mem. ASME.

[3] Senior Project Analytical Engineer, Chance Vought Aircraft, Dallas, Texas. Jun. ASME.

[4] Numbers in parentheses refer to the Bibliography at the end of the paper.

Presented at the National Meeting of the Applied Mechanics Division, Ann Arbor, Mich., June 13–15, 1949, of The American Society of Mechanical Engineers.

Discussion of this paper should be addressed to the Secretary, ASME, 29 West 39th Street, New York, N. Y., and will be accepted until April 10, 1950, for publication at a later date. Discussion received after the closing date will be returned.

Note: Statements and opinions advanced in papers are to be understood as individual expressions of their authors and not those of the Society. Paper No. 49—APM-14.

perfect elasticity and perfect initial shape. It predicts a buckling stress of

$$\sigma_{cl} = [E/\sqrt{3(1-\mu^2)}]t/r \approx 0.605\,Et/r \ldots\ldots [1]$$

The theory does not specify the wave shape ratio m, but if we assume the experimental value $m = 0.75$, the number of waves around the circumference n is predicted to be

$$n_{cl} = \sqrt[4]{12(1-\mu^2)}\,\sqrt{r/t}/(m + 1/m) \approx 0.87\sqrt{r/t} \ldots [2]$$

The check between experiments and the classical theory is shown by the diagrams of Fig. 3, the ratio of the experimental to the classical theoretical buckling stress being given at (*a*), and similarly for the number of circumferential waves at (*b*).

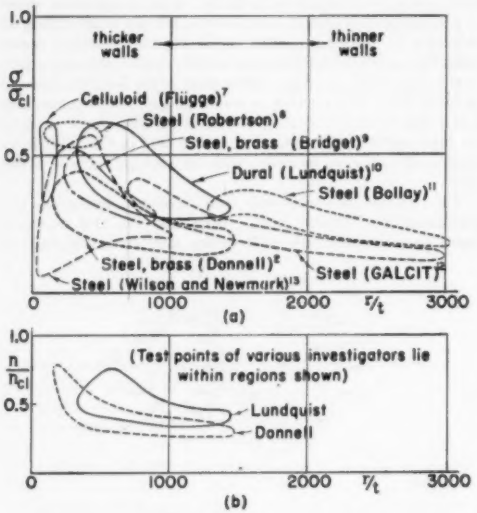

FIG. 3

Experimental points obtained by various investigators (2, 7, 8, 9, 10, 11, 12, 13) lie in the areas indicated, and all the results known to the authors are shown. In general, the experimental values of both σ and n are widely scattered and are all much less than the theory calls for. There seems to be a definite tendency for them to decrease as the cylinders become thinner-walled, except in the case of the tests of Flügge and of Wilson and Newmark (whose specimens were fairly thick-walled and which, as will be seen later, were probably in the plastic or what we would call for columns the "short-column" range).

Many investigators have attempted to explain these large discrepancies between theory and experiment (7, 14, 15, 16, 17, 18). In 1934 one of the authors presented an attempt (2) to investigate the effect of the initial deviations from perfect shape which are always present. A second-approximation shell theory for finite deflections was developed, in which two of the displacement components were eliminated and the following relation between the stress function f of the membrane stresses and the radial displacement w was developed

$$\left(\frac{\partial^2}{\partial x^2} + \frac{\partial^2}{\partial s^2}\right)^2 f = EK\left[\left(\frac{\partial^2 w}{\partial x \partial s}\right)^2 - \frac{\partial^2 w}{\partial x^2}\cdot\frac{\partial^2 w}{\partial s^2}\right] - \frac{E}{r}\frac{\partial^2 w}{\partial x^2} \ldots [3]$$

where $K = 1 + 2w_0/w$ = a constant

The number K involves the ratio between the initial deviation from perfect shape w_0 and the displacement during loading w, and it must be a constant as noted; this means that only the component of the deviation which is of the same shape as the displacements can be taken into consideration. This is the same as is usually assumed in column theory, and this component of the deviation can be shown to be by far the most important component. The second-order terms on the right-hand side of Equation [3] correspond to membrane stresses due to the finite displacements, while the last term on the right-hand side corresponds to membrane stresses due to the curvature. Equation [3] can be considered to be a generalization of Kármán's well-known equation for finite deflections of flat plates (19), and reduces to it for $w_0 = 0$ (so that $K = 1$) and $r =$ infinity.

If w and w_0 are known or assumed, then f can be solved for from Equation [3]. It will be the sum of the easily obtained particular solution and the general solution of the equation obtained by replacing the right-hand side by zero. The latter solution corresponds, in general, to stress distributions which are inconsistent with the physical conditions of the present problem, except for a term $\sigma s^2/2$ which corresponds to the average axial stress σ. The average stress in the circumferential direction will be assumed to be zero, as it would have to be in the middle part of a long cylinder under no internal or external pressure (this will be further discussed in the next paragraph). The use of the stress function f satisfies the two equilibrium equations in the plane of the wall, and the other equilibrium conditions can be approximately satisfied by assuming an expression for w containing arbitrary parameters and choosing these parameters from energy considerations.

In applying this method in the paper (2) of 1934, the energy was minimized for only one parameter and several simplifications and neglections were made to reduce the mathematical difficulties; as a consequence, the solution obtained was unsatisfactory. However, the method itself has proved to be useful. In 1941 von Kármán and Tsien (20) made a very important advance in our understanding of this problem by applying this general method rigorously and assuming a deflection shape of the type

$$w = at\left(\cos\frac{mnx}{r}\cos\frac{ns}{r} + b\cos\frac{2mnx}{r} + c\cos\frac{2ns}{r} + d\right) \ldots [4]$$

where m and n are the wave shape ratio and number of circumferential waves, and a, b, c, and d are other arbitrary parameters. The parameter d defines a uniform inward displacement which is caused by circumferential shortening due to finite deflections; its existence has already been assumed in making the assumption of zero average circumferential stress just mentioned. In practice, d drops out in the differentiations and need not be further considered, although its value can be found if desired from the condition of zero average circumferential stress. This leaves only the parameters a, b, c, m, and n which must be assumed or be determined so as to minimize the energy.

Von Kármán and Tsien assumed c to equal b, minimized the energy for two of the remaining parameters a and b,[5] and for various assumed values of m and n they found relations between the average stress σ and the unit shortening of the cylinder ϵ. These relations were found to be of the type shown by the full line in Fig. 4. They assumed elastic conditions and perfect initial shape, and the peak point p' is at the height given by the classical theory. Such a result is in great contrast to our experience with columns, for which we would obtain a hori-

[5] They also minimized the energy for d, but this amounted to the same thing as our assumption of zero average circumferential stress; in either case this is justified only on the basis of the neglection of end constraints.

zontal or rising curve after buckling, instead of the precipitous drop-off indicated in Fig. 4. Such a drop-off indicates tremendous sensitivity in this type of buckling. Leggett and Jones (21) refined these studies by carrying them a step further;

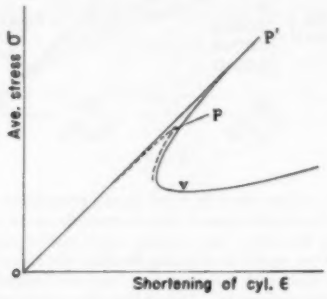

FIG. 4

they also assumed perfect elasticity and initial shape and the constant $c = b$, but they succeeded in minimizing the energy for all four of the remaining parameters, and obtained one curve, namely, the full line in Fig. 4.

The question now arises: What is the exact significance of these highly interesting results? Shall we be content to say merely that this shows great sensitivity to any disturbances (which this idealized solution of course neglects), and that designers must expect that such disturbances will always actually occur and will dull the sharp razor-edge of the resistance curve to something like the shape shown by the dotted line, Fig. 4, with the exact magnitude of the peak resistance at the point p left to tests to determine (24)? This approach merely answers in a general way the question of "why" the large discrepancy between classical theory and experiments, without helping the designer; he is still left to determine from his tests the magnitude of the peak resistance which he needs, just as he had to before.

Or shall we adopt the approach that the low point or "valley" at v, Fig. 4, obviously represents a very stable condition, and that we should use the resistance at this point (which Leggett and Jones found to be about one third of the classical buckling resistance) as a safe and conservative value? Concerning this, it may first be said that under certain conditions (very large r/t ratio, for instance) this value is not at all conservative, while under other conditions (such as a small r/t ratio) it would represent wasteful design, since we can actually safely rely on considerably higher resistance.

Moreover, it seems evident that the magnitude of the actual peak resistance given by a point such as p depends on the shape of the near-by peak part of the idealized curve and that it has little if any relation to the shape of distant parts of this idealized curve such as the region around v. The actual peak resistance would probably be practically the same even if there were no valley in the idealized curve at all and the curve kept on falling; as a matter of fact, as von Kármán and Tsien have pointed out, the "large deflection" theory used is only a second approximation and is probably quite inaccurate at the relatively large displacements (several times the thickness) occurring at the valley, so that this whole region is in doubt and there may really be no valley at all. On the other hand up to the actual peak resistance given by such a point as p (what happens after this point is reached is of little practical interest) the displacements are only a small fraction of the thickness (they are zero along the straight line op' and increase only as we go to the right of this line) and the theory is probably quite accurate for the study of this region.

It seemed to the authors that the only hope of finding out how much the peak resistance is actually reduced under various conditions, and of thus giving the designer some theoretical help, would be to try to make some quantitative study of the factors which are reducing the peak. These are probably rather numerous, and include: (*a*) Initial deviations from the assumed perfect geometrical shape (these can be measured on the inside or outside of the specimen); (*b*) initial stresses; (*c*) deviations from uniform, isotropic elastic behavior (these are obviously not to be ignored in thin-walled sheets of multicrystalline material, where there may be only a few crystals across the thickness); and (*d*) accidental lateral loadings, such as those due to shocks, sound waves, seismographic vibrations, and so on.

It has not been shown that cylinder buckling tests give appreciably lower strengths when made in a boiler factory or a stamping mill than when made in a vibration-proof laboratory, and it seems probable that the first three of these factors are much the most important. Since these first three are all properties of the specimen, rather than of the conditions of loading, there seems some hope of relating some systematic part of them to known properties of the specimen, and thus, by taking them into consideration, of eliminating some part of the variation which at present has to be regarded as unpredictable "scatter."

In any case, all of these factors probably have similar effects, and, since a method is available for considering initial geometric deviations (by using the K in Equation [3]) it is proposed to consider an "equivalent geometric deviation" which would have the same total effect as all these effects together. Its magnitudes may of course be much greater than the geometric deviations alone, which themselves are sometimes large enough to be quite evident to the eye. An attempt will first be made to get some idea of the probable magnitudes of this deviation, and its relation to known properties, by a comparison with the corresponding simpler case of columns, for which considerably more experience and data are available.

Systematic experimental measurements, both for cylinders and columns, are obviously greatly needed, and such work is planned at Illinois Institute of Technology. It is not claimed that the results, which the assumptions which will be made lead to, give a complete answer to this very difficult problem, but it is hoped that they may point out the true nature of the problem involved and the general type of results which can be expected, and indicate further work which is needed for a satisfactory and practically useful solution.

THE CASE OF ACTUAL COLUMNS

Consider a simple hinged end column, say, of rectangular section, with a geometric deviation from perfect straightness at the center of $a_0 t$, as indicated in Fig. 5. The actual average amplitude of this deviation in a number of columns will surely vary with the proportions. For example, if we should cut the column from a bar having a constant small curvature as indicated by the dotted lines, Fig. 5, the deviation would evidently vary as the square of the length. Also, other things being equal, the average deviation will certainly be greater for thin bars than for thick ones. In the present lack of actual data on this subject it seems reasonable to assume a dimensionally consistent relation

FIG. 5

between the average deviation and the dimensions of the column, of the type

$$a_{0l} = Cl^2/t \text{ or } a_0 = C(l/t)^2$$

where the dimensionless number C should have a reasonably constant value for similarly fabricated columns, independent of their proportions.

While the foregoing reasoning was for geometric deviations only, similar reasoning probably applies to the other types of imperfections which are present, and hence also to the equivalent geometric deviation which has an effect equal to all of them combined. The amplitude of the sinusoidal component of this deviation will be approximately the same as the deviation at the center. We will therefore assume this sinusoidal component of the average equivalent deviation to be

$$w_0 = a_{0l} \sin(\pi x/l), \text{ where } a_0 = (U/\pi^2)(l/t)^2 \ldots\ldots [5]$$

The number U is an "unevenness" factor assumed to depend only on the method of fabricating the column. The factor π^2 is introduced to simplify the results.

Using this assumption it is easy to develop by conventional methods a rational column formula which gives the average axial stress σ at which yielding will commence. This computation is made in Appendix 1, and the resulting formula can be expressed as follows

$$\sigma = \sigma_y \left[N - \sqrt{N^2 - \frac{\sigma_{cl}}{\sigma_y}} \right], \text{ where } 2N = 1 + \frac{\sigma_{cl}}{\sigma_y} + \frac{UE}{2\sigma_y} \ldots [6]$$

Here σ_{cl} is of course the Euler stress, obtained by assuming perfect elasticity and shape. This formula considers both yielding and initial imperfections, and can be interpreted to apply to all end conditions and cross sections. It implies a definite yield point of the material σ_y, and gives the condition under which yielding starts; hence it would be somewhat conservative for materials like the aluminum alloys (if their yield point is taken as a value near the proportioned limit) as well as for very short columns in cases where the designer feels that yielding can be permitted and the design can be based on ultimate buckling strength.

Results from Equation [6] are compared in Fig. 6 with several empirical column formulas which have been commonly used for mild-steel construction. The chart[6] used in Fig. 6 is a generalization of the familiar stress versus slenderness-ratio column chart. The horizontal line at which a perfect strut would yield is represented by the line ab, while the Euler curve becomes the 45-deg straight line bc. The points a and c correspond to zero and infinite slenderness ratios. As can be seen, Equation [6] yields curves which approach the broken line abc for small values of U. The depressing effect of initial deviations is greatest in the middle range of slenderness ratios, for values of σ_y/σ_{cl} around 1. Both the theoretical curves and the empirical design curves pass through the points a and c, that is, they coincide with a simple yield condition or with the Euler curve at extreme slenderness ratios. It thus seems evident that the depression of the empirical design curves in the middle range is solely to allow for initial defects. Values of U from 0.0002 to 0.0010 are required to depress the theoretical curves by similar amounts. Such other data as are available (22) on the initial deviations in actual columns indicate that these values of U are not unreasonable.

[6] This type of chart has proved very useful, since it can be used for any kind of buckling problem, and the entire range can be shown on a finite chart. The idea of adjacent plots of a variable from 0 to 1 and of its reciprocal from 1 to 0 (continuous functions remain continuous across the boundary between such plots) can be extended to permit plots of both variables from $-\infty$ to $+\infty$ (23).

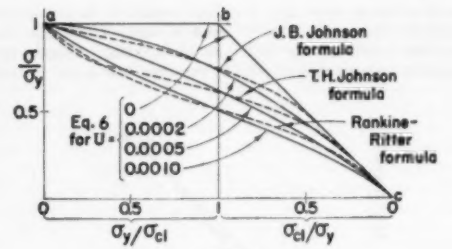

FIG. 6

To be sure, column tests in which special precautions are taken to reduce the column eccentricity or crookedness, or to balance one against the other, may indicate much smaller values of U. These tests are useful for checking idealized theories, but for our present purposes such care in testing tends to eliminate the very thing we are interested in. Design formulas, established through long experience, should be a better guide for estimating the initial deviations which must be expected in actual constructions.

The Case of Thin Cylinders Under Axial Compression

In making a similar analysis for axially compressed cylinders, the deflection under load will be assumed to have the form used by Kármán and Tsien and given by Equation [4]. In order to use the foregoing outlined method of analysis, the component of the "initial equivalent geometric deviation" considered will be assumed to have this same general form. It seems reasonable to assume that its amplitude a_{0l} is related to other properties in a manner analogous to that assumed in Equation [5] for columns. If there were no "preferred directions" in the cylinder wall it would seem reasonable to replace l^2 (which is actually the square of the half wave length of the deviation for columns) by $l_x l_s$ (the product of the half wave lengths of the deviations in the axial and circumferential directions for the cylinder wall). This would give an expression for the amplitude of the cylinder deviation of the form: $a_0 = (U/\pi^2) l_x l_s / t^2$.

However, most thin-walled cylinders in tests and applications are made by bending flat sheets, and this bending into a cylinder tends to flatten out waves which are long in the circumferential direction (as at Fig. 7a) more than those which are long in the axial direction (as at Fig. 7b). To allow for this effect a relation of the form

$$a_0 = (U/\pi^2) l_x^{1+q} l_s^{1-q} / t^2 \ldots\ldots [7]$$

can be used, thereby increasing the amplitudes of components such as those at (b) (Fig. 7), in relation to components such as at (a). Since l_s should obviously not have a negative exponent, the number q should be between zero and one, and in want of definite data the intermediate value of 0.5 will be taken for it. Trials indicate that this choice has comparatively little effect on the results. The expression for the initial deviation is then

$$w_0 = a_{0l} \left(\cos \frac{mnx}{r} \cos \frac{ns}{r} + b \cos \frac{2mnx}{r} + c \cos \frac{2ns}{r} + d \right) [8]$$

where

$$a_0 = (U/\pi^2) l_x^{1.5} l_s^{0.5} / t^2 = Ur^2/(m^{1.5} n^2 t^2)$$

It seems reasonable to assume that the value of the unevenness coefficient U thus defined for the average cylinder formed from metal sheet should be of the same order of magnitude as the corresponding value for metal columns, since the process and

errors of manufacture are much the same; in fact, the same sheet could be cut up into strips to be used for columns or formed into a cylinder. To be sure, the act of forming a sheet into a cylinder tends to reduce the geometric unevennesses, as just discussed. However, this at the same time increases the initial stresses. Also, it should be pointed out that in cylinder buckling

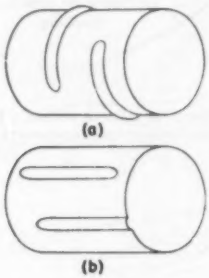

FIG. 7

tests only a small portion of the wall usually buckles, so that, unlike the case of columns, the controlling factor may be the *worst* portion of the wall area (a portion only large enough to contain a few waves), for which the U may be much larger than the average for the entire wall or for a corresponding column. Evidence of the importance of this is presented in Fig. 11 which will be discussed later. In any case it is reassuring that the value of U which is found necessary to explain most of the experimental cylinder strengths turns out to be 0.00015, or a little less than the smallest value which was shown to be possible for columns. It may be noted that cylinder tests are comparable to actual applications, because, unlike column tests, there is no way to reduce or balance initial deviations.

Using the foregoing assumptions and the large-deflection theory which has been described, average stress versus unit shortening curves have been computed for various magnitudes of Ur/t, the results of which are shown in Fig. 8. These computations are presented in Appendix 2. In making these computations it was obviously desirable to determine all five of the arbitrary constants a, b, c, m, and n by minimizing the energy, instead of

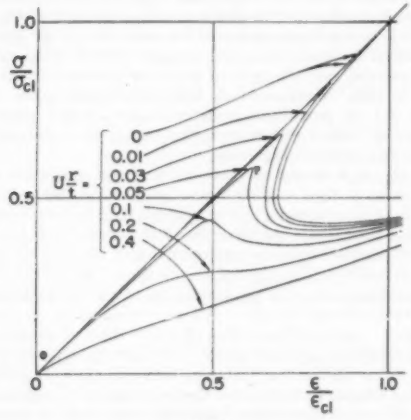

FIG. 8

minimizing it for only two of them as Kármán and Tsien did or for four of them as Leggett and Jones did. In spite of the added complication of considering the initial deviations, an attempt was made to accomplish this result, which involved separate solutions of five simultaneous nonlinear algebraic equations for every point determined. This required a cut-and-try method in which three of the constants b, c, and m had to be guessed at, and if even one of these was not of nearly the right value no useful solution at all resulted. However, success was achieved in getting such a complete solution for small values of Ur/t and values of σ/σ_{cl} from 1.0 down to about 0.75.

When an attempt was made to extend these results down into lower values of σ/σ_{cl} the task became impossibly difficult, but the values of the three constants b, c, and m showed a tendency to center around the values 0.18, 0.03, and 0.728, respectively. A simpler and more practical solution was therefore obtained by taking these values as fixed and minimizing only for the remaining two constants. The results shown in Fig. 8 were obtained with this simpler solution. They are very similar to those obtained from the more complete solution in the region where they can be compared (see Fig. 14b).

It would seem from the foregoing results that the assumptions that $c = b$ made by previous investigators was not a very good guess. As a matter of fact, elementary physical reasoning would indicate that b should be larger than c. As pointed out on page 799 of the paper of 1934 (2), the $b \cos 2mnx/r$ term in the deflection, Equation [4], can eliminate most of the average circumferential strain due to large deflections by increasing the cylinder radius at the peaks of the deflection and reducing it at the nodes of the deflection. On the other hand there is no such simple obvious need for the $c \cos 2ns/r$ term.

Considering now the meaning of the results shown by Fig. 8, it seems evident that a cylinder with a certain value of Ur/t, say, 0.05, will take load smoothly and gradually up to the peak p and will then fail purely elastically and in an explosive manner. As Kármán and Tsien have shown, the elasticity of the testing machine or structure will influence this explosive failure; however, the attainment of the peak p should involve only simple static loading.

Any yielding occurring after this peak is reached will be of no practical importance. However, the stresses increase as we go up the slope op; for some materials, yielding will occur at some point in the cylinder at a loading between o and p, and complete failure will probably then occur at a loading which is not much greater than this. The theory gives the stress condition at any point, and, by using the shear energy yielding condition and assuming from a number of trials that the points most likely to yield first are at the nodes of the waves, the conditions required for yielding at such points were calculated. Two kinds of buckling failure are thus possible in this case. The first kind is a failure precipitated under purely elastic conditions, and it occurs to cylinders which (because they are very thin-walled or made of high-yield material) do not yield until after points such as p are reached. The second kind, occurring to thicker-walled cylinders or those made of lower-yield material, is precipitated by yielding *before* such a peak is reached.

If a cylinder happens to have a Ur/t of 0.2, Fig. 8, it will evidently behave something like a column, with a gradual failure which will be plastic or "elastic" depending upon whether yielding occurs before the plateau is reached. For values of Ur/t greater than this, no elastic failure should occur and all such cylinders should theoretically merely "squash" down until yielding finally occurs. Such failures involve very large displacements, for which the theory is increasingly inadequate, and the results obtained for this range do not seem to be consistent with tests, and are not shown here. This point is beyond the range of most prac-

tical applications and, because of the approximations in the theory and in the assumptions, it may actually very well be beyond the range of the experiments, too. As a matter of fact, other values of b, c, and m can be assumed for this two-parameter solution which yield curves having actual peaks with much lower peak values of σ/σ_{cl} than are obtained with the present assumptions; however, more detailed studies would be required to justify such assumptions.

The foregoing results are shown on an average-stress versus Ur/t chart in Fig. 9. The full line is drawn through points corresponding to the peaks of the curves of Fig. 8, and gives the resistance to the elastic type of buckling for cylinders with any values of U and r/t. The dashed lines are drawn from the computations of maximum stress in the cylinder before the peak is reached; they represent the conditions for the first appearance of yielding in cylinders of a material having the values of $\sigma_y/(UE)$ indicated. Since a cylinder can take a load somewhat higher than that at which yielding first occurs, the "ultimate load" curves should be a little higher than these dashed curves.

As an example of the application of these curves, consider cylinders made of a material and by a fabrication process corresponding to $\sigma_y/(UE) = 5$. Then, according to the results shown in Fig. 9, cylinders having r/t ratios corresponding to values of

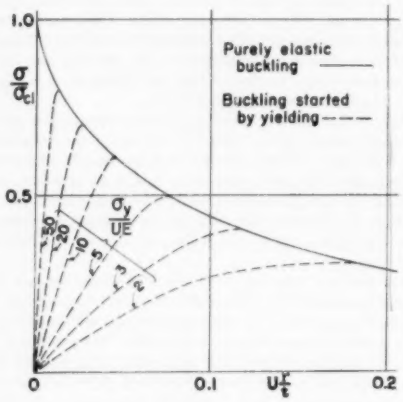

Fig. 9

Ur/t from 0.0 to 0.076 would buckle due to yielding at average stresses given by the dashed line marked 5, while thinner-walled cylinders with higher values of r/t would buckle elastically according to the full line from this point on. For a material with a higher yield point, elastic buckling would start at lower values of r/t.

These results, for $U = 0.00015$, are superposed in Fig. 10 on the test results shown before. The full-line theoretical elastic buckling curve in Fig. 10 (a) fits the average of many of the test groups quite well. The group of tests made by Flügge on celluloid cylinders seems to fit a theoretical yield curve close to that corresponding to this material. The thicker-walled cylinders of Wilson and Newmark, which were made of mild steel, follow the theoretical yield curve for this material quite closely. Some of the test results should doubtless be compared to lower theoretical curves corresponding to larger values of U. The cylinders of Donnell apparently had the largest deviations of any of the groups, and were small-scale specimens made of ordinary

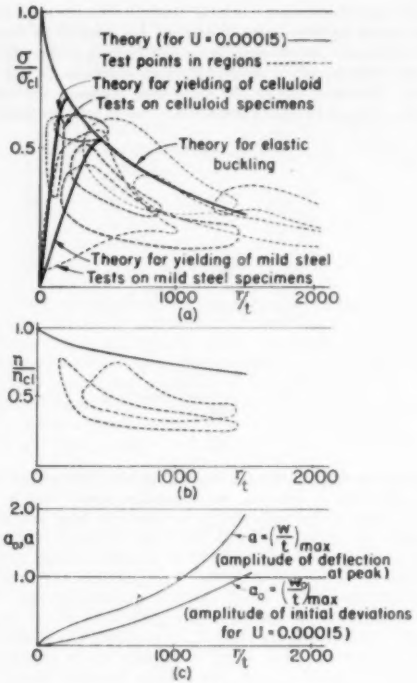

Fig. 10

"shim stock," which does not need to be fabricated very flat for the purposes for which it is ordinarily used.

The number of circumferential waves are compared with the available data at (b). It can be seen that only part of the discrepancy with the classical theory is explained. This result depends greatly on the assumption made in Equation [8] regarding the relation of the amplitudes of different components of the initial deviation to their wave lengths, and this relation apparently needs some modification. The last chart of Fig. 10 at (c) shows that the amplitude of the component of the equivalent initial deviation which was assumed is small compared to the thickness, and only rises to about the thickness for an r/t ratio of 1500. Such extremely thin-walled cylinders are very flimsy and the geometrical deviations alone are very apparent to the eye. The displacement during loading up to the peak is of the same order of magnitude.

Finally, it is desired to point out a rather remarkable fact (24) which perhaps suggests a new approach to this problem. In Fig. 11 is presented a plot of available data for both torsion-test and compression-test strengths of thin-walled cylinders, all plotted together against a parameter which involves the ratio of total wall area to the area of a single wave. Since both kinds of tests were made over the same range of r/t, the inclusion of r/t in the parameter does not explain the remarkable co-ordination achieved. As can be seen, when plotted in this way all the tests group closely along a single curve. This strongly suggests to the authors that the fact that compression-test strengths are so much lower in relation to the classical theory, compared to torsion-test strengths, is to a considerable extent due to the small wave nature of compression buckling, which makes a compression specimen

statistically much more likely to contain one spot with very large initial unevennesses. A theoretical analysis of this statistical side of the question would be difficult, but this represents one more bit of evidence that the effective initial unevennesses in cylinder axial compression specimens can be large.

While much collecting of data and refinement of theory still need to be done on this problem, the authors hope to have demonstrated how our knowledge of this problem can eventually be put on a quantitative basis which will be as satisfactory and as useful for design purposes as that available for other types of buckling problems.

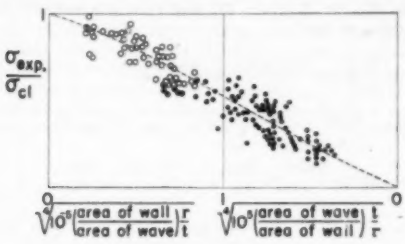

FIG. 11

SYMBOLS USED

E, μ, σ_y = elastic modulus, Poisson's ratio (taken as 0.3), yield point of material

r, t = uniform mean radius and thickness

x, s, z = co-ordinates in axial, circumferential, and radial directions

w_0, w = initial deviation from true shape and deflection

$K = 1 + 2w_0/w$

l_x (l for columns), l_s = half wave lengths of w_0 and w in axial and circumferential directions

$m = l_s/l_x$ = wave-shape ratio

$n = \pi r/l_s$ = number of circumferential waves

a_0, a = amplitudes of w_0, w

b, c, d, α, ν = other parameters defining w and w_0

$A, B, C, D, F, G, H, J, M, N, O, Q, R$ = functions of b, c, and m

U = unevenness factor, depending only on fabrication method

f = stress function of membrane stresses: $\sigma_x = \partial^2 f/\partial s^2$, $\sigma_s = \partial^2 f/\partial x^2$, $\tau_{xs} = -\partial^2 f/\partial x \partial s$

σ, ϵ = average axial compressive stress and unit shortening

$\sigma_{cl}, \epsilon_{cl}, n_{cl}$ = critical values of σ, ϵ, n given by classical theory assuming perfect shape and elasticity

$\mathbf{E}$ = internal strain energy

BIBLIOGRAPHY

1 "The Influence of Curvature on the Buckling Characteristics of Structures," by Th. von Kármán, L. G. Dunn, and H. S. Tsien, *Journal of Aeronautical Sciences*, vol. 7, May, 1940, p. 283.

2 "A New Theory for the Buckling of Thin Cylinders Under Axial Compression and Bending," by L. H. Donnell, Trans. ASME, vol. 56, 1934, p. 795.

3 "Achsensymmetrische Verzerrungen in dünnwandigen Hohlzylinderen," by R. Lorenz, *Zeitschrift des Vereines deutscher Ingenieure*, vol. 52, 1908, pp. 1706–1713.

"Die nicht achsensymmetrische Knickung dünnwandiger Hohlzylinder," by R. Lorenz, *Physikalische Zeitschrift*, vol. 13, 1911, pp. 241–260.

4 "On the General Theory of Elastic Stability," by R. V. Southwell, Philosophical Transactions of the Royal Society of London, England, series A, vol. 213, 1914, p. 187.

5 "Einige Stabilitätsprobleme der Elastisitätstheorie," by S. Timoshenko, *Zeitschrift für Mathematik und Physik*, vol. 58, 1910, pp. 337–385; also Bulletin, Electrotech. Inst., St. Petersburg, Russia, vol. 11, 1914.

6 "The Strength of Tubular Struts," by A. Robertson, Proceedings of the Royal Society of London, England, series A, vol. 121, 1928, pp. 558–585.

7 "Die Stabilität der Kreiszylinderschale," by W. Flügge, *Ingenieur Archiv*, vol. 3, 1932, pp. 463–506.

8 "The Strength of Tubular Struts," by A. Robertson, R. and M. no. 1185, Great Britain Aeronautical Research Committee, Technical Reports, vol. 34, 1928–1929, pp. 935–957.

9 "Some New Experiments on Buckling of Thin-Wall Construction," by F. J. Bridget, C. C. Jerome, and A. B. Vosseller, Trans. ASME, vol. 56, 1934, pp. 569–578.

10 "Strength Tests of Thin-Walled Duralumin Cylinders in Compression," by E. E. Lundquist, NACA Report no. 473, 1933.

11 "Some Investigations of the General Instability of Stiffened Metal Cylinders, I. Review of Theory and Bibliography," by GALCIT, Guggenheim Aeronautical Laboratory, California Institute of Technology, National Advisory Committee for Aeronautics, Technical Note no. 905, 1943.

12 "Some Investigations of the General Instability of Stiffened Metal Cylinders, IV. Continuation of Tests of Sheet-Covered Specimens and Studies of the Buckling Phenomena of Unstiffened Circular Cylinders," GALCIT, Guggenheim Aeronautical Laboratory, California Institute of Technology, National Advisory Committee for Aeronautics, Technical Note no. 908, 1943.

13 "The Strength of Thin Cylindrical Shells," by W. M. Wilson and N. M. Newmark, Bulletin no. 255, University of Illinois, 1933.

14 "Il Cilindro in Parete Sottile Compresso Assialmente, Nuovo Orientamente dell 'Indagine Sulla Stabilita Elastica," by P. Cicala, *L'Aerotecnica*, vol. 24, June, 1944.

15 "Sul Calcolo della Pareti Cilindriche Compresse Secondo le Generatrici," by S. D. Poli, Inst. di Construsio e Ponti, Polytecnico di Milano, June, 1946; also "Il Comportamento Elastico delle Pareti di Forma Cilindrica non Perfetta, Soggette a Compressione," Inst. di Construsion e Ponti, Polytecnico di Milano, October, 1946.

16 "Letter to Editors," by H. L. Cox, *Journal of Aeronautical Sciences*, vol. 14, July, 1947, p. 333.

17 "The Elements of the Buckling of Curved Plates," by H. L. Cox and E. Pribram, *Journal of the Royal Aeronautical Society*, vol. 52, September, 1948, p. 551.

18 "Over de Stabiliteit van het Elastisch Evenwicht," by W. T. Koiter, Doctoral Thesis, University of Delft, Holland, 1945.

19 Th. von Kármán, Encyklopädie der Math. Wiss., vol. 4, art. 27, 1910, p. 349.

20 "The Buckling of Thin Cylindrical Shells Under Axial Compression," by Th. von Kármán and H. S. Tsien, *Journal of the Aeronautical Sciences*, vol. 8, June, 1941, p. 303.

21 "The Behaviour of a Cylindrical Shell Under Axial Compression When the Buckling Load Has Been Exceeded," by D. M. A. Leggett and R. P. N. Jones, RAE Report No. SME 3204, August, 1942 (ARC no. 6135).

22 "Theory of Elastic Stability," by S. Timoshenko, McGraw-Hill Book Company, Inc., New York, N. Y., 1936, p. 187.

23 "A Chart for Plotting Relations Between Variables Over Their Entire Real Range," by L. H. Donnell, *Quarterly of Applied Mathematics*, vol. 1, October, 1943, p. 276.

24 "The Stability of Isotropic or Orthotropic Cylinders or Flat or Curved Panels, Between and Across Stiffeners, With Any Edge Conditions Between Hinged and Fixed, Under Any Combination of Compression and Shear," by L. H. Donnell, National Advisory Committee for Aeronautics, Technical Note no. 918, 1943, pp. 46–47.

Appendix 1

COLUMNS

The condition of equilibrium between the external bending moment M due to an axial load P and the internal resisting moment, for a uniform hinged-end column, Fig. 12, having a bending stiffness EI and an initial deviation w_0, is

$$M = P(w_0 + w) = -EId^2w/dx^2 \quad \ldots\ldots\ldots\ldots [9]$$

If w_0 has the shape given by Equation [5] and the ends of the

column are hinged, this equilibrium condition and the end conditions can be satisfied if

$$w = at \sin(\pi x/l) \quad \ldots\ldots [10]$$

Substituting w_0 and w from Equations [5] and [10] into [9] and simplifying, we obtain

$$P(a_0 + a) = EI(\pi^2/l^2)a$$

or

$$a = a_0/(\pi^2 EI/Pl^2 - 1) = a_0/(P_{cl}/P - 1) = a_0/(\sigma_{cl}/\sigma - 1) \quad [11]$$

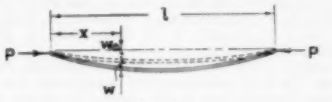

FIG. 12

FIG. 13

where $P_{cl} = \pi^2 EI/l^2$ is the classical buckling load assuming perfect elasticity and shape. The maximum stress in the column will be the sum of the average compressive stress σ and the maximum bending stress $(Mc/I)_{x=l/2} = (Mt/2I)_{x=l/2}$. Using Equations [9], [10], [11], and [5], the condition that this maximum stress has just reached the yield stress σ_y is

$$\sigma_y = \sigma + (Mt/2I)_{x=l/2} = \sigma + \frac{UE}{2(\sigma_{cl}/\sigma - 1)} \quad \ldots\ldots [12]$$

Equation [6] is then obtained by solving Equation [12] for σ.

Equation [6] can be used for columns with any end conditions; it is merely necessary to interpret σ_{cl} as the classical or Euler buckling stress (assuming perfect elasticity and shape) for that particular end condition. To demonstrate that this is true consider a fixed-end column of length $l' = 2l$, Fig. 13, having a deviation from straightness of its middle half of $a_0 l$, as indicated. This middle half will be under the same condition as a hinged-end strut of length l and all the foregoing reasoning and derivation will apply to it. The σ_{cl} in Equation [7] will, as before, be $\pi^2 EI/l^2 = 4\pi^2 EI/l'^2$, which is the same as the classical buckling stress for the fixed-end column of which the hinged-end column is a part.

The foregoing reasoning and Equation [6] can be applied to columns of any symmetrical shape of cross section if t is defined as the height of the section in the plane of symmetry in which buckling is being studied. For more general shapes of cross section this reasoning applies to buckling in the principal planes, provided the amplitude of the initial deviation $a_0 l$ is taken as $(U/\pi^2)(l^2/2c)$, where c is the distance from the corresponding neutral axis to the furthest fiber.

U is supposed to vary with the method of fabrication, and this depends to some extent on the shape of section and end conditions. Hence some variation in the value of U with these conditions might be expected; however, such variations should be small, and in the present state of knowledge would represent meaningless refinements. The best that can be said on the basis of evidence such as that given in Fig. 6, is that the use of Equation [6] with values of U in the range of 0.0002 for "refined" construction to 0.0010 for "rough construction" should give as reasonable an estimate of buckling strength for any kind of column as any present method can, unless closely applicable test data or experience are available.

Appendix 2

CYLINDERS

Substituting the expressions assumed for w and w_0, Equations [4] and [8], into Equation [3], and using trigonometric transformations, we find

$$\left(\frac{\partial^4}{\partial x^4} + \frac{\partial^2}{\partial s^2}\right)^2 f = \frac{Eam^2n^2t}{r^2}\left\{\cos\frac{mnx}{r}\cos\frac{ns}{r} + 4b\cos\frac{2mnx}{r} - \frac{Kn^2at}{2r}\left[4(b+c)\cos\frac{mnx}{r}\cos\frac{ns}{r} + 32bc\cos\frac{2mnx}{r}\cos\frac{2ns}{r} + 4c\cos\frac{mnx}{r}\cos\frac{3ns}{r} + 4b\cos\frac{3mnx}{r}\cos\frac{ns}{r} + \cos\frac{2mnx}{r} + \cos\frac{2ns}{r}\right]\right\} \quad \ldots [13]$$

where

$$K = 1 + 2\frac{w_0}{w} = 1 + 2\frac{a_0}{a} = 1 + \frac{2Ur^2}{m^{1.5}n^2at^2}$$

We will use the new parameters α and ν, defined by

$$\alpha = \frac{\sqrt{3(1-\mu^2)}}{2}\frac{a}{t}$$

$$\nu = \frac{Kn^2at}{2r} = \frac{n^2at}{2r} + \frac{1}{m^{1.5}}\frac{Ur}{t}, \text{ or } \frac{n^2at}{2r} = \nu - \frac{1}{m^{1.5}}\frac{Ur}{t} \quad \ldots [14]$$

Solving Equation [13] in the manner previously discussed, we obtain

$$f = -\frac{Eam^2tr}{n^2}\left[\frac{4\nu(b+c)-1}{(m^2+1)^2}\cos\frac{mnx}{r}\cos\frac{ns}{r} + \frac{2bc\nu}{(m^2+1)^2}\cos\frac{2mnx}{r}\cos\frac{2ns}{r} + \frac{4c\nu}{(m^2+9)^2}\cos\frac{mnx}{r}\cos\frac{3ns}{r} + \frac{4b\nu}{(9m^2+1)^2}\cos\frac{3mnx}{r}\times\cos\frac{ns}{r} + \frac{\nu-4b}{16m^4}\cos\frac{2mnx}{r} + \frac{\nu}{16}\cos\frac{2ns}{r}\right] - \frac{\sigma s^2}{2} \quad \ldots [15]$$

Under elastic conditions the unit strain at the middle surface in the axial direction is, by Hooke's law, equal to $(\partial^2 f/\partial s^2 - \mu\partial^2 f/\partial x^2)/E$, where $\partial^2 f/\partial s^2$ and $\partial^2 f/\partial x^2$ are the membrane stresses in the axial and circumferential directions. This unit strain is composed of two parts:

1 The unit increase in the axial distance between points in the middle surface, which equals $-\epsilon$ since ϵ was defined as unit shortening.

2 The large-deflection strain due to the slope of the middle surface. Using the definition of K, Equation [3], $w_0 = w(K-1)/2$; remembering that K is independent of x, this large-deflection strain due to the slope is equal to

$$\frac{1}{2}\left[\frac{\partial(w+w_0)}{\partial x}\right]^2 - \frac{1}{2}\left[\frac{\partial w_0}{\partial x}\right]^2 = \frac{1}{2}\left[\left(\frac{K+1}{2}\right)^2\left(\frac{\partial w}{\partial x}\right)^2 - \left(\frac{K-1}{2}\right)^2\left(\frac{\partial w}{\partial x}\right)^2\right] = \frac{K}{2}\left(\frac{\partial w}{\partial x}\right)^2$$

We have, therefore, for the axial unit strain at the middle surface

$$\left.\begin{aligned}\frac{1}{E}\left(\frac{\partial^2 f}{\partial s^2}-\mu\frac{\partial^2 f}{\partial x^2}\right) &= -\epsilon+\frac{K}{2}\left(\frac{\partial w}{\partial x}\right)^2\\ \text{or}\qquad \epsilon &= -\frac{1}{E}\left(\frac{\partial^2 f}{\partial s^2}-\mu\frac{\partial^2 f}{\partial x^2}\right)+\frac{K}{2}\left(\frac{\partial w}{\partial x}\right)^2\end{aligned}\right\}\quad\ldots\ldots[16]$$

Using Equations [15] and [4] for f and w and trigonometric transformations, the expression for ϵ can be written out as the sum of numerous periodic terms plus the following two nonperiodic terms: σ/E and $(K/2)(amnt/r)^2(8b^2+1)/4$. The average unit shortening for an entire cylinder containing several waves in the axial direction will be approximately equal to these nonperiodic terms. The average unit shortening of a cylinder ϵ can therefore be written as

$$\epsilon=\frac{\sigma}{E}+\frac{Kn^2at}{2r}\frac{am^2t}{r}\frac{8b^2+1}{4}=\frac{\sigma}{E}+\frac{vam^2t}{r}\frac{8b^2+1}{4}\quad\ldots[17]$$

Solving Equation [17] for σ/σ_{cl}, where $\sigma_{cl}=[E/\sqrt{3(1-\mu^2)}]t/r$ (Equation [1]), and using the symbol $\epsilon_{cl}=\sigma_{cl}/E$ for the unit shortening up to the classical buckling stress, we obtain

$$\frac{\sigma}{\sigma_{cl}}=\frac{\epsilon}{\epsilon_{cl}}-avm^2(8b^2+1)/2\quad\ldots\ldots[18]$$

The internal strain energy $\mathbf{E}$ is

$$\mathbf{E}=\frac{Et^3}{24(1-\mu^2)}\int_0^L\int_0^{2\pi r}\left\{\left(\frac{\partial^2 w}{\partial x^2}+\frac{\partial^2 w}{\partial s^2}\right)^2+2(1-\mu)\left[\left(\frac{\partial^2 w}{\partial x\partial s}\right)^2-\frac{\partial^2 w}{\partial x^2}\frac{\partial^2 w}{\partial s^2}\right]\right\}dxds$$
$$+\frac{t}{2E}\int_0^L\int_0^{2\pi r}\left\{\left(\frac{\partial^2 f}{\partial x^2}+\frac{\partial^2 f}{\partial s^2}\right)^2+2(1+\mu)\left[\left(\frac{\partial^2 f}{\partial x\partial s}\right)^2-\frac{\partial^2 f}{\partial x^2}\frac{\partial^2 f}{\partial s^2}\right]\right\}dxds$$

Substituting in this the expressions of Equations [4] and [15] for w and f, and using the expressions for α and $n^2a t/2r$ from Equation [14], and for σ from Equation [18], we obtain

$$\frac{3(1-\mu^2)r}{\pi ELt^2}\mathbf{E}=\alpha^2(Av^2-Bv+C)+D\left(v-\frac{1}{m^{1.5}}\frac{Ur}{t}\right)^2-F\alpha v\frac{\epsilon}{\epsilon_{cl}}+\left(\frac{\epsilon}{\epsilon_{cl}}\right)^2\quad\ldots\ldots[19]$$

where A, B, C, D, F are functions of b, c, m only

$$A=\left[\frac{4(b+c)m^2}{m^2+1}\right]^2+\left(\frac{8bcm^2}{m^2+1}\right)^2+\left(\frac{4cm^2}{m^2+9}\right)^2+\left(\frac{4bm^2}{9m^2+1}\right)^2+\frac{m^4+1}{8}+\frac{m^4}{4}(8b^2+1)^2$$

$$B=\frac{8(b+c)m^4}{(m^2+1)^2}+b\qquad D=\left(\frac{m^2+1}{2}\right)^2+8(b^2m^4+c^2)$$

$$C=\left(\frac{m^2}{m^2+1}\right)^2+2b^2\qquad F=m^2(8b^2+1)$$

Equation [19] gives an expression proportional to the internal strain energy which involves only Ur/t, ϵ/ϵ_{cl} and the five arbitrary constants α, b, c, m, v. For a given cylinder subjected to a given shortening (as in a test in a rigid testing machine, for example) Ur/t and ϵ/ϵ_{cl} will be given and fixed, and, since there will be no change in length, the external axial compression will do no work during virtual displacements such as provided by small changes in α, b, c, m, and v. By the law of virtual work, therefore, the partial derivations of the internal energy $\mathbf{E}$ with respect to α, b, c, m, and v must be zero. This is equivalent to minimization with respect to the original constants a, b, c, m, and n. The five equations obtained in this way, $\mathbf{E}_\alpha=\mathbf{E}_b=\mathbf{E}_c=\mathbf{E}_m=\mathbf{E}_v=0$ (the subscripts indicating partial derivation), can theoretically be solved for α, b, c, m, v; σ/σ_{cl} can then be determined from Equation [18]. Thus plots of σ/σ_{cl} against the given ϵ/ϵ_{cl} could be plotted for the given values of Ur/t, as in Fig. 8.

These five equations can be put in the following form by combining them in the manner indicated. The first equation $\mathbf{E}_\alpha=0$ is taken as it is

$$2\alpha(Av^2-Bv+C)-Fv\epsilon/\epsilon_{cl}=0\quad\ldots\ldots[20]$$

Eliminating the term in ϵ/ϵ_{cl} between the first and last equations by using the combination $v\mathbf{E}_v-\alpha\mathbf{E}_\alpha=0$, we obtain

$$\alpha^2(Bv-2C)+2Dv\left(v-\frac{1}{m^{1.5}}\frac{Ur}{t}\right)=0\quad\ldots\ldots[21]$$

The third equation $\mathbf{E}_c=0$ does not contain ϵ/ϵ_{cl} and can be solved for $[v-(1/m^{1.5})Ur/t]^2/\alpha^2$. By using the combinations $(8b^2+1)\mathbf{E}_b-16ab\mathbf{E}_\alpha=0$ and $2m\mathbf{E}_m-3v\mathbf{E}_v-\alpha\mathbf{E}_\alpha=0$, we can obtain two more independent equations having a similar form. We thus obtain three equations which can be written together in the form

$$\left(v-\frac{1}{m^{1.5}}\frac{Ur}{t}\right)^2/\alpha^2=Gv-Hv^2=Jv^2+Mv+N=Ov^2+Qv+R\quad\ldots[22]$$

where G, H, J, M, N, O, Q, and R are functions of b, c, and m only. The three independent equations contained in Equation [22] were derived from the equality of the first expression to each of the last three expressions, but the equality of any two of these expressions is of course also implied.

Solutions can then be found as follows: Values of b, c, m are assumed, permitting the values of G, H, J, and so on, to be calculated. The quantity v can then be solved for by using the equality of the second and third expressions of Equation [22]; it can also be solved for from the equality of the third and fourth expressions, and this may give a different value of v; however, by varying b, c, or m and by cross-plotting, values of b, c, m can be found for which both calculations give the same value of v. With sets of values of b, c, m, v so obtained, Equation [21] and the equality of the first and second expressions of Equation [22] can be solved simultaneously for α and Ur/t. Equations [20] and [18] can then be used to determine ϵ/ϵ_{cl} and σ/σ_{cl}. All the equations are thus satisfied, and the resulting sets of values of Ur/t, ϵ/ϵ_{cl}, and σ/σ_{cl} can then be used to plot curves such as those in Fig. 8.

The difficulty in applying such a method lies in finding the proper values of the initially assumed quantities, to obtain real values in the desired range of the final quantities. Values of b, c, m which have been found to fulfill these conditions are shown in Fig. 14(a), while the corresponding values of ϵ/ϵ_{cl}, σ/σ_{cl} and Ur/t are plotted in Fig. 14(b). In this way the upper quarter of the σ/σ_{cl} versus ϵ/ϵ_{cl} diagram can be computed, but

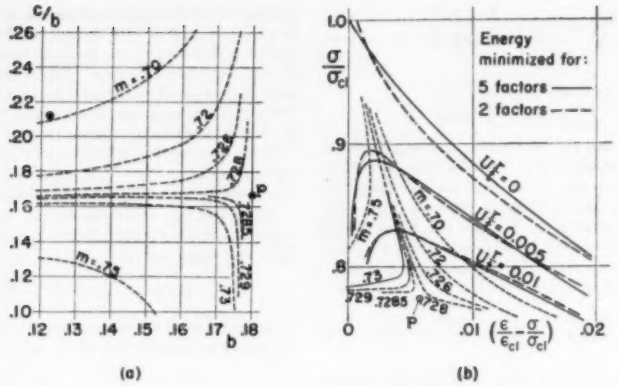

FIG. 14

efforts to extend this solution into the lower part of the diagram were unsuccessful (another family of curves having the same asymptote as the family shown in Fig. 14(a) but with higher values of b can be found, and these yield solutions in the desired region, but these solutions give steadily rising σ/σ_{cl} versus ϵ/ϵ_{cl} curves which are inconsistent with those shown and presumably do not correspond to the "easiest" shape of deformation).

It was therefore decided to use a simpler type of solution in which the energy is minimized for the two parameters α and ν only, and fixed values of b, c, and m are assumed, using the foregoing more complete solution as a guide for choosing b, c, and m. On this basis the values $b = 0.18$, $c = 0.167 \times 0.18 = 0.03$, $m = 0.728+$ (which, it may be noted, is quite consistent with experimental evidence) were chosen, corresponding to the point p in Fig. 14(a) and to approximately the similarily marked point in Fig. 14(b). Using these values in Equation [19] we find $A = 0.361$, $B = 0.382$, $C = 0.185$, $D = 0.666$, $F = 0.666$. Putting these values into Equations [18], [20], and [21] and solving the last two for α, we obtain the three equations

$$\alpha = \frac{0.922\nu\epsilon/\epsilon_{cl}}{\nu^2 - 1.057\nu + 0.513} = \sqrt{\frac{\nu(\nu - 1.61Ur/t)}{0.278 - 0.287\nu}} \quad \ldots [23]$$

$$\frac{\sigma}{\sigma_{cl}} = \frac{\epsilon}{\epsilon_{cl}} - 0.333\alpha\nu \quad \ldots [24]$$

Assuming values of Ur/t and ν (values of ν between $2Ur/t$ and about 0.5 are found to be suitable) we can solve for α and ϵ/ϵ_{cl} from the two equations of Equation [23] and then for σ/σ_{cl} from Equation [24]. Corresponding values of Ur/t, σ/σ_{cl}, and ϵ/ϵ_{cl} obtained in this way are plotted in Fig. 8, and for smaller values of Ur/t are also plotted in Fig. 14 for comparison with the results from the more complete theory in this range. The elastic buckling curve of Fig. 9 is plotted from the peak points of the curves of Fig. 8, each peak giving a set of values of σ/σ_{cl} and Ur/t.

In order to plot the curves for buckling initiated by yielding it is necessary to set up the yielding condition for the most highly stressed point in the cylinder. According to the shear energy theory

$$2\sigma_y^2 = (\sigma_1 - \sigma_2)^2 + (\sigma_1 - \sigma_3)^2 + (\sigma_2 - \sigma_3)^2 \quad \ldots [25]$$

where σ_1, σ_2, and σ_3 are principal stresses at the point. Letting σ_1 and σ_2 represent the principal stresses $(\sigma_x + \sigma_s)/2 \pm \sqrt{(\sigma_x - \sigma_s)^2/4 + \tau_{xs}^2}$ in the plane of the cylinder wall and $\sigma_3 = 0$ be the zero stress in the radial direction, Equation [25] becomes

$$\sigma_y^2 = \sigma_x^2 - \sigma_x\sigma_s + \sigma_s^2 + 3\tau_{xs}^2 \quad \ldots [26]$$

The normal and shear stresses in the axial and circumferential direction, σ_x, σ_s, τ_{xs}, are composed of the sum of the membrane and flexural stresses, and at a distance z from the middle surface they are

$$\left.\begin{aligned} \sigma_x &= \frac{\partial^2 f}{\partial s^2} - \frac{Ez}{1-\mu^2}\left(\frac{\partial^2 w}{\partial x^2} + \mu\frac{\partial^2 w}{\partial s^2}\right) \\ \sigma_s &= \frac{\partial^2 f}{\partial x^2} - \frac{Ez}{1-\mu^2}\left(\frac{\partial^2 w}{\partial s^2} + \mu\frac{\partial^2 w}{\partial x^2}\right) \\ \tau_{xs} &= -\frac{\partial^2 f}{\partial x \partial s} - \frac{Ez}{1+\mu}\frac{\partial^2 w}{\partial x \partial s} \end{aligned}\right\} \quad \ldots [27]$$

Yielding will first occur at the inner or outer surfaces, $z = \pm t/2$, where the flexural stresses are a maximum. Using this and Equations [4] and [15] for w and f in Equation [27], and substituting into Equation [26], yielding will first occur at that value of x and s for which the expression on the right side of Equation [26] is a maximum. To set the derivatives of this expression with respect to x and s equal to zero and solve for the proper value of x and s would involve more complications than seemed justified. Trials for a number of conditions and points indicate that the stress condition is probably as unfavorable at nodes of the primary deformation, on the inner surface, as anywhere else.

If we take $x = \pi r/(2mn)$, $s = \pi r/(2n)$, $z = t/2$, $\mu = 0.3$, and the assumed values of b, c, m, Equation [26] becomes

$$\left(\frac{\sigma_y}{UE}\right)^2\left(U\frac{r}{t}\right)^2 = X^2 - XS + S^2 + 3T^2 \quad \ldots [28]$$

where

$$X = 0.149\alpha\nu + 0.605\sigma/\sigma_{cl} + 0.457(\nu - 1.61Ur/t)$$
$$S = 0.296\alpha\nu - 0.218\alpha + 0.258(\nu - 1.61Ur/t)$$
$$T = -0.135\alpha\nu + 0.200\alpha + 0.560(\nu - 1.61Ur/t)$$

Using the sets of values of α, ν, Ur/t, and σ/σ_{cl} found from

Equations [23] and [24] for points up to the peaks of Fig. 8, in Equation [28], we can solve for σ_y/UE. By cross-plotting, curves of σ/σ_{cl} versus Ur/t for constant values of σ_y/UE are determined and plotted in Fig. 9.

The curves of Fig. 10(a) are obtained from Fig. 9 for $U = 0.00015$.

Fig. 10(b) and Fig. 10(c) were plotted from this value of U and the calculated values of α and ν at the peaks in Fig. 8, by using Equations [2], [8], and [14]

$$\left.\begin{aligned} \frac{n}{n_{cl}} &= \left(m + \frac{1}{m}\right)\sqrt{\left(\nu - \frac{1}{m^{1.5}}\frac{Ur}{t}\right)\Big/(2a)} \\ &= 1.48\sqrt{(\nu - 1.61Ur/t)/a} \\ a &= \frac{2}{\sqrt{3(1-\mu^2)}}\,\alpha \approx 1.21\alpha \\ a_e &= Ur^2/(m^{1.5}n^2t^2) = \frac{0.97\alpha Ur/t}{\nu - 1.61Ur/t} \end{aligned}\right\} \quad \ldots [29]$$

On Plastic Flow and Vibrations

By C. J. THORNE,[1] LOS ANGELES, CALIF.

A general solution is given for the behavior in the linear case of a mechanical model proposed and used by Henry Eyring and others. Four examples are worked in detail. In particular, the steady-state solution for the deflection in periodic vibrations is given in terms of the material constants for any frequency. The transients are given in detail for the three possible cases and inequalities are given to determine which case a particular problem is.

Introduction

HEYRING, G. Halsey, and co-authors[2] proposed a three-element mechanical model to represent the stress-strain curve for textiles. The model was derived by the application of statistical mechanics to the movements of fibers of the material or molecular chains. This work is being extended to the flow, creep, and failure of solid materials under a Navy research contract. Here will be determined mathematical expressions for the one-dimensional plastic deformation of solid materials which satisfy the linear model used by Eyring and others. The steady-state solution is obtained as a function of the physical constants and the transients generally as a function of the roots of the associated cubic equation. Four specific examples are worked out in detail. The examples are primary creep (constant force), vibrations (periodic force), constantly increasing force, constantly increasing elongation. It should be noted that H. Eyring and his co-workers discussed the nonlinear problem when the mass or its acceleration was zero. Example 4 is then included only for completeness.

The Model

The model consists of a spring and dashpot in series, and this combination in parallel with another spring as in Fig. 1. The equivalent circuit is given in Fig. 3. The linear model will mean linear springs ($F = -kx$), and dashpot $F = -c(dx)/(dt)$. In the derivation this is equal to replacing $\sinh x$ by x in the coefficient of c. The term involving c may be thought of as internal friction, and the working of the model as an internal stress adjustment. Temperature effects are not included here. The model under continually increasing stress would result in a stress-strain curve similar to Fig. 2. The initial slope in the stress-strain curve is due to stretching of springs k and k_1 with no motion of the dashpot. The final slope is k, since x is constant, and spring k_1 remains constant in length.

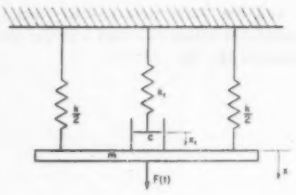

Fig. 1 The Model

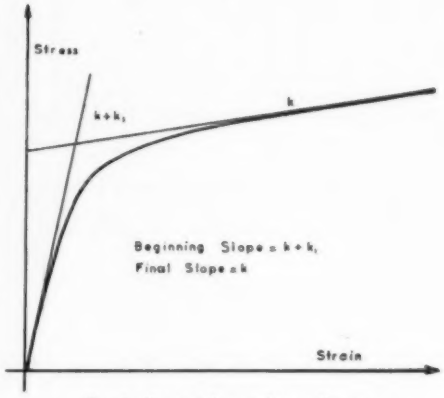

Fig. 2 Typical Stress-Strain Curve

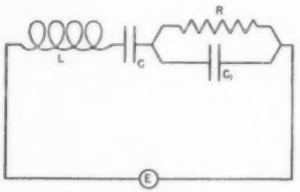

Fig. 3 Equivalent Electrical Circuit

Mild steel has a typical curve reproduced from work of E. A. Davis,[3] in Fig. 4. No attempt is made here to account for the characteristic hump at the yield stress. Here k_1 is approximately 30×10^6 psi, and with a ruler, k can be seen to be about 65×10^3 psi. H. Eyring, G. Halsey, and co-authors have discussed thoroughly the theory of this model and its experimental verification for various textile fibers in a series of papers. Es-

---

[1] Associate Professor of Mathematics, University of Utah; Visiting Associate Professor of Engineering, University of California, Los Angeles, 1948–1949.

[2] "Mechanical Properties of Textiles, I," by G. Halsey, H. J. White, Jr., and H. Eyring, *Textile Research Journal*, vol. 15, 1945, pp. 295–311.

"A General Theory of Elasticity With Application to Partially Rubberlike Substances," by G. Halsey and H. Eyring, *Textile Research Journal*, vol. 15, 1945, pp. 451–459.

Presented at the National Meeting of the Applied Mechanics Division, Ann Arbor, Mich., June 13–15, 1949, of The American Society of Mechanical Engineers.

Discussion of this paper should be addressed to the Secretary, ASME, 29 West 39th Street, New York, N. Y., and will be accepted until April 10, 1950, for publication at a later date. Discussion received after the closing date will be returned.

Note: Statements and opinions advanced in papers are to be understood as individual expressions of their authors and not those of the Society. Paper No. 49—APM-23.

[3] "Yielding and Fracture of Medium Carbon Steel Under Combined Stress," by E. A. Davis, Journal of Applied Mechanics, Trans. ASME, vol. 67, 1945, p. A-13.

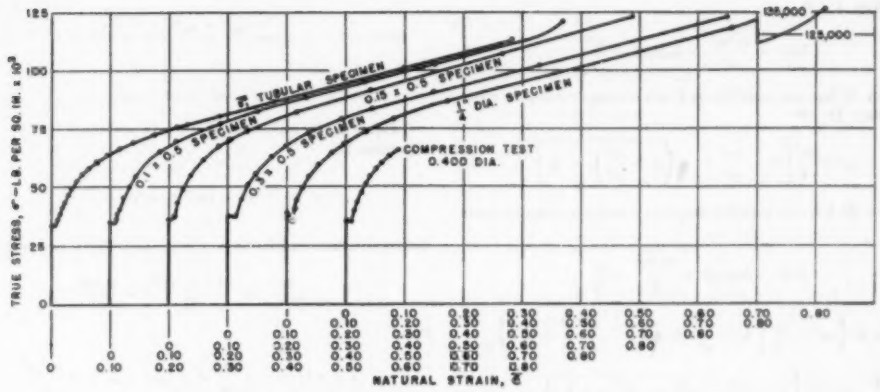

FIG. 4 STRESS-STRAIN CURVES FOR PURE AXIAL TENSION; MEDIUM-CARBON STEEL
(After E. A. Davis.)

pecially the third paper[4] has an excellent discussion of the physical working of the model. More recently J. W. Fredrickson and H. Eyring have discussed metals particularly.[5]

The amplitude of the steady-state motion at resonance is finite, and its experimental determination could be used to evaluate friction coefficient c. If $k >> k_1$, the two resonance frequencies occur at quite different values. For all cases, if $\omega = \omega_0$, the amplitude of motion is

$$(F_0)/m\omega), \text{ and when } \omega = \omega_1, \text{ the amplitude is}$$

$$\frac{F_0\omega}{m\left[\frac{\omega^2(\omega_0^2 - \omega^2)^2}{a^2} + \omega_0^4\right]^{1/2}}$$

THE PROBLEM

The differential equations governing the motion of mass m are

$$m\frac{d^2X}{dt^2} = F(t) - kX - c\left(\frac{dX}{dt} - \frac{dX_1}{dt}\right) \quad \ldots\ldots [1]$$

$$0 = -k_1X_1 + c\left(\frac{dX}{dt} - \frac{dX_1}{dt}\right) \quad \ldots\ldots [2]$$

where $F(t)$ is the driving force; X, X_1 the displacements from equilibrium of the simple spring and the end of dashpot spring, respectively; k, k_1 are spring force constants; and c is the dashpot force constant.

Using the Laplace transform we obtain

$$x(s) = \frac{c_1 + c_2 s + c_3 s^2}{s^3 + \frac{\omega_1^2}{a}s^2 + (\omega_0^2 + \omega_1^2)s + \frac{\omega_1^2\omega_0^2}{a}} + \frac{\frac{\omega_1^2}{a} + s}{\frac{m}{s^3 + \frac{\omega_1^2}{a}s^2 + (\omega_0^2 + \omega_1^2)s + \frac{\omega_1^2\omega_0^2}{a}}} f(s) \quad \ldots\ldots [3]$$

[4] "The Mechanical Properties of Textiles, III," by H. Eyring and G. Halsey, *Textile Research Journal*, vol. 16, January, 1946, pp. 13–25; supplementary data, pp. 284–285.

[5] "Statistical Rate Theory of Metals—I. Mechanism of Flow and Application to Tensile Properties," by J. W. Fredrickson and H. Eyring, Trans. AIME, Metals Technology, vol. 15, August, 1948, 33 pp.

where the Laplace transform of a function with a capital letter is represented by a small letter and

$$\omega_1^2 = \frac{k_1}{m}, \quad \omega_0^2 = \frac{k}{m}, \quad \frac{c}{m} = a, \quad c_1 = \omega_1^2\left[\frac{X'(0)}{a} + X(0) - X_1(0)\right]$$

$$c_2 = \frac{\omega_1^2}{a}X(0) + X'(0), \; c_3 = X(0)$$

also

$$x_1(s) = \frac{d_1 + d_2 s + d_3 s^2}{s^3 + \frac{\omega_1^2}{a}s^2 + (\omega_0^2 + \omega_1^2)s + \frac{\omega_1^2\omega_0^2}{a}} + \frac{\frac{s}{m}f(s)}{s^3 + \frac{\omega_1^2}{a}s^2 + (\omega_0^2 + \omega_1^2)s + \frac{\omega_1^2\omega_0^2}{a}} \quad \ldots\ldots [4]$$

where

$$d_1 = [X(0) - X_1(0)]\omega_0^2, \quad d_2 = X'(0), \quad d_3 = 2X(0) - X_1(0)$$

Consider

$$s^3 + \frac{\omega_1^2}{a}s^2 + (\omega_0^2 + \omega_1^2)s + \frac{\omega_1^2\omega_0^2}{a} = 0 \quad \ldots\ldots [5]$$

Since a is positive, all three roots are negative or imaginary. Call them A_1, A_2, A_3.

There are three cases for the roots of Equation [5]:

Case I (*a*) Three negative roots none equal. (*b*) One negative root and two conjugate complex roots.

Case II Two equal negative roots.

Case III Three equal negative roots.

From the discriminant[6] to Equation [5], we have the following:

Lemma I. Equation [5] has at least two equal roots, one negative root and two complex roots or three negative roots as

$$(\omega_0^2 + \omega_1^2)^2 + \frac{\omega_1^4}{a^2}\left(2\omega_0^4 - 5\omega_0^2 + \frac{\omega_1^4\omega_0^2}{a^2} - \frac{\omega_1^4}{4}\right) \ldots [6]$$

is respectively zero, positive, or negative.

[6] "Elementary Theory of Equations," by L. E. Dickson, John Wiley & Sons, Inc., New York, N. Y. 1914, p. 34.

Corollary I. If

$$2\omega_0^4 + \frac{\omega_1^4\omega_0^2}{a^2} > 5\omega_0^2\omega_1^2 + \frac{\omega_1^2}{4} \quad \ldots\ldots [7]$$

Equation [5] has one negative and two conjugate complex roots,

Corollary II. If

$$\omega_0^2 > \frac{\omega_1^2}{4}\left[5 - \frac{\omega_1^2}{a^2} + \sqrt{\left(5 - \frac{\omega_1^2}{a^2}\right)^2 + 2}\right] \quad \ldots\ldots [8]$$

Equation [5] has one negative and two conjugate complex roots, since

$$2\omega_0^2 - 5\omega_0^2\omega_1^2 + \frac{\omega_1^4\omega_0^2}{a^2} - \frac{\omega_1^4}{4}$$

$$= 2\left\{\omega_0^2 - \frac{\omega_1^2}{4}\left[5 - \frac{\omega_1^2}{a^2} + \sqrt{\left(5 - \frac{\omega_1^2}{a^2}\right)^2 + 2}\right]\right\}$$

$$\left\{\omega_0^2 - \frac{\omega_1^2}{4}\left[5 - \frac{\omega_1^2}{a^2} - \sqrt{\left(5 - \frac{\omega_1^2}{a^2}\right)^2 + 2}\right]\right\} \geq 0$$

if $$\omega_0^2 - \frac{\omega_1^2}{4}\left[5 - \frac{\omega_1^2}{a^2} + \sqrt{\left(5 - \frac{\omega_1^2}{a^2}\right)^2 + 2}\right] \geq 0$$

also

Lemma II. If

$$s^3 + \frac{\omega_1^2}{a}s^2 + (\omega_0^2 + \omega_1^2)s + \frac{\omega_1^2\omega_0^2}{a} = 0$$

has one negative and two conjugate complex roots, the real parts of the complex roots are negative.

Proof: All coefficients of cubic are positive and[7]

[7] "Mechanical Vibrations," by J. P. Den Hartog, McGraw-Hill Book Company, Inc., New York, N. Y., 1947, p. 353.

$$\frac{\omega_1^2}{a}(\omega_0^2 + \omega_1^2) > \frac{\omega_1^2\omega_0^2}{a} \quad \ldots\ldots [9]$$

since

$$\omega_0^2 + \omega_1^2 > \omega_0^2 \quad \ldots\ldots [10]$$

If Equation [5] has three equal roots, we have

Lemma III

$$s^3 + \frac{\omega_1^2}{a}s^2 + (\omega_0^2 + \omega_1^2)s + \frac{\omega_1^2\omega_0^2}{a}$$

has three equal negative zeros $s = -(\omega_1)^2/(3a)$ if and only if

$$\frac{\omega_1^{12}}{729a^6} = \frac{(\omega_0^2 + \omega_1^2)^3}{27} = \frac{\omega_1^4\omega_0^4}{a^2} \quad \ldots\ldots [11]$$

Proof:

$$(s + a_1)^3 \equiv s^3 + \frac{\omega_1^2}{a}s^2 + (\omega_0^2 + \omega_1^2)s + \frac{\omega_1^2\omega_0^2}{a}$$

if

$$a_1 = \frac{\omega_1^2}{3a}, \quad 3a_1^2 = \omega_0^2 + \omega_1^2, \quad a_1^3 = \frac{\omega_1^2\omega_0^2}{a}$$

Also, if Equations [11] are true, the coefficients in the previous function can be written as the coefficients of

$$\left(s + \frac{\omega_1^2}{3a}\right)^3$$

since ω_0^2, ω_1^2, and a are positive real numbers.

Solutions

Case I (a). All roots negative none equal. Let

$$A_1 = -a_1, \quad A_2 = -a_2, \quad A_3 = -a_3$$

$$\left.\begin{aligned} X(t) = {} & \frac{c_1 - c_2a_1 + c_3a_1^2}{(a_2 - a_1)(a_3 - a_1)}e^{-a_1t} + \frac{c_1 - c_2a_2 + c_3a_2^2}{(a_1 - a_2)(a_3 - a_2)}e^{-a_2t} \\ & + \frac{c_1 - c_2a_3 + c_3a_3^2}{(a_1 - a_3)(a_2 - a_3)}e^{-a_3t} + \frac{1}{m}\frac{\frac{\omega_1^2}{a} - a_1}{(a_2 - a_1)(a_3 - a_1)}\int_0^t e^{-a_1\lambda}F(t - \lambda)d\lambda \\ & + \frac{1}{m}\frac{\frac{\omega_1^2}{a} - a_2}{(a_1 - a_2)(a_3 - a_2)}\int_0^t e^{-a_2\lambda}F(t - \lambda)d\lambda + \frac{1}{m}\frac{\frac{\omega_1^2}{a} - a_3}{(a_1 - a_3)(a_2 - a_3)} \\ & \int_0^t e^{-a_3\lambda}F(t - \lambda)d\lambda \end{aligned}\right\} \quad \ldots [12]$$

Call first three terms $X_{T(1)}(t)$

$$\left.\begin{aligned} X_1(t) = {} & \frac{d_1 - d_2a_1 + d_3a_1^2}{(a_2 - a_1)(a_3 - a_1)}e^{-a_1t} + \frac{d_1 - d_2a_2 + d_3a_2^2}{(a_1 - a_2)(a_3 - a_2)}e^{-a_2t} \\ & + \frac{d_1 - d_2a_3 + d_3a_3^2}{(a_1 - a_3)(a_2 - a_3)}e^{-a_3t} - \frac{a_1}{m(a_2 - a_1)(a_3 - a_1)}\int_0^t e^{-a_1\lambda}F(t - \lambda)d\lambda \\ & - \frac{a_2}{m(a_1 - a_2)(a_3 - a_2)}\int_0^t e^{-a_2\lambda}F(t - \lambda)d\lambda - \frac{a_3}{m(a_1 - a_3)(a_2 - a_3)} \\ & \int_0^t e^{-a_3\lambda}F(t - \lambda)d\lambda \end{aligned}\right\} \quad \ldots [13]$$

Call the first three terms $X_{1T(1a)}(t)$

Case I (b). One negative root two conjugate complex roots

$$A_1 = -a_1, \quad A_2 = -a_2 + ib_2, \quad A_3 = -a_2 - ib_2$$

$$X(t) = \frac{c_1 - c_2a_1 + c_3a_1^2}{(a_2 - a_1)^2 + b_2^2} e^{-a_1t} + \frac{1}{b_2}\sqrt{\varphi_1^2 + \varphi_2^2}\, e^{-a_2t}\sin(b_2t + \epsilon_1) + \frac{\frac{\omega_1^2}{a} - a_1}{m[(a_2 - a_1)^2 + b_2^2]}\int_0^t e^{-a_1\lambda}F(t-\lambda)d\lambda \quad \ldots\ldots [14]$$

$$+ \frac{1}{mb_2}\sqrt{\varphi_2^2 + \varphi_4^2}\int_0^t e^{-a_2\lambda}\sin(b_2\lambda + \epsilon_2)F(t-\lambda)d\lambda$$

where

$$\varphi_1 = \frac{(c_1 - c_2a_2 + c_3a_2^2 - c_3b_2^2)(a_1 - a_2) + (c_2b_2 - 2c_3a_2b_2)b_2}{(a_1 - a_2)^2 + b_2^2}$$

$$\varphi_2 = \frac{-b_2(c_1 - c_2a_2 + c_3a_2^2 - c_3b_2^2) + (a_1 - a_2)(c_2b_2 - 2c_3a_2b_2)}{(a_1 - a_2)^2 + b_2^2}$$

$$\varphi_1^2 + \varphi_2^2 = \frac{(c_1 - c_2a_2 + c_3a_2^2 - c_3b_2^2)^2 + b_2^2(c_2 - 2c_3a_2)^2}{(a_1 - a_2)^2 + b_2^2}$$

$$\tan\epsilon_1 = \frac{\varphi_2}{\varphi_1}$$

$$\varphi_3 = \frac{\left(\frac{\omega_1^2}{a} - a_2\right)(a_1 - a_2) + b_2^2}{(a_1 - a_2)^2 + b_2^2}$$

$$\varphi_4 = \frac{b_2\left(a_1 - \frac{\omega_1^2}{a}\right)}{(a_1 - a_2)^2 + b_2^2}$$

$$\varphi_3^2 + \varphi_4^2 = \frac{\left(\frac{\omega_1^2}{a} - a_2\right)^2 + b_2^2}{(a_1 - a_2)^2 + b_2^2}$$

$$\tan\epsilon_2 = \frac{\varphi_4}{\varphi_3}$$

Call the first two terms $X_{1T(1b)}(t)$

$$X_1(t) = \frac{d_1 - d_2a_1 + d_3a_1^2}{(a_2 - a_1)^2 + b_2^2} e^{-a_1t} + \frac{1}{mb_2}\sqrt{\varphi_5^2 + \varphi_6^2}\, e^{-a_2t}\sin(b_2t + \epsilon_3) + \frac{1}{m}\left\{\frac{-a_1}{(a_2 - a_1)^2 + b_2^2}\int_0^t e^{-a_1\lambda}F(t-\lambda)d\lambda + \frac{1}{b_2}\sqrt{\varphi_7^2 + \varphi_8^2}\int_0^t e^{-a_2\lambda}F(t-\lambda)\sin(b_2\lambda + \epsilon_4)d\lambda\right\} \quad \ldots [15]$$

where

$$\varphi_5 = \frac{[d_1 - d_2a_2 + d_3(a_2^2 - b_2^2)](a_1 - a_2) + b_2[d_2b_2 - 2d_3a_2b_2]}{(a_1 - a_2)^2 + b_2^2}$$

$$\varphi_6 = \frac{-b_2[d_1 - d_2a_2 + d_3(a_2^2 - b_2^2)] + (a_2 - a_1)[d_2b_2 - 2d_3a_2b_2]}{(a_1 - a_2)^2 + b_2^2}$$

$$\varphi_5^2 + \varphi_6^2 = \frac{[d_1 - d_2a_2 + d_3(a_2^2 - b_2^2)]^2 + [d_2b_2 + 2d_3a_2b_2]^2}{(a_1 - a_2)^2 + b_2^2}$$

$$\tan\epsilon_3 = \frac{\varphi_6}{\varphi_5}$$

$$\varphi_7 = \frac{-a_2(a_1 - a_2) + b_2^2}{(a_1 - a_2)^2 + b_2^2}, \quad \varphi_8 = \frac{b_2(a_1 - a_2) + b_2a_2}{(a_1 - a_2)^2 + b_2^2}$$

$$\varphi_7^2 + \varphi_8^2 = \frac{a_2^2 + b_2^2}{(a_1 - a_2)^2 + b_2^2}$$

$$\tan\epsilon_4 = \frac{\varphi_8}{\varphi_7}$$

Call the first two terms $X_{1T(1b)}(t)$

Case II. Two equal negative roots. Let

$$A_1 = -a_1, \quad A_2 = -a_1, \quad A_3 = -a_2$$

$$X(t) = \frac{c_1 - c_2a_1 + c_3a_1^2}{(a_2 - a_1)}t + \frac{-c_1 + c_2a_2 - 2c_3a_1a_2 + c_3a_1^2}{(a_2 - a_1)^2}e^{-a_1t} + \frac{c_1 - c_2a_2 + c_3a_2^2}{(a_1 - a_2)^2}e^{-a_2t} + \frac{\frac{\omega_1^2}{a} - a_2}{m(a_2 - a_1)^2}\int_0^t e^{-a_2\lambda}F(t-\lambda)d\lambda + \frac{\frac{\omega_1^2}{a} - a_1}{m(a_2 - a_1)}\int_0^t \lambda e^{-a_1\lambda}F(t-\lambda)d\lambda + \frac{a_2 - \frac{\omega_1^2}{a}}{m(a_2 - a_1)^2}\int_0^t e^{-a_1\lambda}F(t-\lambda)d\lambda \quad \ldots [16]$$

Call the first two terms $X_{T(2)}(t)$

$$X_1(t) = \left[\frac{-d_1 + d_2a_2 - 2d_3a_1a_2 + d_3a_1^2}{(a_2 - a_1)^2} + \frac{d_1 - d_2a_1 + d_3a_1^2}{(a_2 - a_1)}t\right]e^{-a_1t} + \frac{d_1 - d_2a_2 + d_3a_2^2}{(a_1 - a_2)^2}e^{-a_2t} + \frac{-a_1}{m(a_2 - a_1)^2}\int_0^t e^{-a_2\lambda}F(t-\lambda)d\lambda + \frac{-a_1}{m(a_2 - a_1)}\int_0^t \lambda e^{-a_1\lambda}F(t-\lambda)d\lambda + \frac{a_2}{m(a_2 - a_1)^2}\int_0^t e^{-a_1\lambda}F(t-\lambda)d\lambda \quad \ldots [17]$$

Call the first two terms $X_{1T(2)}(t)$.

Case III. Three equal roots. Let

$$A_1 = -a_1, \quad A_2 = -a_1, \quad A_3 = -a_1, \quad a_1 = \frac{\omega_1^2}{3a}$$

$$X(t) = \left[c_2 + (c_2 - 2c_2a_1)t + (c_1 - c_2a_1 + c_2a_1^2)\frac{t^2}{2}\right]e^{-a_1t} + \frac{1}{m}\int_0^t \lambda e^{-a_1\lambda}F(t-\lambda)d\lambda + \frac{\frac{\omega_1^2}{a} - a_1}{2m}\int_0^t \lambda^2 e^{-a_1\lambda}F(t-\lambda)d\lambda \quad [18]$$

Call the first term $X_{T(2)}(t)$.

$$X_1(t) = \left[d_2 + (d_2 - 2d_2a_1)t + (d_1 - d_2a_1 + d_2a_1^2)\frac{t^2}{2}\right]e^{-a_1t} + \frac{1}{m}\int_0^t \lambda e^{-a_1\lambda}F(t-\lambda)d\lambda + \frac{-a_1}{2m}\int_0^t \lambda^2 e^{-a_1\lambda}F(t-\lambda)d\lambda \quad [19]$$

Call the first term $X_{1T(2)}(t)$.

Examples

I Primary Creep. $F = F_0 = \text{const.}$

Steady-state solution (all cases); most easily obtained from the solution in terms of the roots of Equation [5] or directly. As $t \to \infty$

$$X(t) \to \frac{F_0}{k} \text{ and } X_1(t) \to 0 \quad [20]$$

In general

$$X(t) = \frac{F_0}{k} + X_T$$

where X_T is the appropriate transient.

Case I(*a*)

$$X_T(t) = X_{T(1a)}(t) + \frac{F_0}{m}\left\{\frac{\left(1 - \frac{\omega_1^2}{aa_1}\right)e^{-a_1t}}{(a_1-a_2)(a_1-a_3)} - \frac{\left(1 - \frac{\omega_1^2}{aa_2}\right)e^{-a_2t}}{(a_1-a_2)(a_2-a_3)} + \frac{\left(1 - \frac{\omega_1^2}{aa_3}\right)e^{-a_3t}}{(a_1-a_3)(a_2-a_3)}\right\} \quad [21]$$

$$X_1(t) = X_{1T(1a)}(t) + \frac{F_0}{m}\left\{\frac{e^{-a_1t}}{(a_1-a_2)(a_1-a_3)} - \frac{e^{-a_2t}}{(a_1-a_2)(a_2-a_3)} + \frac{e^{-a_3t}}{(a_1-a_3)(a_2-a_3)}\right\} \quad [22]$$

Case I(*b*)

$$X_T(t) = X_{T(1b)}(t) + \frac{F_0}{m}\left\{\frac{\left(a_1 - \frac{\omega_1^2}{a}\right)e^{-a_1t}}{a_1[(a_2-a_1)^2 + b_2^2]} - \frac{\sqrt{\varphi_2^2 + \varphi_4^2}}{b_2(a_2^2 + b_2^2)}e^{-a_2t}\sin(b_2t + e_2 + \delta)\right\} \quad [23]$$

where

$$\tan\delta = \frac{b_2}{a_2}$$

$$X_1(t) = X_{1T(1b)}(t) + \frac{F_0}{m}\left\{\frac{e^{-a_1t}}{(a_2-a_1)^2 + b_2^2} - \frac{e^{-a_2t}}{b_2\sqrt{(a_1-a_2)^2 + b_2^2}}\sin(b_2t + e_4 + \delta)\right\} \quad [24]$$

Case II

$$X_T(t) = X_{T(2)}(t) + \frac{F_0}{m(a_2-a_1)^2}\left\{\frac{a_2 - \frac{\omega_1^2}{a}}{a_2}e^{-a_2t} + \left[\frac{\frac{\omega_1^2}{a} - a_1}{a_1} + (a_2-a_1)\frac{\left(a_1 - \frac{\omega_1^2}{a}\right)}{a_1^2}\right]e^{-a_1t} + t\frac{(a_2-a_1)}{a_1}\left(a_1 - \frac{\omega_1^2}{a}\right)e^{-a_1t}\right\} \quad [25]$$

$$X_1(t) = X_{1T(2)}(t) + \frac{F_0}{m(a_2-a_1)^2}\left[e^{-a_2t} - \frac{a_2}{a_1}e^{-a_1t} + \frac{(a_2-a_1)(a_1t+1)}{a_1}e^{-a_1t}\right] \quad [26]$$

Case III

$$a_1 = \frac{\omega_1^2}{3a}$$

$$X_T(t) = X_{T(3)}(t) + \frac{F_0e^{-a_1t}}{ma_1^3}\left[-a_1^2t - a_1 + {}^1/_2\left(a_1 - \frac{\omega_1^2}{a}\right)(a_1^2t - 2a_1t + 2)\right] \quad [27]$$

$$X_1(t) = X_{1T(3)}(t) + \frac{F_0}{ma_1}e^{-a_1t}({}^1/_2a_1t^2 - 2t) \quad [28]$$

II Oscillations

$$F = F_0R\{e^{i\omega t}\} = F_0\cos\omega t$$

where R means real part. For phase angles or $\sin\omega t$ change t.

Steady-state solution (all cases). Most easily obtained from form of solution in terms of roots of Equation [5].

As $t \to \infty$

$$X(t) \to \frac{F_0\omega_1^2\sin(\omega t + e)}{m\sqrt{\frac{\omega_1^4}{a^2}(\omega_0^2 - \omega^2)^2 + \omega^2(\omega_0^2 + \omega_1^2 - \omega^2)^2}} \quad [29]$$

where

$$\tan e = \frac{\omega_1^2(\omega_0^2 - \omega^2)}{a\omega(\omega_0^2 + \omega_1^2 - \omega^2)}$$

$$X_1(t) \to 0 \quad [30]$$

In general, $X(t)$ = steady solution + X_T where X_T is the appropriate transient.

Case I(*a*)

$$X_T(t) = X_{T(1a)}(t) + \frac{F_0}{m}\left\{a_1\frac{\left(a_1-\frac{\omega_1^2}{a}\right)e^{-a_1t}}{(a_1-a_1)(a_1-a_2)(a_1^2+\omega^2)}\right.$$

$$-a_2\frac{\left(a_2-\frac{\omega_1^2}{a}\right)e^{-a_2t}}{(a_1-a_2)(a_2-a_3)(a_2^2+\omega^2)}$$

$$\left.+a_3\frac{\left(a_3-\frac{\omega^2}{a}\right)e^{-a_3t}}{(a_1-a_3)(a_2-a_3)(a_3^2+\omega^2)}\right\} \quad \ldots [31]$$

$$X_1(t) = X_{1T(1a)}(t) + \frac{F_0}{m}\left\{\frac{a_1^2e^{-a_1t}}{(a_1-a_2)(a_1-a_3)(a_1^2+\omega^2)}\right.$$

$$\left.-\frac{a_2^2e^{-a_2t}}{(a_1-a_2)(a_2-a_3)(a_2^2+\omega^2)^2}+\frac{a_3^2e^{-a_3t}}{(a_1-a_3)(a_2-a_3)(a_3^2+\omega^2)}\right\}$$

$$\ldots\ldots [32]$$

Case I(*b*)

$$X_T(t) = X_{T(1b)}(t) + \frac{F_0}{m}\frac{\left(a_1-\frac{\omega_1^2}{a}\right)a_1e^{-a_1t}}{[(a_2-a_1)^2+b_2^2][a_1^2+\omega^2]}$$

$$+\frac{F_0e^{-a_2t}\sqrt{\varphi_9^2+\varphi_{10}^2}\sin(b_2t+\epsilon_3)}{mb_2[(a_2-a_1)^2+b_2^2][(a_2^2+b_2^2-\omega^2)^2+4a_2^2\omega^2]} \quad \ldots [33]$$

where

$$\varphi_9 = (a_2^2+b_2^2-\omega^2)\left[-a_2\left\{b_2^2+\left(\frac{\omega_1^2}{a}-a_2\right)(a_1-a_2)\right\}\right.$$

$$\left.+b_2^2\left(a_1-\frac{\omega_1^2}{a}\right)\right]-2a_2\omega^2\left[b_2^2+\left(\frac{\omega_1^2}{a}-a_2\right)(a_1-a_2)\right]$$

$$\varphi_{10} = (a_2^2+b_2^2-\omega^2)\left[-b_2\left\{b_2^2+\left(\frac{\omega_1^2}{a}-a_2\right)(a_1-a_2)\right\}\right.$$

$$\left.+a_2b_2\left(\frac{\omega_1^2}{a}-a_1\right)\right]-2a_2b_2\omega^2\left(a_1-\frac{\omega_1^2}{a}\right)$$

$$\tan\epsilon_3 = \varphi_{10}/\varphi_9$$

$$X_1(t) = X_{1T(1b)}(t) + \frac{F_0}{m}\frac{a_1^2e^{-a_1t}}{[(a_2-a_1)^2+b_2^2][a_1^2+\omega^2]}$$

$$+\frac{F_0e^{-a_2t}\sqrt{\varphi_{11}^2+\varphi_{12}^2}\sin(b_2t+\epsilon_4)}{mb_2[(a_2-a_1)^2+b_2^2][(a_2^2+b_2^2-\omega^2)^2+4a_2^2\omega^2]} \quad \ldots [34]$$

where

$$\varphi_{11} = (a_2^2+b_2^2-\omega^2)\left[-a_2\left\{b_2^2-a_2(a_1-a_2)\right\}+a_1b_2^2\right]$$

$$-2a_2\omega^2[b_2^2-a_2(a_1-a_2)]$$

$$\varphi_{12} = (a_2^2+b_2^2-\omega^2)\left[-b_2\left\{b_2^2-a_2(a_1-a_2)\right\}-a_1a_2b_2\right]-2a_1a_2b_2\omega^2$$

$$\tan\epsilon_4 = \varphi_{12}/\varphi_{11}$$

Case II

$$X_T(t) = X_{T(2)}(t) + \frac{F_0}{m(a_3-a_1)}\left\{\frac{a_3\left(a_3-\frac{\omega_1^2}{a}\right)e^{-a_3t}}{(a_3-a_1)(a_3^2+\omega^2)}\right.$$

$$+\frac{a_1\left(\frac{\omega_1^2}{a}-a_3\right)e^{-a_1t}}{(a_3-a_1)(a_1^2+\omega^2)}+\frac{\left(a_1-\frac{\omega_1^2}{a}\right)a_1te^{-a_1t}}{(a_1^2+\omega^2)}$$

$$\left.+\frac{\left(a_1-\frac{\omega_1^2}{a}\right)e^{-a_1t}(a_1^2+\omega_1)}{(a_1^2-\omega^2)^2}\right\} \quad \ldots [35]$$

$$X_1(t) = X_{1T(2)}(t) + \frac{a_3F_0}{m(a_3-a_1)^2}\left\{\frac{a_3e^{-a_3t}}{(a_3^2+\omega^2)}-a_1\frac{e^{-a_1t}}{(a_1^2+\omega^2)}\right\}$$

$$+\frac{F_0a_1}{m(a_3-a_1)}\left[\frac{a_1te^{-a_1t}}{(a_1^2+\omega^2)}+\frac{a_1^2-\omega^2}{(a_1^2+\omega^2)^2}e^{-a_1t}\right] \quad \ldots [36]$$

Case III

$$a_1 = \frac{\omega_1^2}{3a}$$

$$X_T(t) = X_{T(3)}(t) - \frac{F_0}{m}e^{-a_1t}\left\{\frac{a_1t}{a_1^2+\omega^2}+\frac{a_1^2-\omega^2}{(a_1^2+\omega^2)^2}\right.$$

$$\left.+\frac{\frac{\omega_1^2}{a}-a_1}{2}\left[\frac{a_1t^2}{a_1^2+\omega^2}+2\frac{(a_1^2-\omega^2)t}{(a_1^2+\omega^2)^2}+2a_1\frac{(a_1^2-3\omega^2)}{(a_1^2+\omega^2)^3}\right]\right\} \quad \ldots [37]$$

$$X_1(t) = X_{1T(3)}(t) - \frac{F_0}{m(a_1^2+\omega^2)}e^{-a_1t}\left\{a_1t+\frac{a_1^2-\omega^2}{a_1^2+\omega^2}\right.$$

$$\left.-\frac{a_1}{2}\left[a_1t^2+\frac{2(a_1^2-\omega^2)t}{a_1^2+\omega^2}+2a_1\frac{a_1^2-3\omega^2}{(a_1^2+\omega^2)^2}\right]\right\} \quad \ldots [38]$$

III Load Increased at a Constant Rate, $F(t) = F_0t$

Steady-state solution (all cases)

As $t \longrightarrow \infty$

$$X(t) \longrightarrow \frac{F_0}{k}\left(t-\frac{c}{k}\right) \quad \ldots\ldots [39]$$

$$X_1(t) \longrightarrow \frac{F_0c}{kk_1} \quad \ldots\ldots [40]$$

In general, $X(t)$ = steady-state solution plus a transient term X_T.

Case I(*a*)

$$X_T = \frac{F_0}{m}\left\{\frac{\left(\frac{\omega_1^2}{aa_1}-1\right)e^{-a_1t}}{a_1(a_1-a_2)(a_1-a_3)}-\frac{\left(\frac{\omega_1^2}{aa_2}-1\right)e^{-a_2t}}{a_2(a_1-a_2)(a_2-a_3)}\right.$$

$$\left.+\frac{\left(\frac{\omega_1^2}{aa_3}-1\right)e^{-a_3t}}{a_3(a_1-a_3)(a_2-a_3)}\right\}+X_{T(1a)}(t) \quad \ldots [41]$$

$$X_1(t) = X_{1T(1a)}(t) - \frac{F_0}{m}\left\{\frac{e^{-a_1t}}{a_1(a_1-a_2)(a_1-a_3)}\right.$$

$$\left.-\frac{e^{-a_2t}}{a_2(a_1-a_2)(a_2-a_3)}+\frac{e^{-a_3t}}{a_3(a_1-a_3)(a_2-a_3)}\right\}+\frac{F_0c}{kk_1} \quad \ldots [42]$$

Case I(b)

$$X_T(t) = X_{T(1a)}(t) + \frac{F_0}{m}\left\{\frac{\left(\frac{\omega_1^2}{aa_1} - 1\right)e^{-a_1 t}}{a_1[(a_1-a_2)^2+b_2^2]} + \frac{F_0 e^{-a_2 t}\sqrt{\varphi_{13}^2+\varphi_{14}^2}\sin(b_2 t+\epsilon_3)}{mb_2[(a_1-a_2)^2+b_2^2](a_2^2+b_2^2)^2}\right\} \quad [43]$$

$$\varphi_{13} = (a_2^2-b_2^2)\left[\left(\frac{\omega_1^2}{a}-a_2\right)(a_1-a_2)+b_2^2\right] + 2a_2b_2^2\left(\frac{\omega_1^2}{a}-a_1\right)$$

$$\varphi_{14} = 2a_2b_2\left[\left(\frac{\omega_1^2}{a}-a_2\right)(a_1-a_2)+b_2^2\right] + (a_2^2-b_2^2)b_2\left(a_1-\frac{\omega_1^2}{a}\right)$$

$$\tan\epsilon_3 = \varphi_{14}/\varphi_{13}$$

$$X_1(t) = X_{1T(1a)}(t) - \frac{F_0}{m}\left\{\frac{e^{-a_1 t}}{a_1[(a_1-a_2)^2+b_2^2]} + \frac{F_0 e^{-a_2 t}\sqrt{\varphi_{15}^2+\varphi_{16}^2}\sin(b_2 t+\epsilon_4)}{mb_2[(a_1-a_2)^2+b_2^2](a_2^2+b_2^2)^2} + \frac{F_0 ma}{kk_1}\right\} \quad [44]$$

$$\varphi_{15} = [b_2^2 - a_2(a_1-a_2)](a_2^2-b_2^2) - 2a_2b_2^2a_1$$

$$\varphi_{16} = [b_2^2 - a_2(a_1-a_2)]\,2a_2b_2 + (a_2^2-b_2^2)b_2a_1$$

Case II

$$X_T(t) = X_{T(2)}(t) + \frac{F_0\left(\frac{\omega_1^2}{a}-a_3\right)}{m(a_1-a_3)^2}\left[\frac{e^{-a_3 t}}{a_3^2} - \frac{e^{-a_1 t}}{a_1^2}\right] - \frac{F_0\left(\frac{\omega_1^2}{a}-a_1\right)}{m(a_1-a_3)}\left[\frac{2e^{-a_1 t}}{a_1^3} + \frac{te^{-a_1 t}}{a_1^2}\right] \quad [45]$$

$$X_1(t) = X_{1T(2)}(t) - \frac{F_0 a_3}{m(a_1-a_3)^2}\left[\frac{e^{-a_3 t}}{a_3^2} - \frac{e^{-a_1 t}}{a_1^2}\right] + \frac{F_0}{m(a_1-a_3)}\left[\frac{2e^{-a_1 t}}{a_1^3} + \frac{te^{-a_1 t}}{a_1^2}\right] + \frac{F_0 c}{kk_1} \quad [46]$$

Case III

$$a_1 = \frac{\omega_1^2}{3a}$$

$$X_T(t) = X_{T(3)}(t) + \frac{F_0}{m}e^{-a_1 t}\left\{\frac{3}{2}\left(\frac{t^2}{a_1}+\frac{4t}{a_1^2}+\frac{3}{a_1^3}\right) - \left(\frac{t^2}{2a_1}+\frac{t}{a_1^2}+\frac{1}{a_1^3}\right)\right\} \quad [47]$$

$$X_1(t) = X_{1T(3)}(t) - \frac{F_0}{m}e^{-a_1 t}\left\{\frac{t^2}{2a_1}+\frac{t}{a_1^2}+\frac{1}{a_1^3}\right\} + \frac{F_0 c}{kk_1} \quad [48]$$

IV What Force F(t) Will Cause X(t) to Increase Linearly?

From Equations [1], [2]

$$\frac{dX}{dt} = c', \quad X = c't + X(0)$$

$$0 = F(t) - kX - c\left(c' - \frac{dX_1}{dt}\right) \quad [49]$$

$$0 = -k_1X_1 + c\left(c' - \frac{dX_1}{dt}\right) \quad [50]$$

$$F(t) = kX(0) + c'(kt+c) - [kX(0) + c'c - F(0)]\,e^{-\frac{k_1}{c}t} \quad [51]$$

$$X_1(t) = \frac{c_1c}{k_1} + \frac{1}{k_1}[F(0) - kX(0) - c'c]\,e^{-\frac{k_1}{c}t} \quad [52]$$

Flow of Heated Gases

By A. S. THOMPSON,[2] DOWNEY, CALIF.

The purpose of this investigation was to find a convenient method for correlating the variables involved in the transfer of heat from the wall of a passage to a gas moving at high velocity in the passage. A graphical design method has been developed, using the Reynolds analogy between heat transfer and friction, for one-dimensional flow in a passage of variable area, and with variable wall temperature.

Nomenclature

The following nomenclature is used in the paper:

x = distance along passage
A = cross-sectional area of passage for fluid flow
s' = perimeter of passage
m = hydraulic radius of passage $= A/s'$
p = pressure in fluid
w = velocity of fluid
W = weight of fluid per unit of time flowing through A
ρ = mass density of fluid
M = Mach number of fluid $= w/a$
a = velocity of sound in fluid
h = enthalpy of fluid, per unit weight of fluid
q = heat added to fluid from wall, per unit weight of fluid
μ = viscosity of fluid in boundary layer
h' = heat-transfer coefficient for boundary layer
k = thermal conductivity of fluid in boundary layer
f = friction factor in Fanning equation
λ = constant applied to Reynolds analogy to account for "roughness"
T = temperature of fluid
T_t = total temperature of fluid $= T + \dfrac{w^2}{2gc_p}$
T_w = wall temperature of fluid
c_p = specific heat of fluid at constant pressure
c_v = specific heat of fluid at constant volume
γ = ratio of specific heats $= c_p/c_v$
g = acceleration due to gravity
s = entropy of fluid
τ = shearing stress in fluid

Any consistent system of units may be used.

P = Prandtl number
S = Stanton number
N = Nusselt number
R = Reynolds number

Introduction

It has been assumed that the laws for a perfect gas can be used for small steps throughout the range of application of the present method and that the Reynolds analogy between heat transfer and friction is applicable. No discontinuities such as shock waves have been considered.

The use of the chart involves a stepwise approximation to the actual flow composed of processes at constant Mach number occurring in a finite length of passage, and of processes at constant total temperature (isentropic), assumed to occur in a zero length of passage.

Mathematical Development

The equations for compressible fluid flow in the steady state (conservation of momentum, continuity of flow, and conservation of energy) are combined, by means of the Reynolds analogy between heat transfer and friction, with the equation for heat transfer across a fluid boundary. The differential equation thus obtained is integrated for two special cases, an isentropic process, and a process at constant Mach number with constant wall temperature, giving expressions for pressure and area ratios in terms of Mach number and total temperature of the fluid. Next the heat-transfer equation is integrated, for the special case of constant heat-transfer coefficient, to give an expression for total temperature in terms of distance along the fluid passage.

It is assumed, wherever this is necessary to expedite an integration, that all integrations are performed over ranges small enough that the terms for the ratio of specific heats, hydraulic radius, friction factor, heat-transfer coefficient, and wall temperature can be considered constant for the integration interval.

An investigation is made of the limitations imposed by requirements of the second law of thermodynamics to the variables of fluid flow in heating with boundary friction.

The flow is considered to be one-dimensional, that is, the cross section of the passage changes slowly with distance and the passage is essentially straight.

Equation for Fluid Flow[3]

For continuity of flow in Fig. 1, it is required that mass be neither created nor destroyed within the fluid element. This is expressed

$$\frac{\partial}{\partial x}(\rho w A)dx + A dx \frac{\partial \rho}{\partial t} = 0 \qquad [1]$$

For steady-state motion, Equation [1] can be integrated to give

$$\rho w A = \frac{w}{g} = \text{const} \qquad [2]$$

Equation [2] is the continuity equation for steady motion of a fluid.

[1] It has been called to the attention of the author that this paper parallels in certain respects another which became available after the present paper was prepared, namely, "The Mechanics and Thermodynamics of Steady One-Dimensional Gas Flow," by A. H. Shapiro and W. R. Hawthorne, Journal of Applied Mechanics, Trans. ASME, vol. 69, 1947, p. A-317. Shapiro and Hawthorne use the same fundamental equations to develop a formulation suitable for numerical integration for a given problem. The present paper develops a graphical design method by which problems may be solved very quickly, mainly by drawing lines on charts and with a minimum of numerical calculation. The resulting formulations differ from those of Shapiro and Hawthorne primarily because of this difference in aim, and the difference in the forms of equations resulting therefrom.

[2] Research Engineer, North American Aviation, Inc. Mem. ASME.

Contributed by the Heat Transfer Division and presented at the Annual Meeting, New York, N. Y., November 29–December 3, 1948, of The American Society of Mechanical Engineers.

Discussion of this paper should be addressed to the Secretary, ASME, 29 West 39th Street, New York, N. Y., and will be accepted until April 10, 1950, for publication at a later date. Discussion received after the closing date will be returned.

Note: Statements and opinions advanced in papers are to be understood as individual expressions of their authors and not those of the Society. Paper No. 48—A-45.

[3] "Aerodynamics of a Compressible Fluid," by H. W. Liepmann and A. E. Puckett, John Wiley and Sons, Inc., New York, N. Y., 1947.

Conservation of momentum for Fig. 1 requires that the mass in the fluid element times its change in velocity equal the net

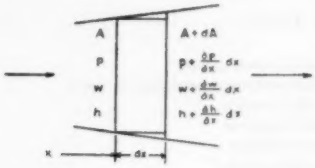

FIG. 1

force on the element times its time of application, or

$$\rho A dx \frac{dw}{dt} = Ap - (A + dA)\left(p + \frac{\partial p}{\partial x} dx\right) + \left(p + \frac{1}{2}\frac{\partial p}{\partial x} dx\right) dA - F_f dx \quad [3]$$

where F_f is the shearing force per unit length of passage on the element due to friction. Equation [3] can be written

$$\rho A \frac{dw}{dt} + A \frac{\partial p}{\partial x} + F_f = 0 \quad [4]$$

Since velocity is, in general, a function of both time and distance along the passage

$$\frac{dw}{dt} = \frac{\partial w}{\partial t} + \frac{\partial w}{\partial x} \frac{dx}{dt} \quad [5]$$

Since, for a given fluid element

$$w = \frac{dx}{dt} \quad [6]$$

$$\frac{dw}{dt} = \frac{\partial w}{\partial t} + w \frac{\partial w}{\partial x} \quad [7]$$

Substituting Equation [7] into [4]

$$\rho A \frac{\partial w}{\partial t} + \rho A w \frac{\partial w}{\partial x} + A \frac{\partial p}{\partial x} + F_f = 0 \quad [8]$$

For steady motion, Equation [8] becomes

$$\rho A w dw + A dp + F_f dx = 0 \quad [9]$$

Equation [9] is the momentum equation for the steady-state flow of fluid.

Since enthalpy is a state function of the fluid, conservation of energy requires that the heat added to the fluid element be accounted for by the change in enthalpy and kinetic energy across the element

$$dq = d\left(h + \frac{w^2}{2g}\right) \quad [10]$$

The definition of the specific heat at constant pressure c_p, is given by the equation

$$dh = C_p dT \quad [11]$$

Also by definition, an increment of total temperature dT_t, is given by the expression

$$dT_t = dT + d\left(\frac{w^2}{2gc_p}\right) \quad [12]$$

Substituting Equations [11] and [12] into [10] gives

$$dq = c_p dT_t \quad [13]$$

Equation [13] is the expression of the conservation of energy for steady-state flow.

Equations for Heat Transfer Across a Fluid Boundary[4]

The heat transfer through a fluid boundary is assumed to be proportional to the difference between wall temperature and total temperature. This is expressed by the formula

$$dq = \frac{h'}{m\rho g w} (T_w - T_t) dx \quad [14]$$

The value of the friction coefficient f, is defined by the equation for shearing stress τ along the wall

$$\tau = f \frac{\rho w^2}{2} \quad [15]$$

The friction force on the element of fluid is given by

$$F_f = s'\tau \quad [16]$$

where s' is the perimeter of the passage. Since the hydraulic radius is defined by

$$m = \frac{A}{s'} \quad [17]$$

Equation [16] becomes on combination with [15] and [17]

$$F_f = \frac{Af\rho w^2}{2m} \quad [18]$$

Relations Between Fluid Flow and Heat Transfer

The equations for fluid flow and heat transfer can now be combined to give a mathematically more useful result. Two more expressions are needed. Defining a quantity R, gives one expression

$$\frac{p}{\rho} = gRT \quad [19]$$

For a perfect gas, R is a constant. Defining Mach number provides the other expression

$$w^2 = M^2 g\gamma RT \quad [20]$$

Combining Equation [18] with [9]

$$dp + \rho w dw + \frac{f\rho w^2}{2m} dx = 0 \quad [21]$$

Eliminating dq between Equations [13] and [14]

$$c_p dT_t = \frac{h'}{m\rho g w} (T_w - T_t) dx \quad [22]$$

This can be rewritten in dimensionless form

$$\frac{f dx}{2m} = \frac{1}{\lambda} \frac{dT_t}{T_w - T_t} \quad [23]$$

where

$$\frac{1}{\lambda} = \frac{f c_p \rho g w}{2h'} \quad [24]$$

Equation [24] can be written alternatively as follows

[4] "Heat Transmission," by W. H. McAdams, second edition, McGraw-Hill Book Company, Inc., New York, N. Y., 1942.

$$\frac{1}{\lambda} = \frac{\mathbf{P}\mathbf{R}}{\mathbf{N}}\frac{f}{2} = \frac{1}{\mathbf{S}}\frac{f}{2} \quad \ldots\ldots\ldots\ldots\ldots\ldots [25]$$

where

$$\mathbf{P} = \text{Prandtl number} = \frac{c_p\mu}{k}$$

$$\mathbf{R} = \text{Reynolds number} = \frac{4m\rho gw}{\mu}$$

$$\mathbf{N} = \text{Nusselt number} = \frac{4h'm}{k}$$

$$\mathbf{S} = \text{Stanton number} = \frac{c_p\rho gw}{h'}$$

The Reynolds analogy between heat transfer and friction, which assumes[5] a similarity of velocity and temperature fields along the wall, gives a value of λ equal to 1. For a more accurate calculation it is necessary to have the functional dependence of friction factor and Stanton number on wall roughness, viscosity, Reynolds number, etc., at high temperatures.

Pressure Ratio Across an Interval in a Heated Passage

Substituting Equation [23] into [21]

$$dp + \rho w dw + \frac{\rho w^2}{\lambda}\frac{dT_t}{T_w - T_t} = 0 \quad \ldots\ldots\ldots\ldots [26]$$

Combining Equations [19], [20], and [26]

$$d[\log p] + \gamma \mathbf{M}^2 \left\{ d\,[\log \mathbf{M}(T)^{1/2}] + \frac{1}{\lambda}\frac{dT_t}{T_w - T_t} \right\} = 0 \ldots [27]$$

An expression for temperature in terms of total temperature and Mach number is obtained by combining Equations [20] and [12]

$$T = \frac{T_t}{1 + \frac{\gamma - 1}{2}\mathbf{M}^2} \quad \ldots\ldots\ldots\ldots\ldots [28]$$

Substituting Equation [28] into [27]

$$d[\log p] + \gamma \mathbf{M}^2 d\left[\log \frac{\mathbf{M}}{\left(1 + \frac{\gamma - 1}{2}\mathbf{M}^2\right)^{1/2}}\right] + \gamma \mathbf{M}^2 \left\{ d[\log (T_t)^{1/2}] + \frac{1}{\lambda}\frac{dT_t}{T_w - T_t} \right\} = 0 \ldots\ldots [29]$$

The second term in Equation [29] can be rewritten

$$\gamma \mathbf{M}^2 d\left[\log \frac{\mathbf{M}}{\left(1 + \frac{\gamma - 1}{2}\mathbf{M}^2\right)^{1/2}}\right] = d\left[\log \left(1 + \frac{\gamma - 1}{2}\mathbf{M}^2\right)^{\frac{\gamma}{\gamma - 1}}\right] \ldots\ldots [30]$$

Then Equation [29] becomes

$$d[\log p] + d\left[\log \left(1 + \frac{\gamma - 1}{2}\mathbf{M}^2\right)^{\frac{\gamma}{\gamma - 1}}\right] + \gamma \mathbf{M}^2 \left\{ d\,[\log (T_t)^{1/2}] + \frac{1}{\lambda}\frac{dT_t}{T_w - T_t} \right\} = 0 \ldots [31]$$

[5] "Compressibility Effects on Heat Transfer and Pressure Drop in Smooth Cylindrical Tubes," by J. N. Nielsen, NACA-ARR No. L4C16, October, 1944.

For the special case of constant wall temperature

$$d\,[\log (T_t)^{1/2}] + \frac{1}{\lambda}\frac{dT_t}{T_w - T_t} = d\left[\log \frac{(T_t)^{1/2}}{(T_w - T_t)^{1/\lambda}}\right] \ldots [32]$$

Substituting Equation [32] into [31]

$$d[\log p] + d\left[\log \left(1 + \frac{\gamma - 1}{2}\mathbf{M}^2\right)^{\frac{\gamma}{\gamma - 1}}\right] + \gamma \mathbf{M}^2 \left[d \log \frac{(T_t)^{1/2}}{(T_w - T_t)^{1/\lambda}} \right] = 0 \ldots [33]$$

Equation [33] is a differential equation relating pressure to Mach number and total temperature. Though it cannot, in general, be integrated analytically, this can be done for two special cases, an isentropic process and a process at constant Mach number. These two processes are shown schematically in Fig. 2.

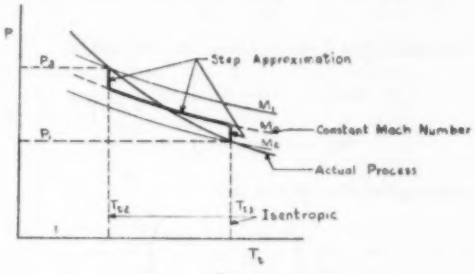

Fig. 2

For the isentropic process

$$\frac{P_2}{P_1} = \left(\frac{1 + \frac{\gamma - 1}{2}\mathbf{M}_1^2}{1 + \frac{\gamma - 1}{2}\mathbf{M}_2^2}\right)^{\frac{\lambda}{\lambda - 1}} \quad \ldots\ldots\ldots\ldots [34]$$

This process is independent of the temperature at which it occurs. It should be noticed that this process must be isentropic as well as adiabatic, for when $d(T_t) = 0$, the friction term $dT_t/T_w - T_t$ becomes indeterminate. In order for this term to disappear also, it is necessary to assume that the process occurs in a zero length, involving a physical discontinuity in the passage (see Equation [23]). For a process at constant Mach number

$$\frac{P_3}{P_2} = \left(\frac{1 - T_a/T_w}{1 - T_a/T_w}\right)^{\frac{\gamma \mathbf{M}_0^2}{\lambda}} \left(\frac{T_a/T_w}{T_a/T_w}\right)^{\frac{\gamma \mathbf{M}_0^2}{2}} \quad \ldots\ldots\ldots [35]$$

This process is assumed to occur in a finite length of passage. The correct value of $\mathbf{M}_0$ is given by the following integration over the actual process

$$\mathbf{M}_0^2 = \frac{\int_1^2 \mathbf{M}^2 d\left[\log \frac{(T_t)^{1/2}}{(T_w - T_t)^{1/\lambda}}\right]}{\left[\log \frac{(T_t)^{1/2}}{(T_w - T_t)^{1/\lambda}}\right]_1^2}$$

By the mean value theorem, for small steps, $\mathbf{M}_1 < \mathbf{M}_0 < \mathbf{M}_2$, and the correct value of $\mathbf{M}_0$ can be bracketed between arbitrarily close limits. Equations [34] and [35] can be combined to give the pressure ratio across the whole step

$$\frac{P_3}{P_1} = \frac{P_2}{P_1}\frac{P_3}{P_2} = \left(\frac{1 + \frac{\gamma - 1}{2}\mathbf{M}_1^2}{1 + \frac{\gamma - 1}{2}\mathbf{M}_2^2}\right)^{\frac{\gamma}{\gamma-1}} \left[\left(\frac{1 - T_{t1}/T_w}{1 - T_{t2}/T_w}\right)^{\frac{1}{\lambda}} \left(\frac{T_{t2}/T_w}{T_{t1}/T_w}\right)^{1/\gamma}\right]^{\gamma \mathbf{M}_2^2} \quad [36]$$

Equation [36] is the expression for the pressure ratio across a small step, composed of an isentropic process and a process at constant Mach number, which can be so adjusted as to approximate any actual process.

Area Ratio Across an Interval in a Heated Passage

It is desired to find the change in area occurring in the same step. Eliminating ρ between Equations [2] and [19]

$$\frac{wAg}{W} = \frac{gRT}{P} \quad [37]$$

Eliminating w and T with Equations [20], [28], and [37]

$$\frac{P}{P_1} = \frac{\mathbf{M}_1\left(1 + \frac{\gamma - 1}{2}\mathbf{M}_1^2\right)^{1/2}}{\mathbf{M}\left(1 + \frac{\gamma - 1}{2}\mathbf{M}^2\right)^{1/2}} \frac{A_1}{A}\left(\frac{T_t}{T_{t1}}\right)^{1/2} \quad [38]$$

Combining Equation [38] with [34]

$$\frac{A_2}{A_1} = \frac{\mathbf{M}_1}{\mathbf{M}_2}\left(\frac{1 + \frac{\gamma - 1}{2}\mathbf{M}_2^2}{1 + \frac{\gamma - 1}{2}\mathbf{M}_1^2}\right)^{\frac{\gamma+1}{2(\gamma-1)}} \quad [39]$$

Combining Equation [38] with [35]

$$\frac{A_3}{A_2} = \left(\frac{T_{t1}/T_w}{T_{t2}/T_w}\right)^{\frac{1+\gamma\mathbf{M}_2^2}{2}} \left(\frac{1 - T_{t2}/T_w}{1 - T_{t1}/T_w}\right)^{\frac{\gamma\mathbf{M}_2^2}{\lambda}} \quad [40]$$

The expression for area ratio across the step becomes

$$\frac{A_3}{A_1} = \frac{\mathbf{M}_1}{\mathbf{M}_2}\left(\frac{1 + \frac{\gamma - 1}{2}\mathbf{M}_2^2}{1 + \frac{\gamma - 1}{2}\mathbf{M}_1^2}\right)^{\frac{\gamma+1}{2(\gamma-1)}} \left(\frac{T_{t1}/T_w}{T_{t2}/T_w}\right)^{\frac{1+\gamma\mathbf{M}_2^2}{2}} \left(\frac{1 - T_{t2}/T_w}{1 - T_{t1}/T_w}\right)^{\frac{\gamma\mathbf{M}_2^2}{\lambda}} \quad [41]$$

Temperature Change as a Function of Distance Along Passage

For a step small enough that f, m, λ, and T_w can be considered constant, the interval of length necessary to change the fluid temperature from T_{t2} to T_{t3} is given by an integration of Equation [23]

$$\frac{\Delta x}{l} = \frac{k}{2}\log_{10}\left(\frac{1 - T_{t2}/T_w}{1 - T_{t3}/T_w}\right) \quad [42]$$

where

$$k = 2\log_e(10)\frac{2m}{\lambda f l}$$

Equation [42] relates the intervals of length along the passage with the variables of Equations [36] and [41].

Entropy Consideration

It is to be expected that certain limitations would be imposed by the requirements of the second law of thermodynamics on heated, nonadiabatic flow. It is the purpose of this section to investigate these limitations. The differential of entropy ds, is given by

$$ds = \frac{du + pdv}{T} \quad [43]$$

The differential of internal energy can be written in terms of enthalpy h

$$du = dh - vdp - pdv \quad [44]$$

Substituting Equation [44] into [43]

$$ds = \frac{dh - vdp}{T} \quad [45]$$

Since $dh = c_p dT$, and $pv = RT$, Equation [45] can be written

$$ds = c_p\frac{dT}{T} - R\frac{dp}{p} \quad [46]$$

where, assuming a perfect gas

$$R = c_p - c_v = c_p\frac{\gamma - 1}{\gamma} \quad [47]$$

Thus

$$ds = c_p\left\{d[\log T] - \frac{\gamma - 1}{\gamma}d[\log p]\right\} \quad [48]$$

Substituting the value of T from Equation [28] into [48]

$$ds = c_p\left\{d[\log T_t] - d\left[\log\left(1 + \frac{\gamma - 1}{2}\mathbf{M}^2\right)\right] - \frac{\gamma - 1}{\gamma}d[\log p]\right\} \quad [49]$$

Substituting the value of $d[\log p]$ from Equation [33]

$$ds = c_p\left\{d[\log T_t] - d\left[\log\left(1 + \frac{\gamma - 1}{2}\mathbf{M}^2\right)\right] + \frac{\gamma - 1}{\gamma}d\left[\log\left(1 + \frac{\gamma - 1}{2}\mathbf{M}^2\right)^{\frac{\gamma}{\gamma-1}}\right] + \frac{\gamma - 1}{\gamma}\frac{\gamma\mathbf{M}^2}{2} d[\log T_t] - \frac{\gamma - 1}{\gamma}\frac{\gamma\mathbf{M}^2}{\lambda}d[\log(T_w - T_t)]\right\} \quad [50]$$

Equation [50] simplifies to

$$\frac{ds}{d\left(\frac{T_t}{T_w}\right)} = c_p\left[\frac{1 + \frac{\gamma - 1}{2}\mathbf{M}^2}{T_t/T_w} + \frac{\gamma - 1}{\lambda}\frac{\mathbf{M}^2}{1 - T_t/T_w}\right] \quad [51]$$

Equation [51] yields several characteristics of the entropy curve. A stationary point exists when $ds/d(T_w/T_t) = 0$, or when

$$\left(\frac{T_t}{T_w}\right)_s = \frac{1 + \frac{\gamma - 1}{2}\mathbf{M}^2}{1 + \frac{\gamma - 1}{2}\mathbf{M}^2\left(1 - \frac{2}{\lambda}\right)} \quad [52]$$

The second derivative of entropy, for constant Mach number processes, has zeros when

$$\frac{T_t}{T_w} = \left(\frac{T_t}{T_w}\right)_s \left(1 \pm \frac{\mathbf{M}}{\sqrt{\lambda}} \sqrt{\frac{2(\gamma-1)}{(\gamma-1)\mathbf{M}^2+2}}\right) \quad [53]$$

For values of T_t/T_w close to zero, the slope is very great; due to the first term of Equation [51] the shape is approximately logarithmic. Due to the second term the slope becomes infinite at $T_t/T_w = 1$, being positive before and negative after this point. The slope tends to zero as T_t/T_w tends to infinity. Schematically then the entropy curve is as shown in Fig. 3.

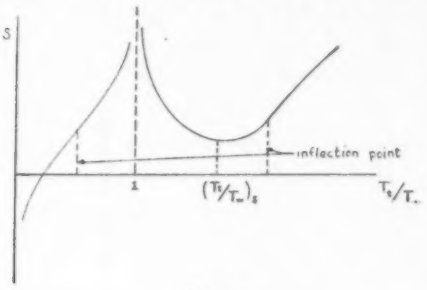

FIG. 3

The interpretation of the curve in Fig. 3 is somewhat as follows: Below $T_t/T_w = 1$, entropy is increasing due both to friction and to the addition of heat. Above $T_t/T_w = (T_t/T_w)_s$, entropy is decreasing faster due to the withdrawal of heat than it is increasing due to friction. Between these two points entropy is increasing faster due to friction than it is decreasing due to withdrawal of heat. As long as the total temperature is below the wall temperature it must rise, and if the total temperature is above the wall temperature it must fall, as would be expected for other reasons. From Equation [52], for $0 < \lambda < 2$, it is necessary (since negative temperatures cannot exist) that the Mach number at the stationary point be limited to

$$\mathbf{M}^2 \leqq \frac{2}{(\gamma-1)\left(\frac{2}{\lambda}-1\right)} \quad [54]$$

As the Mach number approaches the upper limit, the temperature ratio at which the stationary point occurs approaches ∞.

To find the limitations in Mach number as a function of temperature and area, an expression relating these factors will be derived, and the entropy considerations will be applied. From Equations [33] and [38], $d\ [\log P]$ can be eliminated, giving an expression

$$d\left[\log\left(1+\frac{\gamma-1}{2}\mathbf{M}^2\right)^{\frac{\gamma}{\gamma-1}}\right] - d\ [\log \mathbf{M}]$$
$$- d\left[\log\left(1+\frac{\gamma-1}{2}\mathbf{M}^2\right)^{1/2}\right] + \gamma\mathbf{M}^2 d\left[\log\frac{(T_t)^{1/2}}{(T_w-T_t)^{1/\lambda}}\right]$$
$$- d\ [\log A\,] + d[\log (T_t)^{1/2}] = 0 \quad [55]$$

Performing the indicated differentiations and simplifying

$$\frac{(\mathbf{M}^2-1)}{\mathbf{M}^2\left(1+\frac{\gamma-1}{2}\mathbf{M}^2\right)}\, d(\mathbf{M}^2) + \frac{(1+\gamma\mathbf{M}^2)}{T_t}\, d\,(T_t)$$
$$+ \frac{2\gamma\mathbf{M}^2}{\lambda}\,\frac{dT_t}{T_w-T_t} - d[\log(A^2)] = 0 \quad [56]$$

This can be solved for the rate of change of total temperature with Mach number

$$\frac{d\left(\frac{T_t}{T_w}\right)}{d\mathbf{M}^2} = \frac{\frac{T_t}{T_w}\left(1-\frac{T_t}{T_w}\right)\left[\frac{d[\log(A^2)]}{d(\mathbf{M}^2)} - \frac{\mathbf{M}^2-1}{\mathbf{M}^2\left(1+\frac{\gamma-1}{2}\mathbf{M}^2\right)}\right]}{1+\gamma\mathbf{M}^2+\left[\gamma\mathbf{M}^2\left(\frac{2}{\lambda}-1\right)-1\right]\frac{T_t}{T_w}} \quad [57]$$

Since, by Equation [13], dT_t is a measure of the heat added to the stream of fluid, the points where $d\ (T_t/T_w)/d\ (\mathbf{M}^2) = 0$ represent the conditions where the maximum possible amount of heat has been added (or taken away).

One series of these points is given by equating to zero the expression $(1 - T_t/T_w)$. Equation [57] then requires that no combination of area and Mach number exist by which continuous heating or cooling can occur through the condition $T_t/T_w = 1$. The entropy condition requires that the fluid be heated for $T_t/T_w < 1$ and cooled for $T_t/T_w > 1$. A second series of points is given by equating

$$\frac{d\ [\log (A^2)]}{d(\mathbf{M}^2)} - \frac{\mathbf{M}^2-1}{\mathbf{M}^2\left(1+\frac{\gamma-1}{2}\mathbf{M}^2\right)} = 0 \quad [58]$$

This amounts to the statement that, at any Mach number, it is possible to change area in such a way that temperature may be stationary, or increasing or decreasing, provided the entropy condition is fulfilled.

For a cylindrical tube, Equation [58] degenerates to the expression

$$\mathbf{M}^2 - 1 = 0 \quad [59]$$

Equation [59] states that it is impossible either to heat or to cool continuously through Mach number 1, for the cylindrical tube. The entropy consideration requires that, since $d\ (T_t/T_w)$ and $(1 - T_t/T_w)$ are always of the same sign, then $d\ (T_t/T_w)/d(\mathbf{M}^2)$ is positive when $(1 - T_t/T_w)$ and $(\mathbf{M}^2 - 1)$ are of opposite sign, and negative when they are of the same sign. Hence, for heating, the Mach number increases for Mach number less than 1, and decreases for Mach number greater than 1, while for cooling the effect is opposite. The special case of the cylindrical tube is discussed by Nielsen.[5]

Discussion of Charts

Graphical information for the design of passages for the flow of heated gas is presented in charts, Figs. 4 and 5.

The straight lines in the chart, Fig. 4, are solutions (for constant values of K) of Equation [42], giving plots of the ratio of total temperature to wall temperature against fractional distance along the passage. It is to be noted that $K = 1.0$ corresponds to 45 deg on the chart. The parameter K is a direct measure of slope. In an actual process where K varies with gas temperature and distance along the passage, the process is considered for small steps using an average value of K in each step. The total length of passage needed is that which gives the desired temperature rise on the chart in a fractional distance along the passage equal to 1.

The chart in Fig. 5 is divided into four parts, designated as A, B, C, and D. Part A, Fig. 5, gives a family of curves which are the solutions of Equation [39], the parameter being an arbitrary constant. The processes represented by these curves

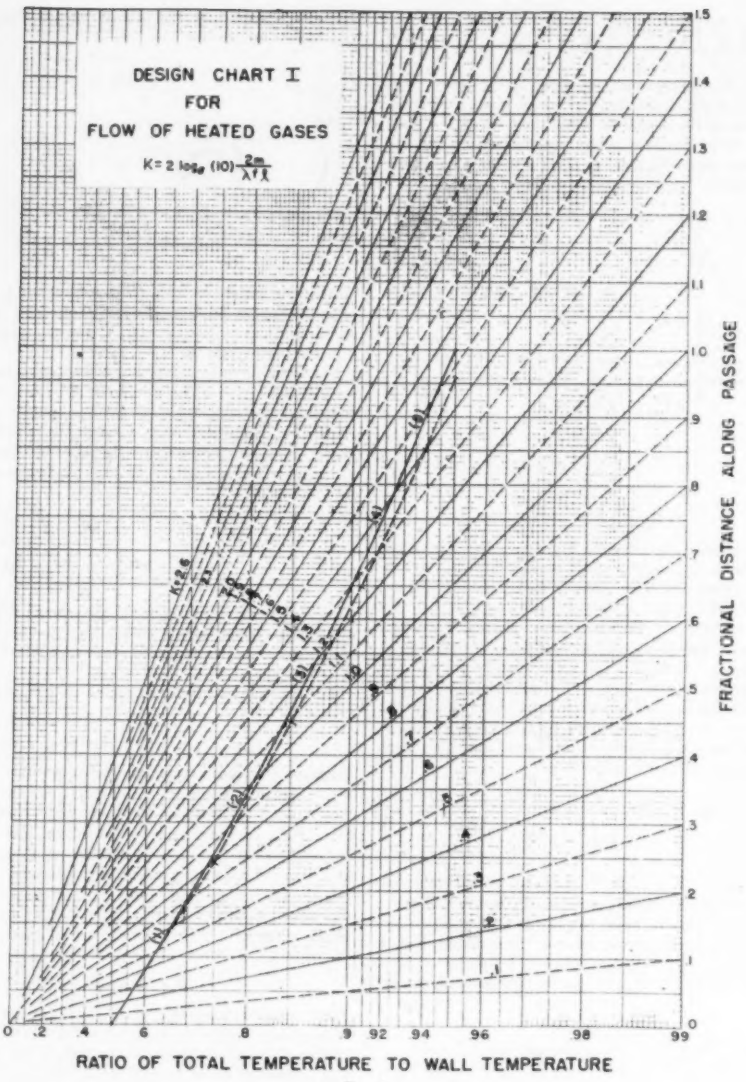
DESIGN CHART I
FOR
FLOW OF HEATED GASES
$K = 2 \log_e (10) \frac{2m}{\lambda' \ell}$
FRACTIONAL DISTANCE ALONG PASSAGE
RATIO OF TOTAL TEMPERATURE TO WALL TEMPERATURE
0 .2 .4 6 8 9 92 94 96 98 99
0 1 2 3 4 5 6 7 8 9 10 11 12 13 14 15

FIG. 4

occur at constant total temperature of the gas. The area ratio necessary to cause the flow at constant total temperature to change between two given Mach numbers is given by the ratio of the ordinates at these Mach numbers, on any curve in Part A. The ratio of the corresponding ordinates on any curve in Part B gives the pressure ratio for the same process at constant total temperature. The family of curves in Part B is the solution to Equation [34]. This ratio gives the isentropic pressure ratio which would exist due to the area ratio in Part A if there were no friction.

The curves of Part C of the chart in Fig. 5 are the solution, with Mach number for a parameter, of Equation [40]. The processes represented by these curves occur at constant Mach number. In flow with friction at a given constant Mach number, the area ratio necessary to cause a change between two given values of the ratio of total temperature to wall temperature is given by the ratio of the ordinates corresponding to these temperatures, on the curve for the given Mach number. The ratio of the corresponding ordinates, in Part D on the curve for the same Mach number, gives the total pressure ratio (pressure ratio due to friction in the passage) for the same process. The family of curves in Part D is the solution to Equation [35].

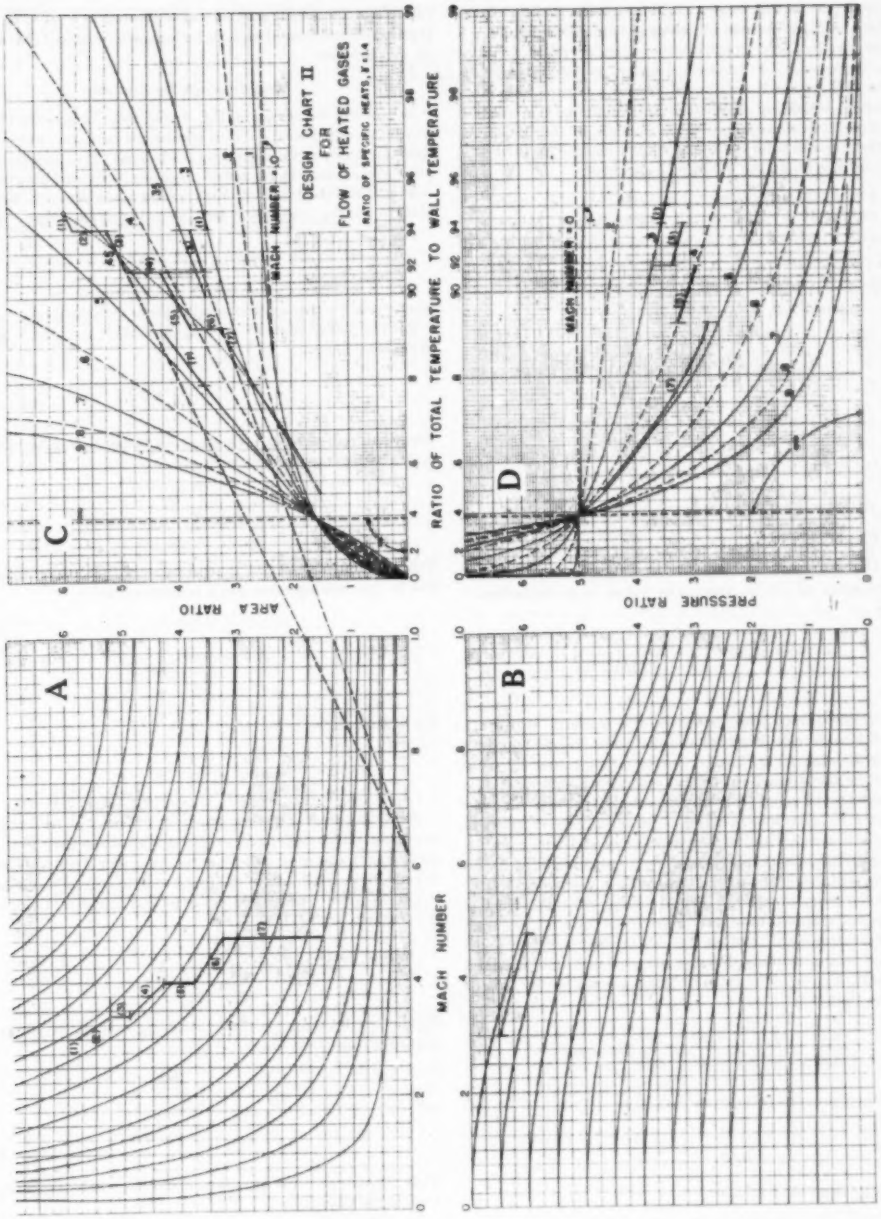
DESIGN CHART II
FOR
FLOW OF HEATED GASES
RATIO OF SPECIFIC HEATS, k = 1.4
MACH NUMBER = 0
A
B
C
D
AREA RATIO
MACH NUMBER
PRESSURE RATIO
RATIO OF TOTAL TEMPERATURE TO WALL TEMPERATURE

FIG. 5

An actual process will, in general, follow neither a line of constant Mach number nor one of constant total temperature. A particular problem may specify either area or pressure ratios through the passage. It is then necessary, on the charts, to approximate this specified variation of area or pressure ratio by a series of steps consisting of constant Mach number and constant total temperature processes. As an example of the use of the charts, the stepwise solution is shown for a circular tapered tube with heated flow under the following conditions:

$\lambda] = 1 = \text{const} = \text{parameter, Equation [23]}$

$T_w = 800$ deg K = constant wall temperature

$\left.\frac{T_t}{T_w}\right]_{x=0} = 0.5$ = ratio of total temperature of gas at inlet to wall temperature

$\left.\frac{T_t}{T_w}\right]_{x=l} = 0.95$ = ratio of total temperature of gas at outlet to wall temperature

$D_0 = 0.25$ in. = diameter of tube at inlet

$$m = \frac{D}{4} = m_0\left(1 + \frac{x}{l}\right) = \frac{D_0}{4}\left(1 + \frac{x}{l}\right) = \text{hydraulic radius}$$

$$A = 4\pi m_0^2\left(1 + \frac{x}{l}\right)^2 = \frac{\pi D_0}{4}\left(1 + \frac{x}{l}\right)^2$$

$\mathbf{M}]_{x=l} = 0.3$ = Mach number at outlet

$\mathbf{R}]_{x=l} = 20{,}000$ = Reynolds number at outlet

$$f = \frac{0.049}{(\mathbf{R})^{0.2}} = \text{friction factor}$$

The viscosity of air in poises was taken from Sutherland's equation

$$\mu = 170.9 \times 10^{-6}\left(\frac{393}{T + 120}\right)\left(\frac{T}{273}\right)^{3/2}$$

where T is the temperature in degrees Kelvin. An estimated value of l, based upon average values, was made ($l' = 71$ in.). Values of K were calculated for the five steps shown, and lines drawn on the chart, Fig. 4, with corresponding slopes for these steps. Since the desired outlet temperature was obtained at a fractional distance equal to 0.96 instead of 1.00, a new trial was made with $l = 71 \times 0.96 = 68$ in. This is the correct length of the tube, as indicated by the fact that the second trial gave the proper temperature at a fractional distance equal to 1.

The plot with $l = 68$ in. on the chart, Fig. 4, gives the relationship between temperature and distance along the tube, which is used to plot, in dotted lines, the desired variation of area ratio with temperature on Part C of the chart, Fig. 5. The seven steps, used to approximate this area are shown in the four parts of the chart, Fig. 5. The ratio of total pressure in the tube is given from Part D as

$$\frac{3.44}{3.51} \times \frac{3.13}{3.32} \times \frac{2.90}{3.22} \times \frac{2.67}{4.52} = 0.492$$

The isentropic pressure ratio, from Part B, is

$$\frac{5.98}{6.50} = 0.92$$

The static pressure ratio is hence

$$0.492 \times 0.92 = 0.452$$

The method of transferring a given constant Mach number area ratio from the Mach number curve plotted in Part C to a new position on the desired area curve is shown for step 3 ($\mathbf{M} = 0.34$) by the dash lines.

Investigation of Errors

In plotting the curves in Fig. 4, the ratio of specific heats γ, was taken equal to 1.4. It is considered pertinent to find what error is involved in neglecting variations in γ. Since, in the plots of constant Mach number processes, γ appears always in the combination $\gamma\mathbf{M}_0^2$, a correction can be made easily in using the plots by taking processes at $\mathbf{M}_0'$ instead of at $\mathbf{M}_0$ where

$$\mathbf{M}_0' = \sqrt{\frac{1.4}{\gamma'}}\,\mathbf{M}_0$$

where γ' is the true ratio of specific heats for a particular process.

For the plot of pressure ratio against Mach number, γ appears in the combination

$$\left(1 + \frac{\gamma - 1}{2}\mathbf{M}^2\right)$$

For numbers $0 < \mathbf{M} < 1$, this expression can be roughly approximated by two terms of a power series

$$\left(1 + \frac{\gamma - 1}{2}\mathbf{M}^2\right)^{\frac{\gamma}{\gamma - 1}} \sim 1 + \frac{\gamma\mathbf{M}^2}{2}$$

The percentage error θ in the pressure ratio across a given step due to a percentage error η in γ is approximately

$$\theta = \frac{\eta\,\gamma\,\frac{\mathbf{M}^2}{2}}{1 + \frac{\gamma\mathbf{M}^2}{2}}$$

For Mach number 1 this error is ($\gamma = 1.4$)

$$\theta_{\mathbf{M}=1} = \frac{0.7}{1.7}\,\eta \sim \frac{1}{2}\,\eta$$

Since this error is approximately a function of $\mathbf{M}^2$, and since the maximum variation of γ from 1.4 is not more than 10 per cent up to 5000 F this error will never be larger than 5 per cent and will, in general, be much less in the range of temperatures considered.

For the plot of area ratio against Mach number, γ appears in the combination

$$\left(1 + \frac{\gamma - 1}{2}\mathbf{M}^2\right)^{\frac{\gamma+1}{2(\gamma-1)}}$$

By the two-term approximation to the power series, the error in area ratio due to error $\eta\gamma$ is

$$\epsilon = \frac{\eta\,\gamma\,\frac{\mathbf{M}^2}{4}}{1 + \frac{\gamma + 1}{4}\mathbf{M}^2}$$

This percentage error is approximately one half the percentage error in pressure ratio.

In plotting the constant Mach number processes in the chart, Fig. 5, it was assumed that $\lambda = 1$. For any other values of λ a new chart must be made.

Discussion

Bending of Rectangular Plates Subjected to a Uniformly Distributed Lateral Load and to Tensile or Compressive Forces in the Plane of the Plate[1]

ROBERTO CONTINI.[2] The problem of a simply supported rectangular plate under uniformly distributed lateral load and uniform compression in the direction of one pair of sides was studied some time ago by Mr. C. H. Heilbron and the writer.[3]

The method of solution adopted was similar to that of the paper, except that, instead of a Fourier series of the type $\Sigma Y_m \sin(m\pi x/a)$, one of the type $\Sigma X_m \sin(m\pi y/b)$ was used. For the case of no end load, the latter solution is more rapidly convergent than the author's in the range of aspect ratios $a/b > 1$; hence less so if $a/b < 1$.[4] As a rule, this is also true if end load is present, although there may be some question as to which solution is preferable in the neighborhood of $a/b = 1$.

In the author's solution, however, advantage should be taken of the relations

$$\frac{4}{\pi}\sum_{m=1,3,5\ldots}^{\infty}\frac{1}{m\left(\alpha_m^2+\frac{P}{D}\right)}\sin\frac{m\pi x}{a}=\frac{1}{(P/D)}\left\{1-\frac{\cosh\left[\frac{a}{2}\sqrt{\frac{P}{D}}\left(1-\frac{2x}{a}\right)\right]}{\cosh\frac{a}{2}\sqrt{\frac{P}{D}}}\right\}$$

for tensile end load, and

$$\frac{4}{\pi}\sum_{m=1,3,5\ldots}^{\infty}\frac{1}{m\left(\alpha_m^2-\frac{P}{D}\right)}\sin\frac{m\pi x}{a}=\frac{1}{(P/D)}\left\{\frac{\cos\left[\frac{a}{2}\sqrt{\frac{P}{D}}\left(1-\frac{2x}{a}\right)\right]}{\cos\frac{a}{2}\sqrt{\frac{P}{D}}}-1\right\}$$

for compressive end load, in order to obtain the best possible convergency. By means of these relations, those parts of the series arising from the last term within braces in Equations [14] and [21] of the paper can be calculated directly rather than as a summation; the second of the foregoing relations cannot be used, however, if, for any m, $\alpha_m^2 = P/D$, i.e., when one of the terms of the author's series requires the application of Equations [22] to [24] of the paper.

As an example, the coefficient γ for the moment M_y at the center of the plate in the case $a/b = 2.0$ and $P/P_E = 0.5$ (compressive) was calculated (1) by the Lockheed method, (2) by the author's method, and (3) by the author's method, modified as suggested. For the Poisson's ratio, the value $\nu = 0.3$ was used. The results are given in Table 1.

TABLE 1 RESULTS COEFFICIENT γ CALCULATIONS

	Lockheed method	Author's method	Author's method modified
Nonseries term	+0.125	....	−0.072279
1st term of series	+0.023896	+0.161312	+0.183427
2nd term of series	0.000000	−0.013960	+0.037642
3rd term of series	....	+0.001947	+0.000125
4th term of series	....	−0.000562	−0.000022
5th term of series	....	+0.000239	+0.000003
6th term of series	....	−0.000125	0.000000
$\gamma = \Sigma$	+0.148896	+0.148851	+0.148896

An important point which was overlooked by the author is that, for certain combinations of aspect ratio and end load (either tensile or compressive), maximum bending moments do not occur at the center of the plate. For the case of compressive end load, the author's assumption that maximum moments occur at the center may lead to serious errors. The considerations which follow apply to this case.

In the previous study,[3] bending moments for the range of aspect ratios $a/b \geq 1$ were investigated, and it was found that in general, as the ratio a/b increases, maximum bending moments move away from the center of the plate, occurring at some other point on the center line parallel to the x-axis. More specifically (the values quoted in the following are for $\nu = 0.3$):

1 For $P = 0$, the maximum moment M_x does not occur at the center of the plate if $a/b > \sim 1.8$; for $a/b = \infty$ it occurs at a distance from the end of the plate equal to approximately $0.6b$ and its value is $0.0445\,qb^2$. The value of a/b for which the maximum moment M_x begins to move away from the center of the plate decreases slightly with increasing values of P.

2 For $P = 0$, the maximum moment M_y occurs always at the center. For $a/b = \infty$, any finite value of the load P will cause the maximum moment M_y to move away from the center, i.e., the maximum moment will occur at a finite distance from the end of the plate. The value of a/b for which the maximum moment M_y begins to move away from the center again decreases as P in-

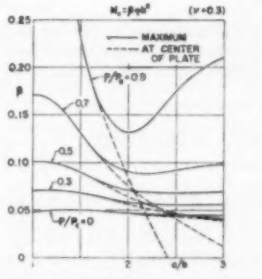

FIG. 1

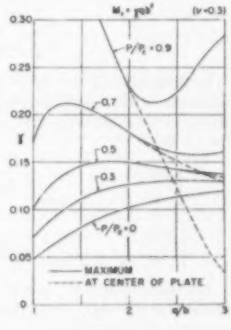

FIG. 2

[1] By H. D. Conway, published in the JOURNAL OF APPLIED MECHANICS, September, 1949, Trans. ASME, vol. 71, pp. 301–309.

[2] Research Engineer, Lockheed Aircraft Corporation, Burbank, Calif.

[3] Lockheed Aircraft Corporation, Report No. 4960, Section B, December, 1945.

[4] "Theory of Plates and Shells," by S. Timoshenko, McGraw Hill Book Company, Inc., New York, N. Y., 1940, art. 29, p. 128.

creases; for instance, for $P/P_E = 0.5$ this value is approximately 2.5, and for $P/P_E = 0.9$ it is approximately 2.

Curves giving maximum-moment coefficients β and γ, using results from the previous study,[3] are shown in Figs. 1 and 2 herewith. These figures should replace the author's Figs. 9 and 10. For comparison, the moment coefficients for the center of the plate are shown in dotted lines for those regions where they are not maximum.

The range of aspect ratios $a/b < 1$ was not investigated, but, under certain conditions, maximum moments may be expected to occur, not at the center of the plate, but at some other point on the center line parallel to the y-axis. Some indication of what happens can be obtained from the solution for the limiting case $a/b = 0$. This is easily derived by introducing a new co-ordinate $z = y + (b/2)$, representing the distance from the edge $y = -b/2$. Substituting for y its value in terms of z, and for A_m and C_m their values, Equations [19], into Equation [18] of the paper and then letting b approach infinity, the following equation for the deflection is obtained

$$\omega = \frac{4q}{\pi} \sum_{m=1,3,5\ldots}^{\infty} \frac{\eta_m{}^2 e^{-\gamma_m z} - \gamma_m{}^2 e^{-\eta_m z} + 2\alpha_m \sqrt{\frac{P}{D}}}{2m\alpha_m{}^2 \sqrt{PD}\left(\alpha_m{}^2 - \frac{P}{D}\right)} \sin \frac{m\pi x}{a}$$

The following equations can then be written for the derivatives of the bending moments along the center line parallel to the y-axis

$$\left[\frac{\partial M_x}{\partial z}\right]_{x=a/2} = \sum_{m=1,3,5\ldots}^{\infty} (-1)^{\frac{m-1}{2}} R_m \left[(\alpha_m{}^2 - \nu\eta_m{}^2)\gamma_m e^{(\gamma_m - \eta_m)z} - (\alpha_m{}^2 - \nu\gamma_m{}^2)\eta_m\right]$$

$$\left[\frac{\partial M_y}{\partial z}\right]_{x=a/2} = \sum_{m=1,3,5\ldots}^{\infty} (-1)^{\frac{m-1}{2}} R_m \left[(\nu\alpha_m{}^2 - \eta_m{}^2)\gamma_m e^{(\gamma_m - \eta_m)z} - (\nu\alpha_m{}^2 - \gamma_m{}^2)\eta_m\right]$$

where

$$R_m = \frac{2q\gamma_m\eta_m e^{-\gamma_m z}}{m\pi\alpha_m{}^2 \sqrt{P/D}\left(\alpha_m{}^2 - \frac{P}{D}\right)}$$

Since an infinitely wide plate buckles essentially as a column, the following inequalities apply for any m

$$\alpha_m{}^2 > P/D$$
$$\gamma_m > \alpha_m > \eta_m > 0$$
$$R_m > 0$$

In investigating the signs of the derivatives of the bending moments, it will be sufficient to consider only the first term of each series, as these converge very rapidly. With this approximation, for $z = 0$

$$\left[\frac{\partial M_x}{\partial z}\right]_{x=a/2;\ z=0} \cong R_1(\gamma_1 - \eta_1)(\alpha_1{}^2 + \nu\gamma_1\eta_1) > 0$$

$$\left[\frac{\partial M_y}{\partial z}\right]_{x=a/2;\ z=0} \cong R_1(\gamma_1 - \eta_1)(\nu\alpha_1{}^2 + \gamma_1\eta_1) > 0$$

For the moments M_x and M_y to have a maximum at a finite distance from the edge $z = 0$, their derivatives would have to become negative for some value of z. Since $e^{(\gamma_1 - \eta_1)z}$ can have any value between $+1$ and $+\infty$ as z varies, this will only happen, for M_x and M_y, respectively, if $(\alpha_1{}^2 - \nu\eta_1{}^2) < 0$ and $(\nu\alpha_1{}^2 - \eta_1{}^2) < 0$. From the inequalities just set forth and from the expression for η_1 in terms of α_1, it follows that M_x cannot have a maximum at a finite distance from the edge while M_y will if

$$P < \frac{\pi^2 D}{a^2}(1 - \nu)^2$$

From the foregoing discussion, the following conclusions—which supplement and modify some of the author's—can be arrived at for the case of compressive end load:

1 Throughout the whole range of aspect ratios from zero to infinity, maximum bending moments are never independent of P. As Figs 1 and 2 herewith show, these moments are always larger than the corresponding maximum moments for the case $P = 0$.

2 For very long plates ($a/b >> 1$), maximum bending moments cannot be calculated by means of cylindrical-surface formulas, except for M_y in the limiting case $P = 0$.

3 For very short plates ($a/b << 1$), it appears that the maximum moment M_x can be calculated by means of cylindrical-surface formulas for all values of P. On the other hand, such formulas will be applicable to the calculation of the maximum moment M_y only if $P > (\pi^2 D/a^2)(1 - \nu)^2$.

Author's Closure

The author is indebted to Mr. Contini for his discussion. For the sake of mathematical elegance it is probably desirable to sum parts of Equations [14] and [21]. However, in the example given by Mr. Contini, the first two terms of the author's series give a result which is only 1 per cent in error; such convergence is quite satisfactory for any practical problem.

The fact that, for certain values of a/b and end load, the maximum bending moments will not occur at the center of the plate is interesting and subscripts "max" in the paper should therefore be changed to "center." However, the author considers this to be of academic interest only and the maximum resultant stress in plates with practical values of a/b and compression end load can usually be calculated as occurring at the center.

The Dynamics of Cavitation Bubbles[1]

Edward Silberman.[2] The writer has made some qualitative observations regarding the initial stages of bubble formation in low-pressure regions which may be of interest to readers of this paper. The observations were made incidental to experiments on resorption of air bubbles in turbulent water.[3] The experimental apparatus consisted essentially of a sealed lucite cylinder, filled with distilled water. A brass rotor was installed in the cylinder near one end and connected by a shaft to an external motor. The liquid inside the cylinder could be made to rotate in a turbulent state at various speeds by controlling the speed of the motor. A pressure connection to the cylinder (through a sealed diaphragm) permitted wide variation in superimposed pressure. Observation was with the unaided eye under a strong continuous light, or with an 18-power microscope in combination with a stroboscopic light.

[1] By M. S. Plesset, published in the September, 1949, issue of the Journal of Applied Mechanics, Trans. ASME, vol. 71, pp. 277–282.

[2] Assistant Professor of Hydraulics, St. Anthony Falls Hydraulic Laboratory, University of Minnesota, Minneapolis, Minn.

[3] "Air Bubble Resorption," by Edward Silberman, Technical Paper No. 1, series B, St. Anthony Falls Hydraulic Laboratory, University of Minnesota, August, 1949.

The water in the cylinder was saturated with air at atmospheric pressure. Cavitation was produced in the rotating liquid by suddenly dropping the mean pressure only 1 or 2 psi. (A similar or much larger drop in pressure in static liquid produced no cavitation.) Immediately after the pressure drop very small bubbles began to form in the liquid. These were merely pin points of light of 0.001 in. diam or less. (The size estimate was obtained by stopping the rotor and watching a bubble in the microscope.) The bubbles continued to form as long as the low pressure was maintained. A further reduction in pressure (or an increase in the speed of rotation) increased the rate of formation of the small bubbles perceptibly, but did not increase their size to a measurable degree. A sudden increase in pressure did not reverse the process; a measurable time was required to make each bubble disappear. Of course the gas inside the bubbles was essentially air rather than water vapor, but the formation process was truly cavitation as it is usually defined. By reducing the saturation pressure of the liquid, small bubbles, consisting mainly of water vapor, could be produced just as well by the same process.

It might be well to mention at this point that the small bubbles were undoubtedly produced in the turbulent vortexes where the pressures were considerably smaller than 1 or 2 psi below atmospheric pressure. The bubbles were first visible at points about one quarter of the distance from the cylinder axis to its walls where the turbulence appeared to be greatest, and where the rotational and irrotational flow were joined. The small bubbles were probably expanded nuclei in accordance with the theory stated by the author; when once expanded, the nuclei maintained their size by virtue of their increased surface energy even though they moved into higher-pressure regions.

After initial formation of the small bubbles, the phenomenon observed by the writer was not cavitation as it is usually described by the engineer. As stated by the author and confirmed by many experimental investigations including those of the writer, the rate of diffusion of air into and out of the bubble is of a much smaller order of magnitude than the rate of evaporation or condensation of water vapor. Therefore as long as the existing pressure exceeds the vapor pressure, individual bubbles grow and shrink only in accordance with the gas laws as the pressure fluctuates rapidly. Incidentally, the principal method of growth of the writer's bubbles was by coalescence following collision, mainly along the cylinder axis.

It is believed that the presence of solid matter, the basis of the author's theory of bubble formation, was demonstrated in the writer's experiments. The distilled water, which was at first perfectly clear, came to have a dirty appearance after many repetitions of the cavitation process. The water was changed many times during the course of the experiments, but it always became dirty. This phenomenon was orginally attributed to wear on the seal where the rotor shaft entered the cylinder, but on dismantling the apparatus no signs of wear could be detected. It is now believed that the dirty appearance is attributable to the coalescence of submicroscopic solid nuclei from the coalescence of small bubbles over a period of time. In a few instances, solid particles were actually observed trapped in the surface of bubbles of about 0.02 in. diam. which had been formed by coalescence of many smaller bubbles.

Perhaps it should have been brought out in the paper that the occurrence of cavitation is not limited to the walls of a solid body, but that any discontinuity in the liquid is a potential cavitating surface by virtue of the vortexes generated thereat. The edges of wakes behind blunt bodies, the edge of the jet in an open-jet water tunnel, and the experiment just described by the writer are examples. The author's three regimes of flow apply to these examples as well as to the solid body.

The phenomenon of rebound, illustrated in Fig. 3 of the paper, requires much further study. Perhaps it may be explained in a homely way as the struggle of the liquid to release the surface energy of the bubble and to return its residual gas and vapor to the nuclear state of low surface energy.

Author's Closure

Mr. Silberman's remark that the occurrence of cavitation is not limited to the neighborhood of solid boundaries is correct, and it was not the author's intention to imply otherwise. It is well known that cavitation may occur in the reduced-pressure fields produced in vortex flow, but it is often difficult to get quantitative information from these experiments.

The author would like to comment on a suggestion of Mr. Silberman that a bubble when once expanded may maintain its increased size by virtue of its increased surface energy even though it moves into a region of higher pressure. An increase in surface energy, that is, the work done against surface tension cannot in itself give a stabilizing effect on a gas bubble in a liquid; in any such configuration, surface tension always acts in the direction of contracting the bubble.

The author disagrees with Mr. Silberman's final remark that the rebound phenomenon is related in some way to the release of the surface energy of the bubble. The cavitation bubbles which we have analyzed collapse from a maximum radius of approximately 0.1 in. The ratio of the surface energy of such a bubble to the pressure potential energy is of the order of 10^{-3}. The surface energy therefore constitutes a trivial portion of the total energy. It is believed that the rebound phenomenon will be explained in terms of the compressibility effects which enter toward the end of the collapse.

An Energy Method for Determining the Dynamic Characteristics of Mechanisms[1]

W. M. Dudley.[2] This paper represents another worthwhile contribution by the author in the field of applying mathematics to the kinematic and dynamic analysis of engineering mechanisms. He shows that if a train of mechanism has rigid parts and only one degree of freedom, then in a given position the velocities of the parts bear fixed ratios to each other. These velocity ratios may be found throughout the motion cycle by the usual methods. At any position, each part contains a fixed percentage of the total kinetic energy. When these have been plotted, it becomes possible to solve two types of problems of practical importance: (1) If a curve of motion versus time is specified, one can find the driving-force function which is necessary to produce it; (2) if the driving force is specified, as by a spring or hydraulic cylinder, the resulting motion can be found.

The latter problem arises frequently in the engineering development of mechanisms. These are usually invented by toolmakers rather than by engineers. The toolmaker has a dual advantage in being skillful with his hands, and blissfully ignorant of high stresses, wear problems, the need for easy repair and adjustment, and other bugaboos which have a paralyzing effect on the thought processes of a trained engineer. When a machine has appeared which is workable on a laboratory basis, it is a very common experience that the inventor is unable to take the remaining steps necessary to make it practical for use without the continual presence of a skilled mechanic.

[1] By B. E. Quinn, published in the Journal of Applied Mechanics, September, 1949, Trans. ASME, vol. 71, pp. 283–288.

[2] Associate Director, Engineering Research Department, Standard Oil Company (Indiana), Chicago, Ill. Mem. ASME.

At this point, the engineer can step in and perform the essential function of redesigning the machine for ease of manufacturing, adjustment, and repair, the elimination of fatigue failures due to excessive stresses, the provision of adequate bearings and lubrication, and a good appearance. To meet these requirements and to be sure that the machine will carry out its operations with the necessary speed and accuracy, he will probably have to make a dynamic analysis of the motions. The existing textbooks on machine design are of little help in such work, as they usually deal with graphical methods and omit mathematics almost entirely. Some of the earlier European treatises are more useful, but they are generally out of print and not available even in libraries.

In the field of cams, in particular, theoretical design methods until recently have lagged far behind the operating problems being encountered. At high speeds, the effects of friction and elasticity of the parts are likely to be of controlling importance, as the author points out. As a result of his earlier paper,[3] together with those of Dudley[4] and Hrones,[5] it is believed that fairly complete mathematical methods are now available for problems in cam geometry, the analysis and control of elastic deflections at high speeds and damping. It is to be hoped that the author will be encouraged to write a more modern "Kinematics and Machine Design" textbook, with adequate use of both analytical and graphical methods, as there is now a great need for such a work.

G. A. Nothmann.[6] The method of this paper constitutes an exceedingly useful tool in mechanism analysis. Since its presentation by the author, the writer has applied the energy method to calculations of the dynamic response of several mechanisms and found it both simple and effective.

The limitations of the process which are described by the author hardly detract from its merits. Specifically, they arise because energy terms corresponding to friction and to elastic deformations of links, depend not only upon the position of the mechanism but also upon velocities and "inertia loads" (which, in turn, are functions of accelerations). The writer would like to suggest an approximate procedure which takes account of these effects and partly controls their cumulative nature.

The velocity-displacement variation of the mass center of link k is represented by

$$v_k = \sqrt{\frac{2\beta_k T}{m_k}} = \sqrt{\frac{2\beta_k}{m_k}(T_0 + E_1 + E_2)}$$

where β_k is the "per cent total KE" and T is the total kinetic energy of the mechanism. T is equal to T_0, the kinetic energy present at the start, plus $(E_1 + E_2)$, the energy added subsequently. Of these, E_1 is a function of displacements only and corresponds to the forces contemplated by the author; E_2 varies with velocities and accelerations, and thus includes frictional and deformation effects. The functional form of E_1 and E_2 is assumed known.

Let the author's method be applied, using phases 1, 2, 3 . . . n . . . of the mechanism. The calculation may then proceed from phase to phase, with the complete velocity and acceleration plan being determined in one phase before proceeding to the next. Since velocities and accelerations are required for the calculation of E_2, it is suggested that this term for phase n be computed on the basis of the preceding phase $(n\text{-}1)$. The remaining error, which arises from changes in E_2 due to differences in velocities and accelerations between phases $(n\text{-}1)$ and n, is insignificant if E_2 is small compared to T_0 and E_1, and if phases are closely spaced. This procedure is capable of further refinement by successive approximation.

D. K. Wright, Jr.[7] The author has presented a clear explanation of a method of dynamic analysis which should be very useful to machine designers. His recognition of this latest example of the power of the energy method, and his careful working out of the details are to be commended.

Although the author has stated correctly that any method of velocity analysis would be satisfactory as a first step in the solution, the "phorograph" method[8] appears to be a natural adjunct to the steps to follow. In this method, a rotating link is chosen as the phorograph link, upon which is found a velocity counterpart or phorograph of each other point in the mechanism. All velocities in the mechanism are thus gathered onto one link, are directly proportional to the angular velocity of that link, and the truth of the basic theorem stated by the author is made evident.

As an example of the use of the phorograph, Fig. 1 herewith shows the slider-crank mechanism used by the author for his first example, with the phorograph velocity solution drawn on the crank, link 2.

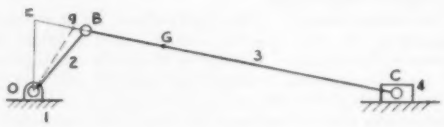

Fig. 1 Phorograph Solution of Slider-Crank Mechanism

Using the notation of Equations [1], [2], and [3] of the paper, and referring to Fig. 1 of this discussion

$$V_c = (Oc)\omega_{21} \quad [1]$$

$$V_g = (Og)\omega_{21} \quad [2]$$

$$\omega_{31} = \frac{Bc}{BC}\,\omega_{21} \quad [3]$$

and

$$\text{KE (crank)} = [I_c]\frac{\omega_{21}^2}{2} \quad [4]$$

$$\text{KE (piston)} = [M_p(Oc)^2]\frac{\omega_{21}^2}{2} \quad [5]$$

$$\text{KE (conn rod)} = \left[M_r(Og)^2 + I_r\left(\frac{Bc}{BC}\right)^2\right]\frac{\omega_{21}^2}{2} \quad [6]$$

The distribution of the kinetic energy in the mechanism can then be determined merely by computing the quantities in the brackets of Equations [4], [5], and [6] of this discussion. No velocity, assumed or otherwise, need enter the calculations.

[3] "An Analytical Method of Cam Design," by B. E. Quinn, Mechanical Engineering, vol. 67, August, 1945, p. 523.

[4] "New Methods in Valve Cam Design," by W. M. Dudley, Society of Automotive Engineers, Quarterly Transactions, vol. 2, January, 1948, pp. 19–33 and 51.

[5] "An Analysis of the Dynamic Forces in a Cam-Driven System," by J. A. Hrones, Trans. ASME, vol. 70, July, 1948, pp. 473–482.

[6] Research Engineer, Armour Research Foundation of Illinois Institute of Technology, Chicago, Ill. Jun. ASME.

[7] Associate Professor of Machine Design, Case Institute of Technology, Cleveland, Ohio. Jun. ASME.

[8] "Applied Kinematics," by J. H. Billings, D. Van Nostrand Company, New York, N. Y., second edition, 1943, chapt. 5.

The sum of the bracketed quantities is the equivalent moment of inertia of the mechanism in that position referred to the crankshaft.

Author's Closure

Dr. Dudley not only has presented a concise and accurate discussion of this method, but has rendered a valuable service by indicating where it can be applied in the development of a machine. The author believes, however, than an ideal text on kinematics and machine design could best be written by several individuals, such as Dr. Dudley, who have made valuable contributions to the subject and who have a broad, comprehensive view of the problems involved in developing machinery.

Dr. Nothmann's suggestion makes possible the analysis of mechanisms in which dissipative forces, and the like, exist, and thus constitutes a valuable addition to the theory. Plans are under way to investigate the behavior of mechanisms experimentally in the Machine Design Laboratory at Purdue University. The spacing of the phases can be determined to give results within the desired limit of error. Dr. Nothmann's method, involving the use of values in phase (n-1), can certainly be justified in view of the fact that, in many approximate methods for solving differential equations, a similar assumption is made. The author is grateful to Dr. Nothmann for extending the usefulness of the original method to problems of much greater complexity.

Professor Wright indicates the simplification that can be made if the "phorograph" method of finding velocities is used. In presenting the energy method it was the intention of the author to leave the manner in which the velocities are to be determined at the discretion of the individual using the method. The author has observed that certain individuals have strong personal preferences for certain methods of velocity analysis, and he did not wish to become involved in a discussion on that subject. This resulted in a slightly longer procedure in applying the energy method, but one in which the velocities could be determined by any means. Professor Wright is to be commended for showing the simplification which can result when an appropriate method of velocity analysis is used.

The Use of the Centrifugal Pendulum Absorber for the Reduction of Linear Vibration[1]

Rupen Eksergian.[2] A large class of machines may have disturbances in an axial or longitudinal direction which bear a constant ratio with the shaft rotation. The problem set forth by the author is to counteract such disturbances in an axial direction in a way similar to the tuned vibration pendulum absorber used for eliminating torsional disturbances.

With the tuned pendulum for torsional oscillations, the counteracting torque exerted by the pendulum on the vibrating shaft, is

$$\Phi_P = \frac{mR(R+L)n^2\omega^2\epsilon}{R - Ln^2} = J_s n^2 \omega^2 \epsilon \quad \ldots\ldots [1]$$

where R = radius to attachment of pendulum, L = length of pendulum, and n = order of harmonic relative to angular speed of shaft ω; J_s is the variable inertia which can be made large by adjusting the denominator toward zero. Moreover, this adjustment is entirely independent of the rotation of the shaft and depends only upon the harmonic order to be tuned, thus making the apparatus effective with variable-speed operation.

For the linear system, in place of the torque reaction of the pendulum on the shaft, we are concerned with a tuned vibration absorber which can make its linear reaction F_s large for any given order n and independent of the rotation of the shaft.

Using the author's nomenclature, if we consider only one pendulum, the kinetic energy is

$$T_P = \frac{1}{2} m[(\dot{x}_1 - r\dot{\theta}\cos\theta)^2 + r^2\dot{\phi}^2\sin^2\theta + (R + r\cos\theta)^2\dot{\phi}^2] + \frac{1}{2} I_1\dot{\theta}^2 + \frac{1}{2} I_2\dot{\phi}^2\sin^2\theta + \frac{1}{2} I_3\dot{\phi}^2\cos^2\theta$$

The applied forces on x_1 and ϕ are $-F_x$ and

$$-F_t R + M_3\cos\phi - M_2\sin\phi$$

hence

$$\frac{d}{dt}\left(\frac{\partial T_P}{\partial \dot{x}_1}\right) - \frac{\partial T_P}{\partial x_1} = -F_x \quad \ldots\ldots [2]$$

$$\frac{d}{dt}\left(\frac{\partial T_P}{\partial \dot{\theta}}\right) - \frac{\partial T_P}{\partial \theta} = -c\dot{\theta} \quad \ldots\ldots [3]$$

$$\frac{d}{dt}\left(\frac{\partial T_P}{\partial \dot{\phi}}\right) - \frac{\partial T_P}{\partial \phi} = M_3\cos\theta - M_2\sin\theta - F_t R \quad \ldots [4]$$

from which

$$m[\ddot{x}_1 - r\cos\theta\cdot\ddot{\theta} + r\sin\theta\cdot\dot{\theta}^2] = -F_x \quad \ldots\ldots [5]$$

in agreement with the author's Equation [4]

$$[I_1 + mr^2]\ddot{\theta} - m\ddot{x}_1 r\cos\theta + (I_3 - I_2)\sin\theta\cos\theta\cdot\dot{\phi}^2 + m(R + r\cdot\cos\theta)r\sin\theta\cdot\dot{\phi}^2 = -c\dot{\theta} \quad \ldots\ldots [6]$$

Equation [4] is the time rate of change of the angular momentum and

$$M_3\cos\theta - M_2\sin\theta - F_t R = \Phi$$

is the torque exerted on the pendulum about the shaft axis. We note $\partial T_P/\partial\phi = 0$, and

$$\frac{\partial T_P}{\partial \dot{\phi}} = [m(R + r\cos\theta)^2 + I_2\sin^2\theta + I_3\cos^2\theta]\dot{\phi} = [AM]_P$$

The equation of angular momentum of the pendulum, is

$$[m(R + r\cos\theta)^2 + I_2\sin^2\theta + I_3\cos^2\theta]\ddot{\phi} - [2m(R + r\cos\theta)r\sin\theta - 2(I_2 - I_3)\sin\theta\cos\theta]\dot{\phi}\dot{\theta} = M_3\cos\theta - M_2\sin\theta - F_t R \quad \ldots\ldots [7]$$

If we combine the author's Equations [8] and [9] and noting the author's Equation [6] we have

$$2[(I_2 - I_3)\sin\theta\cos\theta - m(R + r\cos\theta)r\sin\theta]n\omega\cdot\dot{\theta} = M_3\cos\theta - M_2\sin\theta - F_t R \quad \ldots\ldots [7a]$$

which, noting the author's $n\omega = \dot{\phi}$, is the same as Equation [7] but neglects the acceleration term $\ddot{\phi}$ i.e., it is assumed $n\omega$ = const.

This assumption, in general, cannot be made; $n\omega$ varies with the torsional motion of the system as modified by the torque reaction of the pendulum.

It is important, therefore, to eliminate any coupling between the θ and ϕ co-ordinates in small oscillations of the system. This the author has accomplished in his particular pendulum design.

---

[1] By F. E. Reed, published in the June, 1949, issue of the Journal of Applied Mechanics, Trans. ASME, vol. 71, pp. 190–194.

[2] Senior Staff Adviser, Franklin Institute Laboratories, Philadelphia, Pa.; Chief Consulting Engineer, The Budd Company, Philadelphia, Pa.

Mechanical Impedance of the Pendulum

The linear reaction of the pendulum F_x on the mass M is from the writer's Equation [5]

$$F_x = m(\ddot{x}_1 - r\cos\theta\cdot\ddot{\theta} + r\sin\theta\dot{\theta}^2) \quad [5a]$$

where θ is connected with x_1 through Equation [6], i.e.

$$[I_1 + mr^2]\ddot{\theta} - m\ddot{x}_1 r\cos\theta + [(I_2 - I_3)\cos\theta + m(R + r\cos\theta)r]\dot{\phi}^2\sin\theta = -c\dot{\theta} \quad [6a]$$

For small oscillations, if $\theta = 0$ at the equilibrium position, then $\sin\theta = \theta$, so that if $\dot{\phi} = \omega + \dot{\eta}$ and $\dot{\phi}^2 = \omega^2 + 2\omega\dot{\eta}$, then the coupling due to rotational oscillations can be neglected. This can be effected approximately by using a high gear ratio for the rotational motion of the pendulum, so that the oscillation is around $\theta_0 = 0$, and gravity can be neglected.

In place of the author's nomenclature for the frequency of disturbance, it will be assumed $\dot{\phi} = \omega$ for the rotation of the pendulum, while the disturbance is of the nth order relative to ω, so that $p = n\omega$

$$x_1 = x_{10}e^{jn\omega t}, \quad \theta = \theta_0 e^{j(n\omega t - \phi_1)}$$

Then, neglecting the centripetal term

$$F_x = -mn^2\omega^2[x_{10}e^{jn\omega t} - r\theta_0 e^{j(n\omega t - \phi_1)}] \text{ (approx)} \quad [8]$$

and

$$\left\{-(I_1 + mr^2)n^2 + [I_3 - I_2 + m(R + r)r] + j\frac{cn}{\omega}\right\} \times \omega^2\theta_0 e^{j(n\omega t - \phi_1)} = -mn^2\omega^2 re^{jn\omega t}\cdot x_{10} \quad [9]$$

If

$$Q = \left[\frac{I_3 - I_2}{mr^2} + \frac{R + r}{r}\right] - \left[\frac{I_1}{mr^2} + 1\right]n^2$$

then

$$\left[Q + j\frac{c_1 n}{\omega}\right]r\theta_0 e^{-j\phi_1} = -n^2 x_{10}, \quad c_1 = \frac{c}{mr^2}$$

so that

$$r\theta_0 = -\frac{n^2 x_{10}}{Q + j\dfrac{c_1 n}{\omega}}\left|\cos\phi_1 + j\sin\phi_1\right| = -\frac{n^2 x_{10}}{\sqrt{Q^2 + \dfrac{c_1^2 n^2}{\omega^2}}}$$

where

$$\tan\phi_1 = \frac{c_1 n}{\omega Q}$$

$$\therefore F_x = -mn^2\omega^2\left[x_{10}e^{jn\omega t} + \frac{n^2\cdot x_{10}}{\sqrt{Q^2 + \dfrac{c_1^2 n^2}{\omega^2}}}e^{j(n\omega t - \phi_1)}\right]$$

$$= -mn^2\omega^2\left[\left(1 + \frac{n^2 Q}{Q^2 + \dfrac{c_1^2 n^2}{\omega^2}}\right) - j\frac{c_1 n\cdot n^2}{\omega\left(Q^2 + \dfrac{c_1^2 n^2}{\omega^2}\right)}\right]x_{10}e^{jn\omega t} \quad [10]$$

Without damping, we have

$$F_x = -mn^2\omega^2\left[1 + \frac{n^2}{Q}\right]x_1 \quad [11]$$

The first term augmenting the mass M by m, while the second term can be written

$$F_x' = -\frac{mr^2 n^2\omega^2 x_1}{\left[\dfrac{I_3 - I_2}{m} + (R + r)r\right] - \left[\dfrac{I_1}{m} + r^2\right]n^2} = M_e n^2\omega^2 x_1 \quad [12]$$

which for translation is analogous to Equation [1] for rotation. It is important to note if the disturbing frequency is f then $n = 2\pi f/\omega$ where ω is the actual angular velocity for the pendulum rotation.

Effect of Spring System and Weights in a Pendulum Absorber

Let us consider the system shown in the author's Fig. 4, with a torsional hinge spring at the axis of the pendulum. Its zero position (i.e., without torsion) is assumed at $\theta = \pi/2$. The weights of the pendulum, combined with the centrifugal loadings, pull the pendulum down to its equilibrium position θ_0. Let K = the torsional spring constant. Then the elastic hinge torque is

$$K\left(\frac{\pi}{2} - \theta\right)$$

Let Φ be the applied torque acting on the system. The rotational parts include an additional term I_m for the gear train or the drive motor. We assume the translatory disturbance to be $P_0\sin(pt + \gamma)$ which has the same frequency as the rotational disturbance $\Phi_0\sin(pt + \alpha)$. The hinge torque

$$K\left(\frac{\pi}{2} - \theta\right) = -\frac{\partial V}{\partial\theta}$$

acts on the co-ordinate θ. The virtual work of the gravity forces is

$$Mg\,\delta x_1 + 2\,mg\,\delta[x_1 - r\sin\theta] = (M + 2m)g\delta x_1 - 2mgr\cos\theta\delta\theta$$

Then the Lagrangian equations are

$$\left.\begin{aligned}
&\frac{d}{dt}\left(\frac{\partial T}{\partial\dot{x}_1}\right) - \frac{\partial T}{\partial x_1} = -\frac{\partial V}{\partial x_1} + (M + 2m)g + P_0\sin(pt + \gamma)\\
&\frac{d}{dt}\left(\frac{\partial T}{\partial\dot{\theta}}\right) - \frac{\partial T}{\partial\theta} = -\frac{\partial V}{\partial\theta} - 2mgr\cos\theta - c\dot{\theta}\\
&\frac{d}{dt}\left(\frac{\partial T}{\partial\dot{\phi}}\right) = \Phi_0\sin(pt + \alpha)
\end{aligned}\right\} \quad [13]$$

where

$$T = \frac{1}{2}\{M\dot{x}_1^2 + 2m[(\dot{x}_1 - r\dot{\theta}\cos\theta)^2 + r^2\dot{\theta}^2\sin^2\theta + (R + r\cos\theta)^2\dot{\phi}^2] + 2I_1\dot{\theta}^2 + 2I_2\dot{\phi}^2\sin^2\theta + 2I_3\dot{\phi}^2\cos^2\theta + I_m\dot{\phi}^2\}$$

and

$$V = \frac{1}{2}kx_1^2 + \frac{1}{2}\cdot 2K\left(\frac{\pi}{2} - \theta\right)^2$$

The equations of motion are

$$[M + 2m]\ddot{x}_1 - 2mr\ddot{\theta}\cos\theta + 2mr\dot{\theta}^2\sin\theta = -kx_1 + (M + 2m)g + P_0\sin(\omega t + \gamma) \quad [14]$$

$$[I_1 + mr^2]\ddot{\theta} - mr\ddot{x}_1\cos\theta + (I_2 - I_3)\dot{\phi}^2\sin\theta\cos\theta + m(R + r\cos\theta)r\sin\theta\cdot\dot{\phi}^2 = K(\pi/2 - \theta) - mgr\cos\theta - c\dot{\theta} \quad [15]$$

$$\{I_m + 2[m(R + r\cos\theta)^2 + I_2\sin^2\theta + I_3\cos^2\theta]\}\ddot{\phi} + 2[2(I_2 - I_3)\cos\theta\sin\theta - 2m(R + r\cos\theta)r\sin\theta]\dot{\theta}\dot{\phi} = \Phi \quad [16]$$

Let

$$\theta = \theta_0 + \epsilon, \quad \dot{\phi} = \Omega + \dot{\eta}, \quad x_1 = x'_0 + x$$

Then, for the equilibrium position, we have

$$kx'_0 = (M + 2m)g$$

$$[(I_3 - I_2)\sin\theta_0\cos\theta_0 + m(R + r\cos\theta_0)\, r\sin\theta_0]\,\Omega^2 + mgr\cos\theta_0 = K\left(\frac{\pi}{2} - \theta_0\right)$$

The equations of oscillation about the equilibrium position are

$$[M + 2m]\ddot{x} + kx - 2mr\ddot{\epsilon}\cos\theta_0 = P_0 e^{j(pt+\gamma)} \quad \ldots [14a]$$

$$-mr\ddot{x}\cos\theta_0 + (I + mr^2)\ddot{\epsilon} + c\dot{\epsilon} + [(I_3 - I_2 + mr^2)\cos 2\theta_0 + mRr\cos\theta_0]\Omega^2\epsilon - [mgr\sin\theta_0 - K]\epsilon + 2[(I_3 - I_2 + mr^2)\sin\theta_0\cos\theta_0 + mRr\sin\theta_0]\Omega\dot{\eta} = 0 \quad \ldots [15a]$$

$$[I_m + 2[m(R + r\cos\theta_0)^2 + I_2\sin^2\theta_0 + I_3\cos^2\theta_0]]\ddot{\eta} - 4[(I_3 - I_2 + mr^2)\sin\theta_0\cos\theta_0 + mRr\sin\theta_0]\Omega\dot{\epsilon} = \Phi_0 e^{j(pt+\alpha)} \quad \ldots [16a]$$

If we multiply Equation [15a] by 2, we note the coupling coefficient between ϵ and x is $2mr\cos\theta_0$ and between η and ϵ the gyroscopic coupling coefficient is

$$4[(I_3 - I_2 + mr^2)\sin\theta_0\cos\theta_0 + mRr\sin\theta_0]\Omega$$

The equations, therefore, can be written with

$$x = x_0 e^{jpt}, \ \epsilon = \epsilon_0 e^{jpt}, \text{ and } \eta = \eta_0 e^{jpt}$$

$$\begin{aligned} &[-p^2a_{11} + c_{11}]x + a_{12}p^2\epsilon + 0 = P_0 e^{j\gamma} \\ &+ a_{13}p^2x + [-p^2a_{22} + jp2c + c_{22}]\epsilon + j\beta_{23}p\eta = 0 \\ &0 + j\beta_{32}p\epsilon + [-p^2a_{33}]\eta = \Phi_0 e^{j\alpha} \end{aligned} \quad \ldots [17]$$

where

$$\beta_{23} = -\beta_{32} = 4[(I_3 - I_2 + mr^2)\sin\theta_0\cos\theta_0 + mRr\sin\theta_0]\Omega$$

and

$$a_{12} = a_{21} = 2mr\cos\theta_0, \text{ etc.}$$

Then

$$x_0 = -\frac{p^2}{D}\{[c(a_{22} + jp\cdot 2c - p^2a_{22})a_{33} + \beta_{23}^2]\, P_0 e^{j\gamma} + jpa_{12}\beta_{23}\Phi_0 e^{j\alpha}\} \quad \ldots [18]$$

and

$$D = p^2\{(a_{11}^2 - a_{11}a_{22})a_{33}p^4 + 2ja_{11}a_{33}cp^3 + [(a_{11}c_{22} + a_{22}c_{11})a_{33} - a_{11}\beta_{23}^2]p^2 - j\cdot 2c\cdot c_{11}a_{33}p + c_{11}(\beta_{23}^2 - c_{22}a_{33})\}$$

where

$$a_{11} = M + 2m, \ c_{11} = k, \ a_{22} = 2(I_1 + mr^2)$$

$$c_{22} = 2[(I_3 - I_2 + mr^2)\cos 2\theta_0 + mRr\cos\theta_0]\Omega^2 + 2K - 2mg\cos\theta_0$$

$$a_{33} = I_m + 2[m(R + r\cos\theta_0)^2 + I_2\sin^2\theta_0 + I_3\cos^2\theta_0]$$

along with the coupling coefficients already noted.

Now in the special case where $K = 0$ and neglecting the weight components, the equilibrium position then occurs at $\sin\theta_0 = \theta_0 = 0$. Hence $\beta_{23} = -\beta_{32} = 0$ and

$$c_{22} = 2[I_3 - I_2 + m(R + r)r]\Omega^2$$

$$x_0 = \frac{[(c_{22} - p^2a_{22}) + j\,2cp]P_0 e^{j\gamma}}{(a_{11}a_{22} - a_{12}^2)p^4 - (a_{11}c_{22} + a_{22}c_{11})p^2 + c_{11}c_{22} - j2cp[a_{11}p^2 - c_{11}]} \quad \ldots [19]$$

Following the author's nomenclature, $\Omega = n\omega$ and $p = \omega = mr^2T = [I_3 - I_2 + m(R + r)r]n^2 - [I_1 + mr^2]$, $mr^2\omega C = c$

Then

$$x_0 = \frac{[T + jC]P_0 e^{j\gamma}}{[-\omega^2(M + 2m) + k][T + jC] - 2m\omega^2} = \frac{P_0 e^{j\gamma}}{\left[(-\omega^2(M + 2m) + k) - \dfrac{2\omega^2 mT}{T^2 + C^2}\right] + j\,\dfrac{2C\omega^2 m}{T^2 + C^2}}$$

$$\therefore x_0 = \frac{P_0}{\sqrt{\left[(M + 2m)\omega^2 - k + \dfrac{2mT\omega^2}{T^2 + C^2}\right]^2 + \left[\dfrac{2mC\omega^2}{T^2 + C^2}\right]^2}} \quad [20]$$

in agreement with the author's Equation [22].

From this analysis we conclude that with a spring constant K in the absorber mechanism, the tuning for a given order $1/n$ becomes "dependent" upon a particular rotational speed, and moreover, there is a gyroscopic coupling between the translatory and rotational motion, so that, in general, $n\omega$ is not constant. Thus a spring-governor mechanism would be an absorber but can be tuned for only one shaft speed for an $1/n$ order disturbance.

The author's ingenious mechanism is a close approximation to a true translation pendulum absorber, which, by eliminating springs in the absorber itself and setting the equilibrium position with the pendulum's coplanar, the effect of any variation in the motion of the rotational parts is eliminated.

Author's Closure

The author is indebted to Dr. Eksergian for his additions to the subject. Of particular interest is his analysis of the spring-supported pendulums since springing may be in some cases found necessary, particularly in the case of low-frequency vibrations in a vertical direction.

In view of the detrimental effect of springs on the tuning of the absorber, attention should probably be given to design of constant-force supports, such as are used in some pipe hangers, whose spring constant can be adjusted to zero.

Primary Creep in the Design of Internal-Pressure Vessels[1]

Edward Adams Richardson.[2] It is appreciated that a great deal of effort has been expended by the authors in devising means for designing pressure vessels subjected to high-temperature, whereby the allowable stretch during a limited life is attained safely.

Unfortunately, it is the considered opinion of the partners[2] that the subjection of the structural members of a high-temperature process container, particularly such a one involving high pressure, to a region of temperatures involving both temperature stresses and creep phenomena, should be at least obsolescent at the present time. In the original patent issued to the writer in 1940,[3] it was shown that the structural or vessel wall may be at

[1] By L. F. Coffin, Jr., P. R. Shepler, and G. S. Cherniak, published in the Journal of Applied Mechanics, September, 1949, Trans. ASME, vol. 71, pp. 229–241.

[2] Partner of Edward, (Nellie), and George Richardson; also Publications Department, Bethlehem Steel Company, Bethlehem, Pa. Mem. ASME.

[3] U. S. Patent No. 2,215,532, "Method and Apparatus Relating to Insulated Vessels and Structures of Great Variety," issued to E. A. Richardson, Sept. 24, 1940.

atmospheric temperature throughout, irrespective of the process temperature, if it should be so desired: certainly temperatures well below the limiting one for creep are easily maintained. Thus it should be possible to accomplish two aims: (*a*) remove the limit upon process temperature normally imposed by available structural materials, (*b*) recover virtually all the heat which normally would escape through the walls of such a vessel. In addition, a chemically active reactant which at high temperatures would be highly corrosive may be almost neutral at atmospheric temperatures, greatly simplifying the problem of surface protection.

The method employed is simple. The vessel is lined with an envelope of fluid-permeable material adapted to the temperature gradients to be expected, the temperatures to be attained in the various parts, and the chemical action to be expected. Two cases may be distinguished: (*a*) The permeating fluid is either a reactant in the process or an acceptable diluent thereof; (*b*) the permeating fluid is one other than the reactants and does not mingle with the reactants or products. In cases (*a*) and (*b*), the permeating fluid is distributed over the surface of the permeable envelope, adjacent to the vessel wall which is to be kept cold, at a temperature substantially atmospheric, and at a mass rate of flow such as may be required. The fluid permeates through the permeable envelope from the outer surface to, and through the inner surface thereof.

In the case of (*a*), the fluid leaving the inner surface mingles with the reactants and products; it may be a portion of one of the reactant fluids. In case (*b*), an impermeable envelope is placed inside the permeable one so that the fluid in the space between the two envelopes may be collected and removed. Such fluid being highly heated may be passed through a heat exchanger adapted to recovering the heat therein, either by heating a portion of the reactants or in some other way. Very broadly, any sort of construction or process may be handled by one or other of the methods described.

The laws of the temperatures in the permeable bodies involved have been investigated theoretically and by tests. It is hoped a paper thereon may be presented to the Society. For determining the possibilities, a cracking chamber for oils operating at 850 F and 750 psi, 6 ft diam × 40 ft long, was investigated. Using commercially available permeable bodies, it was found that such a method would be quite practicable. The wall thickness of the vessel was 4 in., in the original design. With cold walls, only 2 in. was necessary. The original and very necessary stainless lining would be desirable but far from essential in the cold-wall design. The fluid flow through the permeable body would be of the order of 1 per cent of the reactants processed. Virtually no heat would be lost from the process, hence no additional heat would be required in the reactants.

It should be remembered that at moderate rates of permeation, the permeating fluid passing through the inner surface of the permeable envelope is at process temperature. If control of the exothermic heat of a reaction is required, the rate of flow of fluid may be increased to lower the reaction temperature.

Later on the partners applied the methods to a furnace with controlled combustion.[4] As the alleged date of the "sweat-cooling" conception is given as September, 1944, it will be seen that the patent specifications of the partners fully anticipated such a development as has been carried on under Navy Project SQUID.

The partners have gone further, applying related methods to very compact heat exchangers, cooling systems, the protection of gas-turbine blading and furnace parts, and have even shown how heat exchange may be secured between fluids, one at high, the other at atmospheric pressure, while avoiding much of the creep effect which must be considered in usual designs. For example, it is possible to build steam generators and furnaces, therefore, for 3500 psi and 1300 F sufficiently compact to generate nearly 200 lb per cu ft of space per hr (as compared with a more usual figure of 12 lb per cu ft per hr for 750 F, 1400 psi), while using materials readily available and of moderate cost. The weight of equipment would be about 10 per cent of the more usual, based upon steam generators for modern ore vessels.

The primary purpose of this discussion, then, is to point out that much work has been done toward the more scientific design of equipment for high temperatures and pressures for the twin purposes of economizing heat, and removing temperature limitations to the process which have been set hitherto by the properties of structural materials. It is impossible to do more than hint at the methods to be used. Obviously, many other useful effects may be secured. Only very limited amounts of material for special purposes should require the application of the methods given in the paper.

Authors' Closure

Mr. Richardson's remarks are of interest. However, they bear little relation to the technical aspects of the problem treated by the authors, and it is felt that no comments regarding them are necessary.

[4] U. S. Patent No. 2,311,350, "Method and Apparatus for Controlling Combustion," issued to E. A. Richardson, Feb. 16, 1943.

Three-Dimensional Solution for Stress Concentration Around a Circular Hole in a Plate of Arbitrary Thickness[1]

M. M. Frocht.[2] This paper has at least two important aspects. It is important because it extends the scope of the mathematical theory of elasticity, in which it is the three-dimensional generalization of Kirsch's plane solution. It is equally important on account of its conclusions regarding the stress concentrations in thick bars with circular holes in tension.

The following remarks are confined to the latter aspects of the paper:

In 1942 the writer, jointly with M. M. Leven, made a photoelastic study[3] of the factors of stress concentration in tensile bars of finite width with circular holes. Our attention at that time was confined to the primary or to the largest principal stress and we were not concerned with the remaining principal stresses.

It is of some interest to compare the conclusions arrived at in 1942, on the basis of optical studies with those arrived at by the authors via the analytical route.

1 *Stress Variation.* In 1942 we found "that in thick bars with circular holes the inner layers carry a somewhat greater stress than the outer layers." The authors find that "if $\Delta \neq 0$

[1] By E. Sternberg and M. A. Sadowsky, published in the Journal of Applied Mechanics, March, 1949, Trans. ASME, vol. 71, pp. 27–38.

[2] Research Professor of Mechanics, Illinois Institute of Technology, Chicago, Ill. Mem. ASME.

[3] "On the State of Stress in Thick Bars," by M. M. Frocht and M. M. Leven, *Journal of Applied Physics*, vol. 13, 1942, pp. 308–313.

the stress-concentration factor is reduced at the faces of the plate and increased in the interior" ($\Delta = t/D$).

2 *Magnitude of Stress Variation and Its Significance.* In 1942 we stated, "the variation in the stresses are, however, small and do not exceed 12 per cent. . . . For practical design purposes the factors of stress concentration for thick plates may be assumed to be equal to the corresponding two-dimensional factors." The authors now find that "regardless of the thickness ratio, the reduction of maximum stress σ_θ does not exceed 10 per cent. . . .," and that, "The foregoing conclusions with regard to σ_θ . . . lend further support to the general assertion that factors of stress concentrations based upon two-dimensional analysis apply to plates of arbitrary thickness ratio."

3 *Vose's Conclusions.* In 1942 we stated that "the results published by Vose . . . are believed to be in error." Commenting on the same results the authors say: "By neglecting σ_z . . . R. W. Vose arrived at the erroneous conclusion that the factor of stress concentration depends sensitively upon the thickness of the plates."

4 *State of Plane Strain.* Although guided by the different evidence, the same conclusions were also reached with regard to the thickness ratio Δ at which a state of plane strain is developed. Thus, in 1942, we found that "no deviation from the state of plane stress (or strain) can be found in bars with central circular holes when r/t is of the order of magnitude of about $^1/_4$ in. (This corresponds to $\Delta = 2$.)

The authors state: "It is noteworthy that the maximum values of σ_θ are practically attained already at $\Delta = 2$. (This maximum value of σ_θ is the value for plane strain.)"

It is now well established that in two-dimensional problems the results from photoelasticity and the theory of elasticity are generally in excellent agreement. The results obtained by the authors bear on the analogous question in the three-dimensional field. It should, however, be kept in mind that the problem solved by the authors deals with a plate of infinite width, whereas the plates studied photoelastically were of finite width with a minimum ratio of diameter of hole to width of plate of 0.14.

One aspect of the paper deserves special mention. The authors show that in three-dimensional problems Poisson's ratio may have a considerable influence on the state of stress. Fortunately, this influence is confined to the secondary stresses as is to be anticipated. In any event, photoelasticians will have to be cognizant of the influence of this factor.

In closing, the discusser wishes to express his admiration for the excellent piece of analytical work done by Drs. Sternberg and Sadowsky.

Authors' Closure

Professor Frocht's comments on experimental corroboration of some of the results obtained in the paper are greatly appreciated. The authors wish to take this opportunity to make reference to a master's thesis[5] in which E. Reissner's method was applied to the determination of three-dimensional corrections for the plane problem of the half-plane under sinusoidal normal tractions along the edge. In view of this application, the statement made on page 28 of the paper, requires modification. At the same time the authors call attention to an alternative solution by A. E. Green[6] of the problem under discussion, which appeared after our work had been submitted for publication.

[4] The same effect was subsequently found in thick slotted plates in tension.

[5] "On Generalized Plane Stress," by R. A. Clark, MS thesis, Massachusetts Institute of Technology, Cambridge, Mass., 1946.

[6] "Three-Dimensional Stress Systems in Isotropic Plates, I," by A. E. Green, *Philosophical Transactions*, Royal Society of London, England, series A, vol. 240, April, 1948, pp. 560–597.

A Strain-Energy Expression for Thin Elastic Shells[1]

W. T. Koiter.[2] The author indicates some inaccuracies in Love's theory of thin shells and particularly in Love's formula for the energy of bending. The arguments put forward to discredit Love's expressions are indeed convincing. Therefore it may be of interest to observe that the corrections indicated by the author are only of small *practical* importance. In effect, the differences between Love's (linear) components of curvature and the linear parts of the author's components of curvature can be shown to amount to

$$\frac{A_2}{E} + \kappa_1 = \text{linear part of } \frac{A_1}{Er_1}$$

$$\frac{B_2}{G} + \kappa_2 = \text{linear part of } \frac{B_1}{Gr_2}$$

$$\frac{C_2}{\sqrt{EG}} + \tau = 0$$

$$\frac{C'_2}{\sqrt{EG}} + \tau = \text{linear part of } \frac{2C_1}{\sqrt{EG}}\left(\frac{1}{r_2} - \frac{1}{r_1}\right)$$

As has been shown elsewhere,[3] it is inherent to the assumptions used in the engineering theory of thin shells that contributions to the strain components of the order zA_1/rE, etc., may be neglected.

Therefore in all cases in which the engineering theory (based upon the assumptions that normals of the undeformed middle surface, remain normals of the deformed middle surface, and direct stresses on planes parallel to the middle surface may be neglected) is applicable, the author's corrections cannot affect the bending energy appreciably.

On the contrary, it may be considered allowable to add to the components of curvature A_2/E, etc., *arbitrary terms* of the order A_1/Er_1, etc., in order to simplify the bending energy as far as possible.

Author's Closure

The author has asserted that Love's formula does not correctly account for the effects of the tangential displacements u and v upon the energy due to bending, since it contains the derivatives u_x and v_y which have no effect upon bending, and it omits the derivative u_y, which, by reason of symmetry, must have an effect similar to that of the derivative v_x. Dr. Koiter has shown that the effects of the derivatives of u and v upon the energy of bending are, in any case, negligible compared to the effects of these derivatives upon the energy of stretching of the middle surface. Consequently, Love's theory may be expected to lead to solutions of special problems which do not differ significantly from solutions derived from the author's equations. Nevertheless, the author's equations have the advantage that they are symmetrical, and that all of the terms in these equations can be explained "physically." Love's equations do not meet these requirements, since they are unsymmetrical with respect

[1] By H. L. Langhaar, published in the June, 1949, issue of the Journal of Applied Mechanics, Trans. ASME, vol. 71, pp. 183–189.

[2] Professor of Applied Mechanics, Technische Hogeschool, Delft, Holland.

[3] "Over de stabiliteit van het elastisch evenwicht" ("On the Stability of Elastic Equilibrium"), by W. T. Koiter, Thesis, Technische Hogeschool, Delft, 1945, chapt. 5 (Theory of Shells for Finite Displacements).

to the surface co-ordinates, and they contain some terms which logically should be deleted.

It has been pointed out that one part of the energy of bending of a shell is due to rotations of elements of the middle surface about their normal lines. In order to reconcile Love's theory with that of the author, this effect must be neglected, since Love's equation cannot correctly account for the rotation, inasmuch as the derivative w_y is lacking. Dr. Koiter indicates that this effect is always negligible if the tangential displacements u and v are small, and the radii of curvature are large compared to the thickness. It then follows that all of the u and v-terms may be discarded from C_2 and C_2' (Equation [8] of the paper), since these terms account for rotations of elements of the middle surface about their normal lines. This conclusion is practically useful, since the u and v-terms in C_2 and C_2' are a source of difficulty in the integration of the differential equations of shells. If the u and v-terms are discarded from C_2 and C_2', and quadratic terms in w are neglected, then $C_2 = C_2'$. This relationship eliminates an anomaly from the theory, since the shearing strain γ_{xy} (Equation [11]) is now given by a linear equation in z, i.e.

$$\gamma_{xy} = 2\,(EG)^{-1/2}\,(C_1 + C_2 z)$$

The approximate expression for C_2 and C_2' is

$$C_2 = C_2' = \frac{E_y w_x}{2E} + \frac{G_x w_y}{2G} - w_{xy}$$

Strictly speaking, the strain energy of a shell is not uniquely determined by the displacements of the middle surface. Analogously, the strain energy of a beam is not uniquely determined by the curvature of the neutral axis. For example, equal and opposite forces, applied laterally to a beam, change the strain energy without changing the curvature of the neutral axis. In order to obtain a unique strain-energy expression for shells, the author has used the usual assumption that the stresses σ_z, τ_{xz}, and τ_{yz} are negligible. Also, quadratic z-terms in the strain tensor have been neglected. Within the limitations of these assumptions, the author's derivation of the linear terms in u, v, and w in the strain-energy expression is rigorous, since the analysis is purely formal mathematics. The fact that some of these terms, although of the first degree, are still negligible, was not contemplated. Dr. Koiter has raised an important point in discussing the relative magnitudes of these terms, since it is essential to discard, from the differential equations of shells, all terms which do not have primary significance, if solutions of special problems are to be achieved.

The Dynamic Response of a Simple Elastic System to Antisymmetric Forcing Functions Characteristic of Airplanes in Unsymmetric Landing Impact[1]

R. L. Bisplinghoff.[2] The author has demonstrated the severity of unsymmetrical landings in producing dynamic stresses. Since landings involving side drift occur frequently in service, and are often unsymmetrical, the critical features demonstrated in the present paper are of considerable importance in dynamic-landing analyses. It should be observed that the increased dynamic response factor in unsymmetrical landings may not be the only reason why dynamic stresses in unsymmetrical landings are more severe. In many cases, the wing configuration and the landing gear location are such that the landing force is applied somewhat closer to the node line in the lowest symmetric mode than in the lowest antisymmetric mode.

The dynamic-response-factor curves for antisymmetric forcing functions given by the author make a valuable addition to those already in the literature for other kinds of disturbances.

Author's Closure

The author wishes to thank Professor Bisplinghoff for his comments. The author agrees that the location of the landing-gear station may be closer to the node line of the lowest symmetric mode than to that of the lowest antisymmetric mode, and that this is an important reason why unsymmetric landings may produce severe dynamic stresses in such a case.

[1] By J. B. Woodson, published in the September, 1949, issue of the Journal of Applied Mechanics, Trans. ASME, vol. 71, pp. 310–316.

[2] Associate Professor of Aeronautical Engineering, Massachusetts Institute of Technology, Cambridge, Mass.

Book Reviews

Philosophy of Mathematics and Natural Science

PHILOSOPHY OF MATHEMATICS AND NATURAL SCIENCE. By Hermann Weyl. Princeton University Press, Princeton, N. J., 1949. Cloth, 6 × 9 in., x and 311 pp., 7 figures. $5.

REVIEWED BY J. ORMONDROYD[1]

THE major concern of Hermann Weyl has been mathematics. He is labeled by himself and the institutions of learning in which he has made his career as a mathematician. But one of his important interests has been in the field of mathematical physics—particularly in the domain of the theory of relativity. Running concurrently and continuously with these interests has been his philosophical outlook on science and mathematics and the relationship between the two. His numerous publications include works in mathematics, relativity, and the philosophy of mathematics and science.

This book is a revised and augmented translation of Professor Weyl's "Philosophy der Mathematik und Naturwissenschaft" which originally appeared in Oldenbourg's Handbuch der Philosophie in 1927. The augmentation consists of six appendixes which cover some aspects of the development of mathematics, physics, chemistry and biology in the last twenty-three years. Dr. Olaf Helmer, versed in mathematics and philosophy, translated the whole Handbuch article with the exception of two sections which were translated by the author's son. The whole translation was reviewed and revised by the original author.

In the original Handbuch text we have the outlook of a philosophically minded mathematician at the time when the theory of relativity had reached completion, and the new quantum mechanics was about to arise. The three parts of this book are intended to be a report on some of the more important philosophical results and viewpoints which have emerged primarily from research within the fields of mathematics and the exact empirical sciences. The book is divided into three parts. The first two parts, Part 1, Mathematics, and Part 2, Natural Science, are the translation of the original Handbuch articles. The third part, which contains six appendixes, forms the augmentation and modernization of the text. The subjects treated in Part 1 are Mathematical Logic, Axiomatics, Number and Continuum, the Infinite, and Geometry. Part 2 discusses Space and Time, the Transcendental External World, Methodology, and the Physical Picture of the World. Appendixes A to F include essays on The Structure of Mathematics, Ars Combinatoria, Quantum Physics and Causality, Chemical Valence and the Hierarchy of Structures, Physics and Biology, and the Main Features of the Physical World.

This book makes tremendous demands on its readers—demands which most of us in the profession of engineering cannot meet. As the outline of the contents indicates the author expects the reader to be completely conversant in details with the foundations of mathematics and most of the physical sciences including chemistry and biology. Besides this he presumes a familiarity with the works of most of the philosophers from Thales to Bertrand Russell. According to the author, "[Sections of historical and supplementary interest not necessary to the main course of development . . . . . are indicated in this volume by opening and closing brackets, such as these]." These "unimportant" sections containing, for the most part, philosophical comments by the creators of mathematics and physics are perhaps the only sections in the book which some engineers can read with understanding. Inevitably those engineers who do have the curiosity and the temerity to take up this book will consider it in comparison with the popular works of Eddington and Jeans on science which were best sellers in the twenties and thirties. They are due for a severe shock. Eddington and Jeans had the light touch, in Eddington even the flippant touch, and in the end they probably said nothing; but Weyl has that deadly serious Germanic approach which may not reach the reader completely, but which actually does say something. This is not a book to be read. It is a book to be studied.

In view of all this, why should this book be reviewed in an engineering journal? (Parenthetically, what right has one who cannot understand most of this book to review it?) To quote the author again, "One of the principal tasks of this book should be to serve as a critical guide to the literature listed in the references." In fact, to any engineer who has a curiosity as to the development and contents of mathematics and the physical sciences, this book could be an invitation and guide to a complete education. It is one of the few books which actually make the reader stop, think, and investigate. For instance, it goaded the reviewer into looking at the much quoted and completely neglected "Elements" of Euclid (in translation, naturally). It made the reviewer ponder on the meaning of Philosophy, Mathematics, and Natural Science. What is the difference between Mathematics and the Philosophy of Mathematics, between Natural Science and the Philosophy of Natural Science? It made the reviewer read several books, write some twenty pages of disconnected notes on many different subjects and engage in quite a few discussions with his friends. Any book that can do that is worth attempting to read.

Engineers who are interested in the modes of thinking of mathematicians and physical scientists in the creative and critical phases of their work will dip into this book over and over again. The mere attempt to answer the numerous questions which it creates in the reader's mind will be a source of great pleasure and might even lead to a more clear-cut approach to his thinking on the problems which arise in his engineering practice. Professor Weyl might resent this last statement since his book in no way attempts to give any rules of action. Man in action is not a philosopher, but Man thinking about action is.

[1] Professor of Engineering Mechanics, University of Michigan, Ann Arbor, Mich. Mem. ASME.

Advanced Calculus for Engineers

ADVANCED CALCULUS FOR ENGINEERS. By F. B. Hildebrand, Prentice-Hall, Inc., New York, N. Y., 1949. Cloth, 6 × 8½ in., illustrations, tables, appendix, xiii and 594 pp., $6.

REVIEWED BY LOUIS A. PIPES[2]

AS stated in the preface, this book was prepared to present an integrated treatment of those topics in mathematics which may be based upon a sound working knowledge of elementary calculus and which are of common importance in a number of fields of application. The practical usefulness of the mathematical

[2] Associate Professor of Engineering, University of California, Los Angeles, Calif.

concepts and techniques developed in the text is illustrated by numerous applications to problems which are of interest to a wide class of readers.

The first five chapters are concerned principally with ordinary differential equations. The material of the first chapter is an introduction to the elementary concepts and techniques associated with linear ordinary differential equations. In the second chapter, the powerful techniques of the Laplace transform are developed and applied to the solution of ordinary linear differential equations with constant coefficients and to the evaluation of certain definite integrals. The standard methods for solving ordinary differential equations numerically are presented in the third chapter. The use of power series for the solution of linear differential equations with variable coefficients and the properties of Bessel, Legendre, and hypergeometric functions are the topics discussed in the fourth chapter.

Boundary-value problems of interest in engineering are used in the fifth chapter to introduce the subjects of orthogonal functions, Fourier series, Fourier-Bessel series, Legendre series, and the Fourier Integral. Chapter 6 develops the useful ideas and tools of vector analysis and together with Chapter 7 serves to introduce the basic concepts associated with the simpler types of partial differential equations. The treatment of the partial differential equations of mathematical physics is illustrated in Chapter 8 by well-chosen problems from the fields of heat flow, fluid flow, mechanical vibrations, traveling waves, and supersonic flow of a compressible fluid. In the concluding chapter those topics in the theory of analytic functions of a complex variable which are needed by the student of engineering are presented. The general theory of the complex variable is applied to the evaluation of definite integrals and to the two-dimensional flow of fluids and allied problems.

In the opinion of the reviewer this is one of the most useful texts in the general subject of applied mathematics that has been published in recent years. Each chapter is concluded with a selection of problems which served to illustrate and extend the theory. These problems are chosen from the fields of physics and engineering as well as from mathematics, and the answers are given. This should be particularly helpful to engineers in industry who wish to review or to extend their knowledge of mathematics. The only possible criticism of the book is the omission of the theory of matrixes and their use in the solution of the differential equations of dynamics.

Analysis and Lubrication of Bearings

ANALYSIS AND LUBRICATION OF BEARINGS. By Milton C. Shaw and E. Fred Macks. McGraw-Hill Book Company, Inc., New York, N. Y. 1949. Cloth, $6^1/_2 \times 9^1/_4$ in., figures, tables, Appendix, xv and 618 pp., $10.

REVIEWED BY L. M. TICHVINSKY[3]

TECHNICAL literature pertaining to the related phenomena of friction, lubrication, and wear is rather abundant; however, it is scattered over a wide range of publications, such as found in mechanical, physical, chemical, petroleum, and metallurgical magazines. For this reason the appearance of "Analysis and Lubrication of Bearings," by Messrs. Shaw and Macks is most welcome as it provides a good source of correlation of special technical information.

As the book is one in the series of publications in aeronautical science, the first four chapters discuss in detail bearing-load analysis produced by cyclic type of loading. Dynamics of reciprocating engines, construction of polar diagrams, and effects of centrifugal and axial forces on bearing loading are included in these chapters.

The subjects of the next six chapters are primarily in connection with hydrodynamic or thick-film lubrication. The classical hydrodynamic theory of lubrication with several examples of simple integration of the Reynolds equation are presented together with the description of the hydrodynamic thrust bearing. Considerable space is devoted to special cases of lubrication which take into account such variables as fluctuating loads, full-floating bearings, oil-film whirl, composite bearing surfaces, and externally pressurized journal bearings.

One chapter is on rolling-contact bearings, with a rather detailed discussion of ball and roller-bearing performance. Relative motion of bearing elements, elastic deformations, and load distribution are presented with respect to a single-row radial ball bearing. Load capacity, in form of design equations and in form of graphs, friction consideration and methods of lubrication are also included in this chapter.

The wide scope of boundary lubrication is covered in one chapter together with short discussions of bearing metals and lubricants.

A few bearing testing machines are described in the last chapter and methods of bearing evaluations are presented.

The appendix contains a detailed table for the determination of piston displacement, velocity, and acceleration of crank mechanisms, and tables with specifications of six modern aircraft engines.

Approximately 300 problems are included at the end of the book and arranged in a sequence of chapter subjects.

The bibliography cites 384 references. There are over 350 figures and numerous tables.

Design engineers, senior and graduate students, especially those who are interested in aircraft construction, will find this book very useful.

[3] Professor of Mechanical Engineering, University of California, Berkeley, Calif. Mem. ASME.

Thermodynamic Charts for Combustion Processes

THERMODYNAMIC CHARTS FOR COMBUSTION PROCESSES: Part I, Text; Part II, Charts. By H. C. Hottel, G. C. Williams, C. N. Satterfield. John Wiley and Sons, Inc., New York, N. Y., 1949. Cardboard, $5^1/_4 \times 8^1/_2$ in., Part I, x and 75 pp., $2.60; Part II, 23 pp. and charts, $2.40.

REVIEWED BY BENJAMIN PINKEL[4]

THE subject publications present thermodynamic charts and methods for analyzing the cycles of various types of power plants including the new types developed for aircraft propulsion during and after World War II. The engine cycles treated are the Otto, Diesel, ramjet, turbine engine, turbine engine with tailpipe burner, and the rocket engine. The working fluids considered are mixtures of air and a hydrocarbon fuel and their products of combustion. For rockets and unconventional engines the general system comprising carbon, hydrogen, oxygen, and nitrogen is discussed.

The material is presented in two volumes titled Part 1 and Part 2. Part 1 contains 75 pages and describes the assumptions, sources of material, and methods of preparation of the various thermodynamic charts and the methods of applying the charts to cycle calculations. Numerical examples are presented to illustrate the application of the charts to engine-cycle computations and include "1, Turbocompressor Power Plant; 2, Com-

[4] Chief, Fuels and Thermodynamics Research Division, Lewis Flight Propulsion Laboratory, Cleveland Airport, Cleveland, Ohio.

pression Ignition Cycle; 3, Otto Cycle Engine With Supercharger; 6, Effect of Flame Travel Across the Combustion Chamber (on temperature distribution in combustion chamber of Otto-cycle engine); 7, Ramjet, 8, Turbocompressor Engine With Tail Pipe Burner; 9, Rocket, Burning Liquid Monofuel; 10, Two-Fluid Rocket, and 11, Liquid-Fueled Rocket Motor Operating Between Pressures Other Than 300 and 14.7 Psia." The several examples illustrate the computation of various types of thermodynamic processes including the compression processes involving air and mixtures of air with a hydrocarbon fuel, combustion at constant volume and constant pressure in which dissociation at the high temperature is taken into account, combustion in a gas flowing through a duct of uniform cross section, expansion of combustion products, and the throttling process. The method of constructing thermodynamic charts for fluids not presented in the subject volumes is discussed for guidance in the computation of thermodynamic charts for systems involving two or more of the elements, carbon, hydrogen, nitrogen, and oxygen.

Part 2 contains 8 large folded charts of the Mollier diagram type. The first chart (approx. 27 × 33 in.) entitled the "Modified Air Chart" gives the thermodynamic properties of air, of octane-air mixtures, and of mixtures of these with their products of combustion. The principal figure on this chart applies for air and has temperature as the ordinate, entropy as the abscissa, and lines of constant pressure and volume. Side figures on this chart provide corrections to be applied to the values in the principal figure for air-octane mixtures and their products of combustion. The temperature range of the chart is from 300 to 2500 deg R.

The remaining seven charts (approximately 25 × 18 in.) are for the products of combustion of air and a hydrocarbon fuel. Each chart applies for a different fuel-air ratio covering a range from 0.8 to 1.5 theoretical fuel. For six of the charts the hydrocarbon fuel is assumed to comprise two atoms of hydrogen per atom of carbon, and for one of the charts the fuel is assumed to comprise 1.625 atoms of hydrogen per atom of carbon. The charts show enthalpy and internal energy as ordinates and entropy as abscissa, and contain lines of constant pressure, temperature, and volume. A range of temperatures from 400 to 5500 deg R are covered and the effects of dissociation are considered.

The charts are derived from the thermodynamic data which have been summarized by R. C. H. Heck, and Hirschfelder, McClure, Curtiss, and Osborne. Only minor subsequent improvements in the basic thermodynamic data have been made.

The subject publication provides data of a type in great demand by engine-cycle analysts. In particular the charts for combustion products in the high-temperature range where dissociation is important fill an important gap in the literature on thermodynamic data. In the attempt to cover a wide range of conditions on each chart some loss in accuracy is incurred. For example, each of the charts on combustion products cover a range of pressures from 0.5 to about 10,000 psi. For many calculations on continuous-flow processes, as encountered in ramjet engines and turbine engines, enlargement of the charts in the low-pressure range would be highly desirable.

The transfer from the modified air chart to the combustion-products chart required in passing from compression to the burning and expansion for some cycles is complicated by the fact that the two charts involved have different temperature bases and one chart is on a per lb mole basis while the other is on a per lb basis. Although the methods for making the transfer are adequately explained a simpler procedure would be appreciated even at some sacrifice in generality in the charts.

In spite of these few shortcomings the charts are a valuable addition to the library of the cycle analyst.

Heat Transfer

HEAT TRANSFER. By Max Jakob. Volume I. John Wiley and Sons, Inc., New York, N. Y., Chapman and Hall, Ltd., London, England, 1949. Cloth, 6 × 9¼ in., xxix and 758 pp., illustrations, Bibliography, $12.

REVIEWED BY JOSEPH KATZ[1]

THIS large treatise represents the first major attempt in the English language to present the subject of heat transfer in great detail from the combined viewpoints of the engineer, physicist, and mathematician. In this first of two planned volumes, Max Jakob has succeeded in creating an authoritative book which will be of great value to many workers in this field, including teachers, researchers, students, and practicing engineers. Two features distinguish this book from others in the field: first, it contains a fairly complete collection of detailed analyses and derivations of important theorems which are difficult to obtain from the literature; second, a conscientious attempt has been made, wherever possible, to explain the macroscopic phenomena from the viewpoint of kinetic theory.

The book is divided into five parts. The first part (the first four chapters) introduces the basic concepts of conduction, convection, and radiation. The second part (chapters 5, 6, and 7) is devoted to discussions of the three properties of matter normally encountered in heat transfer: the viscosity, thermal conductivity, and emissivity. Several small tables of numerical values of these quantities are given, but the major emphasis is placed on understanding the wide variations of the values of such properties from the use of kinetic theory and of the physics of the solid state. The third part (chapters 8 through 20) is labeled simply as heat conduction in simple bodies, but actually covers a large range of subjects; these include steady-state and transient problems, measurements of thermal conductivity, sources and sinks, periodic and nonperiodic temperature changes, special mathematical methods, numerical and graphical methods, and experimental analogs of heat transfer. This third part covers almost 300 pages and serves well to indicate the detailed treatment of subject matter in the book. The fourth part (chapters 21 through 27) treats convection in the absence of change of phase or composition. The subjects covered include a discussion of similarity in flow problems, analytical solutions, free or natural convection, forced convection, and optical methods. The fifth and last part of the book (chapters 28, 29, and 30) treats convection in the presence of change of phase. The problems of heat transfer in evaporation and condensation, as well as a discussion of the similarity between heat and mass transfers, are included in this part.

A section at the end of the book contains problems on most of the thirty chapters for classroom use. An extensive author index, in the form of a bibliography, and a subject index permit one to find points of interest quickly.

Viewing the book as a whole, one finds many favorable features. It will serve as an invaluable source of basic material—it is a gold mine in this respect. It not only evaluates fairly critically the original material in the literature, but also corrects the inevitable mistakes and extends the original work in many cases; in this respect it will be of great service to the worker in this field. It summarizes the state of the art for many of the diverse subjects and brings them up to date for most readers by inclusion of very recent work.

It is regrettable that in a work of this magnitude more attention was not paid to the introduction and presentation of basic concepts in the first few chapters. In several cases, the distinction between a principle and an arbitrary definition is not clearly

[1] Associate Professor of Mechanical Engineering, Massachusetts Institute of Technology, Cambridge, Mass. Jun. ASME.

evident. In this connection, it is the opinion of the reviewer that the book is far more valuable for its presentation of material in theorem form and applications than it is for its treatment of the basic principles of the parent sciences, such as thermodynamics, fluid mechanics, and kinetic theory. One would hesitate, therefore, to use this book for an undergraduate course in heat transfer if one wished to stress the fundamental approach based on a clear and unified statement of the laws of mechanics and thermodynamics together with the arbitrary definitions needed in heat transfer.

In a treatise of 758 pages on an empirical science one would expect to find a great deal of data in tabular or graphical form which could be used in the solution of heat-transfer problems. Such data are almost absent because, as the author states, "It was believed that the present book should not be overloaded with this or any other empirical material, ..." Such a view is shortsighted, perhaps, since some material and some derivations could easily be shortened to permit the addition of some thirty pages of invaluable empirical data without increasing the length of the book. It is hoped that this shortcoming will be removed in the future.

The emphasis on and selection of type of material in the book will reveal to the reader a strong bias in favor of the author's own works. A disproportionate number of the total references in the bibliography refer to the author's own publications; he apologizes for this situation in the preface. Yet, on close examination of the bibliography, one finds no direct reference to the excellent fundamental papers of Hottel and co-workers on radiation. Perhaps these will be included in the second planned volume. This criticism of bias should be interpreted merely in the sense that the book does not have complete objectivity in the eyes of the reviewer; it is not a serious defect.

A second volume is presently in preparation. It will deal mainly with radiation, thermometry, heat exchangers, and selected fields of application.

Rocket Propulsion Elements

ROCKET PROPULSION ELEMENTS. An Introduction to the Engineering of Rockets. By George P. Sutton. John Wiley & Sons, Inc., New York, N. Y., 1949. Cloth, $5^1/_2 \times 8^1/_4$ in., ix and 294 pp., illustrations, $4.50.

REVIEWED BY NEWMAN A. HALL[6]

THE art of rocketry is one of the older expressions of applied physics. Its initial development is intimately associated with the introduction of gunpowder and other explosive combustion systems. In spite of its great age, however, it has resisted to the very present any reduction to an engineering science. During recent years, even, much of what has been written on rockets has had a touch of fiction and the amateur approach. The persistence of a few individuals, however, and the outstanding developments in Germany during the last war have shown that the rocket does deserve a firm place among engineering devices.

In "Rocket Propulsion Elements" the author has made available for almost the first time an introduction fully in keeping with modern engineering practice in design and analysis. Such a treatment will be particularly useful to those currently engaged in research and development in this field.

The first two chapters provide an orientation by reference to the historical development of rockets and to their general configuration and basic mechanical principles of operation.

The action of a rocket is due to the transfer of chemical energy to mechanical energy through the medium of the flow of propellant gases. Consequently, the statement of fluid-dynamic and thermodynamic basis of rocket performance as given in chapter 3 represent an essential starting point.

Chapters 4 and 5 together with a portion of chapter 10 provide a survey of the various types of liquid and solid propellants. Their physical and handled characteristics are discussed in detail. The thermodynamics of the combustion process is developed from the principles of equilibrium reactions and chemical-energy content.

The design of the rocket components, such as the combustion chamber and fuel system as outlined in chapters 6, 7, and 10, is based on well-established engineering practice with reference particularly to careful selection of materials and due attention to heat transfer and fluid-flow principles. These chapters benefit significantly by the inclusion of detailed examples and illustrations of current design practice.

Chapters 7 and 8 present a well-balanced and restrained discussion of testing practice and flight performance. These final stages in development have been frequently minimized and their neglect was the cause of many of the failures of early experiments.

While the needs of the practicing engineer are met very adequately, the arrangement is such that use as a text is equally possible. A large number of illustrative examples are worked out in detail and with most of the chapters a list of examples for the student is included.

The book is well-documented to provide a starting point for those concerned with more advanced phases.

[6] Professor of Thermodynamics, Mechanical Engineering Department, University of Minnesota, Minneapolis, Minn. Mem. ASME.

Helicopter Engineering

HELICOPTER ENGINEERING. By Raymond A. Young. The Ronald Press Company, New York, N. Y., 1949. Cloth, $6 \times 9^1/_4$ in., 163 figures, tables, appendix, xiv and 255 pp., $10.

REVIEWED BY R. H. PREWITT[7]

THE book under review is a timely presentation of practical information concerning the present state of the art of the helicopter industry. Whereas Mr. Young covers a highly technical subject, the absence of lengthy detail solutions and the generous use of graphs and illustrative figures provide a handbook-type source of information of significant value to any engineer desiring to become familiar with rotary-wing engineering.

In Part 1, Theory and Performance, Mr. Young covers substantially all basic data necessary in the design of a successful helicopter. These nine chapters deal with a comparative discussion of various helicopter configurations, design criteria of rotor systems, performance expectations of helicopters in hovering and high-speed flight, theory of stability for helicopters, and a brief introduction to jet-propelled rotor systems.

Part 2, Structural Design: Application and Theory, of Helicopter Engineering presents a discussion of materials and the factors affecting weight. In addition, rotor-blade design and stress-analysis data are listed in sufficient detail to carry out complete calculations. The concluding chapter of Part 2 concerns factors affecting helicopter design, such as flying qualities, performance, disk loading, power transmissions, vibrations, structure, stress concentration factors, and economics.

"Helicopter Engineering" will be genuinely appreciated by the experienced helicopter engineer because of its consolidation of the heretofore widely scattered information. To the engineer starting in the business, it will afford an excellent source of basic data and will provide a constant reference for the daily problems which arise. For other engineers who may wish to broaden their knowledge, "Helicopter Engineering" by Mr. Raymond A. Young, will be interesting and enlightening.

[7] President, Prewitt Aircraft Company, Clifton Heights, Pa.